TUM

Rare-earth metal-mediated synthesis of radical-containing polyvinylphosphonates: Novel materials for battery applications

Thomas Markus Pehl

Vollständiger Abdruck der von der Fakultät für Chemie der Technischen Universität

München zur Erlangung des akademischen Grades eines

Doktors der Naturwissenschaften

genehmigten Dissertation.

Vorsitzender Prof. Dr. Lukas Hintermann

Prüfende der Dissertation 1. Prof. Dr. Dr. h.c. Bernhard Rieger

2. Prof. Dr. Tom Nilges

3. Prof. Dr. Ulrich Schubert

(schriftliche Beurteilung)

Prof. Dr. Klaus Köhler

(mündliche Prüfung)

Die Dissertation wurde am 30.06.2021 bei der Technischen Universität München

eingereicht und durch die Fakultät für Chemie am 07.12.2021 angenommen.

"We can only see a short distance ahead, but we can see plenty there that needs to be done."

Alan Turing

Acknowledgement

In the first place, my special thanks go to my supervisor Prof. Dr. Dr. h.c. Bernhard Rieger for the opportunity to perform my Ph.D. thesis at his chair. I really enjoyed working on this interesting topic, our discussions about it and most of all the support and freedom to pursue my research.

Furthermore, thank you Carsten, for keeping the chair in such a good way, especially concerning the maintenance and repair of our analytic instruments, chemicals and supply of drinks, ice cream and barbecue events, but also to unleash the "Troll" if it was necessary. Concerning maintenance of analytic devices, I would also like to thank Sergei for his support in this matter. I very much enjoyed the discussions with the two of you about analytics and polymer chemistry.

Frau Bauer, thank you for your support in all of the bureaucratic obstacles and your excellent organization.

Next, I would like to thank Moritz and Philipp P., proud how you guys evolved and I'm happy to be still part of your research. Concerning this, I would additionally like to thank-you Moritz, for the valuable discussions and proof-reading of my thesis; this made the creation of my work considerably easier.

I further thank Jonas F., Philipp W. and Marc Kr. for your excellent work. I enjoyed supporting you in your theses and I'm very happy that already two of you found a position in our group. Marc Kr. you know what I expect of you.

Big thanks also to my students Gloria, Flo, Hicran, Nia, Sebastian, Valentin and Tobi for your excellent lab work.

I further thank Xaver Lampbrecht and Lukas Niederegger for your help in electrochemical characterization techniques and your support in our shared projects.

To all of the current and former Ph.D. students of our chair, I really appreciated the nice and helpful atmosphere and wonderful time in- and outside the Lab (especially the skiing trips). A special thanks here therefore to my friends, the "Old Makros" Arzu, Fabi, Basti, Michi and Marc, but also to Matti, Moritz, Jonas B. and Lucas. Especially also a big thank to my coffee and beer collaboration partners from the Fischer Group, Fabi, Stefan and Lena.

My special thanks to my family for supporting me during studying and Ph.D. and who, knowing or unknowing, lay the foundation for my interest in science. Without your support, I would probably not have had the opportunity to study chemistry and to pursue my Ph.D. thesis.

In the end I want to thank Rike, for all the support during my thesis. You were an integral part of it.

List of abbreviations

2VP	2-vinylpyridine
ADMET	acyclic-diene metathesis polymerization
ASSB	all solid-state battery
ATRP	atom transfer radical polymerization
CMC	carboxymethyl cellulose
CNT	carbon nanotube
Cp	cyclopentadienyl
DAVP	dialkyl vinylphosphonate
DEVP	diethyl vinylphosphonate
DIVP	diisopropyl vinylphosphonate
DMVP	dimethyl vinylphosphonate
DNA	deoxyribonucleic acid
DP	degree of polymerization
DPE	1,1-diphenylethylene
DTHVP	di(2,2,6,6-tetramethylpiperidin-4-yl) vinylphosphonate
DTMVP	di(2,2,6,6-tetramethyl-1-methoxypiperidin-4-yl) vinylphosphonate
DTOVP	di(2,2,6,6-tetramethylpiperidin-1-oxyl-4-yl) vinylphosphonate
DTPVP	di(2,2,6,6-tetramethyl-1-(1-phenylethoxy)piperidin-4-yl) vinylphosphonate
EPR	electron paramagnetic resonance
EQCM	electrochemical quartz crystal microbalance
ESI-MS	electrospray ionization–mass spectrometry
I	initiator efficiency
ITO	indium-doped tin oxide
_m_CPBA	meta chloroperbenzoic acid

Me	methyl
MMA	methylmethacrylate
NMP	nitroxide-mediated polymerization
NRC	nitroxide radical coupling
ORB	organic radical battery
ORP	organic radical polymer
PDEVP	polydiethyl vinylphosphonate
PDMS	polydimethylsiloxane
PDTMVP	polydi(2,2,6,6-tetramethyl-1-methoxypiperidin-4-yl) vinylphosphonate
PDTPVP	polydi(2,2,6,6-tetramethyl-1-methoxypiperidin-4-yl) vinylphosphonate
PDTOVP	di(2,2,6,6-tetramethylpiperidin-1-oxyl-4-yl) vinylphosphonate
PEIS	potentiostatic electrochemical impedance spectroscopy
PPP	poly(phosphonate)
P*t*BA	poly(*tert*-butyl acrylate)
PVdF	polyvinylidene difluoride
PVPA	polyvinylphosphonic acid
QCM	quartz crystal microbalance
RAFT	reversible addition-fragmentation chain transfer
REM-GTP	rare earth metal-mediated group transfer polymerization
RFB	redox-flow battery
RNA	ribonucleic acid
ROMP	ring-opening metathesis polymerization
ROP	ring-opening polymerization
ROS	reactive oxygen species
SCXRD	single crystals X-ray diffraction

SEI	solid electrolyte interface
SET-NRC	single-electron-transfer nitroxide radical coupling
SEM	scanning electron microscope
SKA-GTP	silyl ketene acetal-initiated group transfer polymerization
SPE	solid-polymer electrolyte
SQUID	superconducting quantum interference device
sym-**collidine**	2,4,6-trimethylpyridine
*t*Bu-**benzene**	*tert*-butylbenzene
TEMPH	2,2,6,6-tetramethylpiperidine
TEMPOMe	1-methoxy-2,2,6,6-tetramethylpiperidin
TEMPOPE	1-(1-phenylethoxy)-2,2,6,6-tetramethylpiperidin
TFA	trifluoroacetic acid
TMPy	2,3,5,6-tetramethylpyrazine
VGCF	vapor grown carbon nanofiber
VPA	vinylphosphonic acid

1 Abstract

Organic radical polymers (ORPs) are a class of sophisticated functional polymers, addressing a variety of applications including biomedical, organocatalysis, electronics and energy storage, in which the performance of ORPs is directly linked to the polymeric structure. Within this thesis, the scope of ORPs was expanded to phosphorous containing radical polyvinylphosphonates using rare-earth metal-mediated group transfer polymerization (REM-GTP), thus also introducing this sophisticated polymerization technique for the synthesis of organic radical polymers. The compatibility of this polymerization technique was tested with two different approaches: The direct polymerization of a radical vinylphosphonate and the masking of the radical moiety via alkoxyamine protecting groups. Therefore, four different functionalized dialkyl vinylphosphonates (DAVPs) were synthesized via esterification of vinylphosphonic dichloride. While REM-GTP of the radical DAVP failed, for DAVPs functionalized with alkoxyamine protected TEMPO moieties polymerization using di(cyclopentadienyl)lutetium-based systems (Cp_2LuX (X = cyclopentadienyl and pyridine-based systems) as catalyst led to polymers with adjustable molecular weight and narrow molecular weight distributions. End-group analysis confirmed a nucleophilic transfer of the initiator, leading to cyclopentadienyl- or a thiol chain end-groups, which were utilized for polymer immobilization on different surfaces (carbon nanotubes and gold). The oxidative- and the thermolytic deprotection of alkoxyamine-protected polymers resulted in nearly quantitative radical densities per repeating group (99%) for both deprotection approaches, while maintaining the polymers structural integrity. A novel approach utilizing the electrochemical deprotection of alkoxyamines was only successful for monomeric species, alkoxyamine functionalized polymers suffered from solubility issues with the electrolyte. The electrochemical properties of the radical polymers were studied by cyclic voltammetry, revealing a standard potential of $E°(Ag/Ag^+) = 0.72$ V with redox kinetics only limited by diffusion. The generated radical polyvinylphosphonates were additionally investigated in their performance as novel redox active cathode material in an organic radical battery setup. For polymers with increased molecular weights, less capacity fading in the charging/discharging cycling and a better agreement of the theoretical and received capacity was observed. Impedance spectroscopy in combination with scanning electron microscopy reveled agglomeration of the redox active polymer as the mechanism inducing the better performance of higher molecular weight radical polyvinylphosphonates.

2 Theoretical Background

2.1 Polymers as materials for high-tech applications

The chemical modification of natural polymers by pioneers like *Goodyear* (rubber), *Schönbein* (nitrocellulose) or *Fremery* and *Urban* (Rayon) inspired scientists to mimic these materials from available synthetic starting material and thus lay the foundation of the field of polymer science.[1] After basic research on the chemical nature of polymer bonds, sophisticated synthetic pathways were explored tuning not only the material properties, but simultaneously decreasing the overall production costs.[2, 3] These low cost synthetic routes combined with the exceptional processability and enhanced material properties resulted in a plethora of applications for polymers ranging from packaging, building and construction, transportation, electronics, agriculture, medicine to consumer goods.[4] Besides the enormous variety of polymeric structures, 78% of the worldwide polymer production was based in 2018 on only four different polymer types, therefore referred to as commodity polymers in the literature.[5] The remaining polymers are divided up into the segments of engineering or (functional) high-performance polymers. Especially the class of high-performance polymers with its capability to design tailor made functional materials links polymer research with life science, physics and other fields of chemistry thus opening the pathway to cutting-edge technologies offering solutions for highly topical challenges.[6]

One of these challenges is linked to the ongoing growth in population in combination with global climate change, leading to a drastic increase of freshwater demand, while freshwater availability declines simultaneously.[7] This issue is addressed by functional polymers, which can serve as membrane material for the purification of wastewater or desalination thus providing new sources of fresh water (Figure 1).[8, 9] Regarding biomedical applications and especially in the emerging field of drug or RNA delivery – widely noticed by society since the SARS-COV 19 pandemic and RNA based vaccines – functional polymers can serve as nucleic acid delivery vehicle, targeting diseases like cancer, Alzheimer, Asthma, cystic fibrosis and many more.[10-13] In difference to simple vehicles for drug delivery, polymers can be adjusted with the immense power of organic chemistry and thus polymer vehicles can target specific locations and even release the drug/nucleic acid using different stimuli (pH, temperature, redox, UV).[14-16]

However, one of the most discussed challenge society will face within the 21st century is the global climate change and the associated consequences.[17] While carbon dioxide

2

capture and storage approach can utilize high-performance polymer membranes, suitable energy storage system for transportation and grid stability are indispensable for the ongoing transformation from a fossil-based energy production towards unsteady renewable resources.[18, 19]
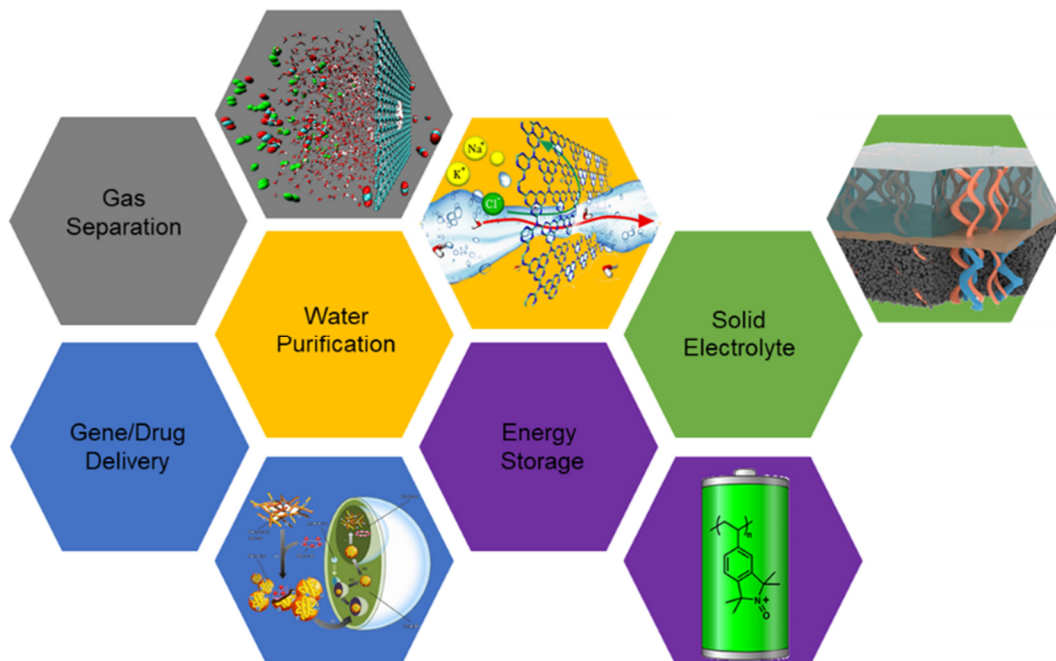

Figure 1: Selection of application sectors functional polymers can serve as sophisticated material. Adapted with permission from references[20-24].

In current energy storage systems like Li-ion batteries or proton exchange fuel cells, the membranes dividing the cell compartments are already based on polymeric materials (Celgard®, Nafion®).[25, 26] To further increase the energy density and adapt more complex battery active materials like silicon or metallic lithium, the concept of all an solid-state batteries (ASSBs) was developed, depending on the exploration of solid electrolytes.[27-29] While research focused on inorganic ceramic solid electrolytes for a long time, solid polymer electrolytes (SPEs) have gained increased scientific interest due to better performance and by combining improved mechanical stability with flexibility.[30-32]

Nevertheless, most commercial energy storage applications depend on metals as their key component, such as fuel cells which employ platinum as electrocatalyst or battery systems storing electrons in redox active metals.[33, 34] However, the exploration of this metals is not only linked to ecological devastation, but in the case of cobalt - commonly used as cathode material for Li-ion batteries – even to child-labor and -soldiers. Besides

this, the utilization of metal-based energy storage systems is also questionable from an economic point of view: The raw materials and especially battery electrodes are produced in high energy consuming processes, whereat suitable metals such as platinum and cobalt are expensive materials and subjected to speculation and price fluctuations.[35-38] In addition, the commercial energy storage systems lack an industrial adaptable recycling process, and most severely the demand for battery metals such as lithium and cobalt is predicted to be twice the amount of available resources for the year 2050.[39-41]

A breakthrough for the replacement of redox active metals was the discovery of reversible oxidation and reduction of poly(acetylene) in the 1970s.[42-45] This discovery laid the foundation for the concept of an all organic energy active material, employing abundant carbon feedstocks and even facilitating the generation of these materials by renewable resources and bio-feedstocks (Figure 2).[46-48] These findings motivated scientists to research different organic redox active molecules and lead to the establishment of the class of stable organic radical polymers. This sophisticated polymer class emerged as the most promising organic redox active material in the literature due to key features such as highly reversible redox chemistry, extremely fast redox kinetics, stable redox potentials and good processability (Figure 2).[49-58]
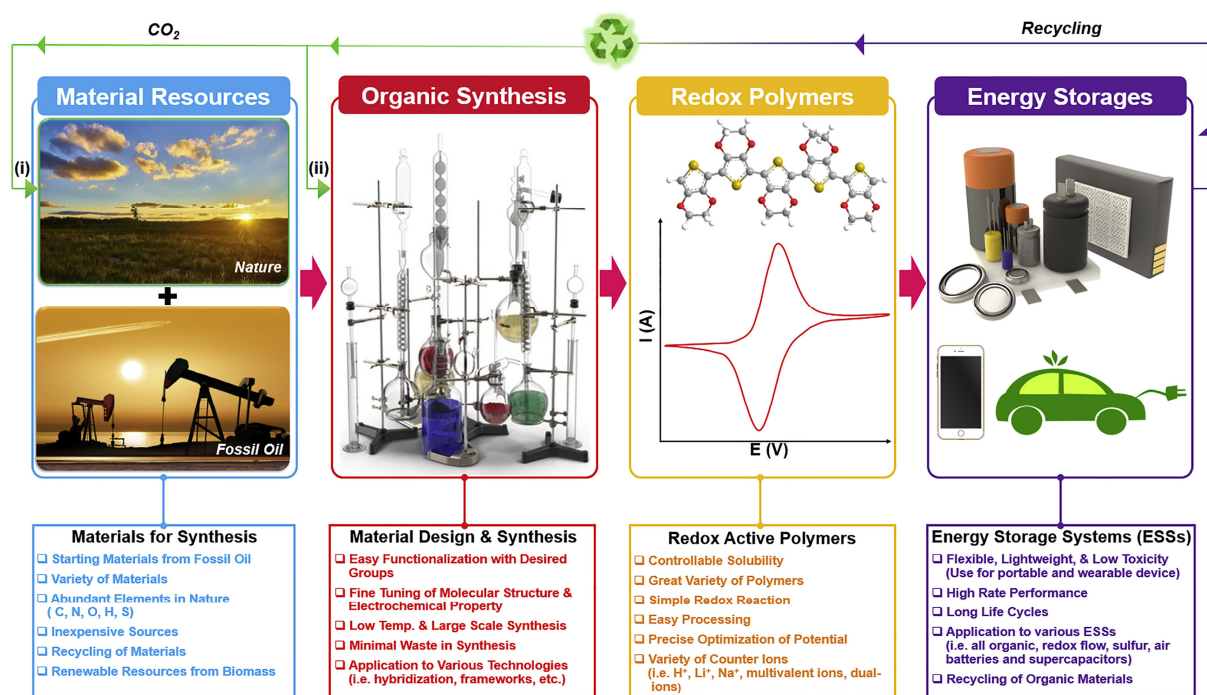

Figure 2:Schematic overview of redox active polymers key features in the areas: Feedstocks, Synthesis, Properties and Applications. Reprinted from reference[59] with permission from Elsevier.

2.2 Organic radical polymers

Via the functionalization of conventional polymer backbones with stable organic radicals as pendant side groups the versatile class of organic radical polymers (ORPs) was established. By this combination of the enormous variety of polymeric materials with their adjustable physiochemical properties and the unique features of stable organic radicals a plethora of different applications is accessible. While organic radicals commonly appear as highly reactive, short-lived reaction-intermediates, in contrast to this, persistent radicals have greater chemical stability and longer lifetimes, in some cases even for several years. This stability is achieved by delocalization of unpaired electrons within a large conjugation system and steric shielding to suppress dimerization. The first stable radical adapting these features was the triphenylmethyl radical introduced by Moses Gomberg in 1900 and therefore referred as *Gomberg* radical in the literature (Scheme 1). While this radical decays in the presence of oxygen, novel radicals based on verdazyl and phenoxyl (galvinoxyl) are unsensitive to air and moisture for a few months. An even further improvement in terms of radical stability was the isolation of nitroxide radicals in 1959.[60, 61] Their higher stability is achieved by delocalization of the unpaired electron on the N-O bond, the absence of α-H and the steric shielding. Additionally, the unfavorable thermodynamics of the N–O–O–N-bond upon dimerization effectively impedes self-termination.[62, 63]
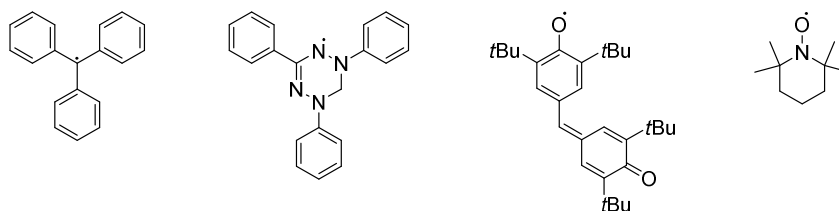

Scheme 1: Examples for typical stable radicals (from left to right): carbon-centered triphenylmethyl radical, nitrogen-centered verdazyl radical, oxygen-centered galvinoxyl radical and the nitroxide radical.

While nitroxide radicals themselves are highly persistent, they readily react with carbon-centered radicals, thereby acting as radical scavengers resulting in the formation of alkoxyamines. For sufficient stabilized carbon-centered radicals this formation is in a thermal equilibrium, serving as basis mechanism for the living radical nitroxide-mediated polymerization (NMP) as well as the nitroxide radical coupling (NRC) click reaction (Scheme 2).[64-67]
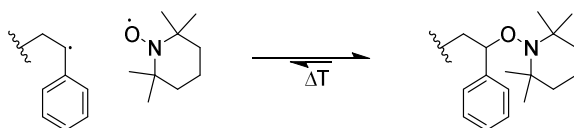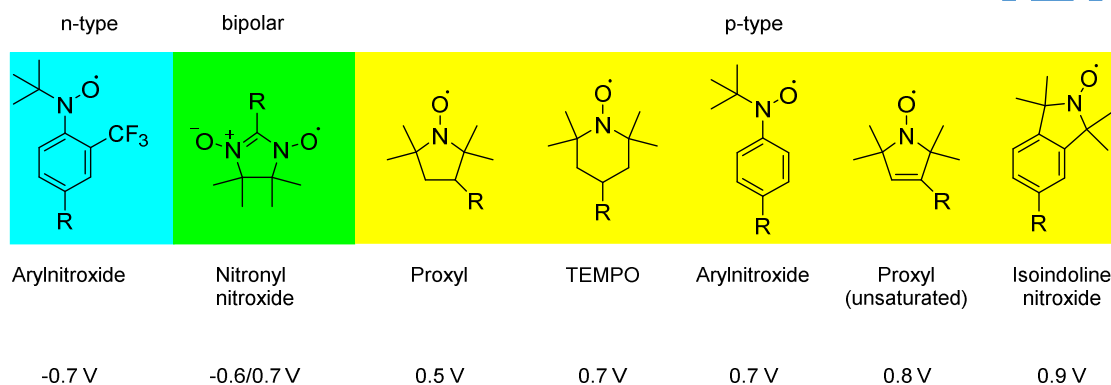
Scheme 2: Reversible formation of an alkoxyamine via a nitroxide and a carbon-centered radical.

Furthermore, as result of their radical character featuring an unpaired electron, nitroxides can undergo one-electron redox reactions. While the oxidation - resulting in an oxoammonium cation ($N=O^+$) - is considered to be fully reversible for tetraalkyl-nitroxides, the reversibility of the reduction forming aminoxyl anions ($N-O^-$) depends highly on the nitroxide structure and the reaction conditions (Scheme 3).[56, 68]
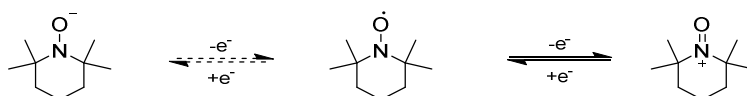
Scheme 3: Redox equilibrium between the nitroxide radical, the reduced oxoammonium cation and oxidized aminoxyl anion.

As more flexible rings are easier oxidized than rigid structures, this fact results in lower oxidation potentials with increasing ring-size, while electron withdrawing groups generally increase the corresponding redox potential. As these materials feature reversible redox reaction towards cationic species at rather high potentials (>0 V vs. Ag/Ag$^+$), they are classified as p-type (positive) materials. In contrast to this, the functionalization with strong electron withdrawing (e.g. trifluoromethane) groups on aromatic nitroxides stabilizes the aminoxyl anion ($N-O^-$) thus forming reversible n-type (negative) anode materials (redox potential < 0 V vs Ag/Ag$^+$).[55, 57, 69, 70] Furthermore, these structural features can also be combined in one structure as reported for the nitronyl nitroxide radicals, resulting in a bipolar material that employs reversible reduction to the anionic as well as reversible oxidation to the cationic species (Scheme 4).

n-type	bipolar		p-type			
Arylnitroxide	Nitronyl nitroxide	Proxyl	TEMPO	Arylnitroxide	Proxyl (unsaturated)	Isoindoline nitroxide
-0.7 V	-0.6/0.7 V	0.5 V	0.7 V	0.7 V	0.8 V	0.9 V

Scheme 4: Common nitroxide radicals and their corresponding redox potentials against Ag/Ag+ reference.[55, 57, 69, 70]

This reversible redox process resulted in the application of nitroxides as organic oxidation catalyst.[71] Additionally, due to their inherent paramagnetism, nitroxide radicals are further investigated as redox-responsive fluorescence quencher or as contrast agent for magnetic resonance imaging, thus replacing the commonly used transition metals.[72-74] Nevertheless, besides these applications it proved even further beneficial to functionalize polymeric materials with these as radical functional side groups.

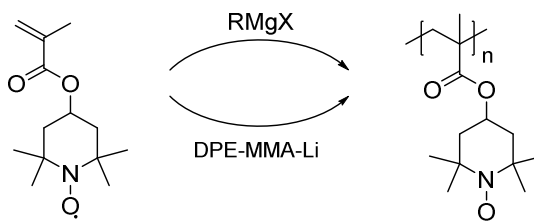### 2.2.1 Synthesis of organic radical polymers

Already in 1967, Griffith *et al*. developed the first polymer with an organic radical as pendant side group by utilization of a polymethacrylate (PMA) backbone which was functionalized with the stable radical (2,2,6,6-tetramethylpiperidin-1-yl)oxyl (TEMPO) as pendant side group resulting in poly(TEMPO methacrylate) (PTMA).[75] Due to its fast redox kinetics ($k_{ex} \approx 10^8$ M^{-1} s^{-1}), feasible standard potential (3.6 V vs. Li/Li+) and straightforward functionalization approaches, TEMPO is up to now the most prominent radical moiety in ORPs.[56, 76] For the synthesis of organic radical polymers, three different approaches exist in literature: Polymerization of stable radical monomers, polymerization of monomers containing suitable radical precursor and the subsequent conversion into the stable radical or post-polymerization modifications of polymers with organic radicals (Scheme 5).
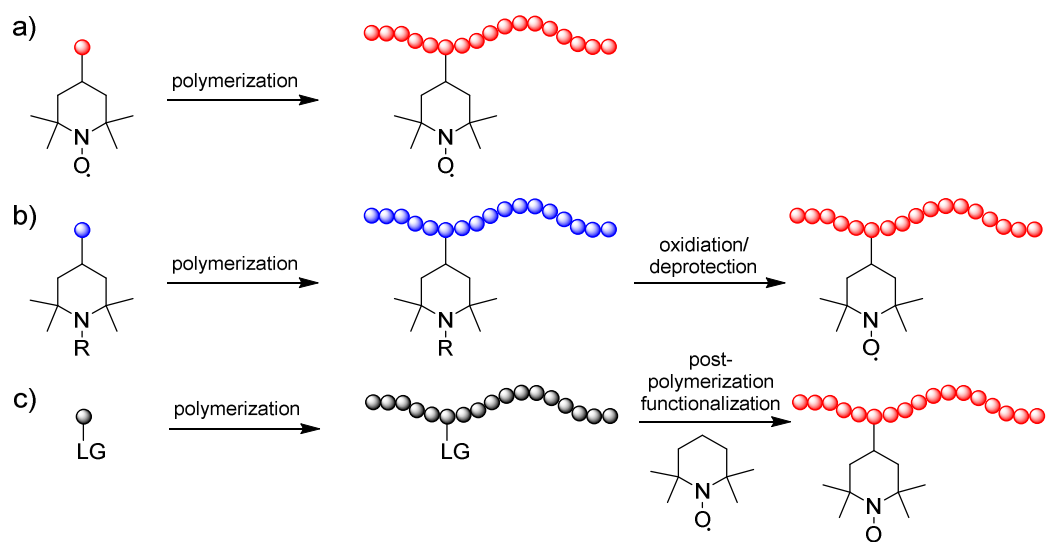
Scheme 5: Synthetic strategies for the generation of radical polymers using TEMPO radicals as an example. a) Direct polymerization of a radical containing monomer, b) polymerization of monomers containing suitable radical precursors and the subsequent conversion into the stable radical and c) post-polymerization modification of polymers with stable radicals.

Direct polymerization of stable organic radical polymers

Direct polymerization of radical containing monomers is a straightforward method for the synthesis of ORPs, without the need of further post-polymerization reactions. Since stable radicals are known to trap reactive carbon radical intermediates, polymerizations techniques employing radical intermediates are not applicable. The initial report on the synthesis of a stable organic radical polymer by Griffith and Coworkers utilized anionic polymerization of TEMPO functionalized methacrylate (TMA) with phenylmagnesium bromide to generate radical PTMA (Scheme 6). However, only low molecular weight polymers were obtained and further analysis revealed a possible crosslinking by side reactions of the nitroxide moiety and the Grignard reagent.[75, 77] By reducing the anionic initiators nucleophilicity via capping 1,1-diphenylhexyllithium with one equivalent methylmethacrylate (MMA) and subsequent polymerization of TMA, polymers up to 20 kg mol^{-1} with narrow molecular weight distributions (Đ < 1.1) were obtained (Scheme 6).[78, 79]
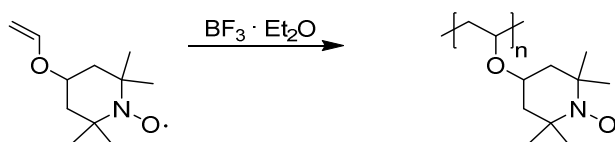
Scheme 6: Anionic polymerization of TEMPO functionalized methacrylates.[75, 77-79]

Similarly, organic radical polyethers are generated via an ionic polymerization of ethylenoxide-based radical monomers (Scheme 7). Unfortunately, these reactions suffered from low conversions, the generated radical polyethers showed broadened molecular weight distributions and most severely if using anionic coordinated ring-opening polymerization with $ZnEt_2/H_2O$, a drastic decrease in radical concentration per repeating unit (62% of the theoretical radical density) was observed.[80]
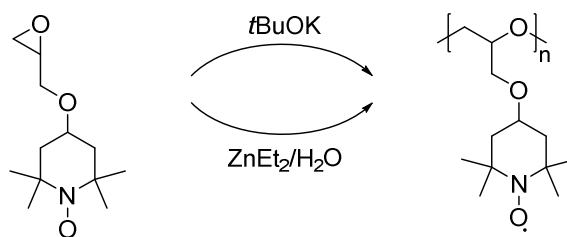
Scheme 7: Anionic synthesis of TEMPO functionalized polyether.[80]

Contrary, for the cationic synthesis of poly(vinyl ethers) catalyzed by the Lewis acid boron trifluoride etherate, a reduction of the radical density could not be observed (Scheme 8).[81, 82] Unfortunately, for this polymerization approach no additional data regarding polymeric properties were reported, thus making a comparison with other ionic polymerization techniques or other approaches for the synthesis organic radical polymers impossible.

Scheme 8: Cationic polymerization of TEMPO functionalized vinyl ether.[81, 82]

Besides ionic mechanism, also catalytic approaches for the direct polymerization of ORPs have been established. Especially the ring-opening metathesis polymerization (ROMP) is well studied for the generation of ORPs, and its applicability was shown by the controlled polymerization of various TEMPO functionalized (oxo)norbornenes by a

second-generation Grubbs catalyst (Scheme 9). With this active polymerization catalyst, high molecular weight polymers (M_n = 200 kg mol^{-1}) were synthesized, however, an increase in molecular weight distributions was observed (Đ > 2). Additionally, it was possible to obtain stereoregular organic radical polymers via stereoselective monomer synthesis (*endo,exo; exo,exo; endo,endo; exo,endo*).[83] The monomers substituents orientation had a strong influence on the respective polymer's properties. While *endo,exo-* and *endo,endo-*oriented polymers were readily soluble in organic solvents, *exo,exo-*oriented polynorbornenes were completely insoluble in common organic solvents.[83, 84]
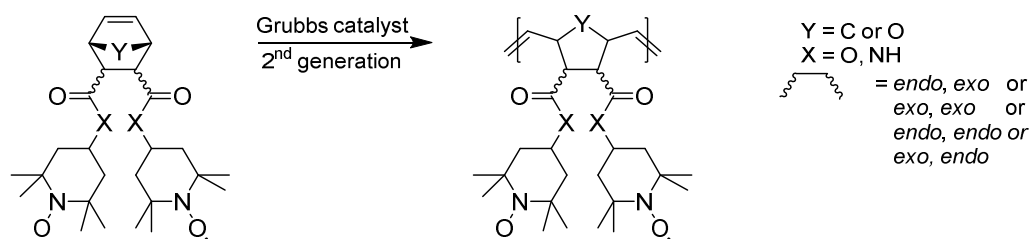
Scheme 9: Synthesis of TEMPO functionalized poly(oxo)norbornenes through ROMP by a 2nd generation Grubbs catalyst.[83]

Schubert and coworkers obtained high molecular weight polynorbornenes with small molecular weight distributions (Đ < 1.1) by switching from TEMPO to various galvinoxyl radical functionalized norbornenes and using a third generation Grubbs catalyst. However, for galvinoxyl radicals with less bulky methyl- instead of *tert*-butyl-substituents, insoluble polymers were obtained. This is attributed to an increased amount of side reactions of radicals due to the decrease steric hindrance.[85]
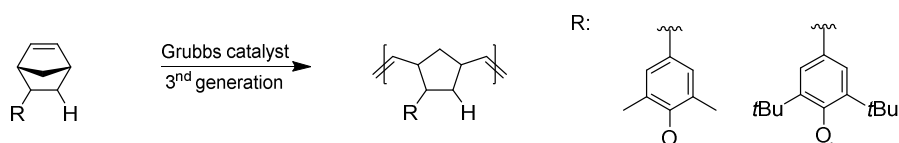
Scheme 10: Synthesis of galvinoxyl functionalized polynorbornenes through ROMP by a 3nd generation Grubbs catalyst.[85]

Besides metal-catalyzed ROMP, various ORP were generated by rhodium-catalyzed acyclic diene metathesis polymerization (ADMET). While the strictly conjugated polymer backbone was assumed to be beneficial for increasing the electric charge conductivity, special ammonia-modified Rh-catalyst had to be employed to suppress catalyst poisoning by the monomers nitroxide functionalities.[86] In a comprehensive investigation, Dulog and Coworkers studied the influence of the functionality linking acetylene and

various nitroxide radicals.[87] While aromatic linkers resulted in defined polymers (M_n up to 15 kg mol^{-1}), for monomers with non-aromatic linkers only oligomeric products were generated. Based on these results, branched polymers with up to four TEMPO functionalities per repeating group were prepared, however a drastic increase in molecular weight distribution was observed (Đ > 4).[84]
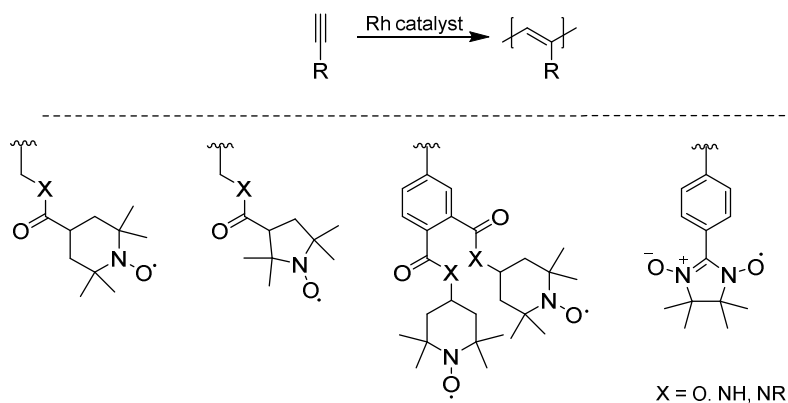

Scheme 11: Synthesis of radical-containing polyacetylenes by acyclic diene metathesis polymerization.[84, 86, 87]

Another catalytic approach was introduced by Bugon *et al*. utilizing silyl ketene acetal-initiated group transfer polymerization (SKA-GTP) of TMA with 1-methoxy-2-methyl-1-trimethylsilyloxypropene and tetrabutylammonium fluoride as the initiating system.[88, 89] For this system, the authors reported on an isotactic enriched (84% *mm*) PTMA as determined via ^{1}H-NMR spectroscopy after reduction of the TEMPO radical to the corresponding hydroxylamine. Unfortunately, the authors made no further explanation or assumption for the underlying mechanism inducing this stereoregularity and the high dispersity (Đ > 1.5) underlined a non-living type polymerization.[88, 89]

**Polymerization of nitroxide precursor monomers**

The use of non-radical containing monomers and polymers bears several synthetic and analytic advantages. Side reactions with the radical moiety are avoided and removal of the paramagnetic unpaired electron enables the applicability of the powerful NMR spectroscopy analysis, leading to improved insight via reaction monitoring, the determination of side reactions, bonding analytic, etc. Via subsequent post-polymerization the so generated polymers are readily converted to their radical form. For the generation of TEMPO based ORP, two strategies exist in the literature: Polymerization of a piperidine-containing monomer and subsequent oxidation to the

TEMPO radical or via polymerization of protected nitroxides that mask the radical species (Scheme 12).[55, 56]
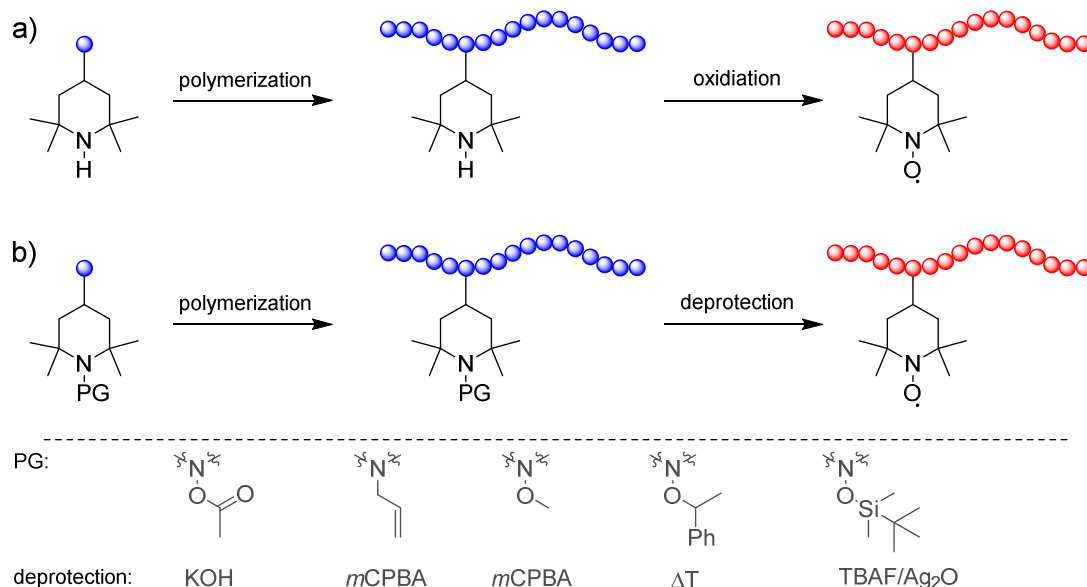
Scheme 12: Polymerization of non-radical nitroxide monomer precursors and post-polymerization modification of the polymers via (a) oxidation of piperidine polymer precursors or (b) cleavage of a protecting group to generate the organic radical polymer.[55, 56]

Kurosaki *et al*. were the first who reported on the generation of ORPs by the post-polymerization approach via free radical polymerization of a 2,2,6,6-tetramethylpiperidine functionalized methacrylate (TMPM) monomer (Scheme 13). The corresponding piperidine functionalized polymer was converted to the radical-species PTMA by oxidation with hydrogen peroxide in the presence of ethylenediaminetetraacetic acid (EDTA) and catalytic amounts of sodium tungstate or by using *meta*-Chloroperbenzoic acid (*m*CPBA) (Scheme 13).[49]
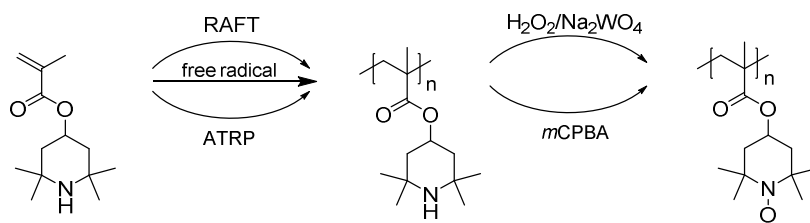

Scheme 13: Preparation of radical PTMA via polymerization of TMPM and subsequent oxidation.[55, 56, 66, 90, 91]

The straightforward nearly quantitative deprotection resulting in high radical densities and the compatibility of the TMPM monomer with living radical polymerization techniques like reversible addition-fragmentation chain transfer- (RAFT) or atom transfer radical polymerization (ATRP) make the resulting TEMPO radical functionalized PTMA

12

by far the most discussed and investigated ORP.[55, 56, 66, 90, 91] These controlled polymerization techniques allowed the synthesis of high molecular weight polymers (up to 131 kg mol^{-1}) while maintaining small molecular weight distribution and the use of sophisticated RAFT or ATRP initiators enabled the synthesis of even more complex polymer architectures or surface initiated polymerizations.[92-95] These results were also transferred to the synthesis of ORPs with acrylamide[96, 97], styrene[98], allyl[99] and acrylate[90] polymer backbones as well as for the synthesis of a plethora of various organic radical copolymers.[100-103]

Nevertheless, this approach is not feasible for polymerization techniques incompatible with secondary amines like NMP, sensitive metal-complexes or for the generation of arylnitroxides ORPs due to the instability of their arylamine precursor, as arylamines are already oxidized by residual oxygen to the corresponding arylnitroxide radical.[90, 104-106] Therefore, different protecting groups have been employed to mask the nitroxide radical, most of them employing the chemistry of alkoxyamines (Scheme 12). The thermal equilibrium of alkoxyamines has already been discussed (see Chapter 2.2 and Scheme 2). This feature was also the basis mechanism of thermolabile protecting groups for nitroxides, which therefore rely on sufficiently stabilized leaving groups like ethylphenyl. This motivated Behrends *et al*. to synthesize an ethylphenyl protected TMA by copper-catalyzed NRC. ATRP was used for the subsequent polymerization of the protected TMA, followed by temperature-induced deprotection.[107] This temperature induced oxidative cleavage was quantitative and no broadening of the molecular weight distribution of the radical polymers was observed, highlighting the potential of this thermolytic bond cleavage for the generation of nitroxide radicals. The versatility of this protecting group was additionally shown by successful deprotection of polymers immobilized on gold or graphene surfaces.[108, 109]
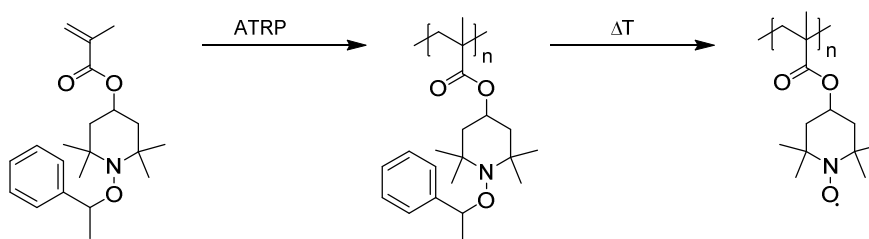

Scheme 14: ATRP of phenylethoxyamine protected nitroxide monomers and the subsequent temperature induced deprotection to generate the nitroxide radical.[107-109]

A different approach for an nitroxide protecting group was reported by Chalmers and Coworkers utilizing an oxidative deprotection of various alkoxyamines with *m*CPBA as oxidant.[110] The authors were able to propose the following mechanism of this cleavage: *m*CPBA generates an *N*-oxide via electrophilic attack at the nitrogen atom. In the subsequent Cope-type elimination, formaldehyde is released, and the corresponding hydroxylamine is formed. This species is further oxidized to yield the corresponding nitroxide radical (Scheme 15).
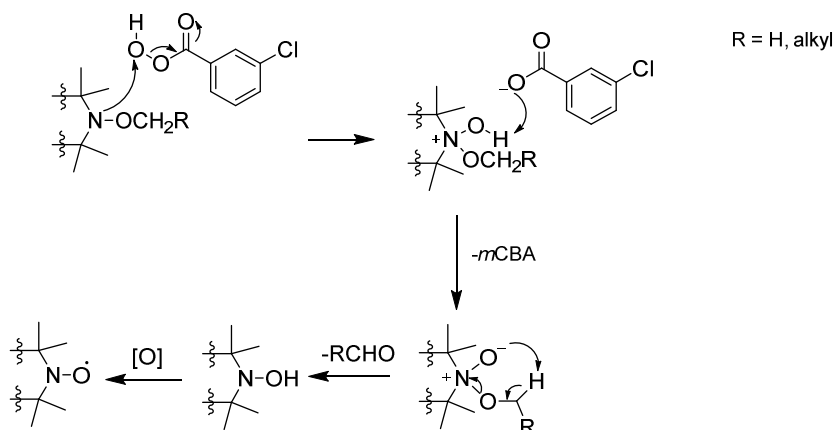

Scheme 15: Oxidative deprotection of alkoxyamines with *m*CPBA as oxidant via a Cope-type elimination.[110]

This approach was recently transferred by Hansen *et al*. for the synthesis of PTMA by RAFT of a methoxyamine protected TMA and also for the synthesis of an *iso*-indoline functionalized polystyrene (Scheme 16).[111, 112] A beneficial feature of the so generated methoxyamine protected polymers is an easier SEC analysis with THF as eluent instead of the special equipment needed for secondary amine containing polymers, which rely on DMF as SEC eluent. The subsequent oxidative deprotection by *m*CPBA yielded nearly quantitative radicals yields (98%) for both polymers, but a severe broadening of the generated ORPs molecular weight distributions was oberserved after deprotection if more equivalents of *m*CPBA were used (Scheme 16).[111, 112]

a)

b)
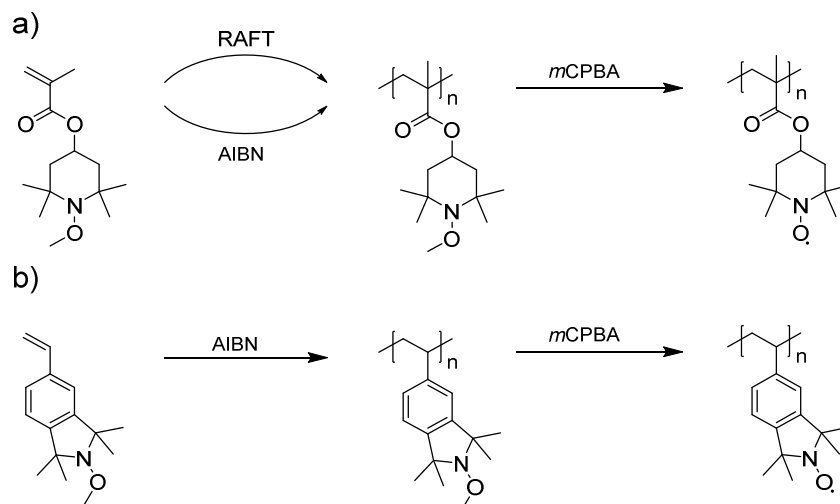
Scheme 16: a) Free and controlled radical polymerization of methoxyamine protected methyl methacrylate and their subsequent oxidation to generate the radical PTMA. b) Free radical polymerization of methoxyamine protected *iso*-indoline functionalized polystyrene and the subsequent oxidative deprotection to generate the corresponding radical polymer.[111, 112]

Nishide *et al*. adapted the *tert*-butyldimethylsilyl (TBDMS) group - widely explored for various alcohol functionalities - for the synthesis of different poly(styrenenitroxides) (Scheme 17).[104] In general, silylethers are due to their selective and mild deprotection an immensely useful protecting group, however this was the only example in the context of organic radical polymers. Via the utilization of the strong electron withdrawing trifluoromethane group in *ortho*-position of the nitroxide radical the redox potential is 1.7 V lower than of the unfunctionalized arylnitroxide making this polymer an interesting candidate as n-type anode active materials in energy applications. [104]
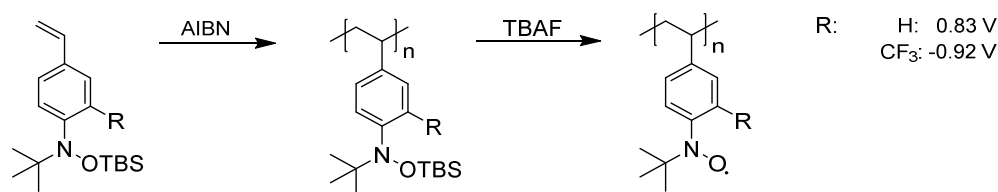

Scheme 17: Free radical synthesis of silylether protected styrenenitroxides and their subsequent deprotection by TBAF as fluoride source.[104]

Post-polymerization modifications of polymers with organic radicals

The post-polymerization modification approach is most widely applied for the functionalization of polymers with isolated radical functionals and only few examples exist focusing on the functionalization of every repetition unit with a radical moiety. The most straightforward approaches are the post-modification of active ester containing poly(*N*-acryloxysuccinimde) with 4-amino-TEMPO or click chemistry of azido

functionalized polythiophene with 4-propagyl-TEMPO.[113, 114] Additionally, post-polymerization modification allows generation of specific backbone compositions not accessible by direct polymerization. A more elaborated approach in this context is the synthesis of radical polysiloxane by post-functionalization of poly(methylhydrosiloxane) with 4-hydroxy-TEMPO by Karsted's catalyst (Scheme 18).[115]
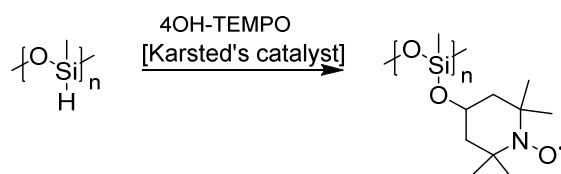
Scheme 18: Synthesis of radical poly(methylsiloxance) via post-polymerization modification with Karsted's catalyst.[115]

2.2.2 Applications of organic radical polymers

The combination of the unique chemical properties of stable organic radicals including selective recombination with carbon-centered radicals, paramagnetic behavior, high chemical and temperature stability and most importantly reversible redox reactivity with the precise adjustable polymeric functions results in a wide field of tailor-made cutting-edge applications. As there is a tremendous amount of ORP application reports, this chapter focuses only on the most important ones as well as special applications linked to the unique radical features of ORPs.

Post-polymerization functionalization and synthesis of complex polymer architectures

With the establishment of a simple and efficient synthesis for various alkoxyamine via the generation of alkyl radicals from organic halides and Cu(I) complexes - similar to the basic mechanism of ATRP - nitroxides are highly susceptible towards radical click-reactions.[116] This mechanism, later know as single-electron-transfer nitroxide radical coupling (SET-NRC), was transferred by Huang *et al*. to the coupling of polyesters featuring a TEMPO end-group and polystyrene synthesized via ATRP to generate block copolymers.[117] Fortunately, polymers generated by ATRP possess inevitable a halide end-group, capable of generating a carbon radical end-group. This feature underlines the versatility and scope of this approach to generate a plethora of different block copolymers.[66] In addition, this coupling reactions are feasible for the partial post-polymerization functionalization of the organic radical polymers pendant radical side groups. Zhang and coworkers utilized SET-NRC of PTMA to generate a fractional pyrene-functionalized copolymer, which self-assembles to layered PTMA on graphene (PTMA-Py-*co*-rGO) or carbon nanotubes (PTMA-Py-*co*-CNT) via their strong π-π stacking (Figure 3).[118, 119]
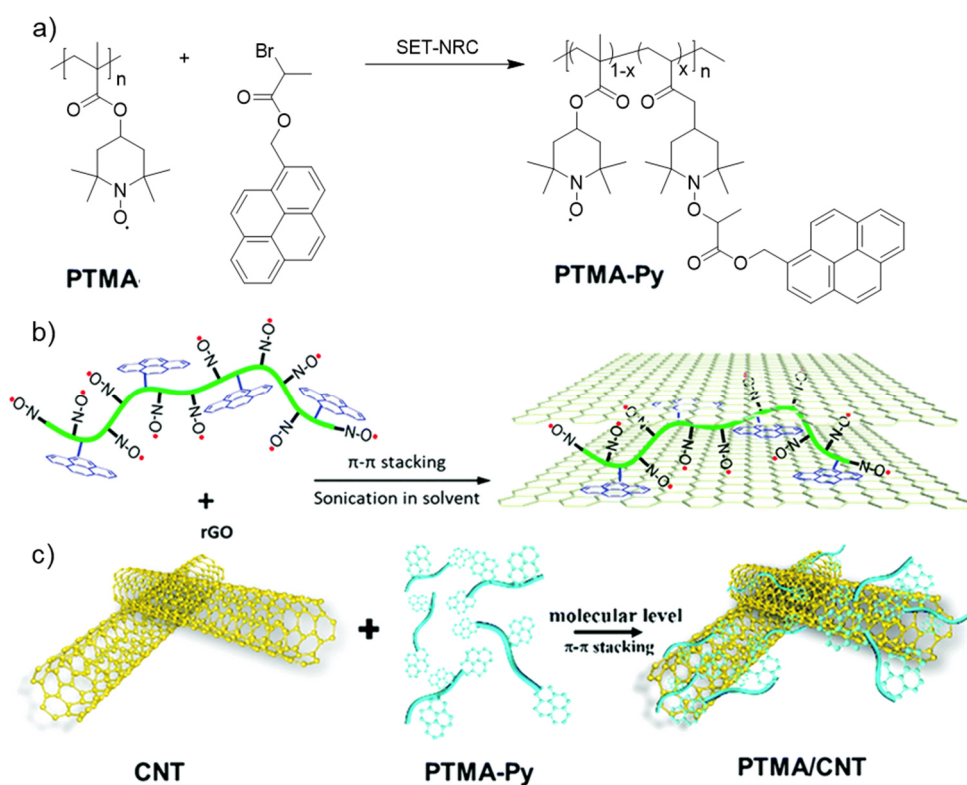
Figure 3: a) Post-polymerization functionalization of PTMA with pyrene by SET-NRC, b) self-assembly of a layered PTMA-Py-*co*-rGO and c) PTMA-Py-*co*-CNT prepared through π-π interaction. Reprinted with permission from reference[57].

An approach aiming at complete functionalization of the radical pendant side group was chosen for the synthesis of different brush polymers. Therefore, a statistical copolymer of 4-glycidyloxyl-TEMPO and ethylene oxide synthesized via anionic polymerization and in addition to this, bromine terminated polystyrene or poly(*tert*-butyl acrylate) (P*t*BA) via ATRP were prepared. Defined polymer brushes of PS or P*t*BA on the ORP were generated via the subsequent ATNRC with radical coupling efficiencies between 82-96% (Scheme 19).[120] Similarly, a grafting from process was applied to generate comb like copolymers of poly(ethylene oxide-g-styrene) from a poly(EO-co-4-glycidyloxyl-TEMPO) macroinitiator by nitroxide mediated polymerization utilizing the radical TEMPO moiety as initiator.[121] The capability of this approach is highlighted by the generation of sophisticated sun-shaped polymeric architectures via a cyclic poly(EO-co-4-glycidyloxyl-TEMPO) macroinitiator and subsequent NMP with styrene (Scheme 19).[122]

grafting to
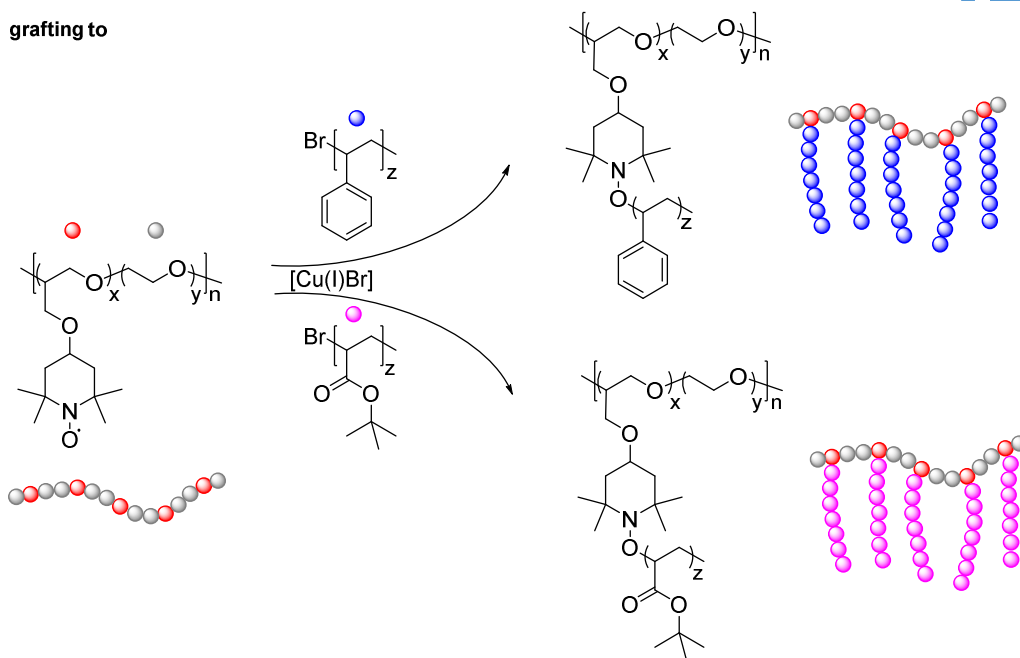
grafting from
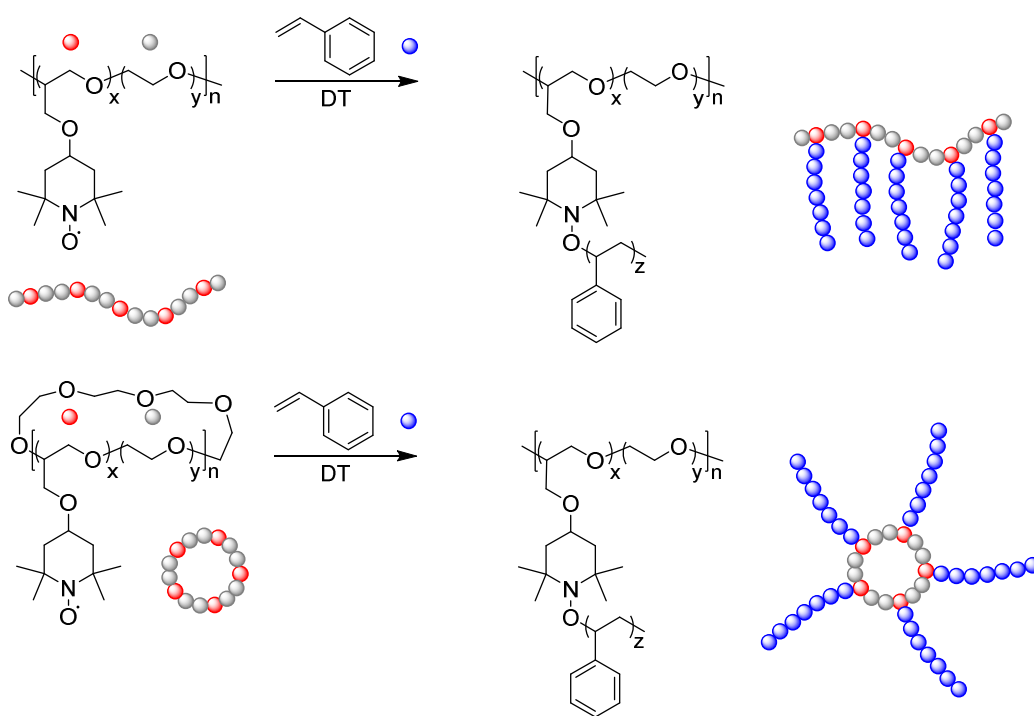
Scheme 19: Top: Grafting to approach for the synthesis of brush PS or PtBA on PEO via SET-NRC of poly(ethylenoxide-co-4-glycidyloxyl-TEMPO) and PS Br or PtBA-Br.[85] Bottom: Grafting from synthesis of a brush-like and sun-shaped poly(ethylenoxide-g-styrene) through NMP with a linear or cyclic poly(ehylenoxide-co-4-glycidyloxyl-TEMPO) macroinitiator.[122]

Conductive polymers

As nitroxide radicals feature in the group of organic molecules one of the highest electron transfer rates of 10^{-1} cm s^{-1} (e.g. ferrocene 10^{-2} cm s^{-1} or ascorbic acid 10^{-4} cm s^{-1}), they are a target of interest for intrinsic charge conductive polymer, featuring fast interfacial electron transfer with surfaces or intramolecularly.[55, 57, 80] The general mechanism of charge transport in ORPs is assumed to follow an electron-hopping mechanism between the radical pendant side groups as illustrated in Figure 4.
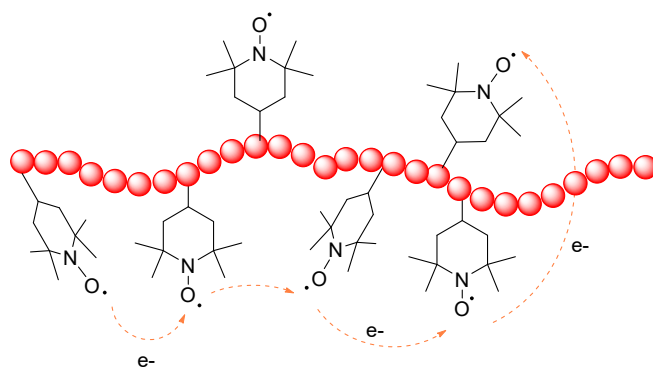
Figure 4: Electron hopping between pendant radical moieties.

However, for the most investigated organic radical polymer PTMA, different results concerning its intrinsic electric conductivity were reported. While first reports considered PTMA as an insulating material, other reports envisioned it as novel class of transparent conductive polymer with values comparable to strictly π-conjugated polymers such as poly(3-alkylthiophenes).[123] Further insights into the capability of TEMPO-based ORPs were given by Boudouris and Coworkers via reducing varying ratios of the TEMPO moieties to the corresponding hydroxylamine (N-OH) in a polynorbornene organic radical polymer. This study revealed a logarithmic dependency on the solid-state electric conductivity and the radical concentration, underlying the immense influence of high radical concentration as well as a short radical-radical distance on the respective charge conductivity.[124] To further elucidate this behavior, the group of Boudouris continued their work in a comprehensive study on the influence of the oxidation time of an amine PTMPM polymer precursor with *m*CPBA as oxidant on the electric charge conductivity. The authors observed that ,with increasing reaction time, the oxidation of the pendant piperidine to the TEMPO radical moiety results in complex follow up reactions.[125] The first one is a partial over-oxidation of the TEMPO radical to the corresponding oxoammonium ion, while further increased reaction time yielded partial hydroxylamine pendant side groups. The subsequent conductivity

20

measurements revealed a severe influence of the initial low radical densities and the complex follow up reaction on the observed solid-state electric conductivity with three appointed regimes (Figure 5). For these radical polymers, a maximum in electric conductivity is obtained for polymers containing high TEMPO radical concentration as well as partial oxoammonium cationic ($^+$N=O) pendant side groups. The authors contribute this dependency to an intramolecular doping effect (p-type) of the oxoammonium cations.
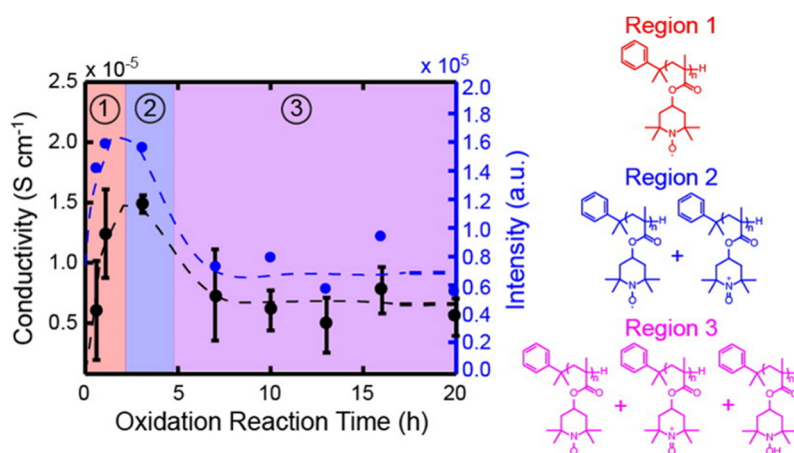
Figure 5: Solid-state electric conductivity of PTMA as a function of oxidation reaction time with three distinctive conductivity regimes. Adapted with permission from reference[125].

A breakthrough in the field of charge conductivity organic radical polymers was achieved by Boudouris and coworkers in 2018 applying a TEMPO functionalized polyether with a glass transition temperature (T_g) close to room temperature instead of rigid polymer backbones (polymethacrylates, polynorbornenes) with high T_g.[126] While for this ORP the initial solid-state electric conductivity was low (10^{-10} S cm^{-1}), an immense increase was observed after annealing the polymer at 80 °C. After this process, the electric conductivity above the T_g (20 °C) reached a drastic increase with values (2 S cm^{-1}) in the range of the most efficient conjugated PEDOT:PSS system (0.1-10 S cm^{-1}).[127] This phenomenon was contributed to the combination of discontinuous radical subnetworks through aggregation to form a macroscopic percolating radical network, which was also verified by DFT calculations (Figure 6).
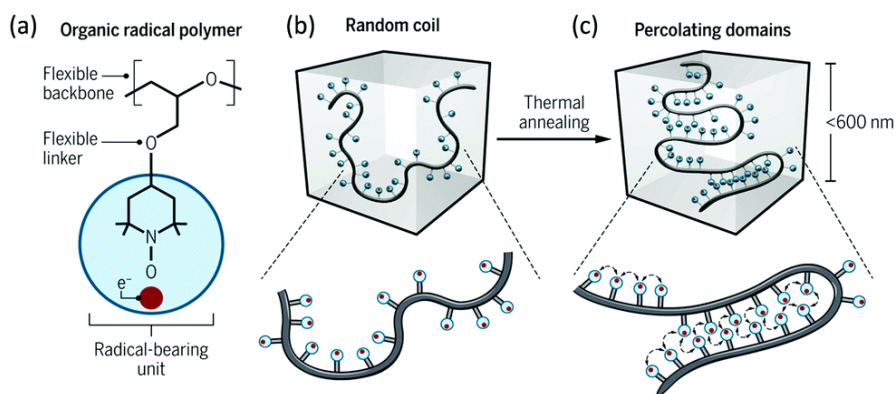
Figure 6: a) A low T_g TEMPO functionalized polyether, b) unannealed polyether in which radical groups are too far apart to transport electrons, and c) after annealing the pendent radicals are organized into percolation domains (about 600 nm) that facilitate electron transport. Reprinted with permission from reference[128].

Energy storage

The reversible redox couple of organic radicals in combination with their high redox potentials and extreme fast electron transfer make them a promising candidate for energy applications. The initial idea for this application was introduced by Nakhahara *et al*. in 2002 by employing PTMA as cathode active material in a metal-organic hybrid battery system.[129] This setup was later transferred to an organic radical battery (ORB) and already the initial study by Nakahara showed remarkable properties. 70% of the theoretical capacity was reached and constant values were obtained for nearly 500 charging/discharging cycles. At high charging/discharging rates of 10 C, 91% of the initial 1C capacity was reached. The C-rate in battery applications is defined as follows: The applied current relative to the current that is necessary to fully charge the battery within 1 hour (C-rate = $i_{applied}/i_{1h}$). While 1 C rates are often used in literature as reference charging rate for different battery types, 10 C rates with a charging/discharging time of 6 minutes is unachieved for commercial ion-intercalating battery systems. Furthermore, ORBs are capable to show immense charging/discharging rates of 10-400 C with only a minor loss of capacity.[51, 130] An additional battery key parameter is the coulombic efficiency (η_C in %), which resembles the ratio of discharging and charging capacity ($\eta_C = C_{discharge}/C_{charge}$) and thus depicts the reversibility of the overall charging process. Organic radical batteries commonly feature coulombic efficiencies higher than 99%, highlighting the highly reversible radical redox process.[130]

As the theoretical capacity depends - according to Faraday's law of electrolysis - reciprocal on the redox active molecular weight, the organic radical polymers capacity

is strongly influenced by the molecular weight of the repeating unit. This effect is depicted in Figure 7 for different TEMPO based ORP backbones.[55]
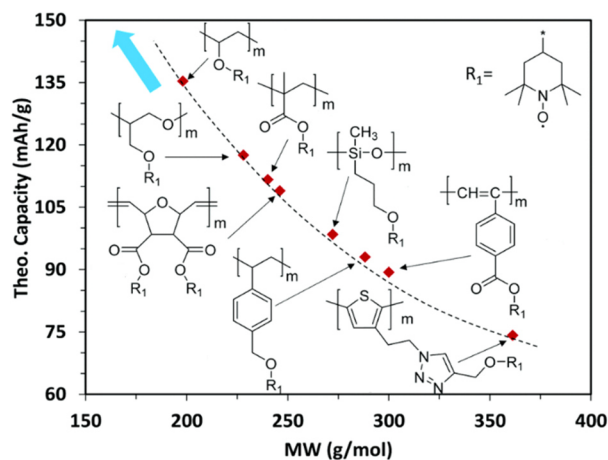

Figure 7: The theoretical capacity vs. molecular weight of the repeating units for various TEMPO based organic radical polymers. Reprinted with permission from reference[55].

Therefore, after the initial study of Nakahara *et al*., an immense variety of different ORP were used as active material in organic radical batteries varying from polyvinylether[82], polyether[80, 98], poly(meth)acrylate[78, 131], poly(oxo)norbornene[83, 132, 133], polysiloxane[115], polystyrene[98], polypyrrole[134], polyphosphazene[135] and polythiophene[113] to name only a few. Nevertheless, for all these different polymers, the initial setup retained some key components: Due to insulating or sluggish electric conductivity, a high surface electric conductive material (e.g. carbon) is added to ensure fast charge transport from the electrode surface to the redox active sites of the ORP. As this support tends to agglomerate and to suppress phase separation between the carbon support, the ORP, and the current collector, a binder like polyvinylidene difluoride (PVdF) or carboxymethyl cellulose (CMC) is added. These additives are until now added in rather high amounts (carbon between 40 to 80 wt%, binder 10 wt%) and thus drastically lower the overall battery capacity.[51] Furthermore, the ORBs capacities often fade with increasing charging/discharging cycling, which is attributed to a partial dissolution of the ORP in the battery's organic electrolyte or agglomeration of the active material. Different approaches were made to inhibit these phenomena, whereat an increase in the molecular weight of the ORP is a straightforward approach. Zhang and Coworkers studied this influence of different molecular weight PTMA (M_n = 14 - 131 kg mol^{-1}) on the ORB electrochemical properties, revealing an immense improved performance with increasing molecular weights.[131] Unfortunately, until now the polymerization techniques

(ionic, radical) applied for the synthesis of ORPs lack an effective method to generate defined high molecular weight polymers.

Further research was conducted to investigate the influence of the polymeric microstructure on the organic radical battery performance. For PTMA synthesized via SKA-GTP an increased oxidation potential for syndiotactic radical pendant side groups was observed and molecular dynamic simulation revealed an optimal charge conductivity with a radical-radical distance of 6-7 Å.[88, 136] Contrary to this, TEMPO functionalized polynorbornenes synthesized from the *endo/endo* monomer featuring shorter radical distance resulted in only 50% capacity compared to the one observed for the polynorbornene prepared from the *exo/endo* monomer.[83] However, a fundamental understanding of the polymeric microstructure in ORB applications was yet not achieved, due to the lack of a polymerization technique capable of synthesizing ORPs with controllable microstructures.

Nevertheless, other approaches were reported in literature to hinder capacity fading induced by dissolution or agglomeration of active material. An elegant multi-step polymerization approach was reported by Oyaizu and Nishide synthesizing a densely grafted radical polymer brush through a sequence of anionic polymerization with a DPE norbornene initiator followed by ROMP of the norbornene polymer end-group (Scheme 20).[137] After spin coating, the resulting ORP thin film was employed without carbon support additives due to an enhanced electric conductivity of the unsaturated polymer backbone and yielded 94% capacity at an extreme fast C rate of 120 C, corresponding to a charging/discharging time of 30 seconds.
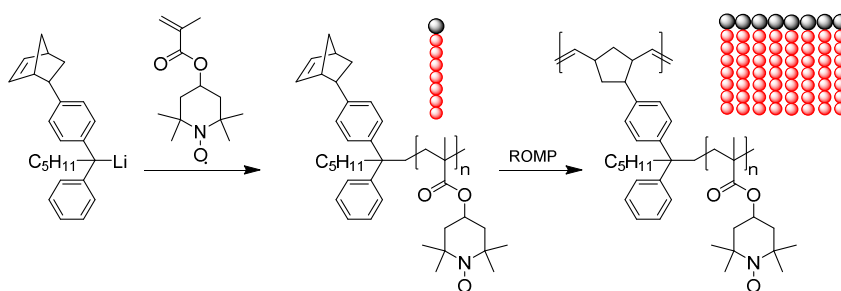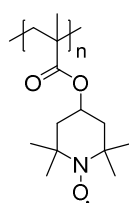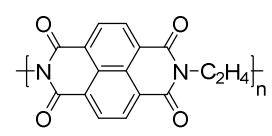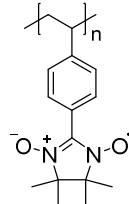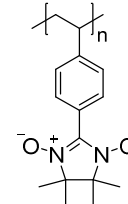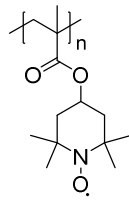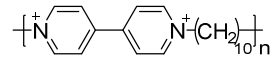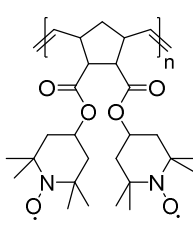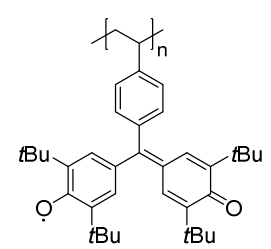

Scheme 20: Synthesis of comb like ORPs by ROMP with an unsaturated polynorbornene backbone.[137]

Other approaches utilized an immobilization of the ORP on the carbon support to impede the solubility of the redox active material. The post-polymerization approaches reported by Zhang and Coworkers - discussed earlier (Figure 3) - were intended to improve the performance of a PTMA-Py-*co*-graphene or a PTMA-*co*-CNT composite

electrode in an organic radical battery setup.[118, 119] Besides the improved C-rate capability and cycling stability of these composite electrodes, a severe drawback of side group functionalization is a loss of redox active centers and thus an overall lowered capacity. Therefore, further immobilization approaches were reported in literature via grafting from and grafting to surface techniques. While the first of these approaches relies on chemical modification of the carbon substrate, the second one includes the post-polymerization modification of the generated ORPs.[108, 109, 138]

As most of the ORBs reported in literature use the respective ORP as cathode active material and a redox active metal (e.g. Li, Zn, Na, Mg) as counter electrode/anode, this setup is often referred to as metal-organic radical battery. In the literature only few examples of fully organic radical battery exist, which replace the metallic anode with a suitable ORP. For this application, a suitable anode should feature a low redox potential (<0 V) to increase the cell voltage thus additionally enhancing the overall energy. However, as already discussed, only few suitable structures for organic radicals with low oxidation potential are reported in the literature. A notable contribution in this sector was reported by Nishide in 2009 by combination of poly(galvinoxylstyrene) and TEMPO-functionalized poly(norbornene) in a full organic radical battery.[105] This allowed for extreme fast C rates of 360 which correspond to a charging/discharging time of 10 seconds. Unfortunately, the overall capacity (32 mAhg^{-1}) was rather low, and the cell voltage reached only 0.66 V (Table 1). Beside these drawbacks, this setup utilized an aqueous-based electrolyte battery systems, unachievable for Lithium based battery systems.[139, 140] Via utilization of polystyrenic backbone functionalized with a bipolar nitronyl nitroxide, this radical polymer is applied as anode and cathode redox active material, resulting in a poleless battery. The subsequent battery cycling revealed a promising cell voltage of 1.3 V and high retention of the capacity up to a rate of 60 C, however, the overall capacity was relative low with 44 mAhg^{-1}, compared to metal hybrid systems.[106] Further improvements were achieved by the utilization of organic redox active anode polymeric materials, which feature only a radical species as charged redox state. Commonly used polymers bear quaternized pyridine[97, 141], polyimide[139] or anthraquinone [142] functionalities (Table 1). Especially polyimides as anode material in combination with a PTMA composite cathode resulted in a promising all-organic battery with a high capacity (136 mAhg^{-1}) and a cell voltage of 1.5 V.[139]

Table 1: Cell potentials and capacities for different all-organic polymer batteries with organic radical polymers as cathode and different organic redox active polymers as counter anode.[55-57]

Cathode	Anode	Cell voltage [V]	Capacity [mAhg^{-1}]
		1.5	136
		1.3	44
		1.25	110
		0.66	32

In a further energy storage technology, organic radical polymers emerged as a promising alternative to metal-based redox active material is the field of redox-flow batteries (RFBs).[53] As this setup is a very suitability candidate for grid-scale energy storage solutions, academic as well as industrial research focused on the development and implementation of this system. While the dissolution of active material in ORB caused severe performance drawbacks, for redox-flow batteries the full dissolution of active material is a basic premise. While small organic molecule based RFBs were already reported in the literature, a fundamental new design for RFB based on an organic radical polymers was introduced by Schubert *et al*. in 2015 (Figure 8).[143, 144] This system featured an aqueous sodium chloride electrolyte instead of extreme hazardous (conc. sulfuric acid for vanadium based RFB) and/or flammable electrolytes, thereby drastically improving the economical, safety, and environmental impact. Furthermore, the use of an ORP instead of small organic molecules as redox active material allowed

the utilization of cheap size-exclusion membranes instead of the costly high-performance membranes (Nafion® or ion-selective membranes) commonly applied for RFBs. By this combination of a cheap size-exclusion cell membrane with an aqueous based electrolyte, the economic cost of these systems are expected to be far lower than for metal-based or small organic molecule systems.[53] A combination of TEMPO and viologen (4,4'-bipyridine) was applied as redox couple resulting in a cell voltage of 1.1 V, a good match for the electrochemical window of water (1.7 V). For the TEMPO pendant radical side group, methacrylate was chosen (PTMA) as polymeric backbone, while for viologen styrene was selected. To improve the solubility in the aqueous electrolyte, a quaternary ammonium functionalized MA/styrene was incorporated by statistical copolymerization. The cell reached 75% of the theoretical capacity and after 10,000 cycles only 20% capacity fading was observed. Transfer of active material between the cell compartments - often reported in RFBs utilizing small molecules - was not observed for the polymer based redox-flow battery, due to the superior selectivity of the size-exclusion membrane.
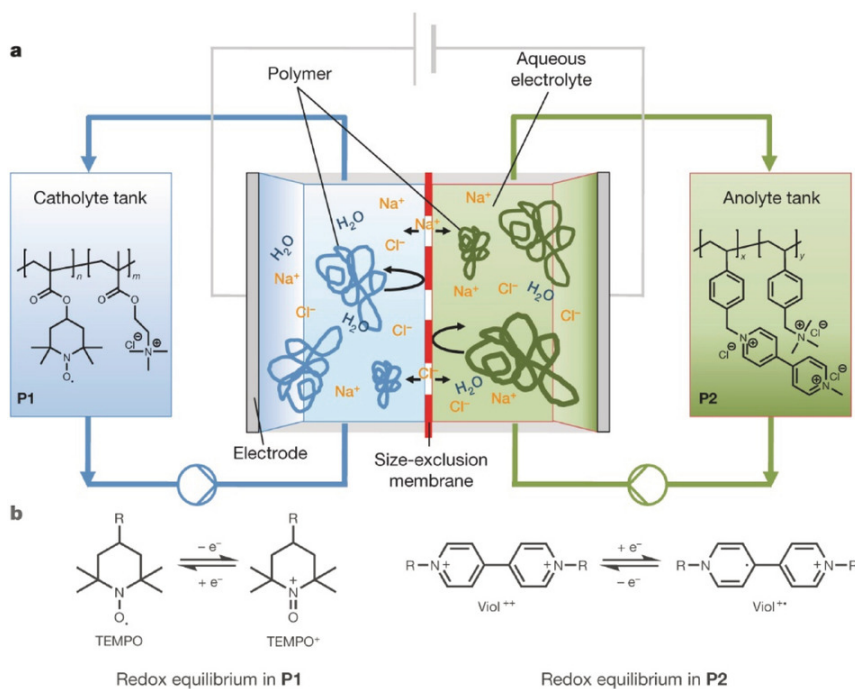

Figure 8: An aqueous polymer based redox-flow battery with TEMPO-copolymer catholyte and viologen-copolymer anolyte. Reprinted with permission from reference [144].

Further reports applied this PTMA copolymer in a PTMA/zinc hybrid-flow battery, a combination of a conventional ORB and RFB, where the organic radical polymer is dissolved in the electrolyte and the counter electrode is apparent in its solid-state form. The low potential of zinc allowed an optimal cell voltage of 1.69 V for aqueous based

electrolytes and a cycling stability test over 1,000 cycles revealed a relatively stable capacity retention of 79%.[145] However, the C rate was relatively low due to the low ionic conductivity of the applied electrolyte.

From an environmental and economic point of view, aqueous electrolyte based RFB systems are the only competitive ones to classical grid energy systems, therefore research focused on enhancing water solubility of the redox active ORPs. [53, 146] To improve this solubility in the aqueous electrolyte as well as to further enhance the ionic conductivity, a zwitterionic PTMA sulfopropylammonium copolymer was developed.[147] Recently, additionally micellar PTMA-*b*-PS structures were investigated as active material in a hybrid zinc system revealing excellent coulombic efficiencies and a constant capacity over 1,000 cycles. Furthermore, the use of the micellar system reduced the viscosity of the electrolyte severely, thus lowering the RFBs steady state energy consumption.[148]

Catalyst for organic reactions

Catalytic oxidations reactions mediated by nitroxide radical moieties are widely applied for the conversion of alcohols to carbonyl functions. Nevertheless, the separation of small molecule nitroxide radicals is challenging and therefore, these catalysts are not recycled. The immobilization of an organic radical polymer or an ORP attached on a surface is a feasible approach, enabling straightforward separation and recyclization approach. This resulted in commercial available systems based on a crosslinked polystyrene matrix, but in addition to this, silicone nanoparticles functionalized via a graft from approach with propargyl-TEMPO were reported in literature (Figure 9).[149] Applying these systems allows for easy separation by centrifugation and the catalysts can be reused multiple times without a loss inactivity.
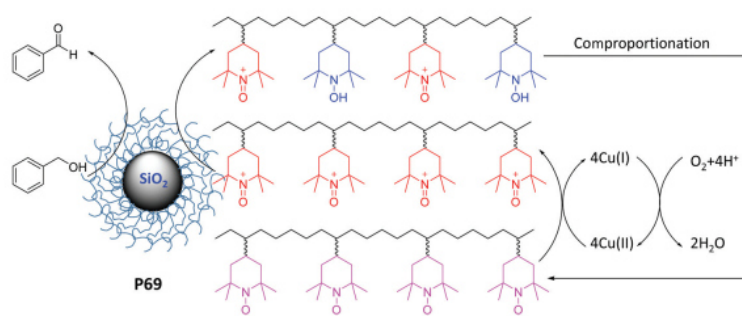

Figure 9: Catalytic oxidation of benzyl alcohol with a nitroxide radical polymer coated silica nanoparticle. Reprinted with permission from reference[55].

28

Biomedical applications

The ability of stable radicals to anticipate in reversible redox reactions in addition to their capability to scavenge reactive radical species results in their antioxidizing behavior. This is especially a feature of interest for biomedical and pharmaceutical applications since an excess of radicals generated by reactive oxygen species (ROS) is linked to several injuries and diseases like inflammation, asthma, stroke, pulmonary hypertension, cancer or aging.[150] As small molecule stable radicals have low *in vivo* lifetimes and show an absence of stimuli responsiveness, ORPs with their tunable functionalities are an emerging alternative. An interesting contribution to this topic was reported by the Nagasaki group utilizing a block copolymer of a pH-sensitive styrene derivative functionalized with amino-TEMPO in *para*-position and polyethylene oxide to enhance water solubility. To study the influence of the pH-switchable amino moiety, a pH-insensitive ether linked copolymer was additionally generated (Figure 10). Both block copolymers self-assembled in water to core-shell-type nanoparticles and the pH-sensitive nanoparticle collapsed in acidic environments (pH < 6), resulting in enhanced therapeutic effects.[151] While the intact nanoparticles showed strong absorption in the electron paramagnetic resonance (EPR) spectroscopy, after acid induced collapsing of the nanoparticles the radical moiety is protonated and the EPR signal vanishes. The nanoparticles are therefore considered a pH-sensitive *in vivo* MRI contrast agent or nanoprobe.[152]
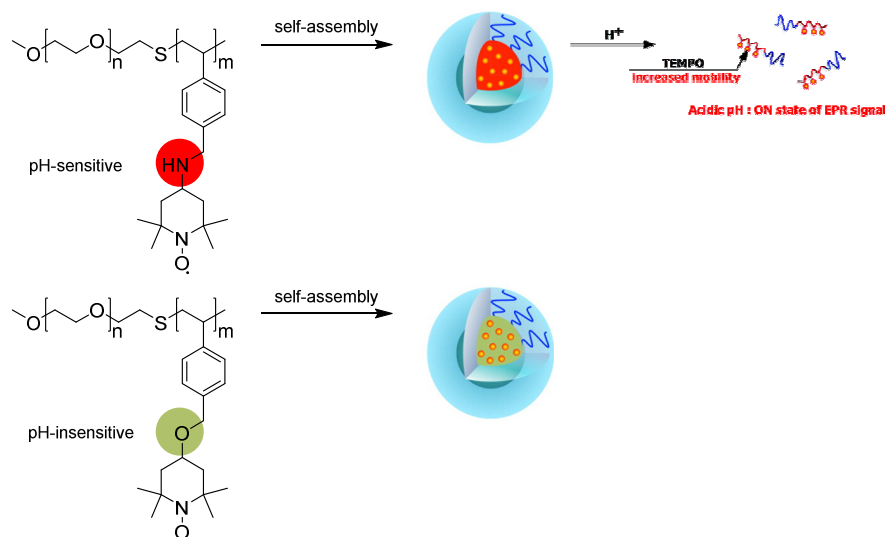

Figure 10: Illustration of pH sensitive and pH-insensitive redox nanoparticles. Adapted from reference[151].

2.3 Phosphorus-containing Polymers

In contrast to industrial application in which phosphorus-containing polymers are only of interest in high-tech applications, life would not be imaginable without it. The two most important macromolecules in cells - the deoxyribonucleic acid (DNA), carrying the genetic instructions, and ribonucleic acid (RNA), conveying this information for the synthesis of proteins - are based on a poly(phosphate) backbone. Since synthetic polymers based on poly(phosphates) are prone to hydrolysis, thus degrading the polymer, two different approaches for implementing more stable phosphorus functionalities to polymers are reported in literature. The first one applies a phosphorus function with a higher chemical stability in the backbone like poly(phosphonate), poly(phosphazenes) or poly(phosphoamidates), while the second one features polymers with a stabile C-C backbone and a phosphorus containing pendant side group.[153-157]

Especially poly(phosphazenes) were intensively investigated due to their straightforward synthesis via ring-opening polymerization (ROP) and their facile post-polymerization functionalization by nucleophilic substitution (Scheme 21 a). This enabled a plethora of varying applications like hydrophilic, hydrophobic or biodegradable elastomers, high refractive index materials, non-linear optic materials, liquid-crystalline thermoplastics, drug-carrier, bone-implant, ion-conducting membrane in fuel cells and batteries and as redox active material in ORPs.[72, 158] The only drawback hindering a greater commercial success of this polymer type is the costly synthesis of the used monomers and the tendency of the prepolymer $(NPCl_2)_n$ to hydrolyze and to cross-link prior to functionalization.[154, 157, 158]

a)

b)

x = 1 or 2
R = OR, R, NHR, NR$_2$

c)

R = OR, R

d)

x, y = 1-9
R = OH, OR, R, NHR
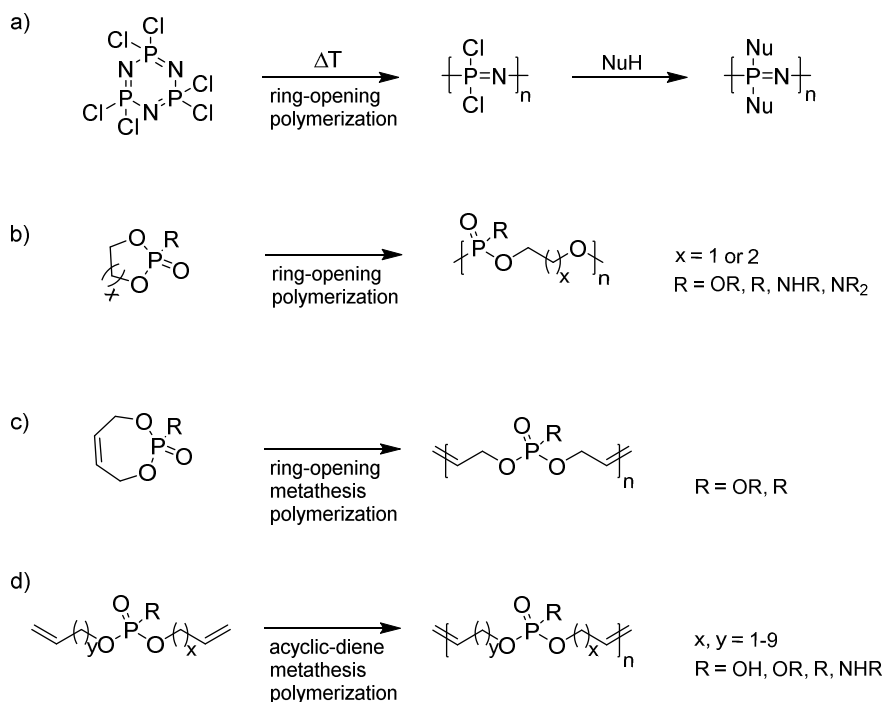
Scheme 21: Different polymers containing phosphor in their backbone and the corresponding polymer synthesis. a) Poly(phosphazenes) and b) poly(phosphoesters) synthesized via ROP, c) ROMP of different cyclodiene organophosphorus compounds and d) ADMET of different dialkylidene organophosphorus compounds.

Due to their biocompatibility and structural analogy to naturally occurring biopolymers, poly(phosphonate)s (PPP) are a target of interest, especially in the biomedical sector. Additionally, these polymers are susceptible towards metabolization via hydrolytic or enzymatic metabolism.[159] In this context, Wurm *et al*. studied the influence of varying PPP alkyl side chain modifications, rendering the physiochemical properties in terms of hydrolytic stability and metabolic degradation.[160] Since the often applied ROP synthesis for PPPs is only feasible for monomers with certain thermodynamic ring strains (5 and 6-mebered cycles), the repetition unit of polymers synthesized via this technique is only slightly adjustable (Scheme 21 b). A sophisticated method independent of the monomers thermodynamic ring-strain is catalytic metathesis polymerization.[153] The group of Wurm *et al*. used ring-opening (ROMP) or acyclic-diene metathesis polymerization (ADMET) of suitable alkene containing monomers to further adjust PPPs physiochemical properties (Scheme 21 c and d).[155, 161] By this approach, not only the hydrophobicity, but also the polymers' morphologies were tailored. With these tools at hand, different applications of PPPs emerged in literature such as polymer-protein conjugates, biodegradable gene carrier, antitumor drug, gene expression enhancer, and many more.[153, 162]

The second approach for phosphorus containing polymers is the relocation of the phosphorus function to the pendant side group. A plethora of different polymer structures can be applied and therefore only the most important ones are discussed in detail. The simplest example of a polymer with a C-C backbone and a phosphorus functionality is polyvinylphosphonic acid (PVPA), which is readily obtained by free radical polymerization of vinylphosphonic acid (VPA). A detailed investigation of the underlying mechanism was published by Bingöl et al., proposing a mechanism via cyclopolymerization of vinylphosphonic anhydride,[163] at which the anhydride of phosphonic acid is formed from the VPA in a temperature dependent equilibrium.[164] While polyvinylphosphonic acid has promising properties for applications as polymer electrolyte membranes for fuel cells, hydrogels for drug delivery and in ion exchange membranes,[165-168] its major drawback impeding further research is the lack of a polymerization techniques with high activity, while maintaining control of the macromolecular parameters and the possibility to synthesize defined (block) copolymers or even more sophisticated tailor-made polymeric architectures. To overcome these disadvantages, a set of phosphorus functionalized monomers including (meth)acrylates[169-172], (meth)acrylamide[173, 174], styrene[175, 176], vinyl(ether)[177-179] and dialkylvinyl phosphonate monomers[163, 167, 180-182] (Scheme 22) were synthesized and polymerized by techniques ranging from free radical,[169, 173, 182, 183] controlled radical[184-189] or ionic[141, 183, 190] to photopolymerization[191-193] approaches.

X = H, R

$P = POR_2, PO(OH)_2, PO(OR)_2, PO(OTMS)_2$
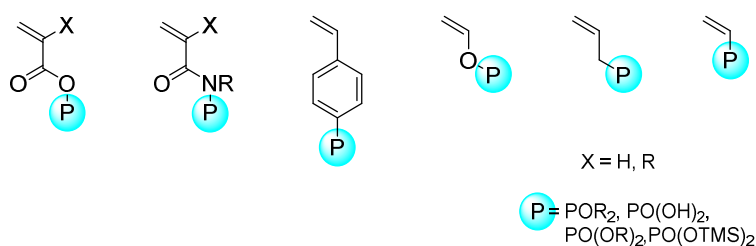
Scheme 22: Selection of common phosphorus functionalized vinyl monomers.

This led to a library of functional polymers for various potential applications, in which the most important ones are located in fields of biochemistry and medicine, metal-complexation and surface coatings, wastewater-treatment and purification, flame retardancy, and membranes in fuel cells and batteries.[194] However surprisingly, the monomer and corresponding polymer with the closest phosphorus distance to the polymer's C-C backbone, the class of dialkyl vinylphosphonates (DAVP), were until 2010 only covered in very few reports.[163, 167, 180-182]

2.4 Polyvinylphosphonates

Vinylphosphonate monomers are known in literature since 1940. The most prominent synthesis route to generate this monomer class is the *Michaelis-Arbusov* rearrangement starting from the corresponding trialkyl phosphite, followed by an $E1_{cb}$ elimination to the desired dialkyl vinylphosphonate (Scheme 21 a). Vinyl-substituted phosphonates with a variety of different and mixed phosphonic ester functionality can additionally be synthesized via palladium-catalyzed cross-coupling reactions from dialkyl phosphites (Scheme 21 b).[195, 196] For more complex synthesis of diaryl or steric demanding dialkyl vinylphosphonates, Rieger *et al*. introduced an alternative metal free approach.[197, 198] Herein, (2-chloroethyl)phosphonic dichloride was synthesized via a *Kabachnik* rearrangement of commercial available tris(2-chloroethyl)phosphite, followed by chlorination with thionyl chloride. The thus generated (2-chloroethyl)phosphonic dichloride can be esterified with various alcohols and the subsequent base induced elimination yields the corresponding DAVP (Scheme 23 c).
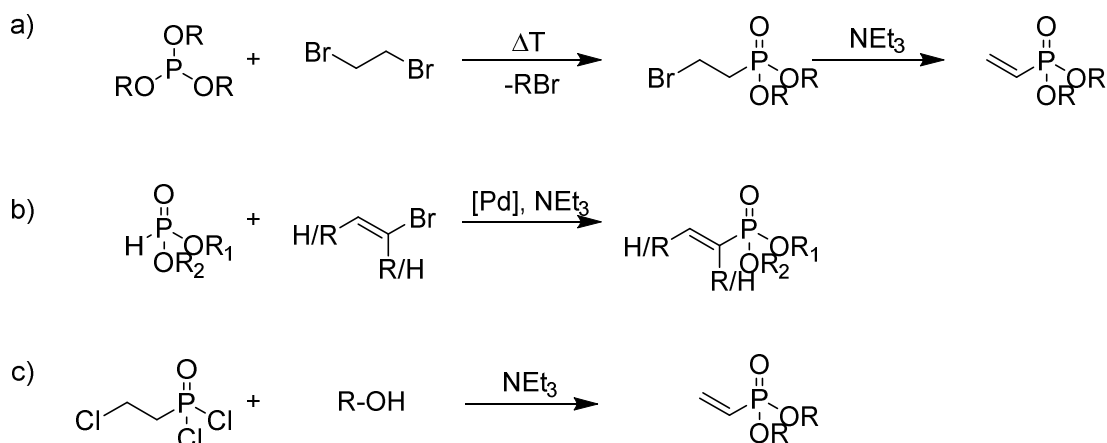

Scheme 23: Synthesis of DAVP a) via *Michaelis-Arbusov* reaction and subsequent elimination, b) palladium catalyzed cross coupling and c) *Kabachnik* rearrangement to yield tris(2-chloroethyl)phosphite followed by nucleophilic substitution and subsequent elimination.

Beside polymerization, DAVPs are already used for the introduction of phosphorus functions in (macro)molecules via *Diels-Alder* cyclization, thiol-ene click reaction, 1,4-*Michael*-addition, and cross coupling reactions.[199-203]

While DAVPs were used as suitable substrate for the incorporation of phosphorus functions for the above-mentioned organic reactions, only few reports cover the polymerization of DAVPs. This can be attributed to the poor performance of this monomer class with classical polymerization techniques like free radical polymerization. While first experiments via this approach were made shortly after the successful

synthesis of diethyl vinylphosphonate (DEVP) and diisopropyl vinylphosphonate (DIVP), the free radical polymerization resulted only in the formation of oligomeric products.[92, 204] One of the attributed reasons for this sluggish performance is the low propagation rate, which is a result of the pronounced stability of the formed radical species. A second and more severe reason is the frequent appearance of chain transfer reactions either to the monomer or to the growing polymer chain, as determined by Bingöl *et al*. via analysis of oligomeric DEVP and DIVP by electrospray ionization–mass spectrometry (ESI-MS).[163] Besides propagation, the generated phosphonate radicals can be relocated via an intramolecular hydrogen transfer of the phosphonate ester moiety, resulting in a PO-alkyl radical species. By propagation of the so formed radical with a new monomer unit a thermolabile P–O–C bond is formed in the backbone, which is prone to undergo chain fragmentation (Scheme 24).
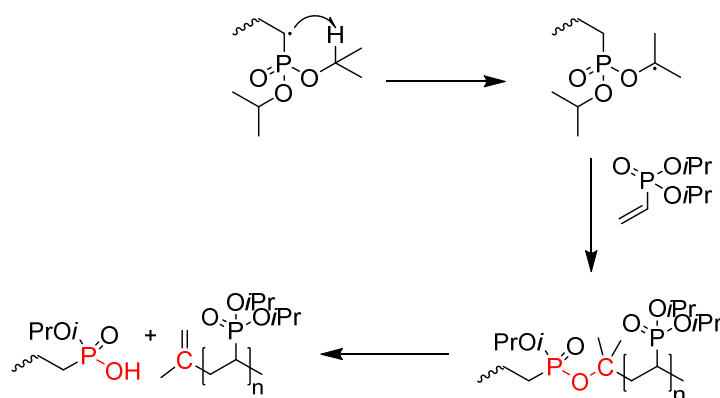
Scheme 24: Intramolecular chain scission of oligomeric DIVP during radical polymerization.[163]

To overcome these drawbacks, research focused on non-radical polymerization of DAVPs. Anionic polymerization of DAVPs exhibits in general higher activity, but similar to radical polymerization approaches anionic pathways suffered from undesired side reactions. The main reason is based on the α-acidic proton of the vinylic group and the resulting termination reactions that occur with the initiating or propagating species (Scheme 25 a). Anionic initiators with high nucleophilicity can attack at the electrophile phosphorus atom, thus subsequently eliminating an alcoholate (Scheme 25 b).[205, 206] Furthermore, the polymerization activity is further decreased due to resonance stabilization of the anionic chain end by the phosphonate moiety, and this again results in the generation of thermolabile P-O-C bonds (Scheme 25 c).
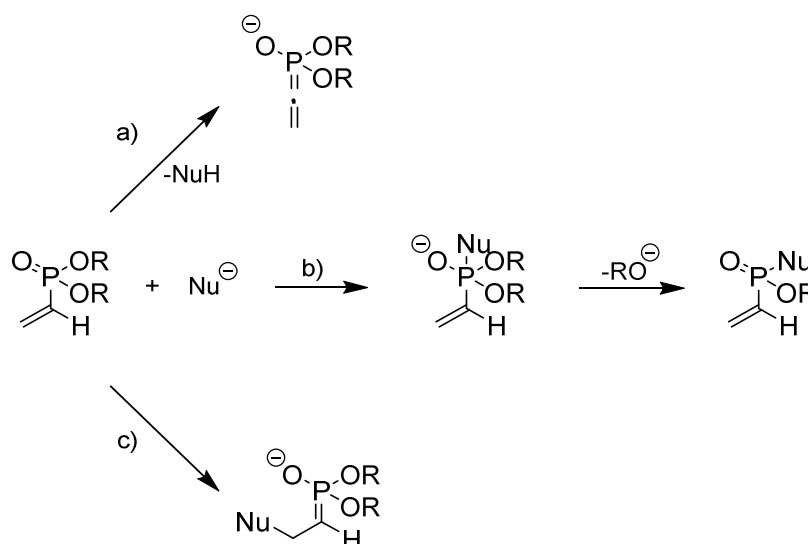
Scheme 25: Possible reaction pathways of the anionic polymerization of DAVPs: a) Abstraction of the α-acidic proton, b) nucleophilic attack at the electrophilic phosphorus and subsequent elimination of an alcoholate and c) nucleophilic attack at the vinyl moiety.[205, 206]

To reduce the anionic nucleophilicity, anionic initiators such as alkyllithiums species are reacted with 1,1-diphenylethylene (DPE) thus generating a sterically shielded tertiary anion. This approach was applied by Jannasch and coworkers for the grafting of diethylvinyl phosphonate (DEVP) onto polystyrene with a PDEVP content up to 57 wt% and side chain lengths between 500 and 5800 g mol^{-1}.[207] The obtained grafted polymers were saponified and afterwards applied as proton conductive fuel cell membrane, revealing an increased proton conductivity for higher phosphoric acid contents (wt%). While a similar approach for the block copolymerization of DIVP and styrene resulted in block compositions up to 7:3 (DIVP:styrene), the homopolymerization of DIVP with DPE and *n*-butyllithium suffered from low initiator efficiencies (10%) and broad molecular weight distributions (Đ = 2.1-3.9).[208]

Therefore, the group of Rieger utilized the electronic and structural similarity between *Michael*-type acceptor DAVP and methacrylates (Scheme 26). For *Michael*-type acceptor monomers like methyl methacrylate (MMA), a plethora of different polymerization techniques is described in literature, whereupon rare earth metal-mediated group transfer polymerization (REM-GTP) is one of the most versatile techniques. Due to the combination of both living and precision coordinative polymerization, strictly linear polymers with very narrow polydispersities (<1.1) are obtained. Furthermore, this enables the synthesis of highly defined block copolymers as well as the introduction of functional polymer end-groups via the GTP-mechanism.[209] The coordination of the active polymer chain-end to the catalyst center suppresses side

reactions and tuning of the metal center alters activity as well changes in the ligand sphere allows stereoregular polymerization. Yasuda *et al.* revealed in a detailed study the underlying mechanism as a repeated 1,4 *Michael* addition.[210]

Scheme 26: Structural and electronic similarity between dialkyl vinylphosphonates and (methyl)acrylates.

Rieger *et al.* transferred this to DAVPs, which are known for their capability to react in *Michael* additions. In an initial study, simple rare-earth metal alkyl precursors produced oligomers of dimethyl vinylphosphonate (DMVP) and DIVP (Scheme 27).[211] The activity and yields for the polymerization with lanthanide tri(bisdimethylsilylamide) complexes (Ln(bdsa)$_3$(thf)$_2$) (Ln = La, Nd, Sm, Y) showed an increase in activity with smaller ionic radius of the metal center.[206] Mechanistic insights via NMR spectroscopy revealed the coordination of the oxygen moiety instead of the vinyl, thus indicating a mechanism proceeding via group transfer polymerization (GTP). However, rather broad polydispersities (Đ > 3) were observed, indicating either a non-uniform, slow initiation, or an initiation by more than one of the σ-donor ligands.


Ln = La, Nd, Sm, Y
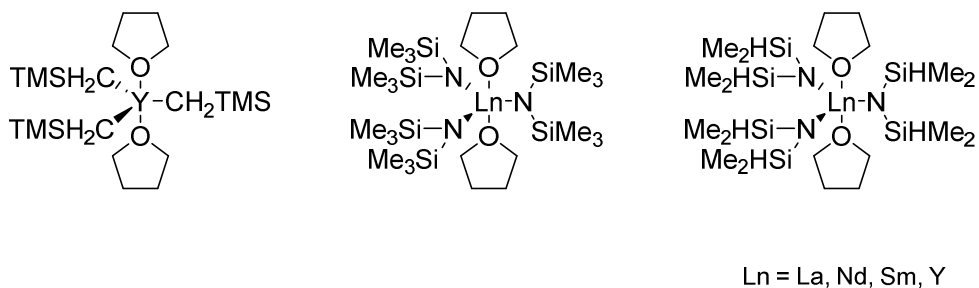
Scheme 27: Rare-earth metal alkyl complexes for the oligomerization of DMVP and DIVP.

To address these issues, late rare-earth metal metallocene (Cp$_2$YbMe and Cp$_2$YbCl) were employed as polymerization catalysts. Cyclopentadienyl (Cp) is a versatile, strongly coordination ligand for a series of different metal complexes (reducing multiple initiations per catalyst), while methyl (Me) is a very strong nucleophile (faster initiation) and chloride (Cl) a rather weak nucleophile (less side reactions).[212] With implementing these alterations, high molecular weight polydiethyl vinylphosphonate (PDEVP) with molecular weights of 1,000 kg mol^{-1} were reported for the first time. While both the methyl and chloro complexes were active in polymerization resulting in polymers with small molecular weight distributions (Đ <1.2), the initiator efficiencies (I) differed heavily:

For the Cp_2YbMe complex the initiator efficiency was around 45%, whereas for the corresponding chloro complex the value was one order of magnitude lower (I = 4%).

In addition to the ytterbium complexes, *bis*(cyclopentadienyl)lanthanide (Ln) chloride complexes in the series of Lu-Er and Y proved to be active in DAVP polymerization.[213] Initial end-group analysis revealed the lack of a defined end-group for the methyl complexes, thus an initiation process via deprotonation was assumed. Surprisingly, Cp end-groups were received for chloro complexes. To gain a deeper understanding in the unexpected initiation of the REM-GTP with chloro complexes, NMR spectroscopic and single crystals X-ray diffraction (SCXRD) studies were conducted to reveal the phosphonate coordination to the REM complexes.[214] Diethyl ethylphosphonate (DEEP) was used due to its similar steric demand in comparison to DEVP, but due to the lack of a vinyl group, it excludes both initiation and subsequent polymerization. The NMR experiments with the chloro complex revealed a monomer (i.e., donor)-induced ligand exchange reaction forming $CpLnCl_2(DEEP)$ and $Cp_3Ln(DEEP)$ in equilibrium with the adduct $Cp_2LnCl(DEEP)$ (Scheme 28). This ligand exchange was also observed for yttrium-complexes in the SCXRD, forming a $Cp_3Y(DEEP)$ complex. Furthermore, single crystals obtained by reacting DEVP with Cp_2LnCl (Ln = Ho, Yb) showed exclusively the coordination via the oxygen and not the vinyl group, a key prerequisite for the ability to polymerize a monomer by a repeated conjugate addition polymerization, i.e., GTP.[206, 209, 212]
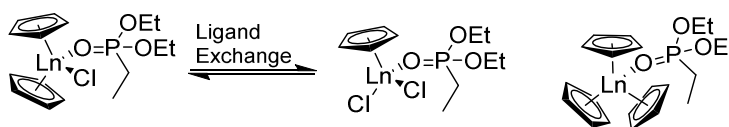
Scheme 28: Ligand exchange of Cp_2LnCl induced by addition of DEEP.[206, 214]

To further understand the ligand's role on the initiation mechanism, a detailed end-group analysis was performed with a series of Cp_2LnX (Ln = Y or Lu, X = Me, Cl, CH_2TMS, Cp, bdsa, OAr, O*i*Pr, S*t*Bu) complexes.[214] This study revealed three different initiation pathways for REM-GTP of vinylphosphonates: Initiation via abstraction of the acidic α-CH of the vinyl moiety is favored for highly nucleophilic ligands like CH_2TMS and Me (Scheme 29 a). For ligands with low nucleophilicity like chloro and alkoxides, a monomer (i.e., donor)-induced ligand-exchange reaction forming Cp_3Ln in equilibrium takes place, which serves as the active initiating species (Scheme 29 b). Only for some

ligands like Cp or thiolates a nucleophilic transfer of the ligand to the coordinated monomer is observed (Scheme 29 c).[214]
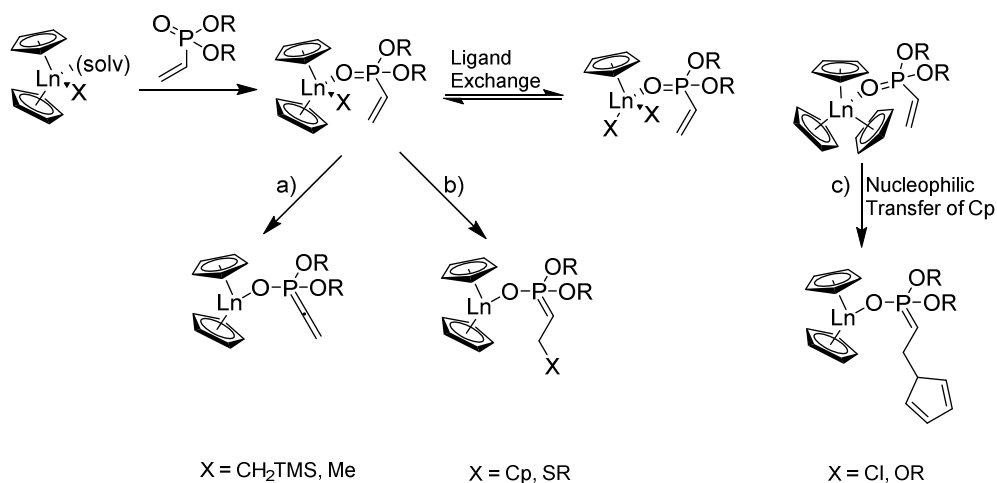
Scheme 29: Initiation of vinylphosphonates using rare earth metallocenes (Cp$_2$LnX): a) via deprotonation of the acidic α-CH, b) nucleophilic transfer of X, or c) a monomer-induced ligand-exchange reaction forming Cp$_3$Ln(DAVP).[214]

In addition, these investigations on the initiation mechanism revealed the mediation of vinylphosphonate polymerization by the Cp$_2$Ln as catalytic active moiety: To understand the influence of the central REM, a series of trivalent Cp$_3$Ln complexes (Ln = Gd to Lu) were synthesized and studied on the subsequent polymerization of DMVP, DEVP and DIVP. Contrary to results for other *Michael* type systems like MMA (activity: Sm > Y > Yb > Lu), the polymerization activity of DAVPs increases with decreasing ionic radius of the REM center (Lu > Gd).[215] Additionally, the steric demand of the vinylphosphonate has an impact on polymerization activity. While the most active complex Cp$_3$Lu showed for DEVP polymerization a normalized turnover frequency of 265,000 h^{-1}, this value decreased by a factor of 14 to 19,400 h^{-1} for the sterically more demanding DIVP.[216] A copolymerization study of different DAVPs (DMVP, DEVP and DIVP) revealed that the rate of vinylphosphonate GTP in statistical copolymerizations is mainly determined by the steric demand of the growing chain end, not by the coordinating monomer.[216] Kinetic investigations for the calculation of activation enthalpy *ΔH* and entropy *ΔS* uncovered that the enthalpy was not affected by the metal ionic radius in DEVP and DIVP polymerizations. In fact, only the entropy term (*TΔS)* affects the activation barrier *ΔG* and this term was shown to decrease with the metal ionic radius, consistent with the experimental activity (Lu > Gd). Taking all these experimental data into account, Rieger *et al*. were able to elucidate the mechanism of DAVP polymerization by REM-GTP.[214] The propagation follows a Yasuda-type monometallic

38

mechanism with a S_N2-type associative displacement of the polymer phosphonate ester by a monomer with a penta-coordinated intermediate. The monomer coordination, i.e., the first transition state, is the rate-determining step of the polymerization. The shorter metalorganic bonds for smaller REM centers lead to a higher steric crowding in the eight membered metallacycle, thus destabilizing the propagation ground state and therefore resulting in its acceleration. Larger pendant side groups of the coordinating polymer chain lead to an increase in rotational and vibrational restrictions in the rate-determining step and therefore to a higher activation barrier.[214]
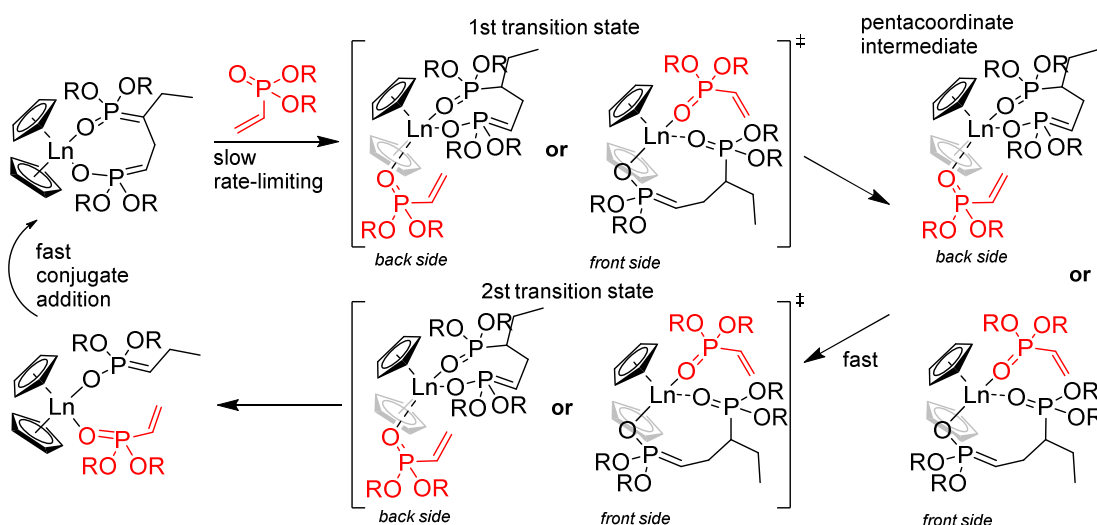
Scheme 30: Reaction mechanism of REM-GTP of DAVPs with the rate-limiting step via an S_N2 type associative displacement of the polymer phosphonate ester by a DAVP monomer, presumably via a pentacoordinated intermediate.[214]

For the elucidation of the REM-GTP mechanism, a set of complexes varying in the central REM (Y and Gd-Lu) and initiating moiety were synthesized and tested for their polymerization performance, regarding activity and initiator efficiency. While the Cp_2LnX moiety was demonstrated to be highly active in DAVP polymerization, only for thiolates and cyclopentadienyl as initiating moiety a chain-end functionalization could be obtained.[205, 206, 214, 215] However, these functional end-groups exhibit severe drawbacks like end-group elimination and limited post-polymerization functionalization.

As trivalent lanthanides and d^0-transition metals do only possess the ability for oxidative addition-and reductive elimination-reactions under harsh conditions, σ-bond or salt metathesis are exclusive synthetic pathways to introduce new initiators to these types of complexes. Unfortunately, salt metathesis reactions for REM complexes tend to form varying amounts of ate complexes, resulting in unpredicted performances of different

catalyst batches.[217, 218] Therefore, σ-bond metathesis for lanthanides emerged as suitable, side-product free catalyst functionalization for REM complexes.[219] The [2σ+2σ] cycloaddition follows a concerted four-membered transition state, leading to hydrogenolysis or alkanolysis depending on the activated substrate (Scheme 31).

$$[M]-CR_3 \ + \ H-CR'_3 \ \longrightarrow \ \left[\begin{array}{c} [M]\text{---}CR_3 \\ \vdots \quad \vdots \\ H\text{---}CR'_3 \end{array} \right]^{\ddagger} \ \longrightarrow \ [M]-CR'_3 \ + \ H-CR_3$$
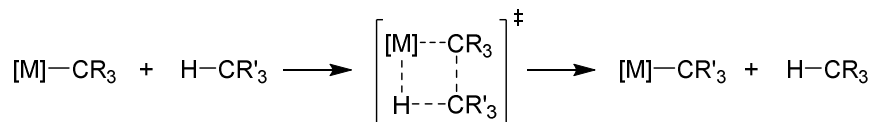
Scheme 31: C-H bond activation by d⁰ transition-metal complexes and trivalent lanthanides through σ-bond metathesis.

The first example for this reaction was introduced by Watson *et al.* in 1983 with the C-H bond activation of benzene, pyridine, and phosphorylidene with the ^{13}C-labeled Cp*$_2$Ln^{13}CH$_3$ (Ln = Lu and Y) complexes.[220] These were the first examples of the activation of a sp³-hybridized C-H bond which is known to be unfavorable to undergo σ-bond metathesis. Additionally, an increase in C-H bond reaction rates with increasing REM centers (Y > Lu) was observed.

The group of Teuben *et al.* investigated different metallocene and non-metallocene complexes towards C-H bond activation of different substrates, including ethylene, propylene, benzene and toluene, but also towards heteroaromatics like pyridine or alkyl substituted pyridine derivatives.[221] For α-picolyl derivates like 2-picoline and ethyl-pyridine a highly selective C-H bond activation occurred at the sp³-alkyl group via a η³-(*C,C,N*)-*aza*-allylic motif as determined by SCXRD (Scheme 32).[222, 223]
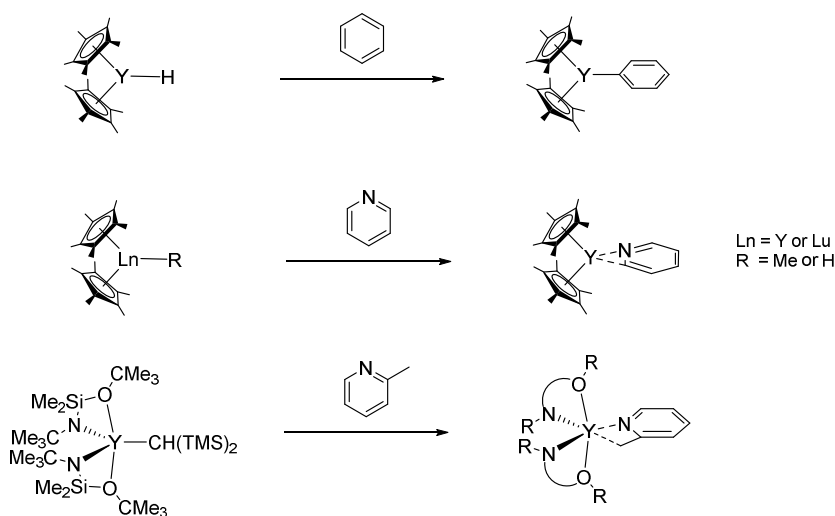

Scheme 32: C-H bond activation of benzene and pyridine by (C$_5$Me$_5$)$_2$LnX (Ln= Y, Lu; X = H or Me) and synthesis of bis(alkoxysilylamido)yttrium-pyridyl-complexes by σ-bond metathesis.[221-223]

This C-H bond activation of yttrium complexes was transferred by Mashima and coworkers for the polymerization of the *Michael*-type system 2-vinylpyridine (2VP), thus introducing a heteroaromatic polymer end-group.[224, 225] Therefore, different catalysts were prepared by in situ σ-bond metathesis of yttrium-en-diamido complexes with a variety of alkynes and α-picolyl derivates such as 1-trimethylsilyl-1-propyne, 2,4,6-trimethylpyridine (*sym*-collidine) or 2,3,5,6-tetramethylpyrazine (TMPy) and the capability of these initiating moieties studied in the subsequent polymerization of 2VP (Scheme 33).
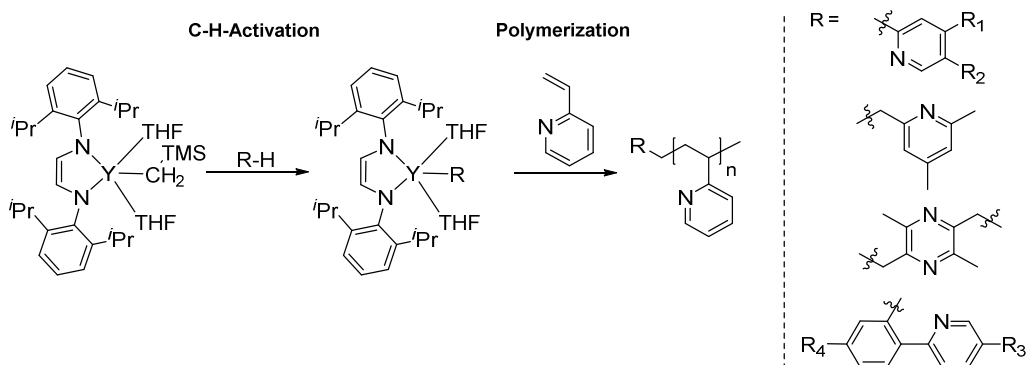
Scheme 33: Polymerization of 2VP with C-H bond activated pyridyl-yttrium-en-diamido complexes.[224, 225]

Rieger and coworkers adapted this technique for the introduction of pyridine initiators for the REM-GTP of DAVPs.[226] Consistent to other REM systems, the cyclopentadienyl systems Cp_2LnCH_2TMS (Ln = Y or Lu) were susceptible towards selective C-H bond activation of *sym*-collidine. While the reaction of the yttrium complexes with one equivalent pyridine showed quantitative yields after short reactions times at room temperature, for the lutetium complexes, prolonged reaction times and elevated temperatures were required for full conversion of the substrate. SCXRD analysis revealed bonding of the pyridine via a sp^3-alkyl group via a η^3-(*C,C,N*)-*aza*-allylic motif, thus resulting in resonance structures of a carbanion or an enamine (Scheme 34).[206, 226]
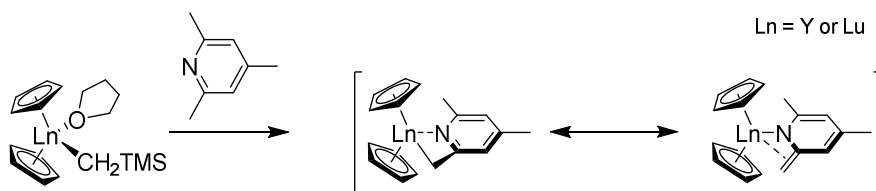
Scheme 34: C-H bond activation of *sym*-collidine with $Cp_2Ln(CH_2TMS)(thf)$ (Ln = Y or Lu) and mesomeric equilibrium of the activated catalyst via the carbanion and the enamide.[206, 226]

Subsequent polymerization studies with these Cp$_2$Ln(*sym*-collidine) (Ln = Y or Lu) catalysts showed high activity in DEVP polymerization (TOF* = 300,000 h^{-1}), combined with high initiator efficiencies (73%), narrow molecular weight distributions (Đ < 1.02) and a living character of the polymerization. End-group analysis via ESI-MS measurements revealed the attachment of (4,6-dimethylpyridin-2-yl)methyl, indicating a nucleophilic transfer of the *sym*-collidine initiator to the first monomer during initiation. This stable C-C bond prevents unwanted side reactions during polymerization and allows for further chain-end functionalization. The authors proposed a mechanism via nucleophilic transfer by a six-membered (6e$^-$ process) or eight-membered (8e$^-$ process) ring (Scheme 35).[206, 226]
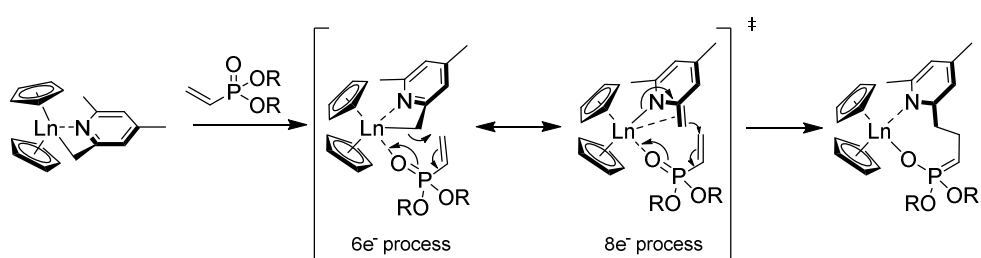
Scheme 35: REM-GTP initiation of DAVP via a proposed eight-membered (8e$^-$ process) or of six-membered (6e$^-$ process) transition state.

Inspired by this work, Pudasaini performed detailed DFT calculations on the activation barrier of different initiators (Me, CH$_2$TMS, S*t*Bu and *sym*-collidine) applied in the REM-GTP of vinylphosphonates as well as other experimental untested initiating moieties (2-propenyl, SMe and NMe$_2$).[227] In contrast to the experimental observations, the addition activation barrier is lower for alkyl ligands than the deprotonation activation, while it is vice versa for the pyridine-based initiators. This is explained by fast barrier tunneling for alkyl initiators to the deprotonation transition state while such a behavior is not observed for pyridine-based initiators (Figure 11).
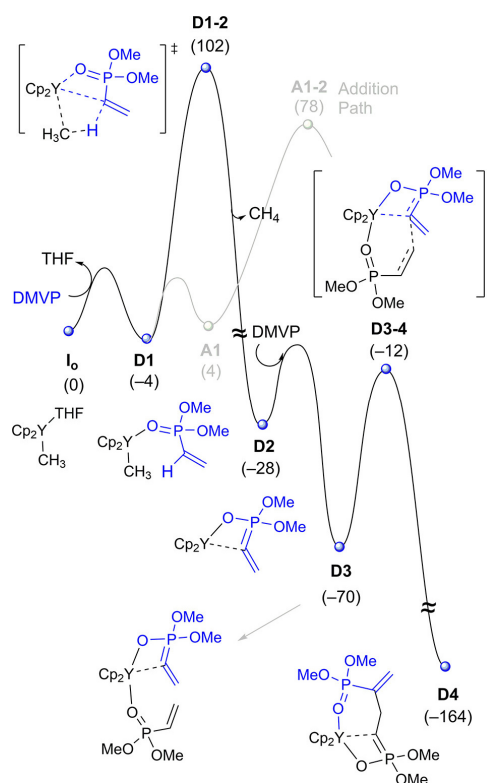
Figure 11: Gibbs energy profile (in kJ mol^{-1}) of the catalytic resting states in the REM-GTP of DMVP. Black curve illustrates the initiation via deprotonation and the gray curve the initiation via addition mechanism. Reprinted with permission from reference[227].

Furthermore, the DFT calculations for π-conjugated (*sym*-collidine and 2-propenyl) initiator systems led to the identification of initiation via *Michael* addition, which has a far lower activation barrier than addition or deprotonation. This suggested that these ligands initiate the polymerization by mimicking the mechanism of propagation, which is consistent with the fast and selective initiation observed in the experimental reports.[227]

These effective initiator systems and the straightforward catalyst functionalization via σ-bond metathesis allowed the introduction of a plethora of different pyridine-based initiators (Scheme 36) and thus to generate tailor-made end-groups and gain a precise control of the polymeric architectures of the synthesized polyvinylphopshonates.[228, 229]

43
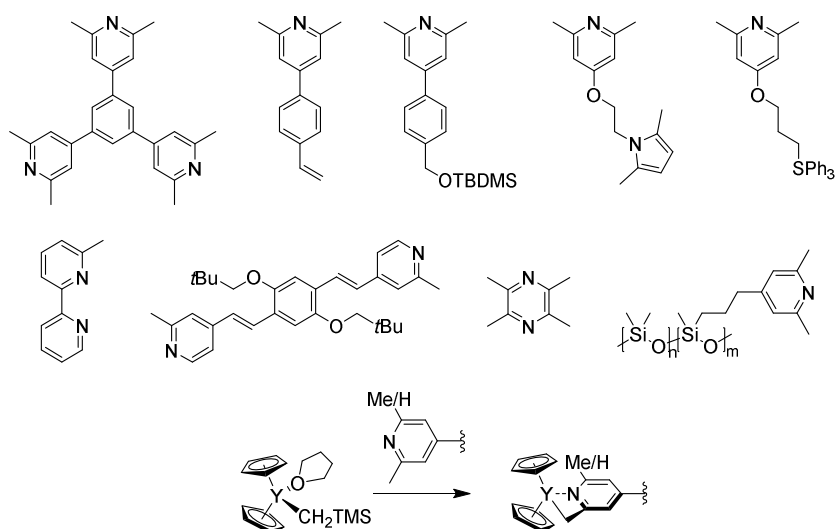
Scheme 36: Functional pyridine-based initiators for the activation of with Cp2Y(CH2TMS)(thf) and subsequent DAVP polymerization.

Even vinylic functionalities were introduced via selective C-H bond activation of 2,6-dimethyl-4-(4-vinylphenyl)pyridine with Cp_2YCH_2TMS. After subsequent polymerization of DEVP, this vinyl end-group allowed coupling to biomolecules like cholesterol or folic acid via efficient thiol–ene click reaction.[198, 230] To introduce other commonly applied reactive functional groups to the polymeric chain-end like thiol, hydroxyl and amine functions, their protic motif must be masked to suppress catalyst degradation. A comprehensive study focused on the suitability of different protecting groups for these functional moieties and their compatibility in σ-bond metathesis reactions.[231] Silyl, pyrrole, and trityl groups proved to be suitable protecting groups, which showed not only quantitative C-H bond activation, but also high initiator efficiencies (41-82%) for DEVP polymerization while maintaining narrow molecular weight distributions of the obtained polymers (< 1.34). The subsequent deprotection was quantitative for the three applied protecting groups and the thus generated functional end-groups were susceptible for post-polymerization modification with cholesteryl chloroformate (OH and NH_2) or N-phenyl maleimide (SH).

With the utilization of an ortho-methylated bipyridine for C-H bond activation the thus generated end-group enables the attachment of metals to this chelating ligand generating metal polymer complexes.[232] Due to the high selectivity towards pyridines also multiple C-H bond activation of macroinitiators are feasible: The control of the polymeric architecture was achieved by synthesis of a trinuclear catalyst via three-fold C–H bond activation of 1,3,5-tris(3,5-dimethyl-4-pyridinyl)benzene with Cp_2YCH_2TMS.[233] This allowed the one-pot synthesis of star-shaped polymeric

44

structures as determined by AFM analysis. A similar approach was chosen to introduce a strong fluorescent marker based on a bifunctional pyridine hydrochinone ether.[234] Recently, the pyridine initiator scope was even expanded to polydimethylsiloxane (PDMS) macroinitiators via the functionalization of PDMS by hydrosilylation with 4-(allyloxy)-2,6-dimethylpyridine.[235] After C-H bond activation of the macroinitiator with Cp$_2$YCH$_2$TMS, different ABA and A-*g*-B copolymers were generated. Another approach for the synthesis of ABA copolymers via the utilization of bifunctional 2,3,5,6-tetramethylpyrazine (TMPy) resulted in the activation of the adjacent rather than opposing methyl groups in TMPy as determined via SCXRD (Scheme 37).[197] This is induced by the generation of an enlarged π-system for adjacent η^3-(C,C,N)-*aza*-allylic coordination yttrium systems, which are thus thermodynamically preferred compared to the activation of opposing methyl groups. Nevertheless, of this adjacent activation product, TMPy initiators proofed active in REM-GTP and therefore emerged as an extremely useful building for the synthesis of defined ABA copolymers.[197, 236, 237]
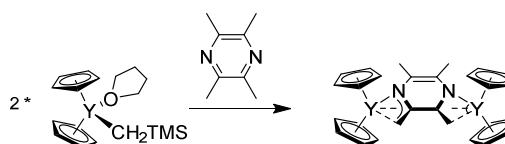
Scheme 37: C-H bond activation of bifunctional 2,3,5,6-tetramethylpyrazine.[237]

After varying the metal center and the initiating group of the REM-GTP catalysts for DAVP polymerization, the last possible motif for tuning the control and performance is within the ligand sphere. For REM-GTP of other *Michael*-type systems, a library of different tailor-made ligands is available, allowing not only the control of activity, but also the introduction of stereoregularity to the received polymers.[209] Initial studies on the influence of the ligand sphere on DAVP polymerization were performed by varying the substitution pattern of simple trivalent REM cyclopentadienyl ligands. In doing so, catalysts with increased steric demand of the coordinated ligand sphere (methyl-, trimethylsilyl-, and tetramethylcyclopentadienyl metallocenes) were synthesized additionally to Cp$_3$Y (Scheme 38).[238]
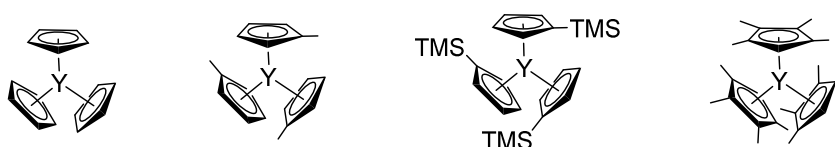
Scheme 38: Trivalent yttrium metallocenes with varying steric demand.[238]

While all catalysts were active in polymerization, a change in activity is observed with the absence of an initiation period. The turnover frequency rose with increasing steric demand of the ligand sphere (Cp_3Y = 21.000 h^{-1}, $(C_5Me_4H)_3Y$ = 95.000 h^{-1}). The authors concluded that the entropy term for substituted cyclopentadienyl REM complexes has a higher influence on the propagation activation barrier than for unsubstituted REM metallocenes. This induces a destabilization of the eight-membered metallacycle ground state (see Scheme 30) allowing a faster S_N2-type associative displacement of the polymer ester by an incoming monomer and thus accelerating the polymerization velocity.[238]

In addition to REM-GTP, yttrium based non-metallocene complexes are commonly utilized for the ROP of various lactones, in which they are highly active and even capable of inducing stereoinformation in some cases.[239] Therefore, Rieger and coworkers adapted a symmetric 2-aminoalkoxy-bis(phenolate)yttrium trimethylsilylmethyl (ONOO)^{tBu}Y(CH$_2$TMS) for the REM-GTP of DAVPs.[197, 236] While this complex was active in polymerization of a plethora of different *Michael*-type systems, the activity for DEVP polymerization was rather low (TOF* = 1,333 h^{-1}) compared to metallocenes and the polymerization suffered from low initiator efficiencies (36%), due to an inappropriate, highly basic alkyl initiator. Remarkably, by altering the initiator to a better suited *sym*-collidine moiety, the initiator efficiency was higher for DEVP polymerization, and for polymerization of the *Michael*-type monomer *N,N'*-dimethylacrylamide (DMAA) the catalyst was even capable of stereospecifically polymerizing DMAA to highly isotactic poly(DMAA) (P_m = 0.94).[240] The analysis of PDEVP stereoinformation prepared with this catalyst was not conducted in this report.
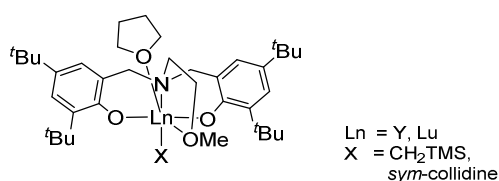
Scheme 39: Non-metallocene (ONOO)^{tBu}Ln(X) (Ln = Y or Lu; X = CH$_2$TMS or *sym*-collidine).

This control of the PDEVP microstructure was not solved until recently. By combination of the well-known constrained geometry (CGCs) as ligand sphere for yttrium with the efficient pyridine-based initiators, isotacticity in PDEVP was induced (P_m = 0.68-0.98) without losing control over other macromolecular parameters.[241] To gain this control, a precise adjustment of the CGC ligand for the stereoselective vinylphosphonate

polymerization was conducted: The indenyl CGC complex showed to be prone to side reactions ($Đ > 1.85$) and suffered from formation of oligomeric side products and incomplete conversion. A switch to a flexible ethylene linker led to a decreased activity and broadened molecular weight distributions ($Đ > 1.48$), but this complex already induced isospecificity ($P_m = 0.73$). The cyclopentadienyl complexes bearing a rigid silyl bridge and a *tert*-butylamine moiety showed to be extremely active in DEVP polymerization ($TOF^* = 45,000 \text{ h}^{-1}$), with so far unreached quantitative (99%) initiator efficiencies, while maintaining high-control over the molecular-weight distribution ($Đ < 1.1$). This complex was also shown to be active over a wide temperature range (-78 °C - +30 °C) and could induce isotacticity ($P_m = 0.68\text{-}0.98$), with higher P_m values at lower temperatures. By increasing the steric demand of CGC by altering the amido moiety to benzyl, an increase in isospecificity was reached at the expense of activity ($TOF^* = 6.000 \text{ h}^{-1}$) and control of the molecular-weight distribution ($Đ < 1.28$).
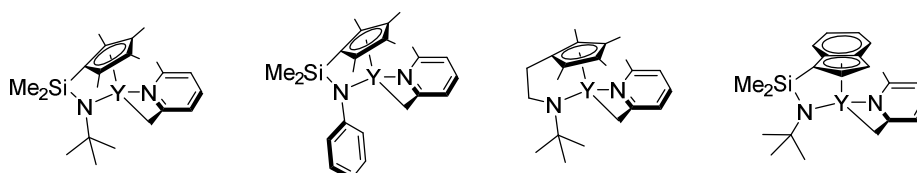
Scheme 40: Yttrium CGCs varying in the amido-moiety, the linker and the substituents of the cyclopentadienyl moiety.

Since phosphorus nuclei feature *J*-coupling in NMR experiments with [1]H- as well as with ^{13}C-nuclei, a detailed NMR study was performed including [1]H–[13]C–[31]P triple-resonance HCP 2D experiment, suppressing this $^1J_{PC}$ coupling. This opened the pathway for triad assignment of the methine polymer triads and thus enabled the determination of tacticity for polyvinylphosphonates.

Furthermore, the authors were able to elucidate the underlying mechanism inducing the stereoinformation by investigating the triad distributions. Due to the isolated r diad stereoerrors an isospecific chain-end control of these C_s-ligated catalysts was concluded. Therefore, the authors were able to propose the stereocontrol mechanism depicted in Scheme 41. This is consistent with the observed temperature dependency of the isospecificity, because chain-end controlled coordination polymerization is more sensitive to the polymerization temperature as site control regiospecific coordination polymerization.
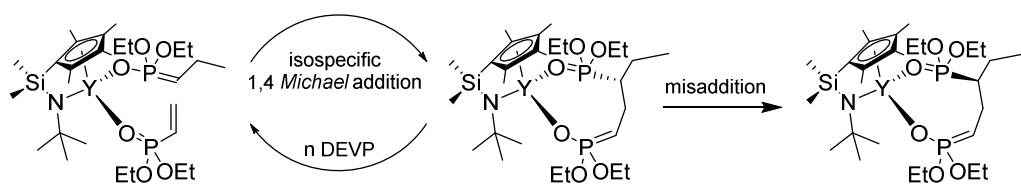
Scheme 41: Proposed Stereocontrol Mechanism and Formation of Stereoerrors for the Isospecific Polymerization of DEVP with CGC.[241]

3 Aim of this thesis

While a plethora of varying organic radical polymers were synthesized so far, the utilized polymerization techniques lack the ability to synthesize high molecular weight polymers, the control of stereoinformation of the generated polymers and a straightforward end-group functionalization without the need of further post-polymerization reactions. A widely applied method for implementing polymers with defined molar masses and stereoinformation is polymerization catalysis using metal-complexes, in which the rare-earth metal-mediated group transfer polymerization is one of the most versatile.

This resulted in the initial motivation to adapt this polymerization technique for the synthesis of functional organic radical polymers. As the polymerization proceeds via a repeated 1,4-conjugate addition (*Michael*-addition), it relies on monomers bearing a 1,4-*Michael*-type acceptor system. To highlight the versatility and activity of REM-GTP, dialkyl vinylphosphonates are targeted as monomers for the synthesis of organic radical polymers. This class of sophisticated monomers is solely polymerizable via REM-GTP and therefore expands the scope of organic radical polymers to polyvinylphosphonates. Furthermore, with the incorporation of phosphorus atoms into the polymers and featuring two functional moieties per repeating group, the so generated ORPs are a promising candidate for application in organic radical batteries or intrinsic charge conducting polymers. The compatibility of REM-GTP with the direct polymerization of radical-containing monomers and the synthesis of suitable polymers for the post-polymerization modification route to yield ORPs is explored (Scheme 42). As protecting groups, alkoxyamines were selected, as they were already shown to be suitable for nitroxide motifs with different deprotection approaches. In general, alkoxyamines generate the corresponding nitroxide radical in high yields via Cope-type elimination induced by peracids. Furthermore, alkoxyamines, in which the cleaved alkyl moiety exhibits a sufficiently stabilized radical (ethylbenzyl), can be deprotected via temperature induced homolysis.

Since the commonly applied *Michaelis–Arbuzov* reaction for the synthesis of DAVP monomers requires high temperatures (>170 °C), this reaction is not suitable to obtain DAVPs functionalized with TEMPO (decomposition temperature 150 °C) or thermolabile protecting groups.[107, 242] Therefore, the already utilized synthetic approach via esterification is explored for the synthesis of the outlined novel TEMPO and TEMPO precursor vinylphosphonates via reaction of (2-chloroethyl)phosphonic dichloride with

4OH-TEMPO or alkoxyamine functionalized 4OH-TEMPO substrates. In addition, the more straightforward approach via esterification of vinylphosphonic dichloride to yield the phosphorous monomer in a single reaction step should be investigated as well (Scheme 42).
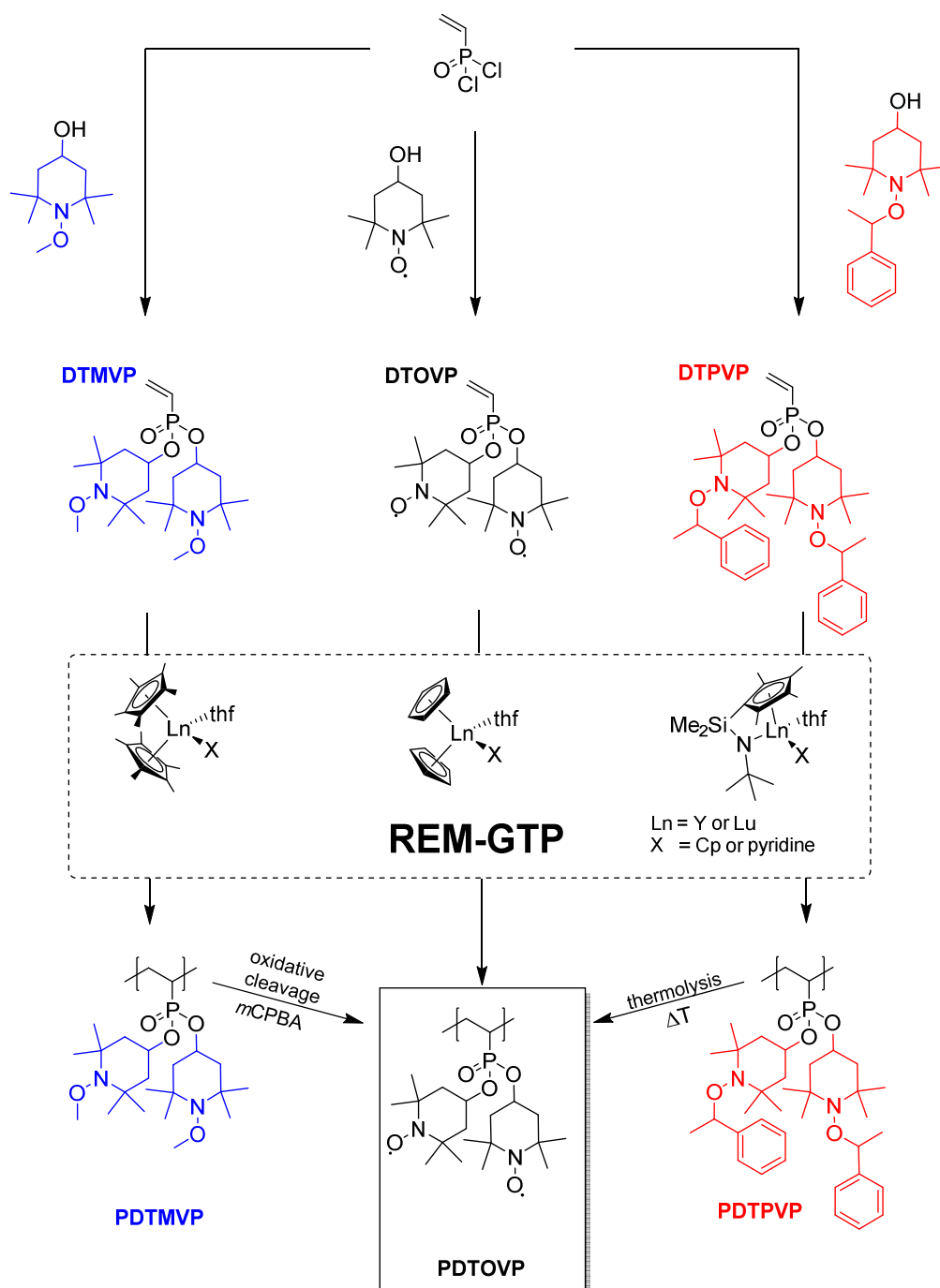

Scheme 42: Synthetic approach for ORPs via a direct REM-GTP of a radical DAVP (black) and post-polymerization-deprotection approaches for alkoxyamine protected DAVPs (blue and red).

Previous studies by our group revealed a dependency of the coordinating monomer's steric demand on the activity in REM-GTP of vinylphosphonates(see chapter 2.4).[206, 216]

Via functionalization of DAVPs with a bulky radical TEMPO and alkoxyamine protected TEMPO radical precursors, the steric demand will drastically be increased compared to DAVPs reported in the literature. Therefore, the polymerization activity of different rare-earth metal centers (Y and Lu) will be investigated and to further enhance the activity, catalysts varying in their ligand sphere (Cp or Cp*) will be synthesized. To introduce various functional end-groups and to investigate their performance in the subsequent REM-GTP of the novel DAVPs - besides the trivalent cyclopentadienyl complexes - pyridine-based initiators are attached to the REM complex via C-H bond activation. Key factors regarding the catalyst and monomer performance in the subsequent REM-GTP are the turn-over frequency (TOF), initiator efficiencies (I) as well as a precise control of the molecular weight distribution. In context of further post-polymerization chain end functionalisation, the initiation via nucleophilic transfer is thoroughly evaluated, especially towards the occurrence of common side reactions such as initiation via deprotonation.

The introduction of stereoinformation to the received polymers can have a huge impact on the properties and the performance of organic radical polymers in different applications, especially in the case of ORB or electric charge conduction polymers. For the simple diethylvinyl phosphonate, stereoselective polymerization was achieved by utilization of yttrium-based constrained geometry complexes (CGCs).[241] Therefore , these complexes will be also investigated in potential isospecific polymerization via the two approaches: The direct polymerization of a radical-containing monomer and polymerization of a masked radical monomer using alkoxyamine protecting groups (Scheme 43).
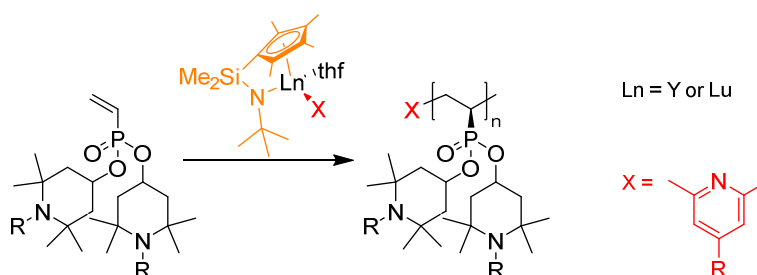

Scheme 43: Investigation of the capability to induce stereoinformation to the synthesized ORP precursors via CGC based REM-GTP catalysts.

For applications utilizing ORPs, a high radical density is a crucial component. While the radical density for the direct polymerization should be close to the theoretical value, for an approach utilizing alkoxyamine precursors, an efficient cleavage of the protecting

groups is necessary and will be investigated in detail. Key parameters are a radical density close to theoretical values, while maintaining the structural integrity of the polymer chains in terms of unchanged molecular weight distributions and molecular weights. Different analytic techniques are utilized for the determination of the radical density ranging from solution-based methods like UV-Vis and EPR analysis to the specialized solid-state magnetometry by a superconducting quantum interference device (SQUID).

Besides the literature known deprotection approaches of alkoxyamines (thermal, oxidative), their compatibility towards the field electrochemical induced reactions will be investigated. This is inspired by the work of Coote and coworkers who reported on utilization alkoxyamines as alkylating agents for various carbonic acids, thus generating TEMPO radicals as byproducts.[243-245] For adapting this approach as a novel deprotecting method for poly(alkoxyamines), the electrochemical deprotection will be tested with small molecule alkoxyamines, optimizing the electrochemical cell in terms of divided and undivided electrode setup as well electrode material (Pt or C). Furthermore, the influence of the used electrolyte and the role of the alkoxyamines chemical structure should be investigated. After this optimization, the results are transferred to the deprotection of the generated alkoxyamineprotected polymers to yield the nitroxide radical functionalized polyvinylphosphonates (Scheme 44).
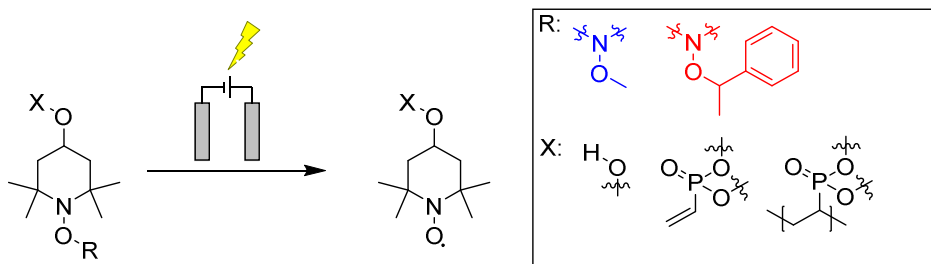
Scheme 44: Electrochemical induced deprotection of various (poly)alkoxyamines.

With their functional polymer end-group, the generated (radical) polyvinylphosphonate are an ideal candidate for the immobilization on various surfaces. ORP surface functionalization has gained increasing interest in the context of organic radical polymers due to enhanced performance or the emerging of novel application like redox-responsive surfaces or sensor devices. Nevertheless, the approaches reported in the literature rely on a further post-polymerization modification step. The suitability of the herein proposed Cp and pyridine-based polymer end-groups could emerge as a

straightforward alternative towards surface functionalization in a graft from approach. Therefore, the direct functionalization of carbon surfaces i.e., carbon nanotubes or fullerenes via Diels-Alder reaction with the cyclopentadienyl end-group of DAVPs will be examined. In addition, a thiol functionalized pyridine-based initiator for REM-GTP was recently reported and could serve as head group for the formation of self-assembled monolayers on gold substrates.[231] A successful surface functionalization is determined via TGA, SEM-EDX, XPS, Raman spectroscopy and for the SAM formation surfaces coverage can be derived via QCM.
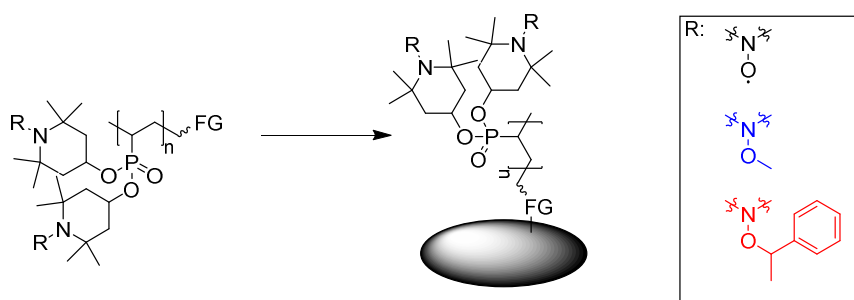
Scheme 45: Surface Immobilization approach of ORP polyvinylphosphonates and the corresponding linker by suitable funtional groups.

After optimization of the polymerization and the subsequent deprotection, the obtained organic radical polyvinylphosphonates will be investigated as novel redox active cathode materials for organic radical batteries (Figure 12). Therefore, composite electrodes of varying amounts of ORP and carbon support will be prepared and their performance regarding electrochemical stability, cycling stability, columbic efficiency and with varying charging/discharging speeds are examined. Furthermore, by impedance spectroscopy the intrinsic resistance of the active material is derived. In the end, battery tests with varying molecular weight radical polyvinylphosphonate are performed to generate a better understanding on the polymers influence on the performance and the derived key parameters.
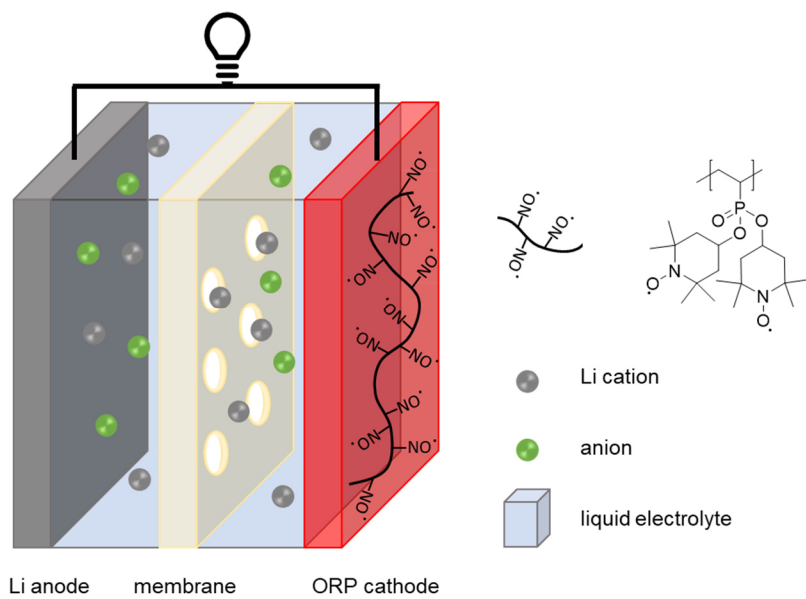
Figure 12: Schematic representation of a metal-organic radical polymer hybrid cell, with radical polyvinylphosphonates as redox active material.

4 Results and discussion

4.1 Monomer synthesis and characterization

For the synthesis of novel TEMPO functionalized PDAVPs, three different synthetic pathways were explored. The basis of these three pathways is the generation of novel TEMPO or TEMPO precursor containing DAVPs via a nucleophilic substitution reaction with the corresponding alcohols. While 4OH-TEMPO and 4-hydroxy-2,2,6,6-tetramethylpipderine (4OH-TEMPH) precursors are commercially available, suitable precursors must be synthesized for the synthetic approach utilizing an alkoxyamine protecting group. With the establishment of nitroxide-mediated polymerization, several methods are reported for the synthesis of alkoxyamines, in which the recombination of nitroxide radicals with alkyl radicals is the most straightforward pathway (Scheme 46). Alkyl radicals can readily be obtained by copper(I)-chloride catalyzed decomposition of the alkyl peroxide intermediates - generated from the corresponding aldehyde and hydrogen peroxide - in the presence of the TEMPO radical in moderate yields, resulting in the alkoxyamines 1-methoxy-2,2,6,6-tetramethylpiperidin-4-ol (4OH-TEMPOMe) and 1-(1-phenylethoxy)-2,2,6,6-tetramethylpiperidin-4-ol (4OH-TEMPOPE).
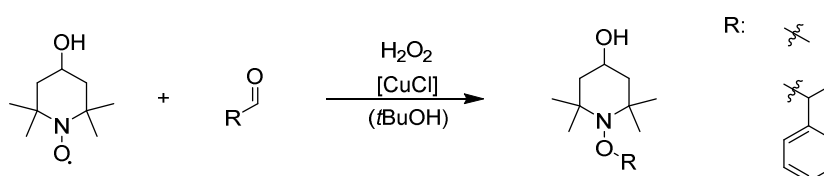
Scheme 46: Copper(I)-chloride catalyzed alkoxyamine synthesis starting from TEMPO radical and the corresponding alkylaldehyde.

Since the common synthesis route for the generation of vinylphosphonates, via *Michaelis Arbusow* reaction, requires temperatures above the decomposition temperature of the TEMPO radical and the cleavage temperature of TEMPOPE, an alternative synthesis approach was chosen. Previous works synthesized various substituted DAVPs in a two-step process via nucleophilic substitution of (2-chloroethyl)phosphonic dichloride with the corresponding alcohol followed by base-induced elimination.[246] While for the alkoxyamines TEMPOMe and TEMPOPE this synthesis route resulted in the formation of the desired DAVPs in moderate yields (45-55%), for the TEMPO radical and the secondary amine TEMPH the subsequent elimination yielded only trace products (< 5%). Therefore, a novel synthesis pathway was explored utilizing the nucleophilic substitution of vinylphosphonic dichloride to

generate the targeted DAVPs (Scheme 47). The synthesis occurred without formation of side products as verified via ^{31}P-NMR spectroscopy if the alkoxyamines TEMPOMe and TEMPOPE or the radical 4-hydroxy-TEMPO were used. For the secondary amine TEMPH, traces of side products were observed caused by amid formation (<5%). After purification by column chromatography, the radical monomer di(2,2,6,6-tetramethylpiperidin-1-oxyl-4-yl) vinylphosphonate (DTOVP), the alkoxyamine monomers di(2,2,6,6-tetramethyl-1-methoxypiperidin-4-yl) vinylphosphonate (DTMVP), di(2,2,6,6-tetramethyl-1-(1-phenylethoxy)piperidin-4-yl) vinylphosphonate (DTPVP) and the secondary amine di(2,2,6,6-tetramethylpiperidin-4-yl) vinylphosphonate (DTHVP) were obtained in moderate to high yields (75-92%). The purity of the compounds was analyzed by elemental analysis and in addition, for the radical precursors DTHVP, DTMVP and DTPVP by NMR spectroscopy. Due to the paramagnetic nature of DTOVP, ^{1}H-and ^{13}C-NMR experiments resulted in broad (^{1}H) or no signals (^{13}C) induced by immense increased spin relaxation times (T_1). Nevertheless, for phosphorous nuclei which already feature a short relaxation time, ^{31}P-NMR spectra of DTOVP was obtained, featuring a signal in the same range as non-radical DAVPs.
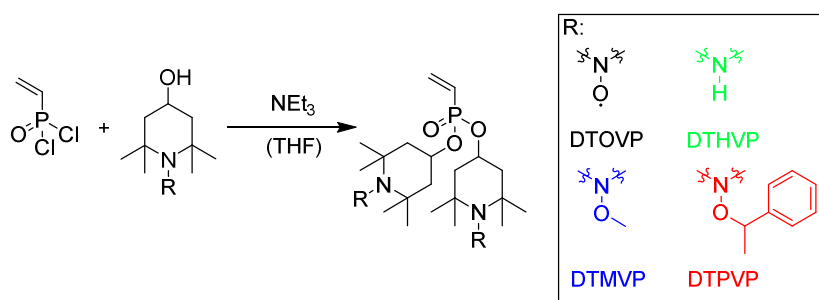
Scheme 47: Synthesis of the substituted DAVP via esterification of vinylphosphonic dichloride.

Because of its paramagnetic nature, the radical DTOVP was further studied with EPR analysis and in addition single-crystal X-ray diffraction measurements were performed, whereat by SCXRD a radical-radical distance of 10 Å in the solid-state phase was derived (Figure 13 d). To suppress undesired exchange and/or electron-electron dipolar interactions with paramagnetic oxygen, the DTOVP benzene solution was deoxygenized by three freeze-pump-thaw cycles prior to EPR measurement. The EPR spectra with a g value of 2.0075 revealed a five-line signal corresponding to the dominant hyperfine coupling of an unpaired electron with the nitrogen nucleus (A_N) in addition to exchange coupling (J) between the two radical moieties (Figure 13 c). Values for A_N and J were elucidated from the simulated spectra (A_N = 43.84 MHz and J = 321 MHz), deriving a

radical-radical distance of 5.4 Å in solution, nearly half of the solid-state value. This could prove beneficial for an intrinsic charge conductive ORP, for which DFT calculations predict an optimal charge conductivity for radical-radical distances of 5-6 Å. [124]

To investigate the phosphonate's influence on the redox behavior on the TEMPO radical cyclic voltammetry measurements were performed, revealing a redox potential of 0.84 V (vs. SHE or 3.88 vs. Li/Li$^+$) and a narrow peak separation of 78 mV (Figure 13 a). The plot of the oxidation peak maximum and reduction peak minimum against the square root of the scan rate showed a linear correlation, highlighting the fast redox kinetics, which were only limited by diffusion. The equal absolute values for the slopes demonstrated fast redox kinetics and the reversibility of the redox process for DTOVP (Figure 13 b), consistent to the radical precursor 4OH-TEMPO. This highlights the compatibility of vinylphosphonates for different applications of organic radical polymers, in which the reversible redox behavior of the radical species is fundamental, e.g. organic radical batteries, redox-flow batteries, redox-responsive materials, etc.
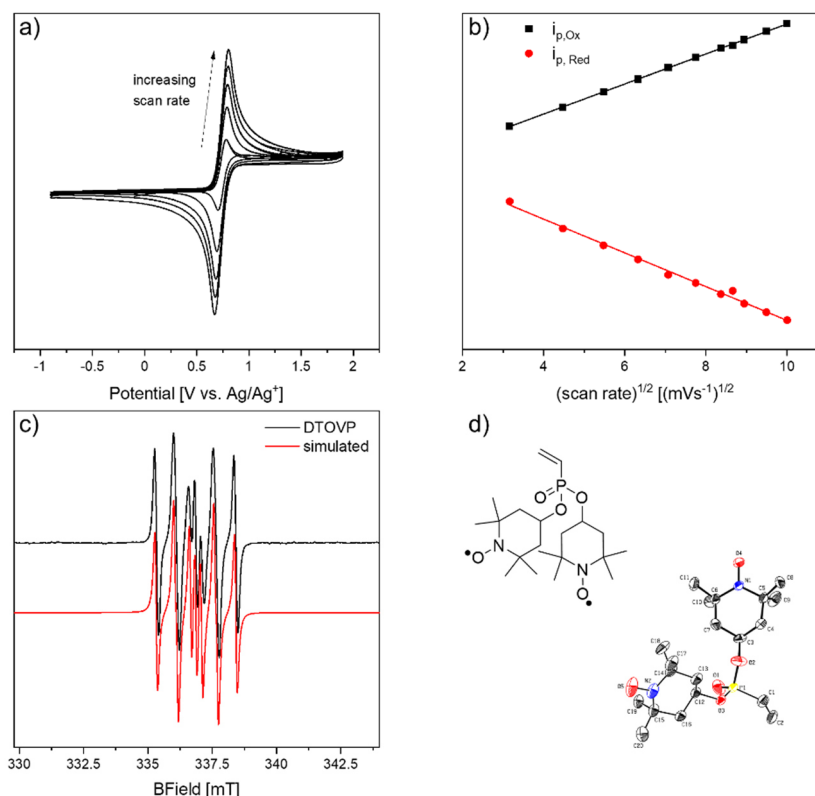
Figure 13: a) Cyclic voltammograms of the radical DTOVP in 5 mM DCM solution with 0.1 M (C$_4$H$_9$)$_4$N$^+$PF$_6^-$ at variable scan rates (10-100mV/s), with a standard potential of E°= 0.73 V (V vs. Ag/Ag$^+$). b) Plot of peak oxidation (black) and reduction (red) peak currents over the square root of the corresponding scan rate. c) EPR spectra of DTOVP in deoxygenized benzene (black) and corresponding simulation (red). d) DTOVP's schematic chemical structure and ORTEP drawing derived by SCXRD.

4.2 REM-GTP catalyst synthesis

Studies from Rieger *et al*. revealed a dependency of activity and steric demand of the coordinating monomer and the coordinating end of the growing polymer chain on REM-GTP activity of various DAVPs.[206, 216] Since the steric demand of the herein reported radical DTOVP and radical-precursor DAVPs (DTHVP, DTOVP, DTMVP and DTPVP) is drastically increased compared to vinylphosphonates reported in the literature, a set of highly active functional catalysts was prepared. Yttrium based systems are - besides REM-GTP of DAVP in which they emerged to the most applied catalytic systems - often applied as catalysts for the polymerization of different *Michael* type systems. The activity of these yttrium catalysts is very high for the polymerization of DEVP (TOF*=21,000 h^{-1} for Cp$_3$Y) and recently also yttrium based CGCs complexes were reported introducing stereocontrolled DEVP polymerization. Besides these yttrium catalysts, lutetium-based systems have shown even higher activities in DEVP polymerization (TOF* = 265,000 h^{-1} for Cp$_3$Lu). Nevertheless, until now only simple Cp$_3$Lu and Cp$_2$LuX (X = CH$_2$TMS, OR, SR, Cl) catalysts were applied in the synthesis of PDAVPs. This scope is therefore extended to different C-H bond activated systems, as well as to Cp* and CGC based ligand systems.

The Cp$_3$Ln (Ln = Y or Lu) complexes were generated according to literature via simple salt metathesis reaction of the corresponding trichloro lanthanide with excess sodium cyclopentadienyl in high yields (68-73%).[212, 213] Since the dicyclopentadienyl lanthanide complexes prepared in a two-step salt metathesis reaction with stochiometric sodium-, lithium- or potassium-cyclopentadienyls and (trimethylsil)methyl)lithium suffer from inseparable byproducts - probably due to the formation of mixed and ate complexes - an alternative approach via alkane elimination was selected. This route utilized the generation of a tris(trimethylsil)methyl) lutetium precursor in a salt metathesis reaction followed by the addition of the corresponding cyclopentadienyl ligand. To further enhance the activity of the Cp$_2$LuX system in addition to Cp ligands, the sterically more demanding pentamethylcyclopentadienyl (Cp*) complexes were generated and additionally a constrained geometry lutetium complex was synthesized via alkane elimination (Scheme 48). The immense selectivity of the alkane elimination reaction resulted in high yields for the dicyclopentadienyl-based complexes (Cp$_2$LuCH$_2$TMS(thf) = 87%, Cp*$_2$LuCH$_2$TMS(thf) = 80%,), and also for the CGC complex (75%).
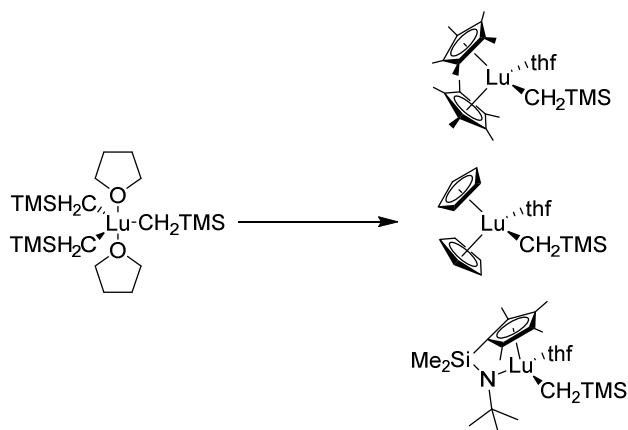
Scheme 48: Preparation of cyclopentadienyl based systems, Cp*$_2$LuCH$_2$TMS(thf), Cp$_2$LuCH$_2$TMS(thf) and CGC-LuCH$_2$TMS(thf).

As the basic CH$_2$TMS alkyl initiator was already shown to initiate the polymerization via deprotonation of the α-acidic proton of DAVPs - leading to unfunctionalized polymer end-groups and a distinctive increase in molecular weight distribution - different pyridine-based initiators were introduced via C-H bond activation of the corresponding CH$_2$TMS complexes. The simple pyridine *sym*-collidine was chosen, due to its literature known fast and selective C-H bond activation and its good performance in the subsequent DAVP polymerization (Scheme 49). In addition, aiming at the immobilization of the generated polymers on gold surfaces via a thiol end-group, the pyridine 2,6-dimethyl-4-(3-(tritylthio)propoxy)pyridine (DTPD) was investigated in its susceptibility towards C-H bond activation with lutetium based complexes. To impede catalyst degradation induced by the protic thiol moiety, a trityl protecting group was utilized, cleavable by acid induced reduction with trifluoracetic acid and alkylsilanes for charge compensation of the leaving trityl cation. While the C-H bond activation of these pyridines with different yttrium-based complexes was already shown to be quantitative within 5 minutes, no data was available for lutetium-based complexes.[226, 231]
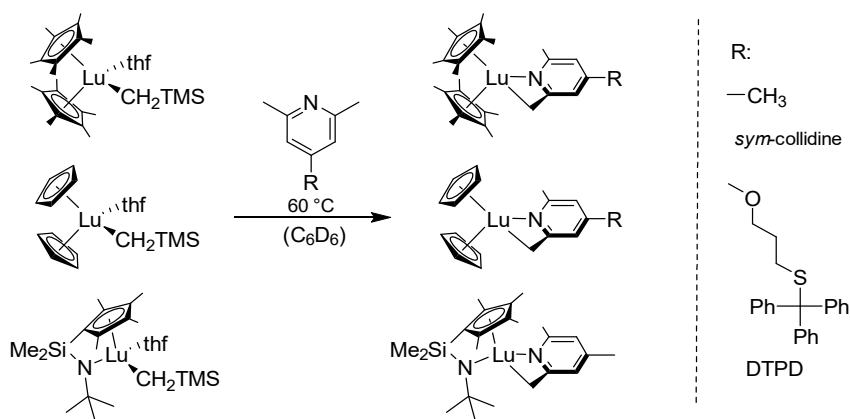
Scheme 49: C-H bond activation of various LuCH$_2$TMS complexes with *sym*-collidine and trityl protected thiol containing DTPD.

To investigate the general activity and conversion of the C-H bond activation with different lutetium complexes, the reaction was monitored in ^{1}H-NMR kinetic experiments. For the ^{1}H-NMR kinetic investigation on C–H bond activation, the lutetium complex and the corresponding pyridine were dissolved in deuterated toluene, the mixture was heated to 60 °C and ^{1}H-NMR spectroscopy was performed at regular time intervals (Figure 14).
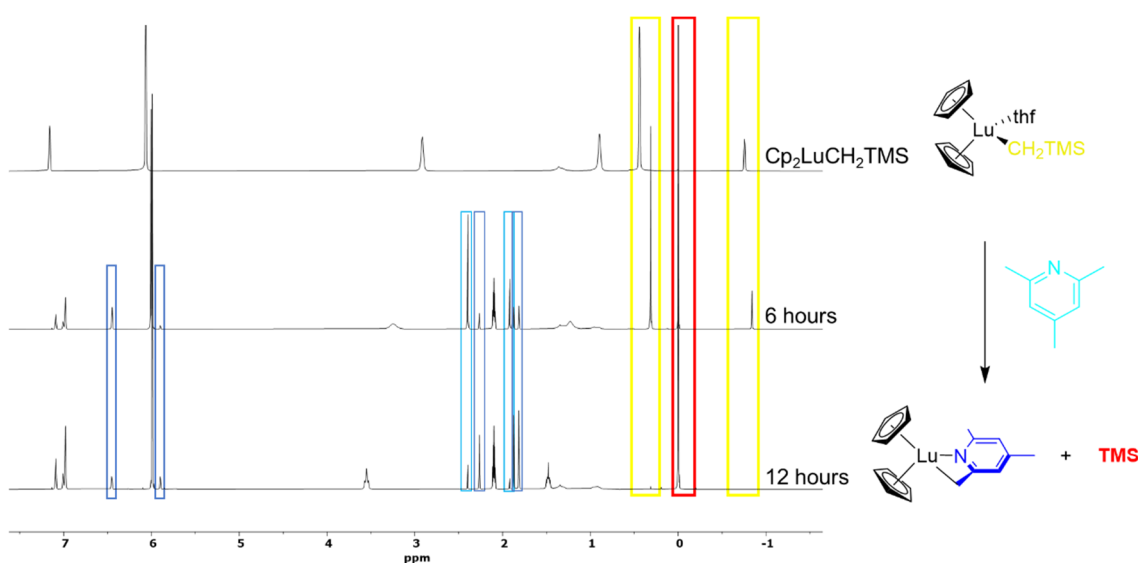
Figure 14: ^{1}H-NMR kinetic reaction of the σ-bond metathesis of Cp$_2$LuCH$_2$TMS with *sym*-collidine to obtain Cp$_2$Lu(*sym*-collidine) in toluene-d$_8$ at 60 °C.

As the reaction progresses, the signals of the CH$_2$-group (δ = -0.80 ppm) and the trimethylsilyl group (δ = 0.32 ppm) of the CH$_2$TMS-initiator attached to the lutetium center decreased, while simultaneously, a new signal emerged at δ = 0.00 ppm corresponding to tetramethyl silane. Likewise, the signal of the pyridine α-methyl groups (δ = 2.39 ppm) decreased over time, while two new signals at δ = 1.87 ppm and

60

δ = 2.26 ppm with an integral ratio of 3:2 were measured. This behavior is consistent with a [2σ + 2σ]-cycloaddition of one of the pyridines α-methyl groups with the CH$_2$TMS ligand of the lutetium complex, resulting in the successful attachment of pyridine to the lutetium center. This functionalization is additionally observed via the shift of the aromatic protons: While a new aromatic signal at δ = 5.90 ppm emerges, the initial signal at δ = 6.45 ppm steadily decreases. This is induced by the attachment of the pyridine to the REM complex, resulting in anisotropic electronic density to the initial symmetric aromatic protons and thus the generation of the observed NMR shifts.

The quantitative attachment was observable for all tested pyridines (*sym*-collidine, DTPD) and lutetium complexes (Cp$_2$LuCH$_2$TMS, Cp*$_2$LuCH$_2$TMS and (CGC)LuCH$_2$TMS), in which the activity in C-H bond activation was solely influenced by the ligand sphere. For the CGC lutetium complex, full conversion was observed after 30 minutes, whereas for Cp*$_2$LuCH$_2$TMS and Cp$_2$LuCH$_2$TMS full conversions were detected after an increased reaction time of 12 hours. This could be explained by two different effects: The steric more demanding ligand sphere of the dicyclopentadienyl complexes in comparison to the less steric demanding ligand sphere of the CGC complex or a difference in the electronic configuration of the lutetium metal induced by the ligand spheres. If the steric hindrance has such a drastic effect on the activity of the C-H bond reaction, also an increase in reaction time for the steric more demanding Cp* complexes compared to the Cp complexes should be observable. As for both complexes the σ-bond metathesis reaction times were in the same range, and in addition a switch to the more steric demanding DTPD pyridine type had no observable effects on the reaction time, the reason for the drastic increased activity of the CGC complexes is induced by electronic effects. It can be assumed that the electron-rich amido moiety with its strong electron donating character increases the electron density at the lutetium metal center. This reduces the Lu-CH$_2$TMS bond energy which induces the high activity in the subsequent C-H bond activation. Further experiments like SCXRD or DFT calculations could support this assumption.

Nevertheless, with these two approaches – simple salt metathesis and σ-bond metathesis – a set of different yttrium and lutetium-based catalytic systems with varying ligand spheres and initiators were synthesized as depicted in Scheme 50.
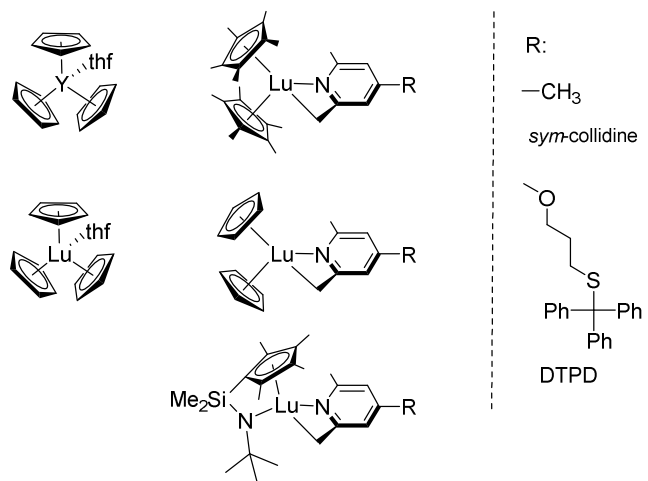
Scheme 50: Set of applied catalysts for the REM-GTP of the novel vinylphosphonates.

4.3 Polymerization of DAVPs

4.3.1 Polymerization of radical DAVPs

As the direct polymerization of radical containing monomers is independent of further post-polymerization reactions, the so generated organic radical polymers feature high or even quantitative radical densities. However, radical groups resemble a reactive moiety, which can interact with the reactive rare-earth metal center, thus terminating the propagation or impede the polymerization initiation. Nevertheless, for other transition metal-based polymerization catalysts (e.g., rhenium or ruthenium) successful polymerization of radical containing monomers were already reported in the literature.[83, 84, 87, 124, 130, 133]

R = Cp, *sym*-collidine
Ln = Y or Lu
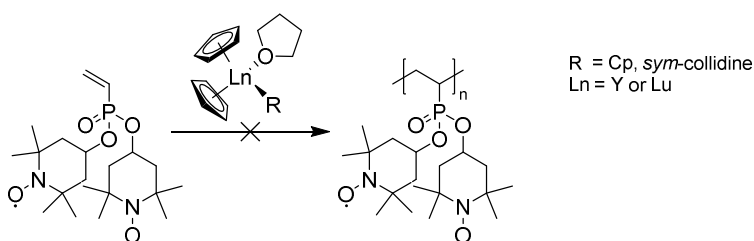
Scheme 51: REM-GTP approaches for the synthesized radical DTOVP catalyzed by $Cp_2Ln(X)(thf)$ (Ln = Y, Lu; X = Cp, *sym*-collidine).

For initial polymerization attempts of the TEMPO-radical monomer DTOVP with different REM complexes $Cp_2Ln(X)(thf)$ (Ln = Y, Lu; X = Cp, *sym*-collidine), a low monomer-to-catalyst ratio of 50/1 was utilized to determine the general compatibility of these monomers towards REM-GTP (Scheme 51). However, no polymerization activity was observed for DTOVP in various solvents (toluene, THF, DCM, $CHCl_3$, DMF) or different temperatures (-78 °C to +90 °C). Evans *et al*. reported the unexpected replacement of REM metallocene ligands with TEMPO anions via a complex redox reaction pathway involving the oxidation of the cyclopentadienyl ligands to the corresponding Cp dimers and the reduction of TEMPO to an aminoxyl anion.[26, 247, 248] Similar considerations were taken into account for the polymerization attempt of the TEMPO radical functionalized DTOVP, and therefore in situ ^{1}H-NMR and ^{31}P-NMR measurements were performed to reveal the underlying mechanism. However, due to the paramagnetic nature of the radical and partial oligomerization of the DTOVP, a distinct product species could not be derived. Consequently, radical monomers seemed to be incompatible with REM metallocenes. A non-metallocene catalyst such as $(ONOO)^{tBu}Ln(CH_2TMS)(thf)$ (Ln = Y or Lu) could feature higher redox stability and thereby be able to polymerize the radical containing DTOVP.[57] Since the lack of an observable polymerization with the radical

DTOVP the direct synthetic pathway was abandoned in favor of the approach utilizing TEMPO precursor moieties.

4.3.2 Polymerization of non-radical precursor and protected DAVPs
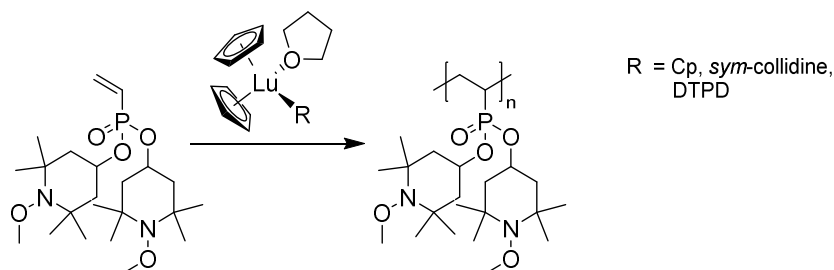
1) Polymerization of DTHVP

In similarity to the polymerization attempts with the radical DTOVP, no polymerization of the tetramethylpiperidine functionalized DTHVP with different REM complexes $Cp_2Ln(X)(thf)$ (Ln = Y, Lu; X = Cp, *sym*-collidine) neither at elevated or decreased temperatures nor in various solvents was observed. This can be attributed to the free secondary amine (pKa ≈ 37), which seems to be able to protonate the highly basic REM complex and thus deactivate the catalyst. Similar results were reported for various polymerization attempts of the secondary amid isopropylacrylamide (pKa ≈ 25). DTHVP was therefore excluded in further studies in favor of the approach utilizing alkoxyamine protected TEMPO moieties.[209]

R = Cp, *sym*-collidine
Ln = Y or Lu
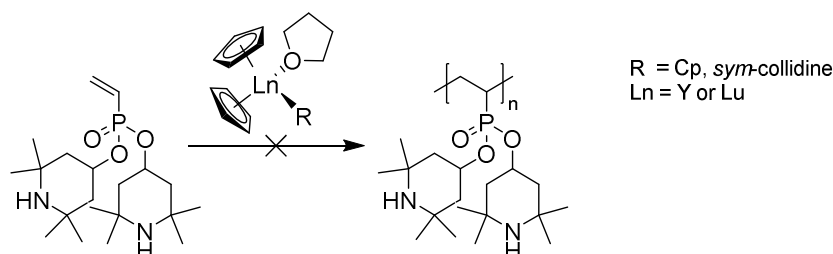
Scheme 52: REM-GTP approach for the synthesized DTHVP catalyzed by $Cp_2Ln(X)(thf)$ (Ln = Y, Lu; X = Cp, *sym*-collidine).

2) Polymerization of DTMVP

Successful polymerization was already observed for preliminary polymerization attempts of methoxyamine protected DTMVP utilizing $Cp_3Lu(thf)$ as catalyst (Scheme 53). To determine the general activity of this monomer and to study the influence of the reaction solvent on REM-GTP with $Cp_3Lu(thf)$, a low monomer-to-catalyst ratio of 50/1 was applied first (Table 2).

Scheme 53: REM-GTP of the methoxyamine protected DTMVP catalyzed by $Cp_2Lu(X)(thf)$ (X = Cp, *sym*-collidine, DTPD).

While the polymerization in toluene led to full conversion of DTMVP within the reaction time of three hours, THF lowered the polymerization activity, attributed to the competing coordination of THF to the REM center, and only a conversion of 17% was observed (Table 2, entry 2).

Table 2: REM-GTP of DTMVP using $Cp_3Lu(thf)$ with various solvents[a]

Entry	Solvent	Conv.[b] [%]	$M_{n,calc}$[c] [kg mol^{-1}]	$M_{n,abs}$[d] [kg mol^{-1}]	Đ[d] [-]	I[e] [%]
1	Toluene	99	22.3	27.0	1.31	82
2	THF	17	3.8	9.6	1.27	40
3	DCM	<3	n.d.	n.d.	n.d.	n.d.
4	DMF	0	n.d.	n.d.	n.d.	n.d.

[a] Reactions performed with [M] = 320 µmol, [M]/[Cat] = 50/1, 2 mL of solvent, reaction time 180 minutes at 25 °C [b] Calculated from ^{31}P-NMR spectrum of aliquots at the end of the reaction via the ratio of signals of the polymer (δ = 30-31 ppm) and the monomer (δ = 15 ppm); [c] $M_{n,calc}$ = M x (([M]/[Cat]) x conversion) [d] Determined via SEC in THF (40 °C, dn/dc(PDTMVP) = 0.102 mL g^{-1}) coupled with triple detection as absolute molar masses, polydispersity calculated from $M_{w,abs}/M_{n,abs}$ [e] Initiator efficiency calculated from I = $M_{n,calc}/M_{n,abs}$ at the end of the reaction.

The catalyst's lower initiator efficiency observed for the polymerization in THF (40%, Table 2, entry 2) compared to the one in toluene (82%, Table 2, entry 1), originates also from this competing coordination of the solvent, thus generating inactive complex

66

species. For the strong coordinating solvent DMF, this behavior was more pronounced, so that the polymerization of DTMVP was completely inhibited, while solvents such as DCM could at least generate a small conversion (<3%,Table 2, entry 3). However, this was not sufficient for isolation of polymers and indicated that propagation only occurs to a small extent.

With toluene as the most suiting solvent for the REM-GTP of DTMVP, the general activity of the different yttrium and lutetium-based catalysts was also explored via in situ ^{31}P-NMR reaction monitoring with a monomer-to-catalyst ratio of 200/1 (Table 3).

Table 3: REM-GTP of the novel DTVMP with various REM catalysts[a]

Entry	Catalyst	Conv.[b]	$M_{n,calc}$[c]	$M_{n,abs}$[d]	Đ[d]	I*[e]	TOF*[f]
		[%]	[kg mol^{-1}]	[kg mol^{-1}]	[-]	[%]	[h^{-1}]
1	Cp$_3$Y	6.3	5.6	n.d.	n.d.	n.d.	n.d.
2	Cp$_3$Lu	99	88.4	147	1.54	60	101
3	Cp$_3$Lu(thf)	99	88.4	101.	1.31	86	105
4	Cp$_2$Lu(CH$_2$TMS)	29	25.9	242	1.45	10	99
5	Cp$_2$Lu(sym-collidne)	99	88.4	102	1.3	87	104
6	Cp$_2$(Lu)(DTPD)	99	88.4	120	1.21	75	102
7	Cp*$_2$LuX[g]	n.d.	0	n.d.	n.d.	n.d.	n.d.
8	CGC-LuX[g]	10	8.9	n.d.	n.d.	n.d.	n.d.

[a] Reactions performed with [M] = 96 µmol, [M]/[Cat] = 200/1, 0.6 mL of solvent [b] Calculated from ^{31}P-NMR spectrum via the ratio of signals of the polymer (δ = 30-31 ppm) and the monomer (δ = 15 ppm); [c] $M_{n,calc}$ from $M_{n,calc}$ = M x (([M]/[Cat]) x conversion) [d] Determined via SEC in THF (40 °C, dn/dc(PDTMVP) = 0.102 mL g^{-1}) coupled with triple detection as absolute molar masses, polydispersity calculated from $M_{w,abs}/M_{n,abs}$ [e] normalized Initiator efficiency calculated from I = $M_{n,calc}/M_{n,abs}$ at the highest slope in time-conversion plot [f] normalized TOF using I*; TOF* = TOF/I* [g] X = CH$_2$TMS, sym-collidine or DTPD.

Consistent to other DAVP polymerizations, the replacement of the REM center from lutetium to yttrium led to a distinctive decrease in activity, resulting in full conversion for the lutetium-based complex within the reaction time of 12 hours, while the yttrium-based cyclopentadienyl complex (Cp$_3$Y) only yielded a conversion of 6.3% (Table 3). In contrast, a switch from Cp$_3$Lu to the corresponding complex with coordinated THF (Cp$_3$Lu(thf)) further increased the activity of the corresponding polymerization, which is

induced by the higher initiator efficiencies of these complexes (Table 3, Entry 3). Fischer *et al*. determined the hapticity of Cp₃Lu as $[(\eta^5\text{-Cp})_2\text{Lu}(\mu\text{-}\eta^1 : \eta^1\text{-Cp})]\infty$ by SCXRD which results in a polymeric structure, while the THF adduct is assumed to have a monomeric or dimeric structure.[249] This resulted in an faster and more complete coordination of DTMVP to the active REM center and thus higher initiator efficiencies. This lethargic initiation process also induced increased polydispersities for Cp₃Lu (Đ = 1.54) compared to Cp₃Lu(thf) (Đ = 1.31). By variation of the initiation moiety from Cp-initiator to CH₂TMS, *sym*-collidine or DTPD, a change in initiation efficiency was observed. The highly basic CH₂TMS led to very low initiator efficiencies (10%) and incomplete conversion resulting in high molecular weights and increased molecular weight distributions (Table 3, Entry 4). Contrary to this, both pyridine initiators revealed a similar polymerization behavior as the Cp₃Lu(thf) catalyst, with high initiator efficiencies and narrow molecular weight distributions (< 1.3). While the initiator efficiency for Cp and *sym*-collidine was nearly quantitative (> 86%), a 10% decreased initiator efficiency was observed for DTPD with a simultaneously decreased molecular weight distribution (Đ = 1.25). It can be assumed that the sterically demanding trityl-functionalized pyridine initiator has a positive effect on the initiation mechanism, thus leading to smaller polydispersities and decreased initiator efficiencies. Since the overall values of the normalized turnover frequencies [TOF*] are independent from the used initiation moiety (Cp, CH₂TMS, *sym*-collidine, DTPD) and are only influenced by the propagation mechanism, the values are in the same range (≈ 100 h⁻¹). These results emphasize Cp₂Lu as the catalytic active moiety in the REM-GTP of DTMVP.

To further tune the catalytic activity and to introduce stereoregularity into the obtained polymers, Cp*₂Lu(X) (X = CH₂TMS or *sym*-collidine) and a lutetium based CGC complex were investigated regarding their general activities in REM-GTP of DTMVP. Unfortunately, the variation of the catalyst ligand sphere by utilization of Cp*₂Lu(X) (X = CH₂TMS or *sym*-collidine) led to immediate gelation of the polymer solution after addition of the catalyst (Table 3, Entry 7). The same behavior was observed with increased monomer dilution or lower temperatures. Only low conversions (<5%) were calculated by ³¹P-NMR spectroscopy. A complete dissolution of the polymer-gel was not achieved, neither with various solvents nor with elevated temperatures. Therefore, these polymers could not be analyzed and the reason for this behavior is therefore based on assumptions: A mechanism inducing this behavior could be linked to an extremely active catalyst suffering from low initiator efficiency. This results in extreme

high molecular weight polymers, which induces the gelation of the reaction mixture. A similar behavior was also observed for the CGC lutetium catalyst (Table 3, Entry 8). However, for this complex also the introduction of stereoregularity to the polymer chains could induce solubility issues, resulting in the gelation and the subsequent insolubility of the polymeric products.

To further elucidate the polymerization activity of DTMVP with $Cp_3Lu(thf)$ as catalyst, turnover frequencies (TOF [h^{-1}]), initiator efficiencies at the highest slope of the activity data (I*) and normalized turnover frequencies (TOF* [h^{-1}]) were determined (Figure 15 a). After plotting conversions vs. time, the highest slope of this plot was used for calculating the turnover frequency and I*. For DTMVP polymerization, the TOF is 208 h^{-1} and taking the incomplete initiation into account (I* = 75%), a normalized TOF* of 277 h^{-1} was calculated. Remarkably, despite the steric demand of the investigated DTMVP, the polymerization lacked an initiation period, which is often reported for trivalent metallocenes in the REM-GTP of DAVPs.[206] The living character of the polymerization of DTMVP was confirmed by a linear growth of the molecular weight with increasing conversion of the monomer and narrow polydispersities (Đ < 1.25) throughout the whole polymerization (Figure 15 b).
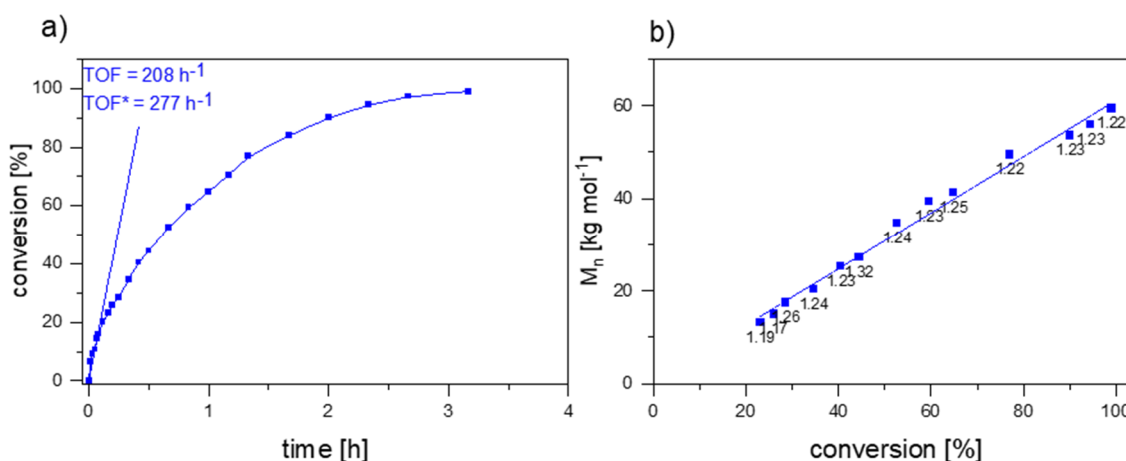
Figure 15: a) Catalytic activity of $Cp_3Lu(thf)$ in the REM-GTP of DTMVP. $Cp_3Lu(thf)$ = 11.2 µmol, [M]/[Cat] = 100/1, toluene = 7 mL, T = 25 °C, measured via the aliquot method (conversions determined via ^{31}P-NMR analysis). b) Linear growth of the absolute of the absolute molecular weight (M_n) as a function of monomer conversion. Polydispersities are shown for each point.

To produce organic radical polymers featuring a cyclopentadienyl end-group with a wide range of molecular weights, a set of different monomer-to-catalyst ratios for the polymerization of DTMVP with $Cp_3Lu(thf)$ in toluene were employed. Thus, polymers ranging from low (18.7 kg mol^{-1}) to ultra-high molecular weight (500 kg mol^{-1}) were

obtained (Table 4, entry 1-7). The overall narrow polydispersities (< 1.34) and the constant initiator efficiencies highlight the controlled, living-type polymerization character of DTMVP with the catalyst Cp$_3$Lu(thf). The slight increase in initiator efficiencies with higher monomer-to-catalyst ratios can be attributed to an increase of coordinating monomer to the catalytic metal center thus facilitating the nucleophilic transfer. Nevertheless, the high and nearly constant initiator efficiencies highlight the living type polymerization and enable the precise synthesis of organic radical polyvinylphosphonates with adjustable molecular weights.

Table 4: REM-GTP of DTVMP with Cp$_3$Lu(thf) with various monomer to catalyst ratios[a]

Entry	Catalyst	[M]/[Cat]	Time	Conv.[b]	$M_{n,calc}$[c]	$M_{n,abs}$[d]	Đ[d]	I[e]
			[h]	[%]	[kg mol^{-1}]	[kg mol^{-1}]	[-]	[%]
1	Cp$_3$Lu(thf)	25	0.45	99	11.2	13.9	1.34	80
2	Cp$_3$Lu(thf)	50	1.5	99	22.3	27.0	1.31	82
3	Cp$_3$Lu(thf)	100	3	99	44.7	59.2	1.25	75
4	Cp$_3$Lu(thf)	200	6	99	89.3	101	1.31	88
5	Cp$_3$Lu(thf)	400	12	99	179	202	1.30	88
6	Cp$_3$Lu(thf)	600	18	99	268	307	1.23	87
7	Cp$_3$Lu(thf)	1000	30	99	447	500	1.24	89

[a] Reactions performed with [M] = 320 µmol, [M]/[Cat] = 200/1, 0.6 mL of solvent[b] Calculated from ^{31}P-NMR spectrum via the ratio of signals of the polymer (δ = 30-31 ppm) and the monomer (δ = 15 ppm); [c] $M_{n,calc}$ from $M_{n,calc}$ = M x (([M]/[Cat]) x conversion) [d] Determined via SEC in THF (40 °C, dn/dc(PDTMVP) = 0.102 mL g^{-1}) coupled with triple detection as absolute molar masses, polydispersity calculated from $M_{w,abs}/M_{n,abs}$ [e] Initiator efficiency calculated from I = $M_{n,calc}/M_{n,abs}$ at the end of the reaction.

In accordance to this, polymers with varying molecular weights via variation of the monomer-to-catalyst ratio were synthesized using pyridine based initiator systems Cp$_2$Lu(*sym*-collidine) and Cp$_2$Lu(DTPD). The catalyst solutions were prepared as described in 4.2 via in situ activation of Cp$_2$Lu(CH$_2$TMS) with the corresponding pyridine and the polymerization was started after observing full C-H bond activation as determined by aliquot ^{1}H-NMR spectroscopy. In difference to PDTMVP synthesized via Cp$_3$Lu(thf), polymers generated with the pyridine-based initiators showed a slightly narrower molecular weight distribution. Similar observations were reported for the polymerization of other DAVP systems and are attributed to a faster initiation process

70

via the capability of the pyridine initiators to mimic the propagation reaction intermediate.[206, 214, 226] While initiator efficiencies decreased for the *sym*-collidine initiator with increased monomer-to-catalyst ratios, the trityl functionalized DTPD system showed constant values over the range of the tested ratios. This could be induced by impurities in the *sym*-collidine used for the C-H bond activation, partly deactivating the catalytic active species, which has an increased effect at higher monomer-to-catalyst ratios. Nevertheless, the pyridine-based system showed a controlled polymerization with predictable molecular weights and narrow polydispersities. Additionally, the straightforward in situ C-H bond activation with $Cp_2Lu(CH_2TMS)$ allows to synthesize polymers with a plethora of different functional polymer end-groups, based on the immense variety of available functional pyridines (see Scheme 36).

Table 5: REM-GTP of DTVMP with in situ activated pyridine based initiators via C-H bond activation of $Cp_2Lu(CH_2TMS)$[a]

Entry	Catalyst	[M]/[Cat]	Time	Conv.[b]	$M_{n,calc}$[c]	$M_{n,abs}$[d]	Đ[d]	I[e]
			[h]	[%]	[kg mol^{-1}]	[kg mol^{-1}]	[-]	[%]
1	Cp_2Lu(*sym*-collidine)	50	1.5	99	22.3	30.4	1.26	73
2	Cp_2Lu(*sym*-collidine)	100	3	99	44.7	60.2	1.29	73
3	Cp_2Lu(*sym*-collidine)	200	6	99	89.3	141	1.27	63
4	Cp_2Lu(*sym*-collidine)	400	12	99	179	289	1.25	54
5	Cp_2Lu(DTPD)	25	0.45	99	11.2	13.1	1.24	84
6	Cp_2Lu(DTPD)	50	1.5	99	22.3	28.6	1.23	77
7	Cp_2Lu(DTPD)	100	3	99	44.7	56.3	1.27	79
8	Cp_2Lu(DTPD)	200	6	99	89.3	120	1.21	73

[a] Reactions performed with [M] = 320 µmol, [M]/[Cat] = 200/1, 0.6 mL of solvent[b] Calculated from ^{31}P-NMR spectrum via the ratio of signals of the polymer (δ = 30-31 ppm) and the monomer (δ = 15 ppm); [c] $M_{n,calc}$ from $M_{n,calc}$ = M x (([M]/[Cat]) x conversion) [d] Determined via SEC in THF (40 °C, dn/dc(PDTMVP) = 0.102 mL g^{-1}) coupled with triple detection as absolute molar masses, polydispersity calculated from $M_{w,abs}/M_{n,abs}$ [e] Initiator efficiency calculated from I = $M_{n,calc}/M_{n,abs}$ at the end of the reaction.

3) Polymerization of DTPVP

A preliminary study similar to DTMVP revealed the influence of the solvent on the polymerization activity (Scheme 54). While the conversion in toluene is nearly complete (80%) within the reaction time of 3 hours, the polymerization in THF only yielded a conversion of 10% (Table 6).
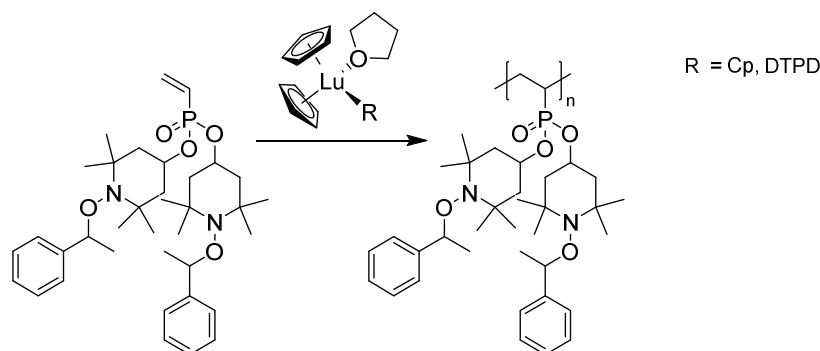
Scheme 54: REM-GTP of the thermolabile phenylethoxyamine protected DTPVP catalyzed by Cp$_2$Lu(X)(thf) (X = Cp, DTPD).

No polymer was formed in either DMF or DCM leading to similar conclusions for the polymerization mechanism of DTMVP and DTPVP. The lower polymerization activity in toluene for DTPVP in comparison to DTMVP is attributed to the considerably higher steric demand of the 1-phenylethoxy protected vinylphosphonate relative to the methoxy protected monomer.

Table 6: REM-GTP of the novel DTPVP using Cp$_3$Lu(thf) in various solvents[a]

Entry	Solvent	Conv.[b] [%]	$M_{n,calc}$[c] [kg mol^{-1}]	$M_{n,abs}$[d] [kg mol^{-1}]	Đ[d] [-]	I[e] [%]
1	Toluene	80	25.1	50.1	1.25	51
2	THF	10	3.1	4.6	1.47	68
3	DCM	0	n.d.	n.d.	n.d.	n.d.
4	DMF	0	n.d.	n.d.	n.d.	n.d.

[a] Reactions performed with [M] = 320 µmol, [M]/[Cat] = 50/1, 2 mL of solvent, reaction time 180 minutes at 25 °C [b] Calculated from ^{31}P-NMR spectrum of aliquots at the end of the reaction via the ratio of signals of the polymer (δ = 30-31 ppm) and the monomer (δ = 15 ppm); [c] $M_{n,calc}$ from $M_{n,calc}$ = M x (([M]/[Cat]) x conversion) [d] Determined via SEC in THF(dn/dc(PDTPVP) = 0.129 mL g^{-1}) coupled with triple detection as absolute molar masses, polydispersity calculated from $M_{w,abs}$/$M_{n,abs}$ [e] Initiator efficiency calculated from I = $M_{n,calc}$/$M_{n,abs}$ at the end of the reaction.

To further reveal the influence of the different alkoxyamine protecting groups on the polymerization activity also for DTPVP polymerization, turnover frequencies (TOF [h^{-1}]), initiator efficiencies at the highest slope of the activity data (I*) and normalized turnover frequencies (TOF* [h^{-1}]) were determined using an aliquot method (monomer-to-catalyst ratio of 100/1 in toluene and Cp$_3$Lu(thf) as catalyst). For the REM-GTP of DTPVP with Cp$_3$Lu(thf) a normalized turnover frequency of 86 h^{-1} was derived, which was three times lower than the obtained TOF* for DTMVP (Figure 16 a). Simultaneously, a decreased initiator efficiency of 50% was observed. These results are induced by the higher steric hindrance of the monomer during polymerization in accordance to REM-GTP of other DAVPs (see Chapter 2.4). Despite the steric demand of DTPVP, the polymerization lacked an initiation period, which is often observed in the REM-GTP of vinylphosphonates. Contrary to literature - which suggest higher initiator efficiencies for steric more demanding vinylphosphonates – the initiator efficiencies are slightly higher for less sterically demanding DTMVP than for DTPVP. Hypothetically, monomers that are too sterically demanding impede the nucleophilic transfer, thus lowering the initiator efficiencies. The linear dependency of the molecular weight with the conversion and narrow molecular weight distributions throughout the polymerization highlight the living character of the polymerization and lay the foundation for (block) copolymers (Figure 16 b).
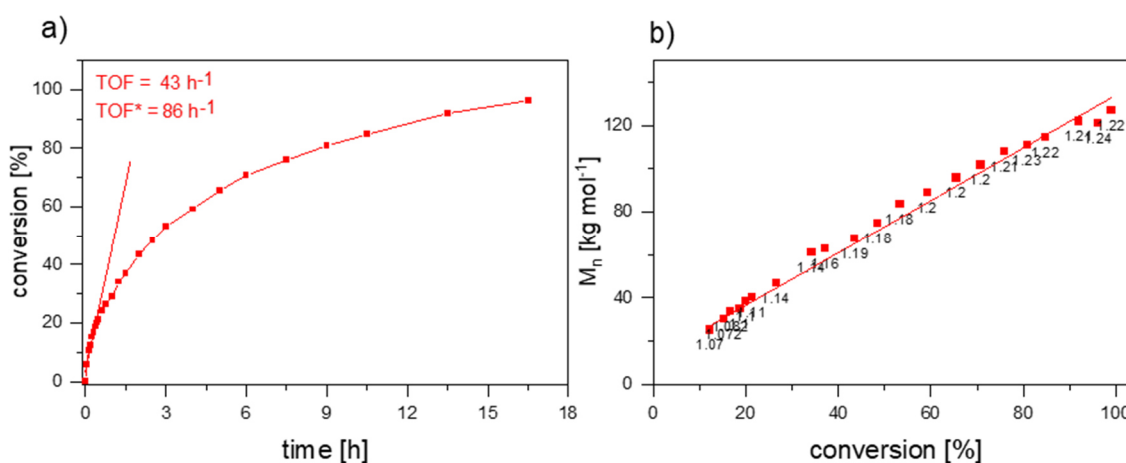
Figure 16: a) Catalytic activity of Cp$_3$Lu(thf) in the REM-GTP of DTPVP. Cp$_3$Lu(thf) = 11.2 µmol, [M]/[Cat] = 100/1, toluene = 7 mL, T = 25 °C measured via the aliquot method (conversions determined via ^{31}P-NMR analysis). b) Linear growth of the absolute of the absolute molecular weight (M$_n$) as a function of monomer conversion. Dispersities are shown for each point.

To produce vinylphosphonates with a thermolabile phenylethoxyamine protecting group over a wide range of molecular weights, different degrees of polymerization (DP)

were targeted. For the synthesis of functional polymer end-groups, as catalytic systems Cp$_3$Lu(thf) (introduces a Cp end-group) and Cp$_2$Lu(DTPD) (introduces a trityl end-group that can be converted to a thiol) were used. This resulted in PDTPVP with low to medium molecular weights (30.0 - 108 kg mol^{-1}), with full monomer conversions up to a monomer-to-catalyst ratio of 100/1. In contrast to DTMVP, the Cp and the pyridine initiators produce polymers with molecular weight distributions in the same range (Đ =1.2 - 1.31). Hypothetically, a fast initiation was induced by steric crowding of the REM center by the sterically demanding DTPVP monomer, accelerating the nucleophilic transfer and thus resulting in narrow molecular weight distributions. With higher monomer-to-catalyst ratios than 100/1 an incomplete conversion and slightly increased polydispersities were observed, while the initiator efficiencies remained constant. Since the incomplete polymerizations resulted in molecular weights in the same range, regardless of the monomer-to-catalyst ratios or conversions, a deactivation of the catalyst system is assumed. Therefore, a maximum turnover number of 167 for the REM-GTP of DTPVP with Cp$_3$Lu(thf) is observed (calculated via the incomplete conversion of DTPVP with a monomer-to-catalyst of 200/1). The variation of the initiating system to DTPD yielded similar results. Possible deactivation pathways are precipitation of the synthesized polymer, entanglement of the active REM complex in the polymer chains or trace impurities in the monomer feed. In difference to DTMVP, for the DTPVP monomer purification was not feasible by distillation - due to the high boiling point and the thermosensitive protecting group – and therefore protic impurities are the most likely cause for catalyst deactivation. The slight decrease in initiator efficiency can also be attributed to a trace impurity deactivating the catalytic active REM complex.

Table 7: REM-GTP of DTPVP with $Cp_3Lu(thf)$ and in situ activated DTPD initiators via C-H bond activation of $Cp_2Lu(CH_2TMS)$[a]

Entry	Catalyst	[M]/[Cat]	Time	Conv.[b]	$M_{n,calc}$[c]	$M_{n,abs}$[d]	Đ[d]	I[e]
			[h]	[%]	[kg mol⁻¹]	[kg mol⁻¹]	[-]	[%]
1	$Cp_3Lu(thf)$	25	4	99	15.7	28.1	1.20	56
2	$Cp_3Lu(thf)$	50	10	99	31.3	52.5	1.24	59
3	$Cp_3Lu(thf)$	100	20	99	62.7	108	1.22	58
4	$Cp_3Lu(thf)$	200	48	48	60.2	107	1.31	56
5	$Cp_3Lu(thf)$	400	96	23	57.7	109	1.31	53
6	$Cp_2Lu(DTPD)$	25	4	99	15.7	25.4	1.20	62
7	$Cp_2Lu(DTPD)$	50	10	99	31.3	51.7	1.24	60
8	$Cp_2Lu(DTPD)$	100	20	99	62.7	102	1.22	61

[a] Reactions performed with [M] = 320 µmol, [M]/[Cat] = 200/1, 0.6 mL of solvent [b] Calculated from ³¹P-NMR spectrum via the ratio of signals of the polymer (δ = 30-31 ppm) and the monomer (δ = 15 ppm); [c] $M_{n,calc}$ from $M_{n,calc}$ = M x (([M]/[Cat]) x conversion) [d] Determined via SEC in THF (40 °C, dn/dc(PDTMVP) = 0.102 mL g⁻¹, dn/dc(PDTPVP) = 0.129 mL g⁻¹) coupled with triple detection as absolute molar masses, polydispersity calculated from $M_{w,abs}/M_{n,abs}$ [e] Initiator efficiency calculated from I = $M_{n,calc}/M_{n,abs}$ at the end of the reaction.

Nevertheless, both alkoxyamine protected monomers are susceptible towards REM-GTP with lutetium-based catalysts in combination with various functional initiators. As both polymerizations follow a living type mechanism by varying the catalyst to monomer ratio a set of polymers with predictable molecular weights were prepared featuring overall narrow molecular weight distributions.

4.4 End-group functionalization of DAVPs

1) End-group analysis

To elucidate the initiation mechanism and to analyze the end-group integrity, an essential prerequisite for efficient end-group functionalization or immobilization on surfaces, a detailed ESI-MS analysis of PDTMVP and PDTPVP was performed to validate the attachment of the used initiators to the polymer chain ends. Therefore, ESI-MS spectra of oligomeric DTMVP and DTPVP were recorded by reacting Cp$_3$Lu(thf) with the corresponding monomer in a 1:3 ratio in toluene, quenching the polymerization with THF after 10 min and immediate measurement of the reaction mixture in acetonitrile (Figure 17). The initiating Cp ligand attachment to the oligomers was verified in the ESI-MS spectrum by a mass shift of 65 m/z, assigned to the cyclopentadienyl ([Cp - H]) moiety of the DTMVP oligomers (m/z = ([M$_{Cp}$ – H] + n × M$_{DTMVP}$ + H + Na)$^+$, n = 2–5) and the DTPVP oligomers (m/z = ([M$_{Cp}$ – H] + n × M$_{DTPVP}$ + H + Na or H)$^+$, n = 2–4).
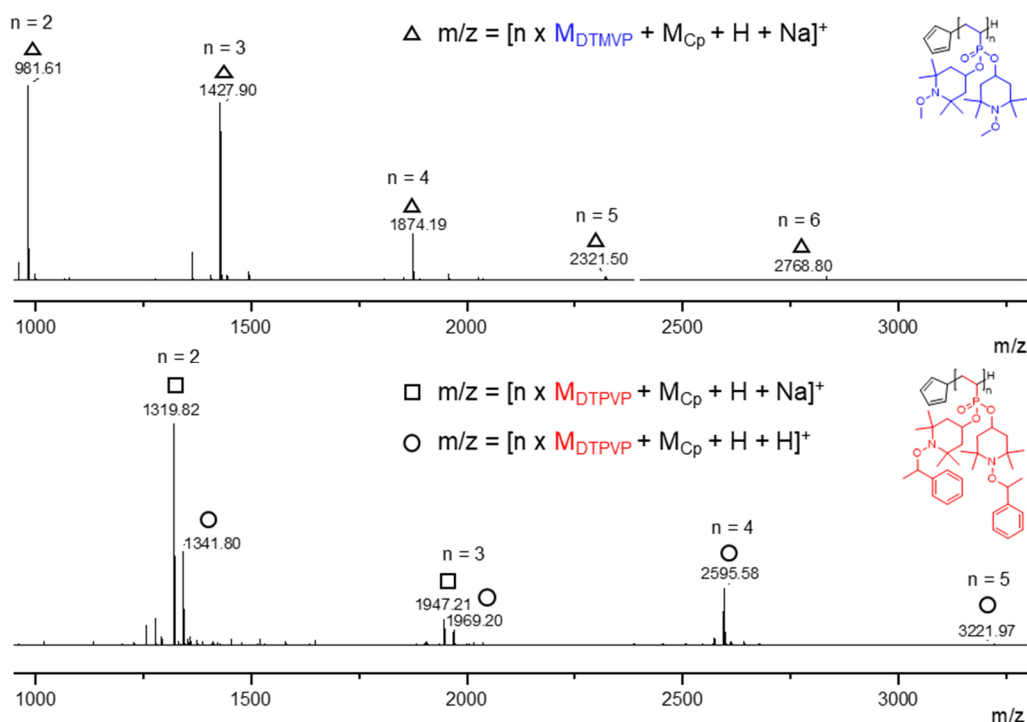
Figure 17: End-group analysis vis ESI-MS of oligomeric DTMVP (top) and DTPVP (bottom) produced with Cp$_3$Lu(thf) ([M]/[Cp$_3$Lu(thf)] = 3/1, 30 min, toluene) and measured in acetonitrile.

Since the initiating groups were clearly visible in the ESI-MS, a nucleophilic transfer reaction of the initiator via a monomer insertion into the lutetium carbon bond during the initiation is evident, leading to the desired Cp end-group. Due to the exclusive

presence of signals corresponding to nucleophilic transfer reaction, an initiation via deprotonation is excluded.

Likewise, for DTMVP and DTPVP, end-group analysis via ESI-MS measurements with the in situ activated pyridine initiators Cp_2LuX (X = *sym*-collidine or DTPD) were conducted. The attachment of this pyridine-based initiators to DTMVP and DTPVP was verified by a mass shift of 120 m/z for the *sym*-collidine and 440 m/z for the DTPD initiator (Figure 18). In contrast to the Cp end-group, which resulted in a very broad ^{1}H-NMR signal of the corresponding chain-end, the trityl end-group resulted in defined ^{1}H-NMR signals, enabling the calculation of the polymers number average molecular weight (M_n). The calculation was performed using the integral of the aromatic triyl end-groups (δ = 7.2–7.5 ppm) and the piperidine protons in α-position of the phosphonate (I_P, two protons per repeating unit), giving $M_{n,NMR} = I_P \times M_{DAVP} + M_{Ini}$. Unfortunately, this was only feasible for PDTMVP, as the aromatic signals of the phenylethoxyamine protecting group of PDTPVP overlapped with the aromatic pyridine end-group signals. The derived values were compared to the absolute number-average molecular weight determined from SEC using triple detection (Table 5). The small variation of only 2–18% for the molecular weights determined via ^{1}H-NMR and SEC indicate full pyridine end-group functionalization and thus opens the pathway for further end-group modification.
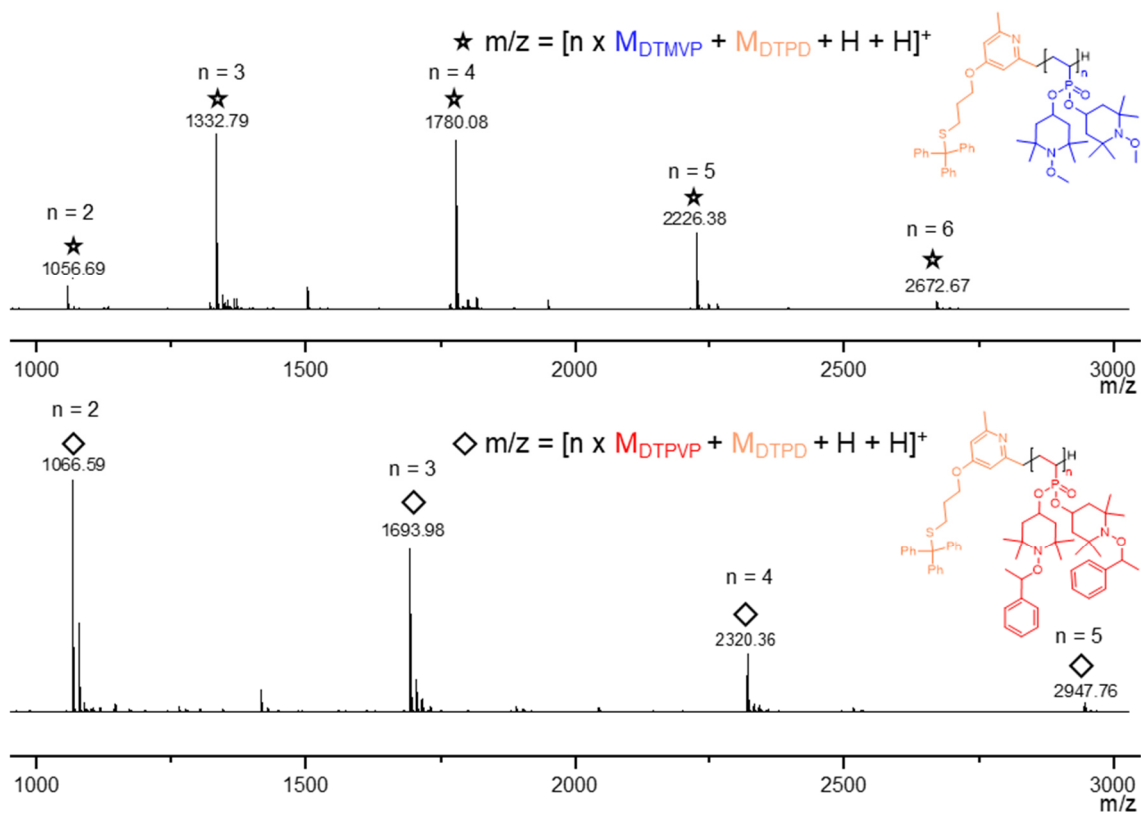
Figure 18: End-group analysis vis ESI-MS of oligomeric DTMVP (top) and DTPVP (bottom) produced with in situ activated Cp$_2$Lu DTDP ([M]//[DTPD]/[Cp$_2$Lu(thf)] = 3/1.05/1, 30 min, toluene) in acetonitrile.

2) Post-polymerization end-group functionalization

The Cp diene chain-end enables straightforward polymer modification via the versatile *Diels-Alder* (DA) reaction or the synthesis of complex comb polymer architectures by ring-opening metathesis polymerization.[85, 250] As a suitable substrate for DA, the dienophile *N*-(1-Pyrenyl)-maleimide was selected, due to its high reactivity and the introduction of an enhanced π-systems with strong fluorescence and π-stacking ability (Scheme 55).
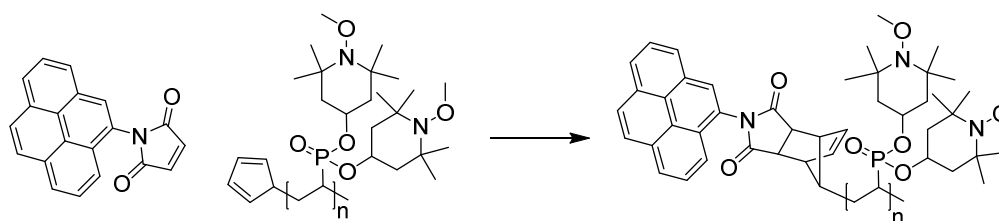
Scheme 55: *Diels-Alder* cyclization of Cp polymer end-group and *N*-(1-Pyrenyl)-maleimide yielding a pyrenic polymer end-group.

The successful attachment via DA post-polymerization was verified by a mass shift of 362 m/z of the prepared DTMVP oligomers in the MALDI-MS spectrum. Furthermore, the introduction of the pyrene end-group allowed the calculation of the number average molecular weight of these polymers. The calculation was performed using the integral of the pyrene end-groups (δ = 8.0–8.3 ppm) and the piperidine protons α-position of the phosphonate (I_P, two protons per repeating unit), giving $M_{n,NMR} = I_P \times M_{DAVP} + M_{Ini}$. Since the results of the M_n calculated via ^{1}H-NMR analysis were in good agreement with the ones derived from absolute SEC measurements, a successful, quantitative end-group modification with pyrene via DA reaction was observed. Additionally, the characteristic adsorption of the pyrene end-group after polymer purification was clearly visible in the UV-Vis spectra.

The ability of the Cp end-group towards DA was further evaluated with surfaces able to serve as dienes or dienophiles. Carbon nanotubes (CNT), especially multi walled carbon nanotubes (MWCNT) or single walled CNT (SWCNT), bear an immense surface area. Due to their conjugated π-network, CNTs additionally exhibit a high electrical charge conductivity. Additionally, this π-network enables CNTs to undergo surface modification via DA reaction, as already reported for different polymeric substrates.[250-253] A combination of an organic radical polymer, or ORP precursor could prove highly

beneficial for various application cases, however a straightforward CNT modification approach by DA reaction in the context of ORP was not reported until now.

Therefore, a Cp end-group containing polymer (PDTMVP, M_n = 180 kg mol^{-1}) was reacted with MWCNT in a DA surface modification approach (Scheme 56). MWCNT was chosen as substrate instead of the more reactive SWCNT due to their lower economic costs, making MWCNT a more suitable candidate for a broad scope for further applications. To enhance exfoliation of the CNT, elevated temperatures (155 °C) were applied and high boiling point solvents (NMP, DMF and mesitylene) were used. To facilitate the exothermic DA formation, the reaction mixture was slowly cooled to room temperature and stirred for an additional day.
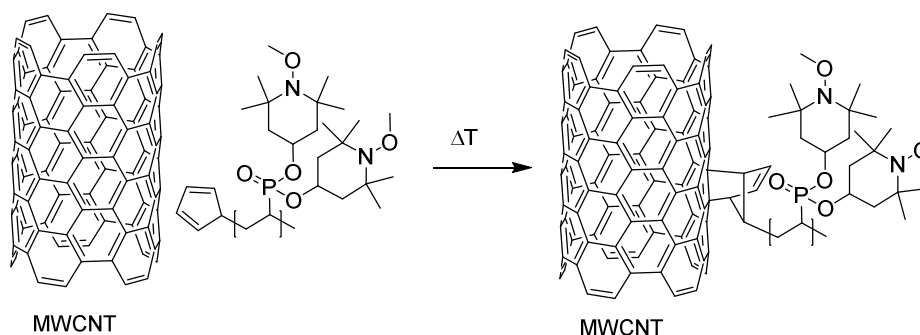
Scheme 56: *Diels-Alder* cyclization of Cp polymer end-group and multi walled carbon nanotubes to immobilize the corresponding polymers on a charge conductive support.

Due to the immense thermal stability of CNTs, the surface immobilization of the attached polymer was derived via the polymer mass loss observed during TGA measurements (see Chapter 4.6 for a detailed discussion of PDTMVPs thermal decomposition). While only low polymer surface attachment was derived for DMF and mesitylene (<2 wt%), a sufficient surface functionalization of 25 wt% polymer on the CNT was observed by utilizing NMP as solvent. This is consistent with the ability of NMP to sufficiently exfoliate CNTs, thus increasing the reactivity of the surfaces and enhancing the heterogeneous DA immobilization. The polymer immobilization on the MWCNT surface was additionally investigated via scanning electron microscopy (SEM). While the MWCNT precursor hollow structures resulted in SEM-images with a sharp contrast, the immobilized polymers suppressed the observation of this hollow structures by the homogeneous attachment on the surface of the CNT (Figure 19). Additionally, an increase in CNT diameter from average values of 21.6 nm for the unfunctionalized MWCNT to 29.2 nm for the composite nanotubes was observed,

consistent with the coverage of the carbon nanotubes with a polymer monolayer. While this is a proof of principle for the successful polymer immobilization, further approaches should focus on the attachment of different molecular weight polymers, the variation of the polymer to MWCNT feed and the utilization of other Cp end-group containing polymers (PDTPVP and PDTOVP). Furthermore, for the utilization of this composite material in ORP applications, the alkoxyamine protecting group has to be removed after CNT modification. While for the thermal phenylethoxyamine protecting group of PDTPVP, the deprotection should proceed during the high temperatures of the immobilization reaction. For the methoxyamine protected PDTMVP, a further post immobilization deprotection step has to be applied (oxidative elimination).
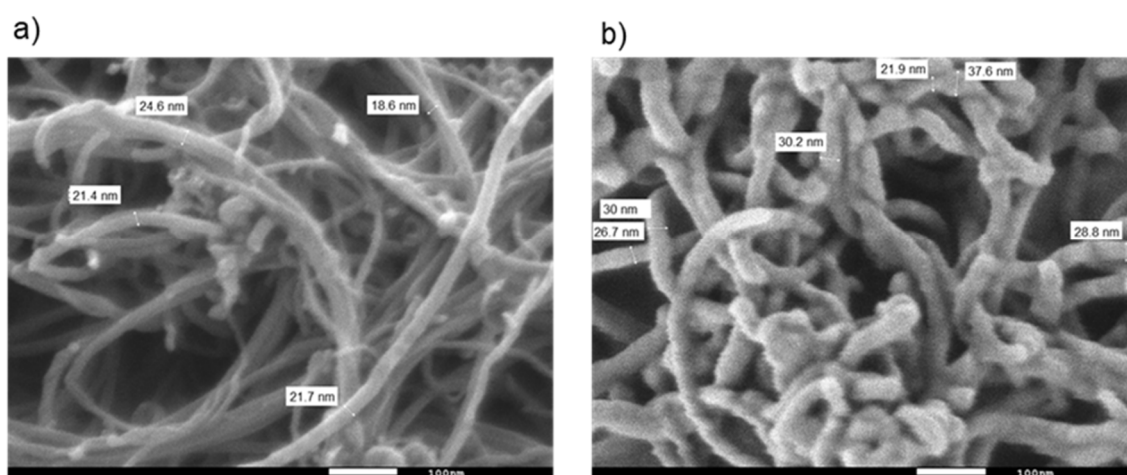
Figure 19: SEM images of a) pristine MWCNT and b) MWCNT functionalized with DTMVP (180 kg mol^{-1}) by *Diels-Alder* cyclization.

Another immensely selective immobilization approach is the formation of self-assembled monolayers (SAMs) via the strong affinity of thiol to gold surfaces.[254] With the introduction of the DTDP initiators to REM-complexes, thiol polymer end-groups were introduced to PDEVP and within this work, this procedure was applied to PDTMVP and PDTPVP(see Chapter 4.3.2). As the protic thiol functionality was masked during GTP via a trityl protecting group, this group must be removed before SAM formation. The protecting group was cleaved in a post-polymerization modification via protonation with trifluoracetic acid (TFA) and scavenging of the trityl cation by triethylsilane in quantitative yields. The cleavage was observed by the vanishing of the trityl signals in the corresponding ^{1}H-NMR and the integrity of the polymer chains was not affected as derived via SEC (Figure 20).
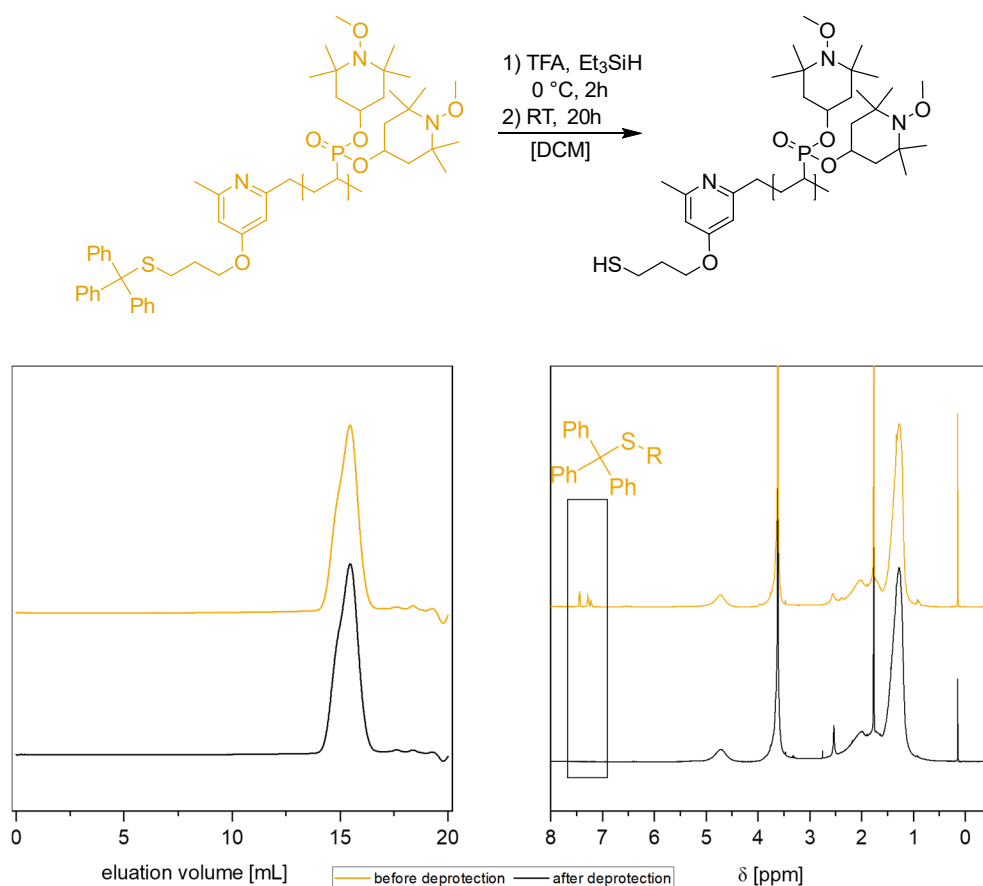
Figure 20: Cleavage of the trityl protecting group, corresponding ¹H NMR Spectra in THF-d8 and SEC traces in THF with the significant regions before (top) and after deprotection (bottom).

The so obtained thiol end-group functionalized PDTMVP and PDTPVP were utilized for the SAM formation on a gold substrate. Therefore, a gold quartz crystal microbalance (QCM) substrate is immersed in a solution (1 mg/mL) of the corresponding thiol end-group containing polymer in THF for 1-2 days. After thoroughly washing of the surface to remove not adsorbed polymer, the decrease in the quartz crystals resonance frequency after functionalization was recorded and the surface functionalization was derived via the Sauerbrey equation:

$$\Delta f = \frac{2 f_0^2}{A \sqrt{\rho_q \mu_q}} \Delta m \qquad (1)$$

Here Δf is the normalized frequency, f_0 the resonant frequency of the fundamental mode of the quartz crystal, A is the surface area, ρ_q is the density of quartz (2.648 gcm^{-3}), μ_q is the shear modulus of quartz (2.947x10^{11} gcm^{-1}s^{-2}) and Δm is the observed mass change. The general Sauerbrey equation can therefore be simplified for the used 5 MHz quartz crystals:

$$\Delta m = -C_{QCM}\, \Delta f \qquad\qquad (2)$$

Where C_{QCM} is the mass sensitivity constant (17.7 ngcm^{-2}Hz^{-1}). Here for PDTMVP and PDTPVP a linear increase with increasing degree of polymerization was observed, consistent with the formation of a self-assembled close packed polymeric monolayer.

4.5 Deprotection of DAVPs

4.5.1 Oxidative elimination deprotection

Blinco *et al*. recently reported on the oxidative cleavage of methoxyamine moiety to generate defined TEMPO radical functionalized PTMA.[111] As oxidant, a peracid was utilized to generate an *N*-oxide and the subsequent deprotection follows a Cope-type mechanism (Scheme 15). In a preliminary study for the deprotection of methoxyamine protected PDTMVP, various peroxy species such as peracetic acid, performic acid, *tert*-butylhydroperoxide and *meta*-chloroperbenzoic acid, and other oxidants like dimethyl dioxirane were tested. However, solely *m*CPBA yielded observable radical generation, as indicated by the emerging of a strong orange coloring of the reaction solution.

Nevertheless, in this preliminary study, *m*CPBA showed to be an inseparable impurity of such prepared organic radical polyvinylphosphonates (Scheme 57). For secondary amine (R_2NH) systems an over-oxidization of the nitroxide radical into an oxoammonium group ($R_2^+N=O$) with increased reaction times was already reported.[66] This over-oxidation is attributed with an increase in polydispersities and lower radical yields frequently observed for ORPs generated by peracids.[131] To optimize the oxidative deprotection of high molecular-weight PDTMVP and to maintain narrow molar mass distributions, the influence of different equivalents of *m*CPBA and reaction time on the deprotection of methoxyamine were studied (Figure 21). Therefore, the generation of the radical species of PDTMVP (202 kg mol^{-1}) was quantified by in situ EPR spectroscopy (Figure 21 a). The herein appointed equivalents correspond to the methoxyamine protecting groups (two per repeating unit).
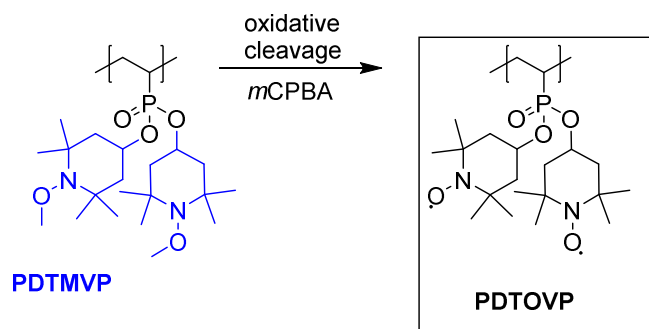
Scheme 57: Oxidative deprotection of PDTMVP to generate radical polyvinylphosphonate.

Regardless of the stoichiometric ratio, a fast increase in conversion occurred, followed by constant conversion values. While for 1.5 eq. *m*CPBA a maximum conversion of 45%

was reached after 30 minutes, 3 eq. led to a quantitative conversion of 99% within 75 minutes. For high excess of *m*CPBA (4.5 eq.), a maximum of 93% conversion was observed 10 minutes after addition, but the value steadily decreased to a final value of 90%. This decrease in conversion was induced by over-oxidation of TEMPO radicals to oxoammonium cations as indicated by ATR-FTIR spectroscopy (Figure 21 b). Only PDTMVP that was oxidized by 4.5 eq. *m*CPBA, exhibited a characteristic $^+$N=O band at 1540 cm^{-1}, while the IR spectra of PDTMVP oxidized with fewer equivalents showed no observable signals in this region.
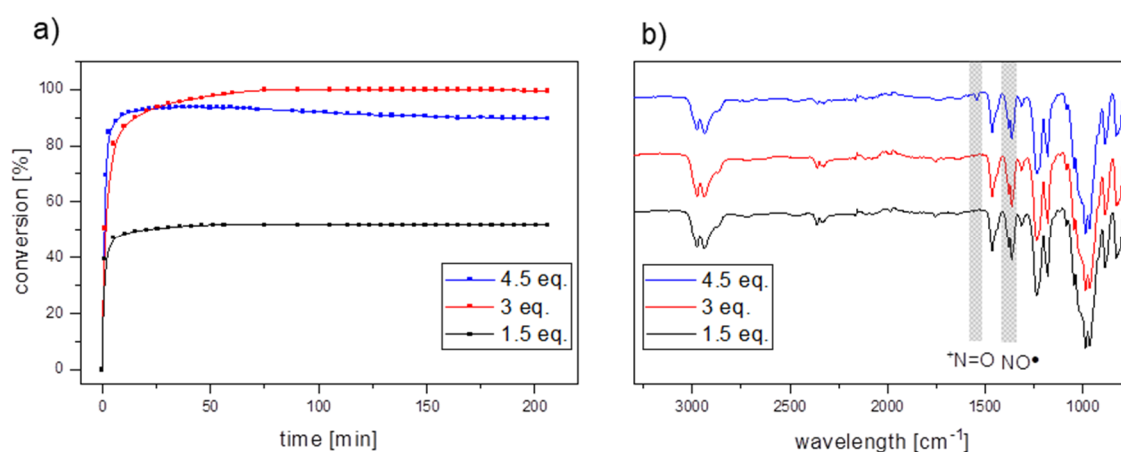
Figure 21: a) Time-conversion plot for the oxidative deprotection of PDTMVP (202 kg mol^{-1}) using different equivalents of *m*CPBA (1.5, 3, and 4.5) with respect to methoxyamine groups. Conversions are determined with an EPR calibration curve based on 4OH-TEMPO (Figure S1). b) Corresponding normalized ATR-FTIR spectra after workup of the polymers from (a); the band at 1360 cm^{-1} is associated with nitroxide radical (N−O$^•$) while the signal at 1540 cm^{-1} is associated with oxoammonium cation ($^+$N=O).

The PDTOVP prepared with 3 and 4.5 eq. *m*CPBA were analyzed by SEC after work-up and the radical yield was determined by EPR and UV-Vis analysis (Figure S1 and Figure S3). The radical yields for the deprotection with 3 eq. of *m*CPBA were consistent with conversions obtained by the in situ EPR experiment. Unchanged molecular weight distributions before and after deprotection demonstrated the structural integrity of the polymer chains and the absence of cross-linking or backbone degradation (Table 8). For the polymer deprotected with 4.5 eq. *m*CPBA, the radical yield is 7% lower than estimated by in situ EPR measurements. Additionally, the radical yield of the corresponding radical-containing polymer could only be derived by EPR, as strong light scattering affected the UV-Vis measurement. SEC analysis revealed a broad and bimodal molecular weight distribution (Table 8, entry 6) with increased molar masses above the limit of the SEC calibration. These observations indicated a crosslinking or agglomeration induced by over-oxidation if using high excess of *m*CPBA.

The optimized deprotection was additionally tested with different molecular weight PDTMVPs ranging from 18.7 to 500 kg mol^{-1} (Table 8). For the lower M_n polymers, almost quantitative deprotection was achieved. For the highest molecular weight PDTMVP (500 kg mol^{-1}), a deprotection yield of 96% was determined. The slight decrease in radical yield could be explained by coiling of the polymer chains resulting in an inaccessibility of the oxidant to the entangled inner methoxyamine protecting group. The structural integrity of the deprotected polymers was shown by similar values for Đ before and after deprotection for PDTPVPs up to 202 kg mol^{-1}. Higher molecular weight DTOVP could not be analyzed due to insolubility in the SEC eluent (DMF) or other SEC eluents (THF, chloroform, 1,3,5-trichlorbenzene).

Table 8: Deprotection of PDTMVP via oxidative cleavage induced by mCPBA[a]

Entry	M_n	Radical conc. UV	Radical con. EPR	Đ$_{before}$	Đ$_{after}$
	[kg mol^{-1}]	[%][b]	[%][c]	[-][d]	[-][d]
1	18.7	99.1	98.8	1.34	1.26
2	27.0	98.2	98.2	1.31	1.30
3	59.2	98.5	97.8	1.25	1.33
4	133	98.6	97.8	1.31	1.34
5	202	97.8	97.8	1.3	1.32
6[e]	202	n.d.	83.1	1.3	2.31
7	307	96.5	96.8	n.d.	n.d.
8	500	96.1	95.8	n.d.	n.d.

[a] Reactions performed with 0.56 mol PDTMVP and 3 equivalents of mCPBA in 60 mL DCM; conversions determined by [b] UV-Vis analysis and [c] EPR analysis in NMP with TEMPO based calibration curves (Figure S1 and Figure S3). [d] determined via SEC in DMF at 30 °C relative to PMMA; [e] reaction performed with 4.5 equivalents of mCPBA.

To further analyze the purity and chemical composition of the radical PDTOVPs, elemental analyses were performed. While consistency of theoretical and measured values highlights the controlled deprotection with 3 equivalents mCPBA, increased carbon and decreased nitrogen values for 4.5 eq. indicate the occurrence of impurities. This can be attributed to the occurrence of positive charged oxoammonium species, which must be compensated by a counterion to ensure charge neutrality. Likely,

generated benzoic acid during deprotection or perbenzoic acid serve as counter-anion. For samples with high amounts of impurities as determined by EA, IR measurements indicated such carbonate species ($\approx$1700 cm^{-1}) with their distinctive band as one of the main byproducts.

4.5.2 Thermolytic homolysis of DAVP

The phenylethoxyamine motif is, due to its selective and fast temperature-induced homolytic cleavage of the NO-C bond, one of the most applied initiators in nitroxide-mediated polymerizations.[68] This concept was transferred to a thermal protection motif for the synthesis of ORPs by Behrends *et al.*[107] The deprotection was shown to proceed byproduct-free with almost quantitative radical yields and more significantly, without the use of auxiliary oxidizing agents. The effectivity of the herein synthesized thermocleavable phenylethoxyamine protected polyvinylphosphonate (PDTPVP) was studied regarding the deprotection rate and activity (Scheme 58).
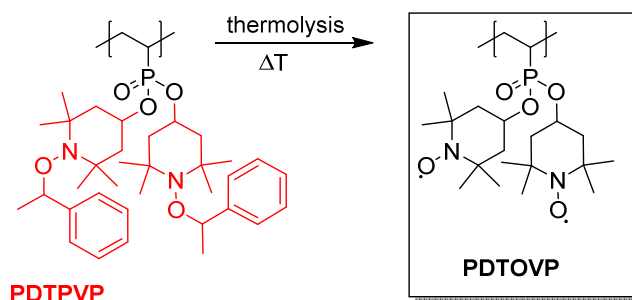
Scheme 58: Thermolysis of the PDTPVP to generate radical polyvinylphosphonate.

Therefore, PDTPVP (59.4 kg mol^{-1}) was dissolved in *tert*-butylbenzene (*t*Bu-benzene) or mesitylene (10 mg/mL), saturated with oxygen by sparging with air for 30 min, and heated to 135 °C. Reaction aliquots were taken from the reaction mixture after different time intervals and the respective conversions were analyzed with EPR and UV-Vis measurements.

For both reaction solvents, a fast increase in conversion was followed by a region of linear increase (Figure 22). However, while deprotection in *t*Bu-benzene reached full radical conversion after 8 hours, for mesitylene only a deprotection rate of 36% was observed. Two different phenomena can be considered to induce this behavior: The first assumption includes a better stabilization of the generated phenylethyl radical in mesitylene, resulting in the recombination of adjacent TEMPO radical and the cleaved phenylethyl radical to generate the phenylethoxyamine precursor in an equilibrium reaction and thus inducing the incomplete conversion. The second hypothesis includes the formation of radical solvent species, at which aromatic radicals were already shown to accelerate the temperature induced decay of the TEMPO radical via the formation of the instable nitrogen radical (anthrone) and tetramethylpiperidine.[69] Especially the formation of an aromatic radical is consistent with the different behavior of mesitylene

and *t*Bu-benzene, as mesitylene is able to stabilize a radical species more sufficiently and thus decay the formed TEMPO radical.

Additionally to these studies, polydispersities were measured via SEC for deprotection reactions in *t*Bu-benzene. Aliquots obtained over the course of the reaction showed that a high temperature had no detrimental effect on the polymers structure as indicated by unchanged molecular weight distributions of the analyzed aliquots (Figure 22, insets).
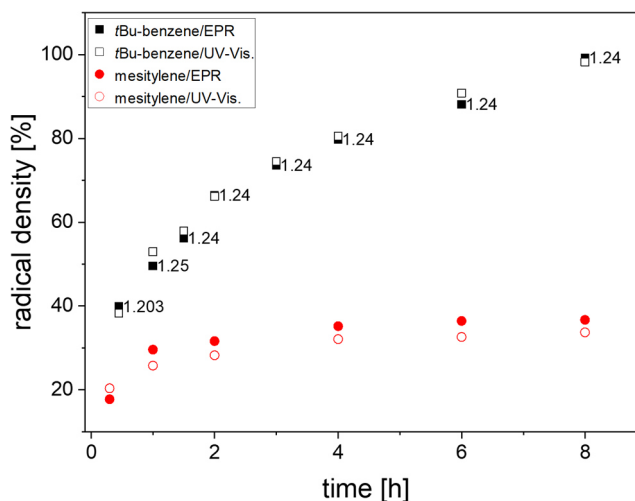
Figure 22: Time-conversion plot for the thermolytic deprotection of PDTPVP (59.4 kg mol^{-1}) in *tert*-butylbenzene (black squares) and mesitylene (red circles). Conversions were determined with an EPR (solid symbols) and UV-Vis (blank symbols) calibration curve based on 4OH-TEMPO (Figure S1 and Figure S3). Insets show for the deprotection in *tert*-butylbenzene the corresponding molecular weight distributions measured via SEC in DMF.

The efficiency of the temperature-induced deprotection was also investigated with different molecular-weight PDTVPs (Table 9). Regardless of their molecular weight, all polymers reached quantitative (99%) radical yield. In addition, their structural integrity was verified by the unchanged molecular weight distributions before and after deprotection.

As the ethylbenzyl protecting group was observed to cleave during thermogravimetric analysis (Chapter 4.6, Figure 29) also a solid-state deprotection approach was applied. Therefore, TGA crucibles were loaded with 20 mg of PDTPVP (59.4 kg mol^{-1}) and an isotherm measurement at the desired temperature (135 °C and 155 °C) performed until a mass loss of 33% - which corresponds to quantitative deprotection – was received. While 33% mass loss was obtained at 155 °C after 10 hours, for the measurement at 135 °C the reaction time was prolonged five-fold and reached the desired mass loss after 50 hours (Figure 23). Surprisingly, side reactions resulting in broadening of

molecular weight distributions often induced by high temperatures were less observed for the solid-state deprotection at higher temperatures (Table 9). The crucial factor inducing side reactions, which resulted in broadening of the polydispersities, was therefore correlated to prolonged reaction time.
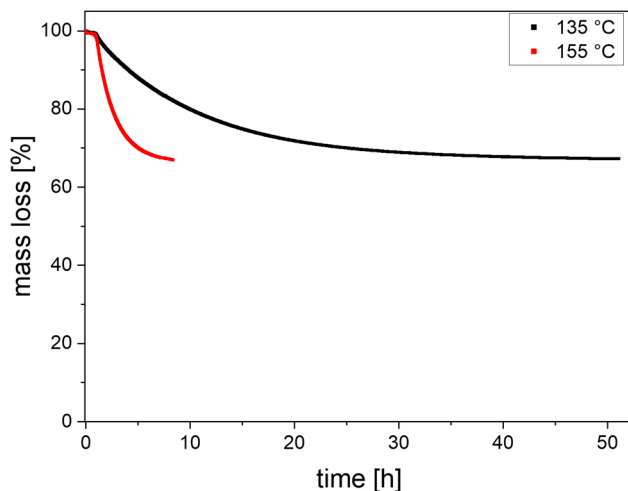
Figure 23: TGA isothermal plots for PDTPVP (59.4 kg mol^{-1}) at 135 °C (black squares) and at 155 °C (red squares).

Nevertheless, the solution-based method is the method of choice for the synthesis of highly defined radical polyvinylphosphonates, while the solid-state method is a convenient method for the synthesis of organic radical polymers on surfaces or applications utilizing solid organic radical polymers. Consistent to PDTOVPs prepared by oxidate elimination of PDTMVP with *m*CPBA, the purities of the radical PDTOVPs prepared by thermolytic cleavage of PDTPVP were additionally analyzed by elemental analysis. The overall consistency of theoretical and measured values highlight the controlled thermolytic deprotection technique, while maintaining the structural integrity of the polymers as also shown by SEC in DMF.

In conclusion, these two different deprotection approaches of alkoxyamine protected polymers, allow for sequential post polymerization modification of the polyvinylphosphonate pendant groups via stepwise nitroxide radical coupling reactions induced by an oxidative or a thermolytic trigger.

Table 9: Deprotection of PDTPVP[a]

Entry	M_n	Method	T	Radical conc. UV	Radical conc. EPR	Đ$_{before}$	Đ$_{after}$
	[kg mol^{-1}]		[°C]	[%][b]	[%][c]	[-][d]	[-][d]
1	33	solution	135	99.2	99.4	1.20	1.21
2	33	solid	155	97.1	96.8	1.20	1.42
3	52.5	solution	135	99.5	98.8	1.24	1.29
4	52.5	solid	135	96.4	97.0	1.24	1.73
5	52.5	solid	155	97.1	97.0	1.24	1.6
6	108	solution	135	99.1	99.0	1.22	1.33
7	108	solid	155	97.7	97.2	1.22	1.55

[a] Reactions performed with 0.56 mol PDTMVP and 3 equivalents of *m*CPBA in 60 mL DCM; conversions determined by [b] UV-Vis analysis and [c] EPR analysis in NMP with TEMPO based calibration curve [d] determined via SEC in DMF at 30 °C relative to PMMA; [e] reaction performed with 4.5 equivalents of *m*CPBA.

4.5.3 Electrochemical deprotection DAVP

The electrochemical deprotection approach is based on the work by Coote and coworkers, who applied alkoxyamines in an electrochemical induced alkylation of various carbonic acids in the presence of a base.[243] The authors suggested a reaction mechanism involving the oxidation of the alkoxyamine (E_R) followed by a chemical irreversible reaction (C_{irr}) leading to the alkylated species and the TEMPO radical (E_R) as a byproduct, resulting in the overall $E_R C_{Irr} E_R$ mechanism as observed via CV. This led to the motivation to utilize this kind of electrochemical reaction as a novel deprotection technique for the herein synthesized alkoxyamine protected polymers PDTMVP and PDPVP. An electrochemical deprotection approach could prove extremely beneficial for the synthesis of organic radical polymers: Zhang and coworkers could show in one of their reports that the formation of oxoammonium ions ($^+N=O$) by overoxidation leads to some kind of doping mechanism (p-type doping) enhancing the intrinsic electrical charge conductivity.[78] Nevertheless, as already discussed in the case of a chemical oxidant like *m*CPBA these overoxidation simultaneously induces crosslinking, presumably due to ionic interactions between different polymer chains (see Chapter 4.5.1). Furthermore, the use of *m*CPBA led to benzoate and perbenzoate as counterions of the oxoammonium cations as indicated by IR spectroscopy (see chapter 4.5.1 and Figure 21) which is assumed to lower the overall charge conductivity due to its high steric bulk and the thus increased radical-radical distance.

Herein, an electrochemical deprotection could serve as a more generally adaptable technique, allowing the use of different counterions (Cl^-, PF_6^-, ClO_4^-, NO_3^-, etc). In addition, this approach has a better efficiency from an economic point of view, not only compared to the approach utilizing a chemical oxidant, for which a high excess of *m*CPBA is applied (3 equivalents), but also in the case of the thermal deprotection approaches depending on high temperatures for prolonged reaction times. However, the most striking advantage of this approach is a control of the ratio between nitroxide radical and oxoammonium cation, thus enabling to control the degree of cation doping, which was already shown by Zhang and Coworkers to have a severe impact on the intrinsic electric charge conductivity.[78]

To gain a fundamental understanding on the influence of the electrolyte and the utilized electrochemical setup instead of polymers - which show broad and low signals in voltametric analytic techniques due to the slow diffusion (see Randles-Sevcik

equation[255]) – the alkoxyamine monomers DTMVP and DTPVP were utilized as model compounds for initial reaction optimization.

Surprisingly, if the methoxyamine DTMVP and the non-coordinating electrolyte combination of acetonitrile (MeCN) and tetrabutylammonium hexafluorophosphate (TBAPF$_6$) was chosen, a highly reversible redox reaction of the methoxyamine (E$_R$) was observed instead of an electrochemical irreversible E$_R$C$_{Irr}$E$_R$ reaction (Figure 24 a).
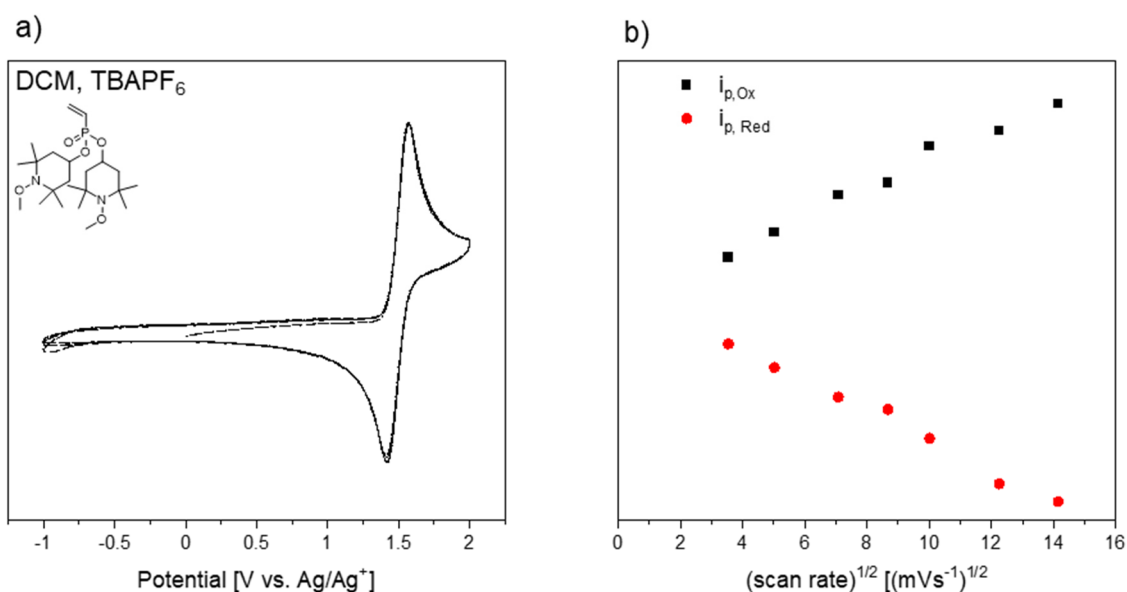
Figure 24: a) Cyclic voltammogram of DTMVP in DCM with 0.1 M TBAPF$_6$ at 250 mV/s with an Ag/Ag$^+$-reference electrode and b) plot of the i$_{p,Ox}$ (black) and i$_{p,Red}$ (red) against the square root of the corresponding scan rate.

The plot of the oxidation peak maximum (i$_{p,Ox}$) and reduction peak minimum (i$_{p,Red}$) against the square root of the scan rate showed - similar to the radical DTOVP (Figure 13) - a linear correlation, demonstrating extremely fast redox kinetics only limited by diffusion. Furthermore, the equal absolute values for the slopes highlight the reversibility of the redox process for the methoxyamine functionalized DTMVP. However, the standard potential was distinctively shifted compared to the radical TEMPO (0.72 V (vs. Ag/Ag$^+$) to an increased potential of 1.49 V (vs. Ag/Ag$^+$), while maintaining a narrow peak-to-peak separation of 0.14 mV. This is the highest reversible redox potential reported for an organic molecule and, in combination with the observed fast-redox kinetics, TEMPOMe could emerge as a novel organic redox battery material. The utilization of this promising active material in an electrochemical cell would result in a raised cell potential, and therefore lead to a further increase in the battery's electric power.

However, a switch in the alkoxyamine substituent from methyl to the ethylphenyl moiety (DTPVP) resulted in complete inverse CV traces. While the oxidation of the corresponding phenylethoxyamine was clearly visible (E_R) in the corresponding CV, a reversible reduction was not observed and a new reversible redox signal at a potential of 0.7 V (vs. Ag/Ag$^+$) emerged. This can be attributed to the reversible redox process of the TEMPO radical (E_R) and thus this electrochemical induced reaction followed an ideal $E_R C_{Irr} E_R$ mechanism of C–O cleavage.[255] This suggests that alkyl substituents that are able to sufficiently stabilize a charged or a radical species – similar to the thermolytic deprotection approach which is only possible with this kind of stabilizing alkyl substituents (see chapter 4.5.2) – are able to undergo a $E_R C_{Irr} E_R$ mechanism, without the need of further reactants. This assumption was confirmed by the group of Coote, who reported on the effect of different alkyl substituents on the electrochemical cleavage of alkoxyamines.[244] In this comprehensive study supported by DFT calculations, the kinetics of fragmentation were studied, revealing the highest fragmentation kinetics of a purely alkyl substituent for the herein applied phenylethoxyamine. Hetero-alkoxyamine substituents like oxazolone or methyl ester analogs showed even faster NO-C cleavage kinetics, however in the context of REM-GTP the compatibility of this coordinating groups is uncertain and this protecting groups were therefore not applied in the context of this work.
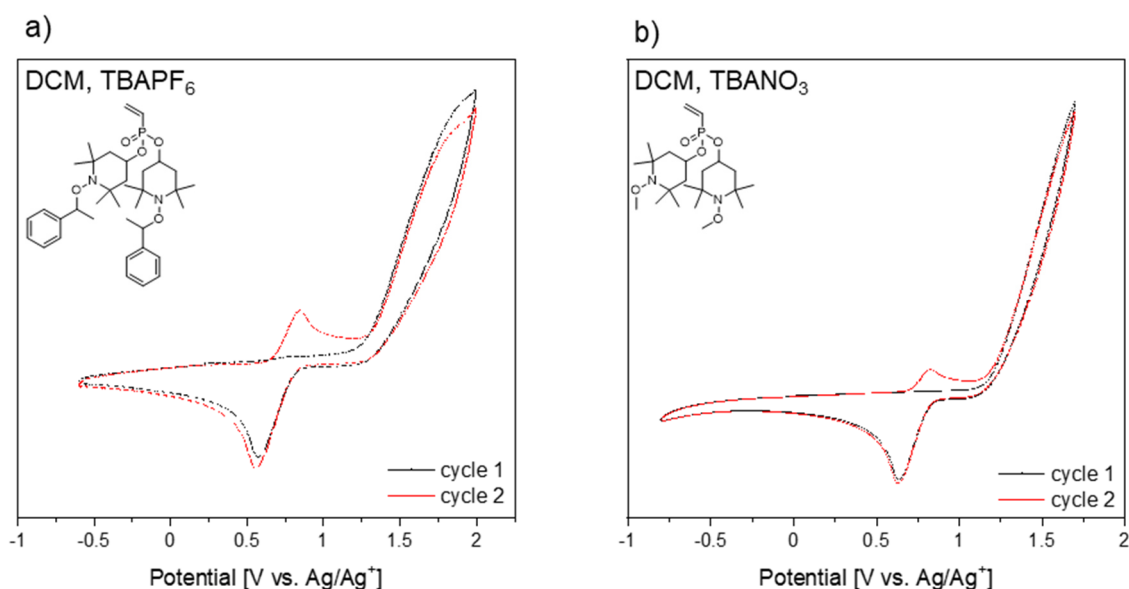
Figure 25: a) Cyclic voltammogram of DTPVP in DCM with 0.1 M TBAPF$_6$ at 250 mV/s and b) of DTMVP in DCM with 0.1 M TBANO$_3$ at 250 mV/s both with an Ag/Ag$^+$-reference.

While the phenylethoxy moiety itself is a sufficient electrochemical protecting group, methoxyamine deprotection is dependent on further electrophilic reaction partners to which the charged nucleophilic methyl can be transferred onto. As the initial approach by Coote *et al*. utilized pyridine bases and carbonic acids, different combinations of these reactants for the electrochemical deprotection of methoxyamine were tested. Surprisingly, a simple switch in solvent from non-coordinating DCM to THF or DMF already showed some generation of nitroxide radical without the need of additional reaction partners. Similarly, by variation of the non-coordinating PF_6^- to ClO_4^- or NO_3^- as electrolyte counterion in DCM, a successful electrochemical deprotection of methoxyamine was also observed as indicated by CV measurements (Figure 25 b). This resulted in an optimized combination of a coordinating solvent (THF or DMF) and coordinating electrolyte ($TBANO_3$ or $TBAClO_4$).

Since only minimal amounts of analyte in the diffusion layer at the working electrode are converted in the cyclic voltammetry measurement setup, voltametric bulk techniques were applied for the synthetic deprotection approach. In general, two different setups (Figure 26) are available: In the undivided cell setup, working and counter electrode are in the same compartment, whereas in the divided setup counter and working electrode are separated by a membrane (Nafion®), a salt bridge or a porous glass frit. In general, a divided cell setup features lower reaction times, however, due to the unseparated electrode at the counter electrode the reverse redox reaction takes place. In some cases, this is utilized as a benefit or even required: During *Shono* oxidation, the working electrode is used for oxidation of carbamates and simultaneously alcohols are reduced at the counter electrode, yielding nucleophilic alcoholates to generate the desired *N,O*-acetals. As TEMPO radicals can be reduced electrochemically irreversible to aminoxyl groups (≈ -1.0 V), a scavenger like methanol or carbonic acid was applied for the electrochemical deprotection in an undivided cell setup. This scavenger was reduced instead of the generated TEMPO radical and can additionally serve as an electrophile partner for the electrochemical generated nucleophilic alkyl species and thus accelerate the electrochemical deprotection.
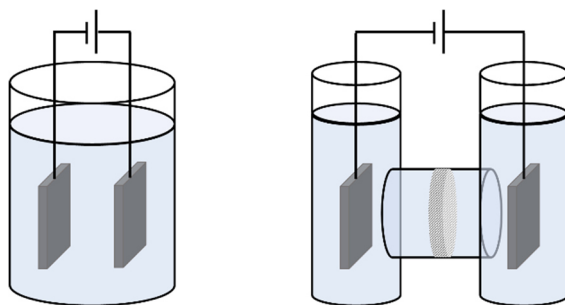
Figure 26: Schematic bulk electrolysis setups: left undived cell setup, right divided cell setup.

The synthetic electrochemical deprotection of methoxyamine was studied with $TBANO_3$ as electrolyte, different solvents (DCM, MeCN, THF, DMF) and scavengers (none, MeOH, formic acid, pyridine). The voltametric bulk steps were adapted from results derived via CV: The working electrode was set to a potential of 1.5 V (vs. Ag/Ag^+) for one hour inducing the E_RC_{Irr} reaction, yielding a mixture of TEMPO radical and oxoammonium cation as indicated by aliquot IR measurements. Full conversion of alkoxyamine is indicated by the absence of the corresponding oxidation currents after this first bulk oxidation step. Afterwards, the oxoammonium cations were reduced to TEMPO radicals (E_R) by altering the potential of the working electrode to 0 V (vs. Ag/Ag^+) and the radical yield was determined by EPR (Figure S3). However, only low radical yields were obtained with maximum values of 20% for the combination of DCM as solvent and MeOH as scavenger. Due to full conversion of alkoxyamine as derived via vanishing of the corresponding oxidation current in the CV, it can be assumed that the low radical yields were induced by different side reactions of the TEMPO radical species. Unfortunately, it was not possible to elucidate the exact composition of these byproducts, due to a low reactant concentration and the occurrence of a mixture of paramagnetic and diamagnetic species. However, the irreversible reduction of the TEMPO radical to the aminoxyl species is assumed to be the main reason for this low radical yields.

To suppress this unwanted redox side reaction a divided cell setup with a porous glass frit (POR 4) instead of the simple undivided cell was utilized. With this setup, only one distinctive redox reaction takes place in the working electrodes compartment, while in the separated counter electrodes compartment solvent, electrolyte or a scavenger (e.g. ferrocene/ferrocenium) is reduced/oxidized for charge equalization. The advantage of a higher selectivity is often accompanied by longer reaction times.

As only one distinct redox process takes place at the electrode in the reactions compartment, the consumed current of the working electrode enables to derive the conversion of the redox process or even to stop after a set current (corresponding to a set chemical conversion). Therefore, this enables the monitoring of the alkoxyamine deprotection rate and allows the precise adjustment of the TEMPO radical and oxoammonium cation ratio. While the deprotection of the methoxyamine DTMVP resulted in high radical yields (98%) for the electrolyte TBANO$_3$ in DMF or MeCN after a reaction time of two hours (Figure 27 a), the same conversion was observed in DCM after a prolonged reaction time of 16 hours. In difference to this, a maximum in conversion of 45% was recorded in THF as solvent after 16 hours. Similar results were obtained for phenylethoxyamine protected DTPVP (97% conversion in MeCN).
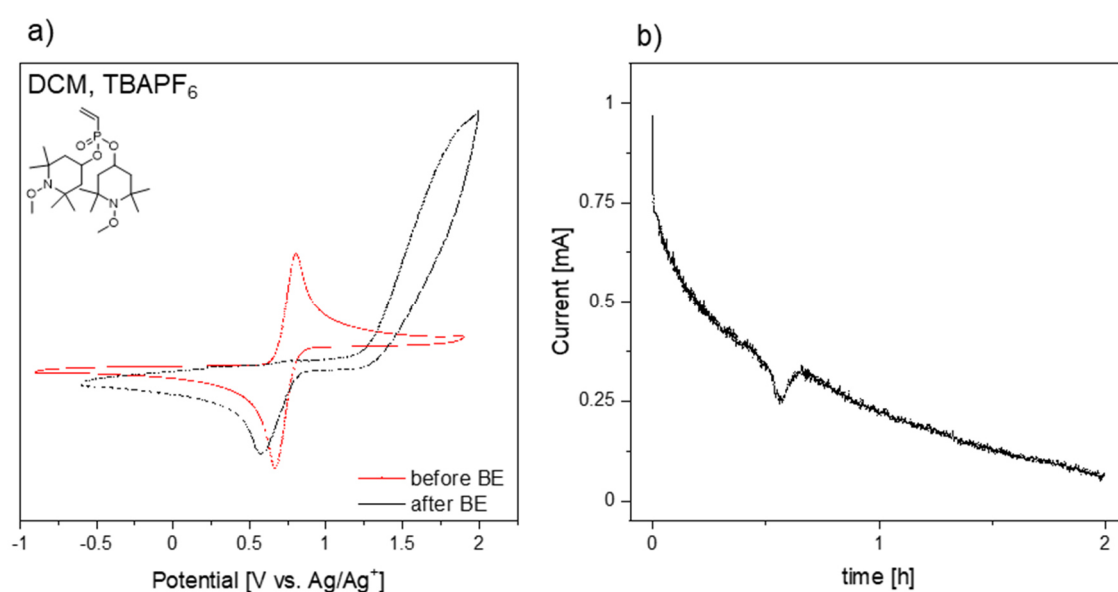
Figure 27: CV traces before (black curves) and after (red curves) electrochemical deprotection of DTMVP in a divided cell setup at a scan rate of 250 mV/s. b) Current time plot for the bulk electrolysis step at constant potential of 1.5 V (vs. Ag/Ag$^+$). All measurements with 0.1 M TBANO$_3$ in MeCN and an Ag/Ag$^+$ reference electrode.

This increased performance of polar solvents is often observed for electrochemical reactions and is attributed to a better polarization of the solvents, enhancing the heterogeneous electron transfer from electrode onto the substrate. Additionally, the different wetting behavior of the applied solvents is assumed to influence this heterogenous process. However, due to the relatively new field of electro-organic synthesis, literature results are often difficult to compare, since the lack of standardized setups (divided, undivided, semi-divided) and the plurality of influences on the reaction conditions (solvent, reactant concentration, ohmic resistance, electrolyte, electrode

97

material, etc). Nevertheless, these results serve as a proof of principle for the general selective electrochemical induced deprotection of alkoxyamines. Unfortunately, the influence of the solvent on the deprotection reaction time and conversion is detrimentally for the electrochemical deprotection of the polymers PDTMVP and PDTPVP, since both alkoxyamine protected polymers were insoluble in the most suitable solvents DMF or MeCN.

Therefore, the electrochemical deprotection of the methoxyamine polymer PDTMVP was performed in DCM. In difference to the monomeric species DTMVP – which yielded full conversion after 16h - only 12% conversion were received for the corresponding polymer PDTMVP (18.7 kg mol^{-1}) after 16 hours, and extended reaction times (up to 24 hours) only lead to a slight increased conversion (14%). This lower conversion of the polymer compared to the small molecule analog can be attributed to the slow diffusion of polymer chains to the electrode surface and in addition to the incomplete heterogenous electron transfer, likely due to inaccessible polymer entanglements.

Since the tool of REM-GTP has already proven to be a potent tool for end-group functionalization and surface immobilization (see chapter 2.4), this feature was extended to the preparation of polymer SAMs on gold QCM and their application as working electrode in the electrochemical quartz crystal microbalance (EQCM) (Figure 28). Experiments studying the electrochemical deprotection of polymer SAMs in the EQCM setup and the utilization of the generated radical thin films as battery material are currently performed in cooperation with the Bandarenka Group, TU Munich. The advantage of this setup is not only the exclusion of reactant diffusion, but also a further in situ technique to monitor the deprotection rate linked to the observed mass loss on the EQCM substrate. The utilization of this setup could evolve to be beneficial for further organic radical thin film applications like (optical transparent) organic radical thin film batteries, sensors detecting radical species, for further surface functionalization by NRC or in analogy to the initial publication as heterogenous electrochemical alkylating catalyst (regeneration by NRC).
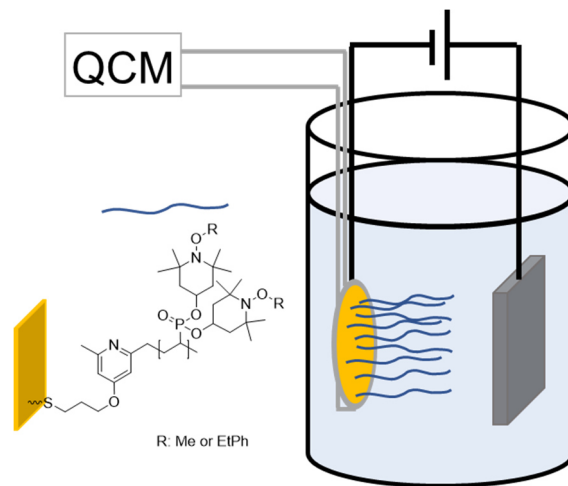
Figure 28: EQCM setup with SAM gold working electrodes generated with thiol end-group functionalized PDTMVP and PDTPVP.

4.6 Thermal analysis of PDTMVP, PDTPVP and PDTOVP

The obtained polymers PDTMVP, PDTPVP, and the radical PDTOVP were analyzed regarding their thermal properties using thermogravimetric analysis coupled with mass spectrometry (TGA-MS), and differential scanning calorimetry (DSC). PDTMVP had - similar to other polyvinylphosphonates - two distinct decomposition steps. The first observed mass loss at 210 °C was assigned to the elimination of TEMPOMe, leading to polyvinylphosphonic acid, which was then decomposed in a second step at a temperature range between 420-700 °C. In contrast to this, three distinct decomposition regimes were observed for PDTPVP, with the first regime in a temperature range between 120-180 °C. With a mass of 104 m/z derived via MS (Figure S4), this can be attributed to a phenylethyl radical species, assigning the first decomposition step clearly to the homolytic cleavage of the phenylethoxyamine NO-C bond. The mass loss of 32.3% for PDTPVP was in excellent agreement with the mass loss corresponding to the thermolysis of the phenylethyl moiety (theoretical mass loss 33%). The second and third regimes were consistent with the results obtained for PDTMVP, attributed to the cleavage of the TEMPO radical pendant side group (onset 190 °C) and the decomposition of the PVPA backbone. The radical PDTOVPs, generated by oxidative deprotection or thermolysis, showed a similar behavior, consistent with the cleavage of the TEMPO radical starting at 190 °C and a mass loss of about 73% (theoretical mass loss 74%). The decomposition of the polyvinylphosphonic acid backbone was not affected by the TEMPO side group. Since DSC analysis showed no detectable change in heat capacity in the scan range (-150 to 175 °C for PDTOVP and PDTMVP, -150 to 100 °C for PDTPVP), no melting or glass transition temperatures could be determined. This is consistent with other polyvinylphosphonates, which also lack observable melting or glass transitions temperatures, only with the exception of highly isotactic PDEVP (P_m = 0.90), featuring a melting temperature of 18 °C.[241] The absence of visible melting temperatures indicates complete amorphous polymers, which could be beneficial for application as electrical charge conducting organic radical polymers or thin film applications.
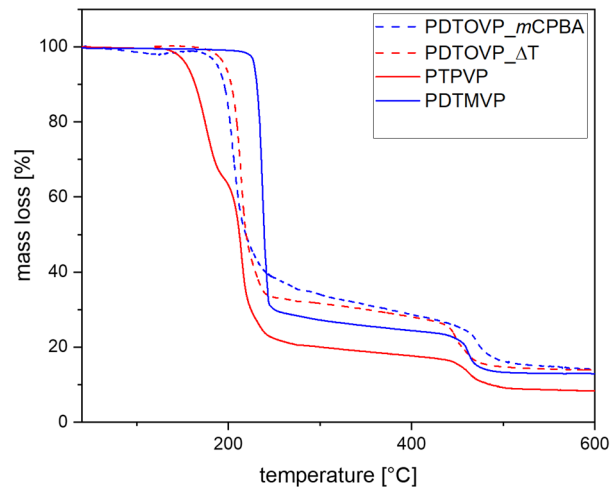
Figure 29: TGA plots for PDTMVP (blue), PDTPVP (red) and PDTOVP received by oxidative deprotection (blue dashed) and by thermolytic deprotection (red dashed). All measurements performed with a heating rate of 1 Kmin^{-1}.

4.7 PDAVPs as novel redox-active materials for organic radical batteries

For the general applicability of the generated radical polyvinylphosphonates as redox active materials for various energy applications, their fundamental standard potentials as well as their redox kinetics were investigated by CV measurements (Figure 30 a). With a standard potential of 0.73 V (vs Ag/Ag$^+$), the redox behavior of the TEMPO radical side group was not affected by the attachment onto the PDAVP backbone or the applied deprotection technique. The higher signal intensity of the PDTOVP prepared by oxidative deprotection (M_n = 27.0 kg mol^{-1}, red trace) compared to the one generated by thermolysis (M_n = 52.5 kg mol^{-1}, blue trace) is attributed to the faster diffusion of shorter polymer chains to the working electrode. Furthermore, the fast redox kinetics of the TEMPO radical were not affected by attachment of TEMPO to the vinylphosphonates backbone as indicated by the linear correlation of the plot of the oxidation peak maximum ($i_{p,Ox}$) and reduction peak minimum ($i_{p,Red}$) against the square root of the scan rate (Figure 30 b) (redox kinetics only limited by diffusion). In addition, the equal absolute values of the slopes underline the highly reversible redox behavior, mandatory for battery applications to enable repeated charging/discharging as well as long cycle lifetimes.
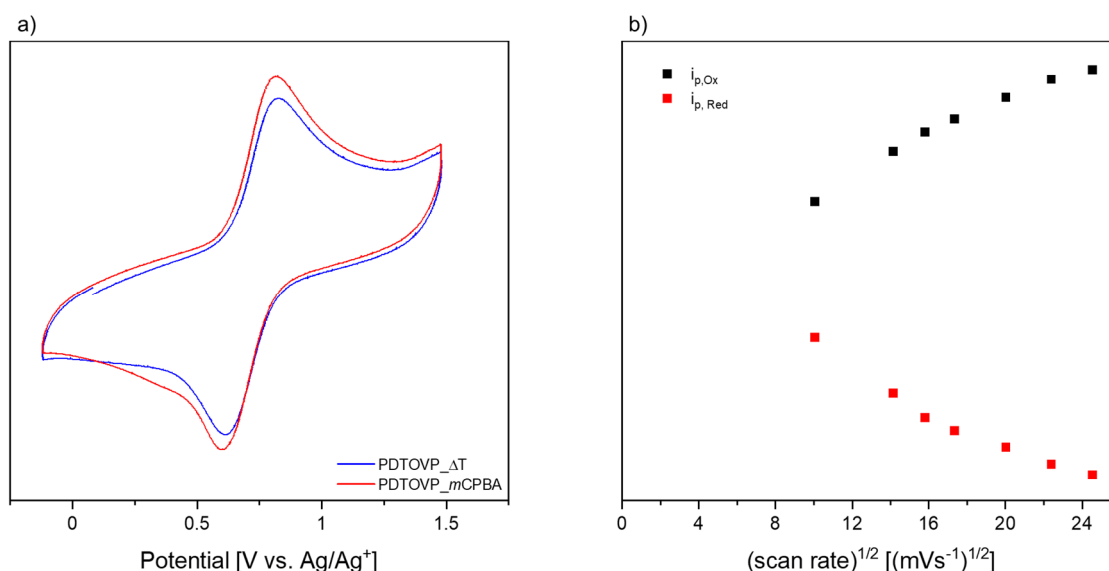
Figure 30: a) Cyclic voltammograms of the radical PDTOVPs in 5 mM DCM solution with 0.1 M TBAPF$_6$; scan rate 100mV/s, E°(V vs. Ag/Ag$^+$) = 0.73 V. The blue trace represents PDTOVP prepared by oxidative deprotection of PDTMVP (27.0 kg mol^{-1}) by mCPBA, the red traces PDTOVP by temperature-induced homolytic cleavage of PDTPVP (52.5 kg mol^{-1}). b) plot of the $i_{p,Ox}$ (black) and $i_{p,Red}$ (red) for PDTOVP prepared by oxidative elimination of PDTMVP (27.0 kg mol^{-1}) against the square root of the corresponding scan rate.

As organic radical polymers do not feature sufficient electric conductivity for the utilization as pristine electrode material in organic radical batteries, ORP composite electrodes with charge conductive additives were prepared. Commonly, electric conducting carbon materials like vapor grown carbon nanofibers (VGCF) or spherical carbon in combination with a binder which enhances the mechanical stability were utilized. To ensure an ideal homogeneous distribution of the radical PDTOVP (M_n = 106 kg mol^{-1}) and the carbon support, water or NMP dispersions were prepared through planetary mixing and coated on an aluminum current collector via the doctor blade method. The homogeneity of this composite electrodes was analyzed by scanning electron microscope (SEM). While the composite electrodes prepared from the water dispersion yielded isolated polymer flakes on the VCGF support (Figure 31 a), the electrodes prepared via NMP dispersion showed a more homogenous polymer distribution, with a thin polymer film covering the carbon nanotubes (Figure 31 b). This better distribution was consistent with the solubility behavior. While the radical polyvinylphosphonates were fully dissolvable in NMP, water led only to partial gelation of the polymers. In addition, NMP is a more suited solvent for CNT exfoliation and therefore more homogeneous composite electrodes could be generated with this slurry combination.
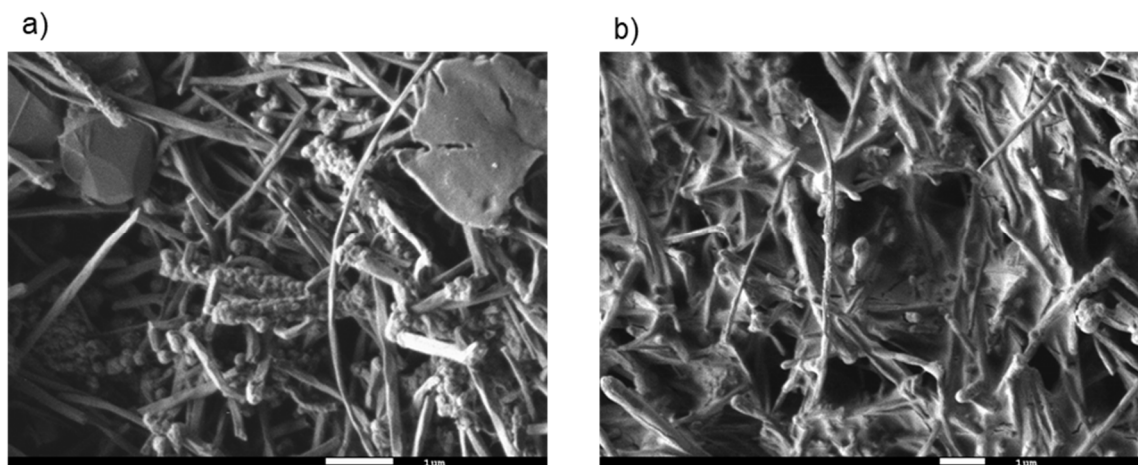
Figure 31: SEM images of the radical polyvinylphosphonate VCGF composite electrodes prepared by a) a water-based coating and b) a NMP-based coating.

To examine the influence of the homogeneous distribution of the redox active PDTOVP on the organic radical battery performance, coin cells with composite electrodes from the water or NMP slurry were prepared. For the respective cycling test with a C-rate of 1 (corresponds to 1 hour for a full charge/discharge), the NMP based composites electrodes revealed with 40% of the theoretical capacity nearly twice the values

observed for the water-based electrodes (20% of the theoretical capacity) (Figure 32 a). This is consistent with the results obtained via SEM; the better attachment of the redox active PDTOVP to the carbon support for NMP based electrodes led to a better overall electric charge conductivity. Besides electric charge conductivity, another key prerequisite is the diffusion of electrolyte to compensate the charge of the generated oxoammonium cation ($^+$N=O). This ion diffusion to the redox active centers is assumed to be faster for the more homogeneous distributed NMP based electrodes than for the water-based electrodes with bigger redox active polymer particles. However, the electrodes prepared from the NMP slurry suffered from higher capacity fading for the repeated charge/discharge cycling at 1 C compared to the water-based electrodes. Capacity fading is an often-observed issue for organic radical batteries, unfortunately the exact reason for this is so far not sufficiently understood. A widely supported theory attributes the capacity fading to a (partial) dissolution of the redox active polymer in the electrolyte (ethylencarbonate/dimethylcarbonate 7/3 with 1 M LiPF$_6$), while newer investigations supported by neutron scattering measurements assume agglomeration of the polymer, resulting in inaccessible redox sites.[48, 131, 205]
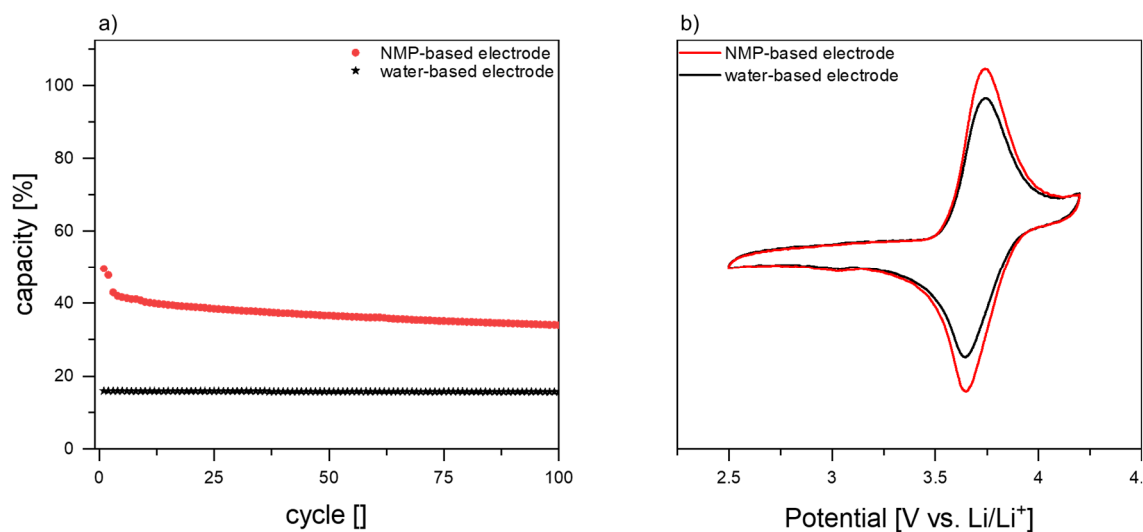
Figure 32: a) Cycling at 1 C of the half-cells prepared form radical polyvinylphosphonates from a water-based coating (black stars) and NMP based coating (red dots). b) Cyclic voltammograms of the half-cells from a water-based coating (black line) and NMP based coating (red line) at a scan rate of 10mV/s, E°(V vs. Li/Li$^+$) = 3.65 V.

Furthermore, capacity loss in general can also be attributed to electrochemical induced degradation of the redox active material. As the cyclic voltammetry analysis revealed for both composite electrodes solely the expected reversible redox signals of the TEMPO radical at 3.65 V (vs. Li/Li$^+$) (Figure 32 b) and no observable irreversible currents

in the charging/discharging potential range (2.5-4.2 V vs. Li/Li$^+$), electrochemical degradation was excluded for the radical polyvinylphosphonates.

To analyze capacity fading induced by dissolution in the electrolyte, coin cells were dissembled after the charge/discharge cycling experiments and the battery electrolyte transferred to EPR analysis. Despite the immense sensitivity (µmol) of the EPR technique, no radical species were detected and thus capacity fading due to solubility issues can be neglected. Therefore, the main issue for capacity fading was assumed to be induced by agglomeration of the radical polymer chains or unknown loss/inactivity of redox active centers.

To further study the impact of molecular weight on the perspective battery performance, composite electrodes with varying molecular weight (M_n = 50-312 kg mol^{-1}) based on the better suited NMP dispersion method were prepared (Figure 33 a).
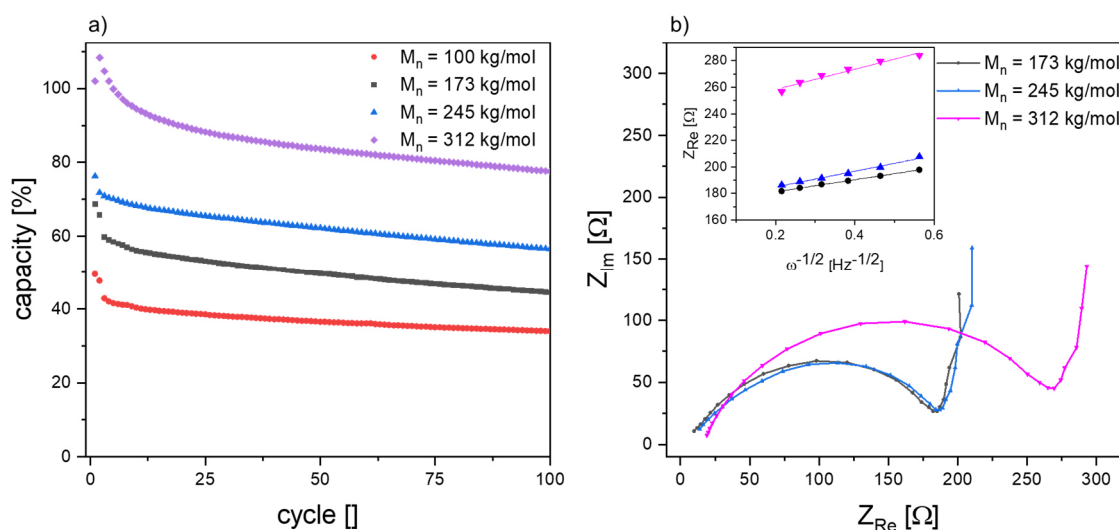
Figure 33: a) Cycling at 1 C of the half-cells prepared form radical polyvinylphosphonates with varying molecular weight (M_n = 50-312 kg mol^{-1}). b) Nyquist impedance plots of the corresponding half-cells before the cycling test. Inset shows the plot inverse square root of the frequency ($\omega^{-1/2}$) against the real part of the impedance (Z_{re}) at low frequencies to derive R_{CT} and the ionic diffusion of electrolyte to redox-active centers.

Independent of the molecular weight, a strong capacity fading of up to 15% was observed for the initial charge/discharge cycles, followed by regimes with constant values or only slight capacity decreases. One effect inducing the initial capacity fading is attributed to the formation of the electron consuming reducing of electrolyte to the solid electrolyte interface (SEI). This is consistent with the discrepancy of charge and discharge capacity observed in the first cycles, as derived for the first charge discharge cycle of the half-cell utilizing PDTOVP with a molecular weight of 312 kg mol^{-1}. For this

half-cell, the first discharge capacity was 12% higher than the corresponding charge capacity and with 112% even higher than the calculated theoretical capacity. As the SEI build-up only affects the initial cycles, other effects induce the exponential decrease in capacity until the nearly constant regimes. This exponential decrease was additionally affected by the different molecular weight of the redox active PDTOVP. While the decrease for the longest molecular weight polymer (312 kg mol^{-1}) was monitored over 15 cycles, this process was accelerated for the shorter M_n polymers and only lasts up to 5 cycles (Figure 33 a). Furthermore, half-cells based on higher molecular weight radical polymers revealed a better agreement of the theoretical and measured capacities. This dependency is consistent with the literature, often observing similar trends.[52, 55, 57, 116, 130, 131] However, as already described these effects are not fully understood. Therefore, to gain further insights additionally to the cycling tests potentiostatic electrochemical impedance spectroscopy (PEIS) were performed (Figure 33 b).

The thus derived Nyquist plots showed the characteristic semi-circle of a charge transfer control region and the linear slopes of a diffusion-controlled regime (Warburg Impedance). The initial intercept with the real part of the impedance (Z_{Re}) in the high frequency region (corresponding to low impedances) represents the resistance of the electrolyte (R_e). Since this was only determined by the utilized electrolyte (EC/DMC 7/3 with 1 M LiPF$_6$), the values of 12-18 Ω vary only slightly. However, the charge-transfer resistance (R_{CT}), corresponding to the intercept of the semicircles at low frequencies, revealed an observable increase in R_{CT} for electrodes prepared from higher molecular weight radical PDTOVP. The exact value was derived from the plot of the inverse square root of the frequency ($\omega^{-1/2}$) against the real part of the impedance (Z_{re}) at low frequencies (<14 Hz) (Inset Figure 33 b). While the intercept of Z_{Re} produces the R_{CT} value, the slope of this plot allows calculation of the ionic diffusion of electrolyte to redox active centers via the following equations:

$$D = R^2T^2/(2A^2n^4F^4C^2\sigma^2) \tag{3}$$

$$Z_{Re} \approx \sigma\omega^{-1/2} \tag{4}$$

R is the universal gas constant, T is the Temperature, A is the electrode surface (electrode diameter 15 mm), n is the number of electrons for the redox process (for TEMPO one electron process), F is the Faraday constant, C is the electrolyte

concentration and σ is the Warburg factor, which can be determined by the plot of Z_{Re} over $\omega^{-1/2}$ according to equation (4). The respective values for R_e, R_{Ct} and ionic diffusion are summarized in Table 10.

While the charge-transfer resistance rose with increasing molecular weight of the redox active PDTOVP, the ionic diffusion to the redox active centers decreased. This behavior can be ascribed to different effects: As the smaller molecular weight polymers bear shorter polymer chains, the intrinsic charge transport via electron hopping or charge transfer via the redox reaction of a neighboring radical is accelerated. This is explained by shorter distances of inner sphere radical centers to outer sphere radical centers, resulting in a reduction of the charge transfer and increasing the ionic diffusion. Additionally, longer polymer chains tend to have higher fractions of polymer entanglements thus further decelerating these processes. This is contrary to the charging/discharging results, in which higher molecular weight active materials resulted in a better agreement of the observed and theoretical capacities. According to the PEIS results, redox active centers of shorter polymers were easier susceptible towards the ionic diffusion process and electric currents, therefore allowing faster and more complete redox processes. To investigate a change in ionic diffusion and electric conductivity after the initial cycling at 1 C, additional PEIS were recorded after 100 charging/discharging cycles (Table 10). For the electrodes based on shorter molecular weight polymers, a significant increase in charge transfer resistance and decrease in ionic diffusion were observed, while values for the highest molecular weight (312 kg mol^{-1}) only slightly increased. These observations indicate a stronger tendency of shorter molecular weight polymers to form agglomerates, increasing - due to the increased surface-volume of the agglomerates - the charge transfer resistance as well as the ionic diffusion. Therefore, less radical centers were susceptible during the redox process, thus lowering the received capacities.

Table 10: Effect of molecular weight on the charge-transfer resistance (R_{CT}) and ionic diffusion coefficient (D) before and after 100 cycles at charging rate of 1 C.

Entry	M_n	Cycle[a]	R_e	R_{CT}	D
	[kg mol^{-1}]	[-]	[Ω][b]	[Ω][c]	[cm^{2}s^{-1}][d]
1	173	0	12	172	5.47 x 10^{-12}
2	173	100	13	220	1.32 x 10^{-12}
3	245	0	12	173	3.22 x 10^{-12}
4	245	100	12	225	8.12 x 10^{-13}
5	312	0	18	243	1.95 x 10^{-12}
6	312	100	18	255	1.72 x 10^{-12}

[a] PEIS measurement before or after 100 charge/discharge cycles at 1 C [b] Intercept of the Nyquist plot in the high frequency region [c] Intercept and [d] slope of the plot of Z_{Re} and $\omega^{-1/2}$ in the low frequency region.

For the application as novel battery material, the best performing electrode with the highest molecular weight (312 kg mol^{-1}) was additionally studied with higher current densities, resulting in accelerated charging/discharging times (Figure 34). Therefore, the initial C-rate of 1, corresponding to a full chare/discharge in 1 hour, was stepwise enhanced up to 40 C, lowering the charging/discharging time to only 90 seconds. While the received capacities reach at the lowest C-rate the highest values of up to 81%, at 40 C a capacity of 47% is measured, corresponding to 58% of the initial 1 C value. After utilizing the high current densities, the initial capacities of the corresponding C-rates were restored, indicating a redox process only limited by kinetics without any electrochemical degradation of redox-active or support material at high current densities. In addition, the observed capacity fading was depending on the C-rate: While nearly no capacity fading was observed at high C-rates and additionally the coulombic efficiency was higher than 99%, a slight capacity fading with less ideal coulombic efficiencies was observed for 1 C. Therefore, a time dependent process as main reason for the observed capacity can be concluded and this in combination with the precious results leads to the assumption of agglomeration as process inducing the observed capacity fading.
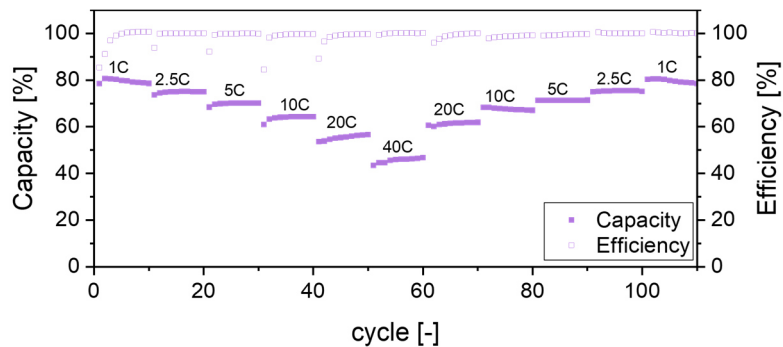
Figure 34: Cycling at various C-rates of the half-cells prepared form radical polyvinylphosphonates with the best performance at the initial C-rate of 1 (M_n = 312 kg mol^{-1}). Filled squares resemble the received capacity, dashed squares the Coulombic efficiency. Inset shows the corresponding C-rate of the corresponding cycle.

5 Summary

The scope of organic radical polymer was expanded to polyvinylphosphonates synthesized via REM-GTP, thus introducing this sophisticated polymerization technique for the synthesis of organic radical polymers. To study the compatibility of this polymerization technique with two different approaches – the direct polymerization of a radical TEMPO monomer and the conversion of a suitable radical precursor– four different functionalized DAVPs were prepared in high yields (75-92%). However, the radical and secondary amine containing DAVP monomer were incompatible with the REM-GTP catalysts, due to inactivation of the REM complex. Nevertheless, alkoxyamine protected TEMPO moieties were susceptible towards REM-GTP. While yttrium-based catalysts were inactive, for catalysts based on lutetium as central metal, highly controlled polymerizations were observed. Activity studies for $Cp_3Lu(thf)$ revealed a TOF* of 277 h^{-1} for methoxyamine protected DTMVP and 86 h^{-1} for the sterically more demanding phenylethoxyamine protected DTPVP, featuring moderate to good initiator efficiencies (50-91%) and narrow molar mass distributions ($Đ < 1.35$). A linear correlation of molecular weight against conversion showed the living character of the polymerization, which enables the straightforward synthesis of functional (block) copolymers. By varying the catalyst-to-monomer ratio, low to high molecular weight polymers based on DTMVP (18.7-500 kg mol^{-1}) and DTPVP (33-108 kg mol^{-1}) were synthesized and the overall narrow polydispersities highlight the controlled polymerization. In an approach to introduce stereoinformation, a novel constrained geometry complex based on lutetium (CGCLu(*sym*-collidine)) was synthesized. However, completely insoluble products for the polymerization of DTMVP with this complex were obtained, impeding further polymer analysis.

The corresponding post-polymerization deprotection of the alkoxyamine protecting groups towards stable TEMPO radicals via oxidative elimination of methoxyamine (PDTMVP) and thermolysis of phenylethoxyamine (PDTPVP) polyvinylphosponates were optimized, regarding radical yield as well as the perseverance of the structural integrity of the polymers. This resulted in almost quantitative deprotection of PDTMVP (96-99%) with 3 equivalents of *m*CPBA over a wide range of M_n (18.7-500 kg mol^{-1}), while simultaneously a small increase in molecular weight distributions was observed. The thermal deprotection of PDTPVP in *tert*-butylbenzene at 135 °C resulted in nearly quantitative radical yields (98-99%) and unchanged polydispersities, while for the solid-state deprotection approach at 155 °C similar conversions (96-98%) in combination

with increased molecular weight distribution were observed. Cyclic voltammetry studies of the small molecule methoxyamine and methoxyamine protected PDTMVP revealed highly reversible redox potentials at 1.49 V (vs Ag/Ag$^+$) for non-coordinating electrolytes, whereas a switch to coordinating electrolytes resulted in electrochemical cleavage of the alkoxyamine to the TEMPO radical via an $E_R C_{Irr} E_R$ mechanism. Different approaches were tested to utilize this method as a new efficient alkoxyamine deprotection technique, receiving promising results for small molecule alkoxyamines. However, for polymeric materials an efficient deprotection failed, due to insolubility of the polymers in the electrolytes (MeCN, DMF) which is required for an efficient electrochemical reaction. Thermal analysis of the generated polymers revealed high decomposition onset temperatures at 190 °C for PDTMVP and PDTOVP, while a decomposition temperature of 125 °C was observed for PDTPVP, due to thermolysis of the protecting group. All synthesized polymers lack an observable melting temperature during DSC analysis, indicating entirely amorphous polymers.

For the utilization of thiol functionalized pyridine initiators, C-H bond activation of Cp$_2$LuCH$_2$TMS was performed resulting in Cp$_2$LuDTPD (DTPD = thiol functionalized pyridine). End-group analysis confirmed a nucleophilic transfer reaction of the Cp$_3$Lu(thf) and Cp$_2$LuDTPD via a monomer insertion into the lutetium carbon bond, leading to the corresponding Cp or thiol polymer end-groups. While the surface immobilization of Cp end-group containing polyvinylphosphonates on carbon nanotubes via *Diels-Alder* cyclization resulted only in moderate polymer to CNT ratios (0.25), the thiol end-group served as effective anchor point for the formation of polymeric self-assembled monolayers on gold surfaces. A correlation between the surface coverages of the generated SAMs with the degree of polymerization of the utilized polyvinylphosphonate was observed. Cyclic voltammetry measurements revealed a highly reversible redox reaction for the radical PDTOVP with a standard potential of E°(Ag/Ag$^+$) = 0.72 V.

The generated radical polyvinylphosphonates were additionally investigated in their performance as novel redox active cathode material in an organic radical battery setup. The polymer composite electrodes showed increased capacities with increasing molecular weight of the redox active polymer with a maximum of 95% of the theoretical capacity for PDTOVPs with molecular weights of 312 kg mol^{-1}. Cycling and impedance studies in combination with SEM revealed polymer agglomeration during battery cycling as the most plausible reason for this behavior, as smaller molecular weight polymer tend to agglomerate faster. Variation of the current densities lead to 50% of the theoretical

capacity values at the immense fast charging/discharging time of 90 seconds and full recovery of the initial 1 C capacity, underlining the extreme reversible redox process of the TEMPO radical functionalized polyvinylphosphonates.

The two redox active TEMPO pendant groups per repeating unit, the potential to synthesize high-molecular weight ORPs and the introduction of phosphorus to the polymers make radical vinylphosphonate an immensely promising candidate for further organic radical polymer applications. This class of functional polymers will further improve from the expansion of polymerization techniques to the field of rare-earth metal-mediated group-transfer polymerization, with its unique possibility to synthesize tailor-made polymers and quantitative end-group functionalization, opening the pathway for future applications.

6 Outlook

The utilization of single site catalytic REM-GTP could open the pathway to a new era for the synthesis of organic radical polymers. The capability of this approach is linked to the application of suitable protecting groups such as the herein reported alkoxyamines, but also silyl ethers were shown to be a suitable protecting group for nitroxide radicals as well as to be compatible with REM-GTP.[41, 104, 106, 231] Based on these two developments, a plethora of different *Michael*-type monomers beside vinylphosphonates, such as alkoxyamine functionalized methacrylate, acrylamide or vinylpyridines are susceptible to the sophisticated REM-GTP or other single-site catalytic techniques. ORPs therefore benefit from this powerful polymerization technique, allowing the synthesis of adjustable block copolymers, boost the activity and thus synthesize ultra-high molecular weight ORP. These techniques additionally enable a precise control of the polymeric architecture and, most visionary in the case of ORPs, to gain for the first time a precise control of the polymeric microstructure. While this was not achieved for the herein reported polyvinylphosphonates, due to the lack of a suitable catalyst for the stereocontrolled synthesis of sterical demanding vinylphosphonates, for various alkyl functionalized methacrylates or acrylamides (Scheme 59) such systems are reported in the literature.[209]
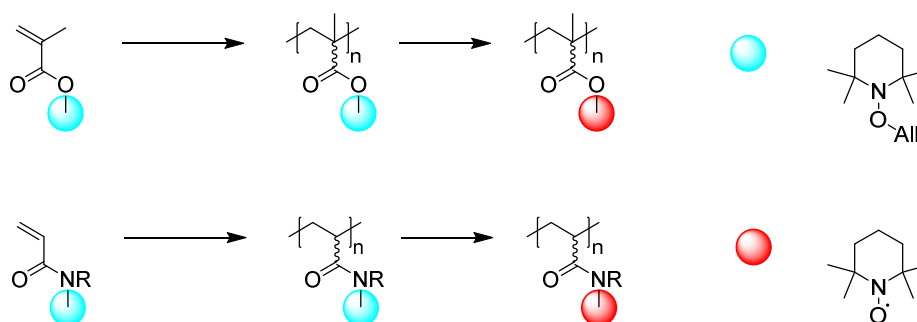
Scheme 59: Schematic pathway for the generation of stereocontrolled organic radical polymers based on alkoxyamine funtionalized methacrylates and acrylamides.

This control of the tacticity would alter the radical-radical distance in the received ORPs, especially in the context of electric charge conductive radical polymers this could be a notable development. As this charge conductivity is a key parameter in the application of ORP as active material in organic radical batteries, it could additionally enhance the performance, while simultaneously reducing the ratio of electric charge conductive support and thus increase the overall performance of such organic radical batteries. Furthermore, as ORBs suffer from capacity fading due to dissolution of active material

in the liquid electrolyte or the agglomeration of the redox active polymer, a change in microstructure could efficiently solve these application issues.

However, not only *Michael*-type monomers benefit from this powerful adaption of single-site catalytic precision polymerization for the generation of ORP. The herein reported alkoxyamine protecting group chemistry is transferable to other monomers such as functionalized epoxides or vinylethers (Scheme 60).
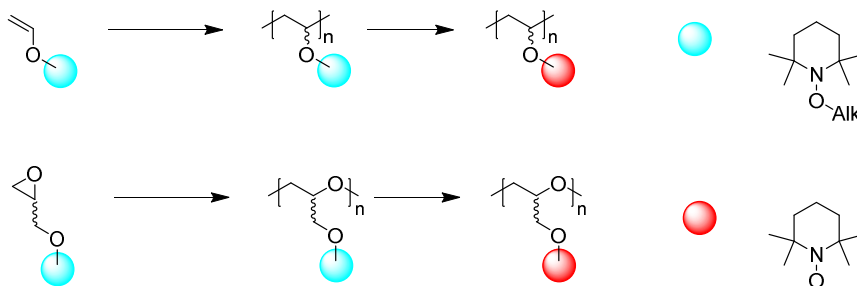
Scheme 60: Schematic pathway for the generation of stereocontrolled organic radical polymers based on alkoxyamine funtionalized vinylethers and epoxides.

However, one of the main features of REM-GTP besides the high activity and precision, is the ability to introduce functional polymeric end-groups during initiation of the polymerization. Especially for vinylphosphonates, our group established a plethora of functional pyridine initiators, which are readily susceptible as REM-GTP initiators via C-H bond activation (see Scheme 36). As outlined in the scope of this work, the functional cyclopentadienyl end-group allowed immobilization on multi-wall carbon nanotubes (polymer/CNT 0.25/0.75). This immobilization could proof highly beneficial as it suppresses dissolution and agglomeration of the redox active ORPs. Furthermore, the increased homogeneity of the insulating OPR active material on the electric charge conductive support allows higher ORP loading and thus increases the overall capacity as well as accelerates the charging/discharging processes. To increase the immobilization ratio to values required for the application as composite electrode in ORBs, azide or diazonium salt functionalized pyridine end-groups could be employed. To introduce azide functionalities to the pyridine, two different approaches are outlined here: Direct C-H bond activation of 4-azido-2,6-dimethylpyridine or post-polymerization modification of 4-bromo-2,6-dimethylpyridine by nucleophilic substitution with sodium azide (Scheme 61). Other approaches for efficient functionalization of CNT with polymeric material employ the in-situ generation of diazonium salts. While alkyl amines as end-groups of polyvinylphosphonates introduced via REM-GTP were recently

reported, the more active aryl amines could be established via C-H bond activation of TMS protected 2,6-dimethylpyridin-4-amine.
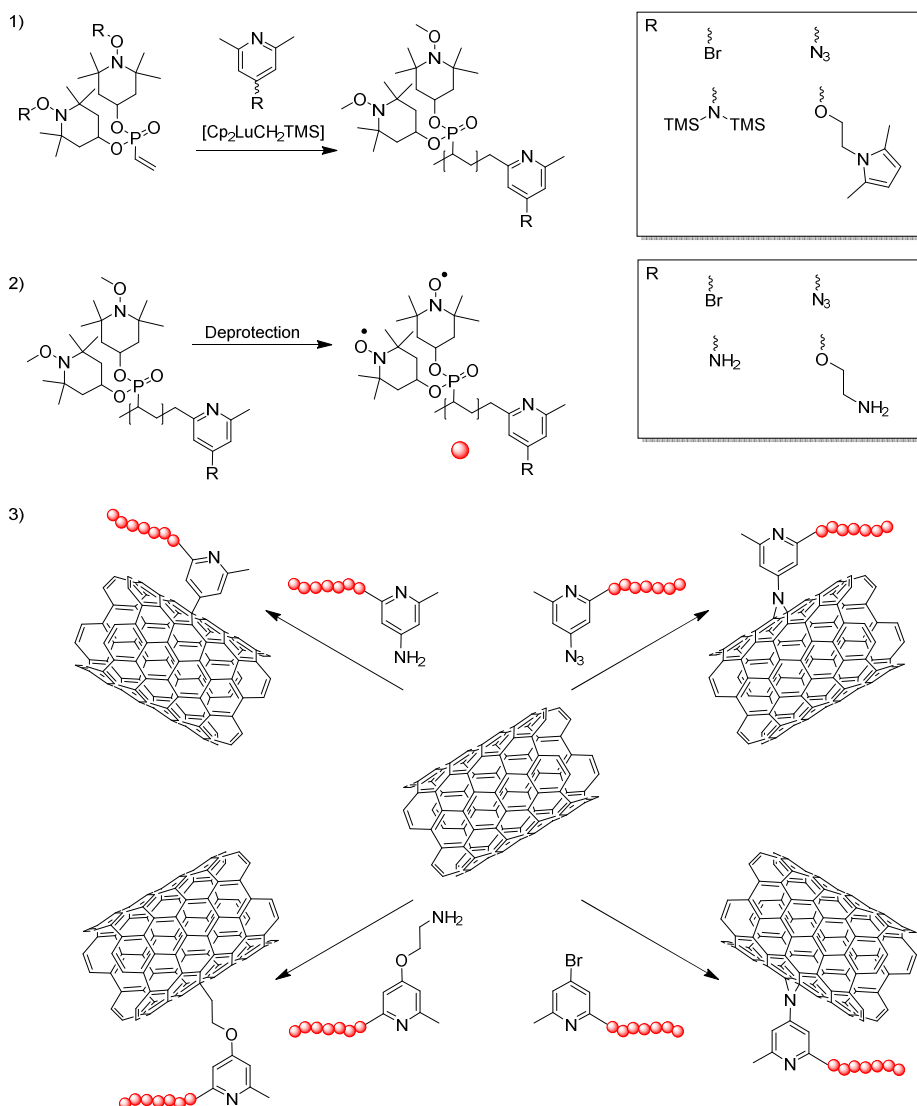
Scheme 61: Various synthetic pathways for the immobilization of organic radical polyvinylphosphonates via the introduction of suitable end-groups through REM-GTP.

Despite CNT functionalization, REM-GTP already enables the precise surface attachment of gold surfaces with thiol end-group functionalized polyvinylphosphonates; a technique that is transferable to a plethora of different monomers and the corresponding polymers. As the generated thin films already showed promising electrochemical features after electrochemical deprotection of the alkoxyamine to the corresponding TEMPO radical, thin film batteries on this system could emerge (Figure 35). Initial research should focus on the establishment of an organic counter electrode (anode) to the herein developed cathode material (PDTOVP). While different systems based on spin-coated redox active organic polymers exist in the literature, the

approach utilizing a redox active polymer SAM as anode material could emerge as a powerful alternative. In general, the approach of the herein generated TEMPO based organic radical polyvinylphosphonates could be transferred to generate anode redox active organic polymers (Figure 35).
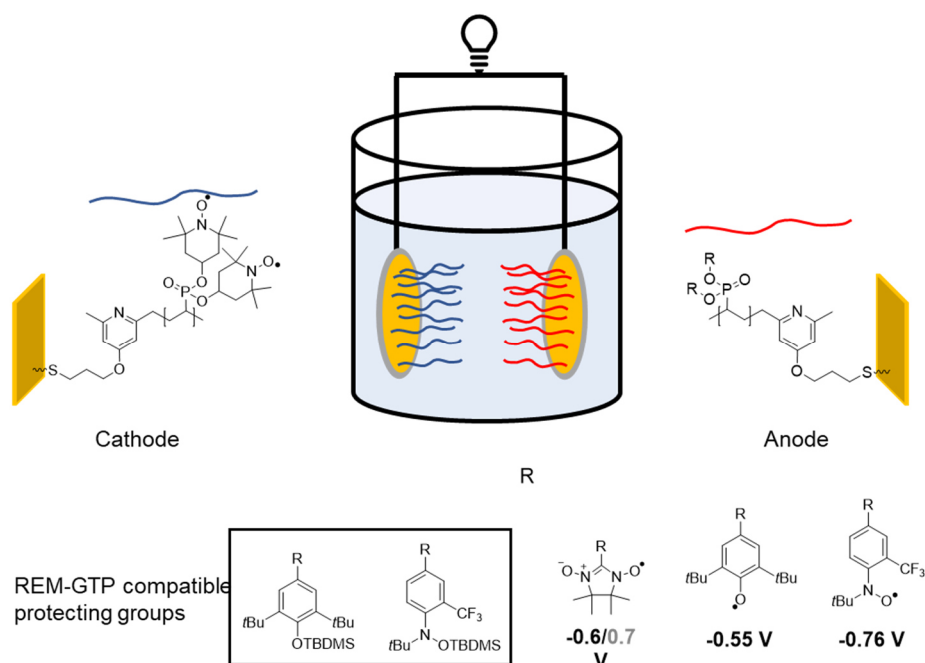
Figure 35: All organic thin film battery based on thiol end-group functionalized polyvinylphosphonates. The herein reported TEMPO based radical polyvinylphosphonates is proposed as the corresponding cathode. For the corresponding anode, different suitable redox-active motifs and potential protecting groups for the polymerization via REM-GTP are presented.

These materials should feature redox potentials below 0 V and one of the most suitable candidates for this approach are nitroxylbenzyl groups. While unsubstituted nitroxylbenzyl features a standard potential of 0.7 V (vs. Ag/Ag$^+$), the functionalization with a strong electron withdrawing trifluoromethane in ortho position results in the stabilization of the n-type (NO$^•$ to NO$^-$) process. This features a reversible redox potential of -0.8 V (vs. Ag/Ag$^+$) and therefore offers a suitable anode material. In addition, organic radical polymers prepared with this redox active moiety already utilized a *tert*-butyldimethylsilyl protecting group, which was already shown to be compatible with REM-GTP.[231]

While thin film batteries prepared with such redox active SAMs can employ economic and hazardous free aqueous electrolytes, these systems could be further improved via attachment to other conductive metal surfaces or even transparent conductive surfaces such as indium-doped tin oxide (ITO). Especially REM-GTP offers suitable initiators,

resulting in styrene or pyrrole functionalized polymer end-groups, which are susceptible to electro-polymerization, generating current/cycling dependent thin films. Additionally, graft from approaches are feasible, which employ in an initial step the immobilization of trichlorsilane, alcohol or trialkoxysilane functionalized collidine initiators. This immobilized collidine can serve as anchor point for C-H bond activation with various REM complexes and subsequent polymerization from the surface. However, these initiators can alternative be utilized in a post-polymerization graft to approach, forming defined polymer films on ITO.
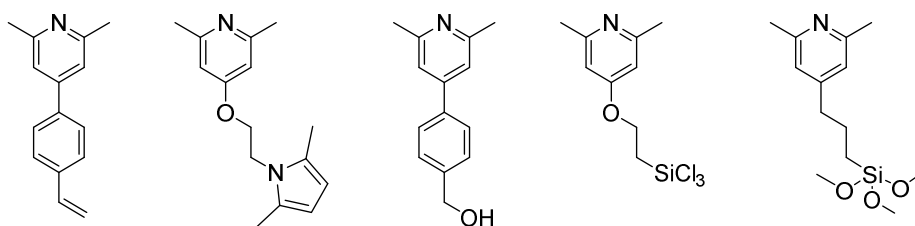
Scheme 62: Potential functionalized pyridine REM-GTP initiators for the immobilization via eletro-polymerization or silanization in a graft from or graft to approach.

While a so generated thin film battery could emerge as fruitful setup, the utilization of REM-GTP allows the establishment of a forward-looking organic all-solid-state battery design. Therefore, a combination with the currently investigated solid-polymer electrolytes (SPE) based on a polyvinylphosphonate backbone with pendant oligoethylenoxide functionalities and the developed TEMPO based redox active polyvinylphosphonates is proposed. A key premise for this ASSB design is the separation of the cathode (radical PDTOVP) and the counter electrode (e.g. Lithium) by the SPE. This is only feasible by the utilization of REM-GTP to design defined XAB block copolymers, with the redox active block as the first block A and the SPE as the second block B. Finally, the initiator X serves as anchor point to a current collector - e.g. thiol on gold – to ensure the separation of cathode and anode (Figure 36).
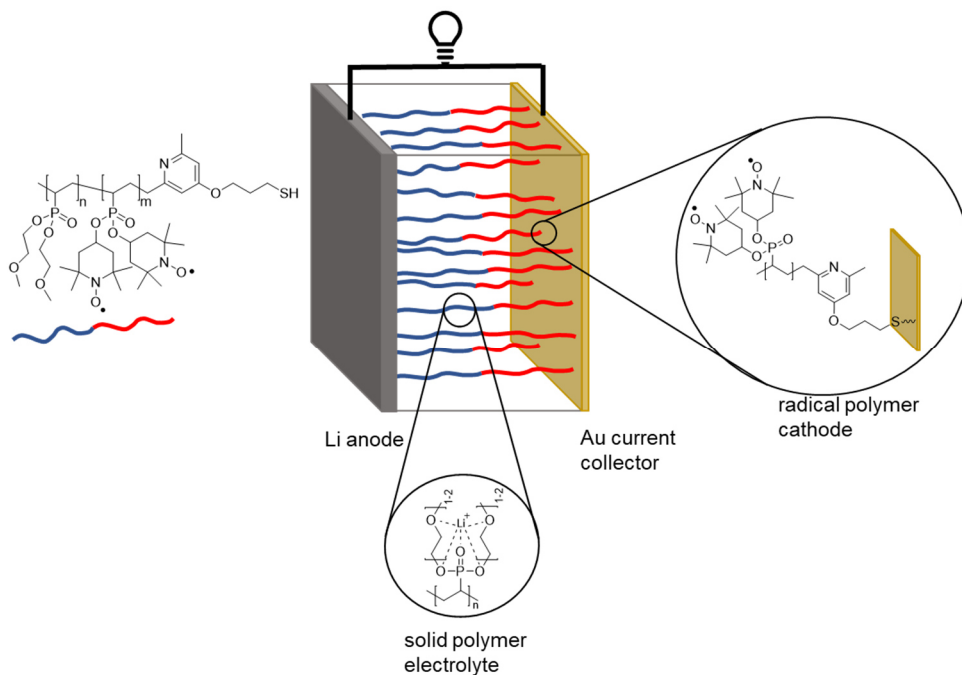
Figure 36: Lithium metal organic radical polymer hybrid all solid-state battery based on polyvinylphosphonates.

While the setup with a counter anode e.g. metallic lithium is readily feasible, the incorporation of an organic redox active anode material like nitroxylbenzyl as last block in a XABC triblock-polymer enables the establishment of a visionary all organic all solid state battery design (Figure 37). As the applied polymers are transparent even in their charged redox state, the combination with suitable transparent electrode materials (ITO) would allow a truly transparent battery design, which could emerge highly beneficial for applications like mobile screens or other portable smart devices. This design is based on the powerful tool of REM-GTP enabling the necessary end-group functionalization and the precise synthesis of the XABC triblock copolymer, in which the capacity is adjustable by the block length of the redox active block A and B.
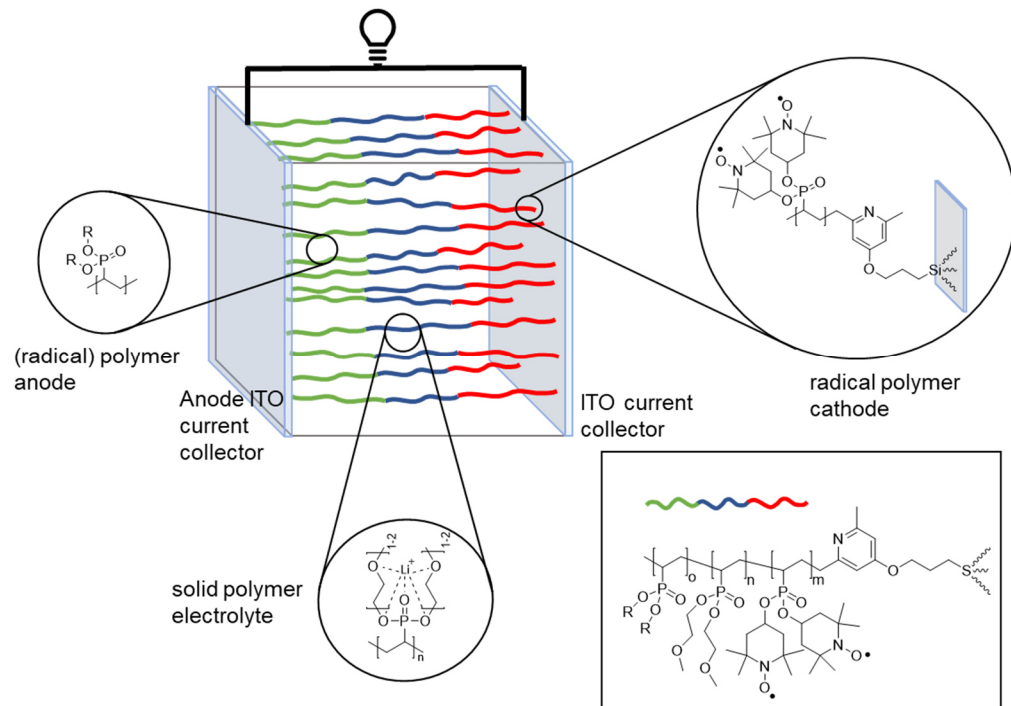
Figure 37: A transparent all organic all solid-state battery based on polyvinylphosphonate triblock polymers.

7 Experimental

7.1 General considerations

All reactions with air and moisture-sensitive substances were carried out under an argon atmosphere using standard Schlenk techniques or in a glovebox. Prior to use, all glassware was heat-dried under vacuum. Unless otherwise stated, all chemicals were purchased from Sigma-Aldrich, ABCR, or TCI Europe and used without further purification. Toluene, THF, and DCM were dried using an MBraun SPS-800 solvent purification system and stored over 3 Å molecular sieves. DMF was dried over calcium hydroxide and stored over 4 Å molecular sieves after distillation. The alkoxyamines (2,2,6,6-tetramethyl-1-(1-phenylethoxy)piperidin-4-ol (TEMPOPE) and 2,2,6,6-tetramethyl-1-methoxy-piperidin-4-ol (TEMPOMe), 2,6-Dimethyl-4-(3-(tritylthio)propoxy)pyridine and $(C_5Me_4H)SiMe_2NHBu$ were prepared according to literature procedures.[5, 34, 241]

7.2 General analytic methods

NMR spectra were recorded on a Bruker AVIII-300, AV-400HD or an AVIII-500 Cryo spectrometer. ^1H and ^{13}C NMR spectroscopic chemical shifts δ were reported in ppm relative to the residual solvent signal of the deuterated solvent. Unless otherwise stated, coupling constants J were the averaged values and refer to couplings between two protons. All deuterated solvents (C_6D_6, $CDCl_3$, CD_2Cl_2) were obtained from Sigma-Aldrich. Elemental analyses were measured on a Vario EL (Elementar) at the Laboratory for Microanalysis at the Institute of Inorganic Chemistry at the Technical University of Munich. UV–Vis measurements were performed with a Cary 50 UV–Vis Spectrophotometer (Varian) with different 4OH-TEMPO calibration curves (). EPR measurements were recorded on a Magnettech MS5000 (Freiberg Instruments) in 50 µL microcapillary pipettes or EPR quartz tubes (I.D. 3 mm) with 100 kHz modulation and a frequency of 9.46 GHz. IR spectra were measured on a Vertex 70 FTIR using a Platinum ATR (Bruker). Absolute molecular weights and polydispersities of PDTMVP and PDTPVP were determined by triple detection using two angle light scattering (45° and 90°), a refractive index detector, and a viscometer in tetrahydrofuran with 0.22 g/L 2,6-di-tert-butyl-4-methylphenol as eluent at 40 °C. The dn/dc was determined via SEC measurement of three samples with different concentrations of polymers with various

molar masses. It was determined as 0.102 mL/g for PDTMVP and 0.129 mL/g for PDTPVP. Polydispersities of the oxidized radical PDTOVP were measured on an Agilent PL-GPC 50 (Santa Clara, CA, USA) with an integrated RI unit with two Agilent PolarGel M columns. As eluent, *N*,*N*-dimethylformamide with 2.096 g/L lithium bromide at 30 °C was used. PMMA standards were used for calibration. TGA-MS measurements were performed with a Netzsch TG 209 F1 Libramachine at a heating rate of 0.5 K/min in an argon flow of 20 mL/min (Ar 4.8) coupled with a QMS Aëolos® MS system. DSC analysis were performed on a DSC Q2000 from TA Instruments. The measurement was performed in exo down mode with a heating rate of 10 K/min in a temperature range of -150 °C to 175 °C for PDTMVP and PDTOVP, for PDTVP from -150 °C to 100 °C with samples of 6-9 mg. Three cycles were run per measurement (heating, cooling, heating). Cyclic voltammetry was recorded on a Metrohm PGSTAT302N or a PalmSens4 with a glassy carbon working electrode and counter electrode, and an Ag/AgCl reference electrode in a sperate compartment (double junction or porous glas tip separator). ESI-MS was measured on an ExactivePlus Orbitrap from Thermo Fisher Scientific in positive ionization mode. Battery tests were performed at 25.0 °C on a Biologic VSP-300. Commercial Au-coated quartz crystal microbalances (QCM, Q-Sense, diameter 14 mm, thickness 0.3 mm, AT cut, fundamental frequency 4.95 MHz) were used as the QCM substrates and the shift in frequency recorded on BEL-QCM-4.

7.3 Monomer synthesis

Dichlorovinylphosphonate
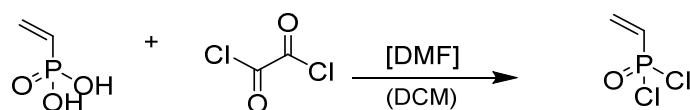
In an oven dried schlenk flask with magnetic stirrer was added vinylphosphonic acid (60 g, 555 mmol, 1 eq.) in 500 mL dry CH_2Cl_2. The solution is cooled to 0 °C in an ice-water bath and after addition of 0.11 mL DMF (104 mg, 1.42 mmol, 0.26 mol%) followed by addition of 140 mL of oxalyl chloride (207 g, 1.63 mmol, 2.93 eq.) *via* a dropping funnel over an period of 2 h. Attached overpressure valve to prevent moisture and release of evolved gases. After the addition of oxalychloride the reaction was kept at 0 °C for another hour and was allowed to proceed at rt for 12 hrs. Solvent and excess oxalyl chloride was removed under reduced pressure. The brown-colored oily residue was purified by vacuum distillation (85 °C, 15 mbar) to obtain 48.3 g (333 mmol, 60%) of a clear liquid.

^{1}H-NMR (500 MHz, C_6D_6, 300 K): δ (ppm) = 5.84 (dd, J = 34.7, 18.1 Hz, 1H, CH_{Vinyl}), 5.69 – 5.48 (m, 1H, CH_{Vinyl}), 5.12 (dd, J = 70.7, 11.9 Hz, 1H, CH_{Vinyl}).

^{13}C-NMR (100 MHz, C_6D_6, 300 K): 135.52 (s, C_{Vinyl}), 133.06 (d, *J* = 143.7 Hz, PC_{Vinyl})

^{31}P-NMR (162 MHz, C_6D_6, 300 K): δ (ppm) = 28.44 (s, $RPOCl_2$)

General Monomer synthesis procedure

The corresponding alcohol (116 mmol, 2.2 eq) and vinylphosphonic dichloride (6.00 g, 4.29 mL, 41.4 mmol, 1.0 eq) were dissolved in 100 mL THF in an oven-dried two-necked round bottom flask. After cooling to 0 °C NEt$_3$ (16.8 g, 23.1 mL, 165 mmol, 4.0 eq) was added dropwise to the reaction solution. After complete addition, the reaction was heated to 66 °C. The course of the reaction was monitored via ^{31}P-NMR spectroscopy. After the disappearance of signals for vinylphosphonic dichloride (28 ppm) and the monosubstituted species (≈25 ppm), the reaction was quenched by the addition of 50 mL H$_2$O. The solution was filtered and THF removed *in vacuo*. 200 mL DCM was added to the viscous residue and the organic phase was extracted with water (2 × 200 mL) and brine (1 × 200 mL), dried over MgSO$_4$, filtered and the solvent removed *in vacuo*, yielding a viscous liquid. The product is then dried over a neutral Al$_2$O$_3$ column yielding DAVP.

Di(2,2,6,6-Tetramethylpiperidin-1-oxyl) vinylphosphonate (DTOVP)
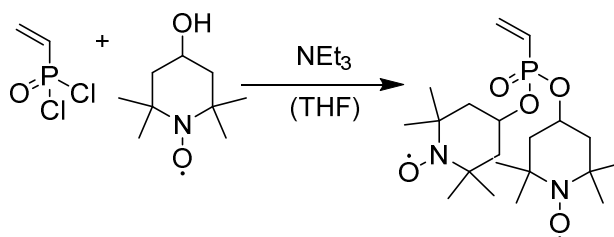
87%, red crystals

EPR (9.46 GHz, C$_6$H$_6$, 300K): 2.0075 g

EA: Calc. C 57.68, H 8.95, N 6.73, O 19.21, P 7.44. Found: C 57.66, H 9.07, N 6.78

Di(2,2,6,6-tetramethyl-1-(1-phenylethoxy)piperidin-4-yl) **vinylphosphonate (DTBVP)**
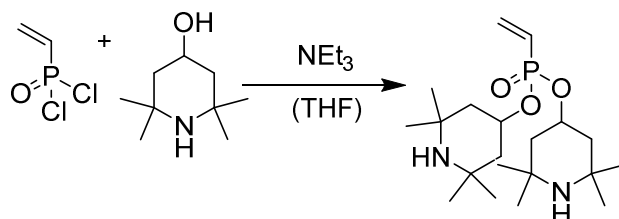
69%, white solid

¹H-NMR (400 MHz, CD_2Cl_2, 300K): δ (ppm) = 6.40 – 5.89 (m, 3H, , CH_{Vinyl}), 4.76 (m, 2H, $NOCH_2$), 2.01 (m, 4H, CH_2), 1.24 (m, 4H, CH_2), 1.19 (d, J = 5.2 Hz, 12H, CH_3), 1.14 (d, J = 3.7 Hz, 12H, CH_3).

¹³C-NMR (100 MHz, CD_2Cl_2, 300K): δ (ppm) = 134.19 (s, C_{Vinyl}), 128.63 (s, C_{Aryl}), 126.80 (s, C_{Aryl}), 71.67(d, J = 6.0 Hz, POC), 51.83 (s, CH_2), 46.22 (s, CH_2), 46.19 (s, CH_2), 46.06 (s, CH_2), 46.02 (s, CH_2), 34.83 (s, CH_3), 29.06 (s, CH_3).

³¹P-NMR (162 MHz, CD_2Cl_2, 300K): δ (ppm) = 15.74 (s, $RPO(OR)_2$).

Di(1-methoxy-2,2,6,6-tetramethylpiperidin-4-yl) vinylphosphonate (DTMVP)
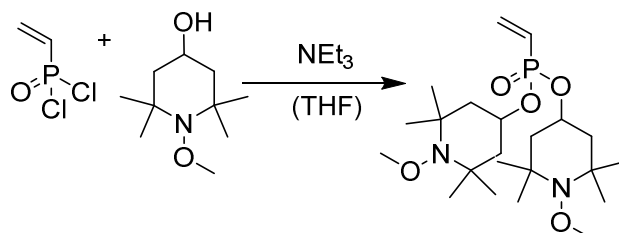
92%, white crystals

¹H-NMR (500 MHz, $CDCl_3$, 300K): δ (ppm) = 6.33 – 5.90 (m, 3H; CH_{Vinyl}), 4.58 (m, 2H, POCH), 3.59 (s, 6H, $NOCH_3$), 1.89 (m, 4H, CH_2), 1.64 (m, 4H, CH_2), 1.20 (s, 12H, CH_3), 1.13 (s, 12H, CH_3).

¹³C-NMR (100 MHz, $CDCl_3$, 300K): δ (ppm) = 134.83 (s, C_{Vinyl}), 127.38 (d, J = 185.0 Hz, PC_{Vinyl}), 69.48 (d, J = 5.6 Hz, POC), 65.60 (s, NOC), 60.10 (s, CH_2.), 46.29 (s, CH_2), 46.24(s, CH_2), 33.11 (s, CH_3), 20.89 (s, CH_3)

³¹P-NMR (162 MHz, $CDCl_3$, 300K): δ (ppm) = 15.91 (s, $RPO(OR)_2$)

124

EA: Calc. C 59.17, H 9.71, N 6.27, O 17.91, P 6.94. Found: C 59.16, H 9.83, N 6.11

Di(2,2,6,6-tetramethyl-1-(1-phenylethoxy)piperidin-4-yl) vinylphosphonate (DTPVP)
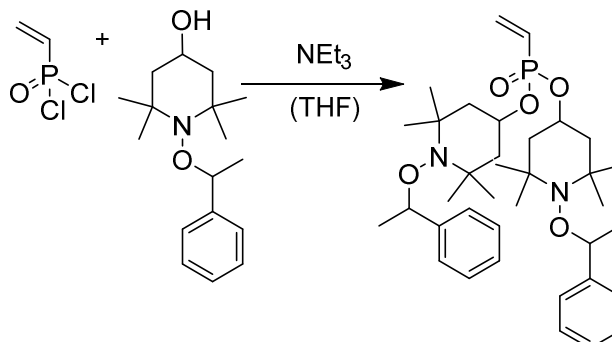
85%, clear viscous liquid

^{1}**H-NMR** (400 MHz, CD$_2$Cl$_2$, 300K): δ (ppm) = 7.38 – 7.18 (m, 10H, CHaryl), 6.27 – 5.94 (m, 3H, CH$_{Vinyl}$), 4.78 (qd, J = 6.7, 3.9 Hz, 2H, NOCH$_2$), 4.57 (m, 2H, POCH), 1.94 (m, 2H, CH$_2$), 1.81 (m, 2H, CH$_2$), 1.66 (m, 2H, CH$_2$), 1.56 (m, 2H, CH$_2$), 1.48 (dd, J = 6.7, 3.3 Hz, 6H, CH$_3$), 1.34 (s, 6H, CH$_2$), 1.23 (s, 6H, CH$_2$), 1.09 (s, 6H, CH$_3$), 0.67 (s, 6H, CH$_3$).

^{13}**C-NMR** (100 MHz, CD$_2$Cl$_2$, 300K): δ (ppm) = 145.76 (s, C$_{Aryl}$), 134.73 (s, C$_{Vinyl}$), 128.45 (s, C$_{Aryl}$), 127.88 (d, J = 184.2 Hz, , PC$_{Vinyl}$) 127.40 (s, C$_{Aryl}$), 127.12 (s, C$_{Aryl}$), 83.70 (s, NOC), 69.60 (d, J = 5.6 Hz, POC), 60.59 (s, CH$_2$), 60.35 (s, CH$_2$), 47.26 (s, CH$_2$), 47.08(s, CH$_2$), 34.55 (s, CH$_3$), 34.29(s, CH$_3$), 23.40 (s, CH$_3$), 21.30 (s, CH$_3$).

^{31}**P-NMR** (162 MHz, CD$_2$Cl$_2$, 300K): δ (ppm) = 15.66 (s, RPO(OR)$_2$).

EA: Calc. C 68.98, H 8.84, N 4.47, O 12.76, P 4.94. Found: C 69.03, H 8.64, N 4.46

7.4 Catalyst synthesis

General procedure for the synthesis of Cp₃Lu(thf)

LnCl₃   ⟶ (THF)   Ln = Y or Lu
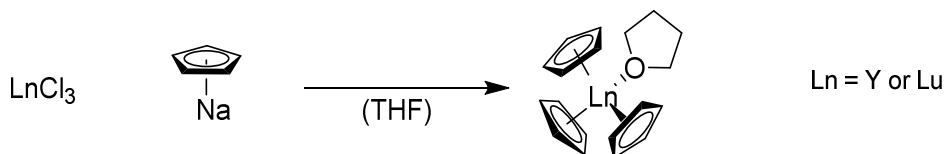
626 mg (7.11 mmol, 4.0 equiv.) sodium cyclopentadienide dispersed in 10 mL THF were added dropwise to the corresponding amount (1.78 mmol, 1.0 equiv.) $LnCl_3$ (Ln = Y or Lu) dispersed in 10 mL THF. The solution was stirred vigorously at room temperature for one hour and afterward, the solvent was removed in vacuo. The crude product was heated overnight to 110 °C in vacuo (10^{-2} mbar) and colorless crystals (Cp₃Lu) were collected using a cooling finger. For the synthesis of the THF adduct, Cp₃Lu was dispersed in THF (0.1 M) and stirred for 24 hours. After removal of the solvent, the residue was recrystallized from toluene at -35 °C yielding colorless crystals.

Cp₃Y

^{1}H-NMR (300 MHz, C_6D_6, 300 K): δ (ppm) = 5.92 (s, 15H).

Cp₃Y(thf)

Yield: 70% (colorless powder)

^{1}H-NMR (300 MHz, C_6D_6, 300 K): δ (ppm) = 5.94 (s, 15H), 3.40 (s, 4H), 1.24 (s, 4H).

Cp₃Lu

Yield: 70% (colorless powder)

^{1}H-NMR (300 MHz, C_6D_6, 300 K): δ (ppm) = 5.93 (s, 15H).

Cp₃Lu(thf)

Yield: 98% (colorless powder)

^{1}H-NMR (300 MHz, C_6D_6, 300 K): δ (ppm) = 5.92 (s, 15H), 3.35 – 3.25 (m, 4H), 1.13 – 1.04 (m, 4H).

^{13}**C-NMR** (126 MHz, C_6D_6, 300 K): δ (ppm) = 110.26 (s, C_{Cp}), 73.54 (s, C_{THF}), 25.26 (s, C_{THF}).

Lu(CH$_2$TMS)$_3$(thf)$_2$
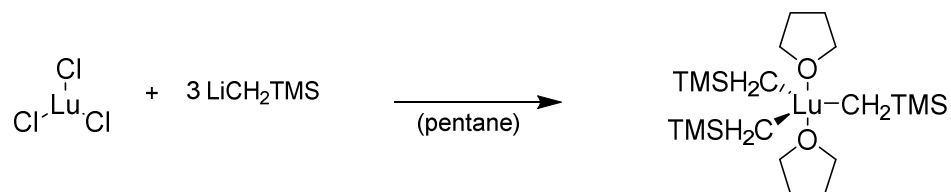
1.16 g (4.12 mmol, 1.0 eq.) LuCl$_3$ is suspended in 90 mL THF an heated to 66 °C for 90 minutes, after removing the solvent by evaporation and thoroughly drying, the received white solid is suspended in 30 mL pentane and cooled to 0 °C. A solution of 1.18 g (12.5 mmol, 3.03 eq.) trimethylsilylmethyl lithium in 15 mL pentane is added dropwise and the solution is stirred at 0 °C for 2 h. The solution is filtered using a filter cannula and the remaining residue is extracted with pentane (3 x 15 mL). The solvent is removed in vacuo and the product is obtained as white solid. For synthesis yielding after purification a viscous clear liquid, the liquid is redissolved in pentane and the filtration repeated. The solid can be recrystallized from pentane at -35 °C, however degradation can alter the complex.

^{1}**H-NMR** (400 MHz, C_6D_6, 300 K): δ (ppm) = 3.97 (s, 9H), 1.31 (s, 9H), 0.34 (s, 27H), -0.89 (s, 4H).

Cp₂LuCH₂TMS
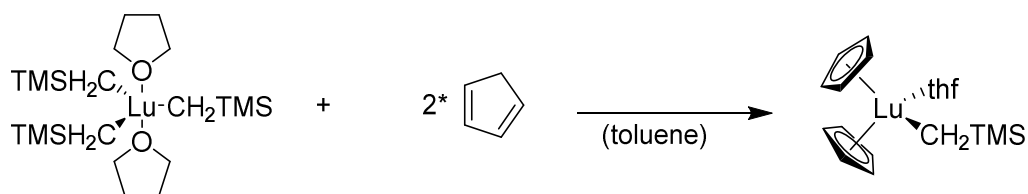
800 mg (1.38 mmol, 1.0 eq.) Lu(CH₂TMS)₃(thf)₂ are dissolved in 20 mL toluene and 182 mg (2.75 mmol, 2.0 eq.) of freshly cracked Cp are added dropwise at room temperature. The mixture is stirred overnight and volatile compounds removed in vacuo. The product is recrystallized from 1:1 pentane toluene at -35 °C and freeze dried from benzene.

¹H-NMR (500 MHz, C₆D₆, 300 K): δ (ppm) = 6.07 (s, 10H), 2.92 (s, 4H), 0.90 (s, 4H), 0.44 (s, 2H), -0.76 (s, 4H).

¹³C-NMR (126 MHz, C₆D₆, 300 K): δ (ppm) = 110.33, 71.10, 30.23, 27.28, 24.84, 5.02.

²⁹Si-NMR (100MHz, C₆D₆, 300 K): δ (ppm) = -0.82.

Cp*₂LuCH₂TMS
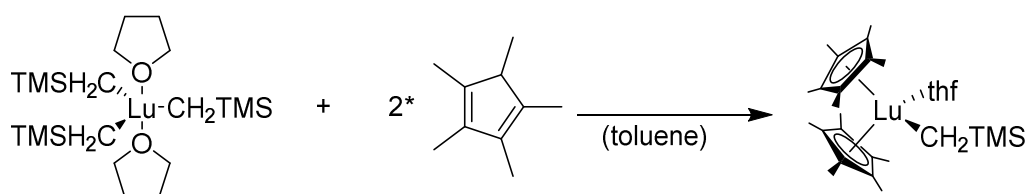
800 mg (1.38 mmol, 1.0 eq.) Lu(CH₂TMS)₃(thf)₂ is dissolved in 20 mL toluene and 375 mg (2.75 mmol, 2.0 eq.) of Cp* are added dropwise at room temperature. The mixture is stirred for 24 h and volatile compounds removed in vacuo. The product is recrystallized from pentane at -35 °C and freeze dried from benzene.

¹H-NMR (500 MHz, C₆D₆, 300 K): δ (ppm) = 3.32 (s, 4H), 1.99 (s, 30H), 1.15 (s, 4H), 0.49 (s, 9H), -1.00 (s, 2H).

¹³C-NMR (126 MHz, C₆D₆, 300 K): δ (ppm) = 116.34, 71.69, 28.65, 25.44, 12.15, 6.40.

²⁹Si-NMR (100MHz, C₆D₆, 300 K): δ (ppm) = -1.12.

CGCLuCH₂TMS
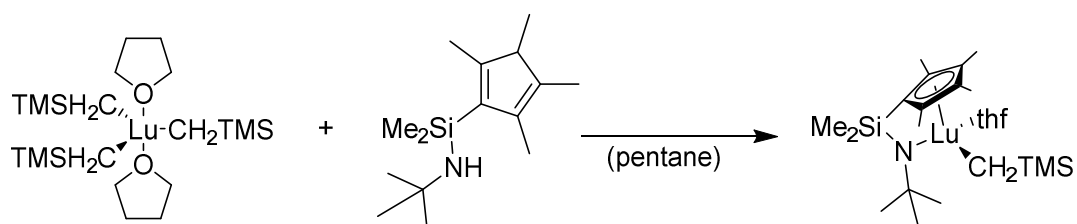
425 mg (0.73 mmol, 1.0 eq.) Lu(CH₂TMS)₃(thf)₂ is dissolved in 20 mL pentane and 375 mg (2073 mmol, 1.0 eq.) of (C₅Me₄H)SiMe₂NHBu in 5 mL pentane are added dropwise at room temperature. The mixture is stirred for 24 h and volatile compounds removed in vacuo. The product is recrystallized from pentane at -35 °C and freeze dried from benzene.

¹H-NMR (500 MHz, C₆D₆, 300 K): δ (ppm) = 3.40–3.13 (m, 4H), 2.19 (s, 12H), 1.38 (s, 9H), 1.03–0.96 (m,4H), 0.78 (s, 6H), 0.31 (s, 9H), -0.90 (d, J = 3.2 Hz, 2H).

¹³C-NMR (126 MHz, C₆D₆, 300 K): δ (ppm) = 126.38, 122.31, 106.63, 70.59, 54.15, 36.12, 26.25, 24.72, 14.01, 11.52, 8.49, 4.65.

²⁹Si-NMR (100MHz, C₆D₆, 300 K): δ (ppm) = = -2.71, -25.16.

C-H bond activity measurements

The corresponding YLuCH$_2$TMS (10 µmol, 1.0 equiv.) is dissolved 0.3 mL Toluene-d8 and 0.3 mL of 30 µM solution corresponding pyridine (10 µmol, 1.0 equiv.) in Toluende-d8 is added in one portion. The solution turns immediately yellow and is transferred to a NMR-tube and heated in the NMR cavity to 60 °C. At regular time intervals NMR measurements are performed.

C-H bond activity

The corresponding lutetium CH$_2$TMS complex (20 µmol, 1.0 equiv.) is dissolved 0.6 mL Toluene and 0.6 mL of 30 µM solution corresponding pyridine (20 µmol, 1.0 equiv.) in Toluene is added in one portion. The solution turns immediately yellow heated overnight at 60 °C in a screw cap vial. The reaction was monitored by ^{1}H-NMR spectroscopy until full conversion was detected and immediately used for polymerization reactions.

7.5 Polymer synthesis

Activity measurements

To measure the activity of $Cp_3Lu(thf)$ of DTMVP and DTPVP polymerization, 1.12 mmol (100 equiv.) of DAVP were weighed into an oven-dried screw cap vial in the glovebox and were dissolved in 6.5 mL anhydrous toluene. Under vigorous stirring, 0.5 mL of a 2.24 µM (1.12 µmol, 1.0 equiv.) solution of $Cp_3Lu(thf)$ was added in one portion. At certain time intervals, 0.2 mL aliquots of the reaction mixture were taken out and quenched by the addition of 0.2 mL wet $CDCl_3$. The conversion was calculated using ^{31}P-NMR spectroscopy. The number-average molecular weight and polydispersity were determined using SEC analysis. The turnover frequency was determined from the highest slope in the time–conversion plots. Normalized turnover frequencies were determined taken the average initiator efficiency of these points into account. The living-type character of the polymerizations were determined from a linear increase of molecular weight in a conversion–molar mass plot.

General polymerization procedure

For the polymerization of DTOVP, DTMVP, or DTMVP, 320 µmol (133 m DTOVP, 143 mg DTMVP or 200 mg DTPVP, 1.0 equiv.) were weighed into an oven-dried screw cap vial and dissolved in 2 mL anhydrous solvent. Under vigorous stirring the calculated amount of a 5 mM catalyst solution (1/25 equiv., 1/50 equiv., 1/100 equiv., 1/200 equiv., 1/400 equiv., 1/600 equiv. or 1/1000 equiv). was added in one portion and the reaction was stirred at 25 °C for the stated reaction time (Table 1-6). An aliquot of 0.2 mL of the reaction mixture was taken and quenched in wet $CDCl_3$ before stopping the reaction with 0.5 mL wet THF. The polymers were precipitated in 25 mL acetone, centrifuged, and the solution was decanted off. The residue was freeze-dried from benzene. All polymer samples were analyzed by NMR, SEC, and elemental analysis.

7.6 Polymer deprotection

End-group deprotection of tritylpyridine functionalized polymers

The experimental conditions were adopted from a literature procedure.[34] 200 mg of the corresponding polymer is dissolved in 10 mL absolute DCM and cooled to 0 °C. At this temperature 2 equivalents of triethylsilane and 30 equivalents trifluoracetic acid in correspondence to the respective polymer end-group are added in one portion and the solution stirred at 0 °C for two hours and afterwards for one day at room temperature. The volatiles are removed in vacuo and the residue dissolved in a minimal amount of THF. The polymer is precipitated in 25 mL acetone and the residue freeze dried form benzene yielding 90% white polymer flakes.

PDTMVP

^{1}H-NMR (500 MHz, CDCl$_3$, 300K): δ (ppm) = 4.62 (s, 2H, POCH), 3.58 (s, 6H, NOCH$_3$),0.58-2.5 (m, 35H, polymer backbone and 2,2,6,6-tetramethylpiperdidin).

^{13}C-NMR (100 MHz, CDCl$_3$, 300K): δ (ppm) = 66.8-71.5 (m, POC), 65.87 (s, NOC), 59.42 (s, CH$_2$), 44.2-48.8 (m, CH$_2$), 33.07 (s, CH$_3$), 20.98 (s, CH$_3$).

^{31}P-NMR (162 MHz, CDCl$_3$300K): δ (ppm) = 24.2-38.5 (m, RPO(OR)$_2$).

PDTPVP

^{1}H-NMR (500 MHz, CD$_2$Cl$_2$, 300K): δ (ppm) = 7.31 (s, 10H, aryl) 4.3-5.28 (m, 4H, POCH and NOCH$_2$), -0.58-2.47 (m, 42H, polymer backbone,2,2,6,6-tetramethylpiperdidin and CH$_3$).

^{13}C-NMR (100 MHz, CD$_2$Cl$_2$, 300K): δ (ppm) = 145.81 (s, C$_{Aryl}$), 128.50 (s, C$_{Aryl}$), 127.53 (s, C$_{Aryl}$), 83.48 (s, NOC), 60.55 (s, CH$_2$), 47.34 (s, CH$_2$), 34.11 (s, CH$_2$), 23.28 (s, CH$_3$), 21.96(s, CH$_3$).

^{31}P-NMR (162 MHz, CD$_2$Cl$_2$, 300K): δ (ppm) = 24.1-38.2 (m, RPO(OR)$_2$).

In situ EPR oxidative deprotection of PDTMVP

For the oxidative deprotection, 20 mg (44.8 µmol, 1.0 equiv.) of PDTMVP (M_n = 202 kg mol^{-1}) were dissolved in 2.5 mL absolute DCM. A solution of the respective equivalents (1.5, 3.0, or 4.5) of 77 wt% *m*CPBA in correspondence to methoxyamine (thus 3.0, 6.0, or 9 equiv. in correspondence to the repetition group) dissolved in 2.5 mL DCM was added in one portion. The solution was stirred at RT and an aliquot of 0.4 mL was transferred to an EPR tube and the spectra were recorded every 5 minutes with a sweep time of one minute for 4 hours. After the reaction time, the solution was filtered over a neutral Al_2O_3 column and precipitated in 5 mL MeOH and afterwards dissolved in a minimal amount of DCM and precipitated in 5 mL hexane. The precipitate was freeze-dried from 1,4-dioxane.

Oxidative deprotection of PDTMVP

For the oxidative deprotection, 200 mg (448 µmol, 1.0 equiv.) of PDTMVP was dissolved in 25 mL absolute DCM and a solution of 622 mg (2.77 mmol, 3.0 in correspondence to methoxyamine, thus 6.0 equiv. in correspondence to the repetition group) of 77 wt% *m*CPBA dissolved in 25 mL DCM was added in one portion. The solution was stirred at room temperature for 4 hours and afterward, the solution was filtered over a neutral Al_2O_3 column and precipitated in 20 mL MeOH and in 20 mL hexane. The precipitate was freeze-dried form 1,4-dioxane, yielding 75-82% of red powder.

PDTOVP

EPR (9.46 GHz, DCM, 300K): 2.0086 g

EA: Calc. C 57.68, H 8.95, N 6.73, O 19.21, P 7.44. Found: C 56.76, H 8.99, N 6.61

Thermolytic deprotection of PDTPVP

For the thermolytic deprotection, 200 mg (319 µmol, 1.0 equiv.) of PDTPVP were dissolved in 20 mL *tert*-butylbenzene (10 mg/mL) and the solution was saturated with oxygen by bubbling air for 30 minutes. The solution was heated to 135 °C for 8 hours. Afterward, the solvent was removed in vacuo and the residue was dissolved in a minimum amount of THF. The polymer was obtained by precipitation in 25 mL hexane/ethyl acetate (1:1) and acetonitrile in 93-95% yield as red flakes.

EPR (9.46 GHz, DCM, 300K): 2.0078 g

EA: Calc. C 59.17, H 9.71, N 6.73, O 19.21, P 7.44. Found: C 59.17, H 9.07, N 6.78

7.7 Self-assembled monolayer formation

The Au-cut quartz crystals (A = 1.54 cm^{-2} for QSX 301) are thoroughly cleaned by piranha solution 3 three times for one minute, followed by intensive washing of the surface with DE water and isopropanol and drying the crystal with a stream of argon. The surface is additionally cleaned by ozone for 10 minutes and the fundamental frequency of the crystal recorded. Afterwards the crystal is immersed in a solution of the respective thiol end-group containing polymer (1-10 mg mL^{-1}) in THF for 12-72 h, followed by intensively rinsing the coated substrate by THF, CHCl$_3$ and isopropanol to remove physiosorbed polymer. After drying the crystals surface in a stream of argon and 15 minutes at 60 °C the shift in resonance frequency is recorded and the surface coverage determined according to equation (2).

7.8 Fabrication of ORBs

The working electrodes were prepared by mixing 10 wt% PDTOVP, 80 wt% of VGCF, and 10 wt% of poly(vinylidene fluoride) (PVdF) in NMP (solid content 10 wt%) to form a homogeneous slurry. Then the slurry was pressed on an aluminium current collector by the doctor blade method and the composite electrodes dried at 100 °C at 10^{-2} mbar for 12 hours. As counter and reference electrode Lithium foil was used and a porous polyethylene membrane (Celgard® 2500) used as separator. A solution of ethylene carbonate/diethyl carbonate (3:7 v/v) containing 1M of $LiPF_6$ was used as an electrolyte. Cyclic voltammetry was performed a scan rate of 10 mV s^{-1} ranging from 2.0 to 4.0 V, potentiostatic electrochemical impedance spectroscopy (PEIS) with a potential amplitude set at 10 mV from 1.0-10,000 Hz. The galvanostatic cycling test were performed in the range of 2.5-4.5 V with varying C-rates derived from the weight of the dried working electrode.

8 References

1.   Feldman, D., Polymer History. *Designed Monomers and Polymers* **2012,** *11* (1), 1-15, doi: 10.1163/156855508x292383.

2.   Mulhaupt, R., Hermann Staudinger and the origin of macromolecular chemistry. *Angew Chem Int Ed Engl* **2004,** *43* (9), 1054-63, doi: 10.1002/anie.200330070.

3.   Wilke, G., Fifty years of Ziegler catalysts: consequences and development of an invention. *Angew Chem Int Ed Engl* **2003,** *42* (41), 5000-8, doi: 10.1002/anie.200330056.

4.   Koltzenburg, S.; Maskos, M.; Nuyken, O., *Polymer Chemistry*. 2017.

5.   Distribution of Plastic Production Worldwide in 2018, by Type. https://www.statista.com/statistics/968808/distribution-of-global-plastic-production-by-type/ (accessed 03.4.2021).

6.   Abd-El-Aziz, A. S.; Antonietti, M.; Barner-Kowollik, C.; Binder, W. H.; Böker, A.; Boyer, C.; Buchmeiser, M. R.; Cheng, S. Z. D.; D'Agosto, F.; Floudas, G.; Frey, H.; Galli, G.; Genzer, J.; Hartmann, L.; Hoogenboom, R.; Ishizone, T.; Kaplan, D. L.; Leclerc, M.; Lendlein, A.; Liu, B.; Long, T. E.; Ludwigs, S.; Lutz, J. F.; Matyjaszewski, K.; Meier, M. A. R.; Müllen, K.; Müllner, M.; Rieger, B.; Russell, T. P.; Savin, D. A.; Schlüter, A. D.; Schubert, U. S.; Seiffert, S.; Severing, K.; Soares, J. B. P.; Staffilani, M.; Sumerlin, B. S.; Sun, Y.; Tang, B. Z.; Tang, C.; Théato, P.; Tirelli, N.; Tsui, O. K. C.; Unterlass, M. M.; Vana, P.; Voit, B.; Vyazovkin, S.; Weder, C.; Wiesner, U.; Wong, W. Y.; Wu, C.; Yagci, Y.; Yuan, J.; Zhang, G., The Next 100 Years of Polymer Science. *Macromolecular Chemistry and Physics* **2020,** *221* (16), doi: 10.1002/macp.202000216.

7.   Vorosmarty, C. J.; Green, P.; Salisbury, J.; Lammers, R. B., Global water resources: vulnerability from climate change and population growth. *Science* **2000,** *289* (5477), 284-8, doi: 10.1126/science.289.5477.284.

8.   Lu, X.; Feng, X.; Yang, Y.; Jiang, J.; Cheng, W.; Liu, C.; Gopinadhan, M.; Osuji, C. O.; Ma, J.; Elimelech, M., Tuning the permselectivity of polymeric desalination membranes via control of polymer crystallite size. *Nat Commun* **2019,** *10* (1), 2347, doi: 10.1038/s41467-019-10132-0.

9.   Silva, T. L. S.; Morales-Torres, S.; Figueiredo, J. L.; Silva, A. M. T., Polymer Membranes for Water Desalination and Treatment. In *Nanostructured Polymer Membranes*, 2016; pp 251-286.

10.   Dammes, N.; Peer, D., Paving the Road for RNA Therapeutics. *Trends in Pharmacological Sciences* **2020,** *41* (10), 755-775, doi: 10.1016/j.tips.2020.08.004.

11.   Wadhwa, A.; Aljabbari, A.; Lokras, A.; Foged, C.; Thakur, A., Opportunities and Challenges in the Delivery of mRNA-based Vaccines. *Pharmaceutics* **2020,** *12* (2), doi: 10.3390/pharmaceutics12020102.

12.   Hajj, K. A.; Whitehead, K. A., Tools for translation: non-viral materials for therapeutic mRNA delivery. *Nature Reviews Materials* **2017,** *2* (10), doi: 10.1038/natrevmats.2017.56.

13.   Hartl, N.; Adams, F.; Merkel, O. M., From adsorption to covalent bonding: Apolipoprotein E functionalization of polymeric nanoparticles for drug delivery across the blood-brain barrier. *Adv Ther (Weinh)* **2021,** *4* (1), doi: 10.1002/adtp.202000092.

14.   Fliervoet, L. A. L.; Engbersen, J. F. J.; Schiffelers, R. M.; Hennink, W. E.; Vermonden, T., Polymers and hydrogels for local nucleic acid delivery. *J Mater Chem B* **2018,** *6* (36), 5651-5670, doi: 10.1039/c8tb01795f.

15.   Uz, M.; Alsoy Altinkaya, S.; Mallapragada, S. K., Stimuli responsive polymer-based strategies for polynucleotide delivery. *Journal of Materials Research* **2017,** *32* (15), 2930-2953, doi: 10.1557/jmr.2017.116.

16.   Chatterjee, S.; Chi-Leung Hui, P., Review of Stimuli-Responsive Polymers in Drug Delivery and Textile Application. *Molecules* **2019,** *24* (14), doi: 10.3390/molecules24142547.

17.   *The Global Risk Report 2019*; World Economic Forum®: Geneva, Switzerland, 2019.

18.   Wang, W.; Zhou, M.; Yuan, D., Carbon dioxide capture in amorphous porous organic polymers. *Journal of Materials Chemistry A* **2017,** *5* (4), 1334-1347, doi: 10.1039/c6ta09234a.

19.   *Urban Energy Transition*. 2 ed.; Elsevier: 2018; p 706.

20.   Lai, W. F.; Wong, W. T., Design of Polymeric Gene Carriers for Effective Intracellular Delivery. *Trends Biotechnol* **2018,** *36* (7), 713-728, doi: 10.1016/j.tibtech.2018.02.006.

21.   Lee, J.; Aluru, N. R., Water-solubility-driven separation of gases using graphene membrane. *Journal of Membrane Science* **2013,** *428*, 546-553, doi: 10.1016/j.memsci.2012.11.006.

22.   Liu, Y.; Xie, D.; Song, M.; Jiang, L.; Fu, G.; Liu, L.; Li, J., Water desalination across multilayer graphitic carbon nitride membrane: Insights from non-equilibrium molecular dynamics simulations. *Carbon* **2018,** *140*, 131-138, doi: 10.1016/j.carbon.2018.08.043.

23.   Hansen, K. A.; Nerkar, J.; Thomas, K.; Bottle, S. E.; O'Mullane, A. P.; Talbot, P. C.; Blinco, J. P., New Spin on Organic Radical Batteries-An Isoindoline Nitroxide-Based High-Voltage Cathode Material. *ACS Appl Mater Interfaces* **2018,** *10* (9), 7982-7988, doi: 10.1021/acsami.7b18252.

24.   Cheng, X.-B.; Zhao, C.-Z.; Yao, Y.-X.; Liu, H.; Zhang, Q., Recent Advances in Energy Chemistry between Solid-State Electrolyte and Safe Lithium-Metal Anodes. *Chem* **2019,** *5* (1), 74-96, doi: 10.1016/j.chempr.2018.12.002.

25.   Sapkota, P.; Boyer, C.; Dutta, R.; Cazorla, C.; Aguey-Zinsou, K.-F., Planar polymer electrolyte membrane fuel cells: powering portable devices from hydrogen. *Sustainable Energy & Fuels* **2020,** *4* (2), 439-468, doi: 10.1039/c9se00861f.

26.   Martins, P. M.; Nunes-Pereira, J.; Lanceros-Méndez, S.; Costa, C. M., Synthetic polymer-based membranes for lithium-ion batteries. In *Synthetic Polymeric Membranes for Advanced Water Treatment, Gas Separation, and Energy Sustainability*, 2020; pp 383-415.

27.   Ding, Z.; Li, J.; Li, J.; An, C., Review—Interfaces: Key Issue to Be Solved for All Solid-State Lithium Battery Technologies. *Journal of The Electrochemical Society* **2020,** *167* (7), doi: 10.1149/1945-7111/ab7f84.

28.   Xia, S.; Wu, X.; Zhang, Z.; Cui, Y.; Liu, W., Practical Challenges and Future Perspectives of All-Solid-State Lithium-Metal Batteries. *Chem* **2019,** *5* (4), 753-785, doi: 10.1016/j.chempr.2018.11.013.

29.   Kim, J. G.; Son, B.; Mukherjee, S.; Schuppert, N.; Bates, A.; Kwon, O.; Choi, M. J.; Chung, H. Y.; Park, S., A review of lithium and non-lithium based solid state batteries. *Journal of Power Sources* **2015,** *282*, 299-322, doi: 10.1016/j.jpowsour.2015.02.054.

30.   Zhao, Q.; Stalin, S.; Zhao, C.-Z.; Archer, L. A., Designing solid-state electrolytes for safe, energy-dense batteries. *Nature Reviews Materials* **2020,** *5* (3), 229-252, doi: 10.1038/s41578-019-0165-5.

31.   Zheng, Y.; Yao, Y.; Ou, J.; Li, M.; Luo, D.; Dou, H.; Li, Z.; Amine, K.; Yu, A.; Chen, Z., A review of composite solid-state electrolytes for lithium batteries: fundamentals, key materials and advanced structures. *Chem Soc Rev* **2020,** *49* (23), 8790-8839, doi: 10.1039/d0cs00305k.

32.   Wu, Z.; Xie, Z.; Yoshida, A.; Wang, Z.; Hao, X.; Abudula, A.; Guan, G., Utmost limits of various solid electrolytes in all-solid-state lithium batteries: A critical review.

Renewable and Sustainable Energy Reviews **2019,** *109*, 367-385, doi: 10.1016/j.rser.2019.04.035.

33.   Vielstich, W.; Lamm, A.; Gasteiger, H., *Handbook of fuel cells. Fundamentals, technology, applications*. Wiley: United Kingdom, 2003; p 3826.

34.   Sun, C., *Advanced Battery Materials*. Wiley: United Kingdom, 2019; p 672

35.   Talens Peiró, L.; Villalba Méndez, G.; Ayres, R. U., Lithium: Sources, Production, Uses, and Recovery Outlook. *Jom* **2013,** *65* (8), 986-996, doi: 10.1007/s11837-013-0666-4.

36.   Zeng, X.; Li, J., On the sustainability of cobalt utilization in China. *Resources, Conservation and Recycling* **2015,** *104*, 12-18, doi: 10.1016/j.resconrec.2015.09.014.

37.   Wood, D. L.; Li, J.; Daniel, C., Prospects for reducing the processing cost of lithium ion batteries. *Journal of Power Sources* **2015,** *275*, 234-242, doi: 10.1016/j.jpowsour.2014.11.019.

38.   Mudd, G. M.; Weng, Z.; Jowitt, S. M.; Turnbull, I. D.; Graedel, T. E., Quantifying the recoverable resources of by-product metals: The case of cobalt. *Ore Geology Reviews* **2013,** *55*, 87-98, doi: https://doi.org/10.1016/j.oregeorev.2013.04.010.

39.   Velázquez, M.; Valio; Santasalo, A.; Reuter; Serna, G., A Critical Review of Lithium-Ion Battery Recycling Processes from a Circular Economy Perspective. *Batteries* **2019,** *5* (4), doi: 10.3390/batteries5040068.

40.   Vaalma, C.; Buchholz, D.; Weil, M.; Passerini, S., A cost and resource analysis of sodium-ion batteries. *Nature Reviews Materials* **2018,** *3* (4), doi: 10.1038/natrevmats.2018.13.

41.   Weil, M.; Ziemann, S.; Peters, J., The issue of metal resources in Li-ion batteries for electric vehicles. In *Behaviour of lithium-ion batteries in electric vehicles*, Springer: 2018; pp 59-74.

42.   Wang, Y. J.; Yu, G., Conjugated polymers: From synthesis, transport properties, to device applications. *Journal of Polymer Science Part B: Polymer Physics* **2019,** *57* (23), 1557-1558, doi: 10.1002/polb.24911.

43.   Heeger, A. J., Nobel Lecture: Semiconducting and metallic polymers: The fourth generation of polymeric materials. *Reviews of Modern Physics* **2001,** *73* (3), 681-700, doi: 10.1103/RevModPhys.73.681.

44.   Etemad, S.; Heeger, A. J., Polyacetylene, (CH)x: The Prototype Conducting Polymer. *Annual Review of Physical Chemistry* **1982,** *33* (1), 443-469, doi: 10.1146/annurev.pc.33.100182.002303.

45.   Heinze, J.; Frontana-Uribe, B. A.; Ludwigs, S., Electrochemistry of conducting polymers--persistent models and new concepts. *Chem Rev* **2010,** *110* (8), 4724-71, doi: 10.1021/cr900226k.

46.   MacInnes, D.; Druy, M. A.; Nigrey, P. J.; Nairns, D. P.; MacDiarmid, A. G.; Heeger, A. J., Organic batteries: reversible n- and p- type electrochemical doping of polyacetylene, (CH) x. *Journal of the Chemical Society, Chemical Communications* **1981,** (7), doi: 10.1039/c39810000317.

47.   Novak, P.; Muller, K.; Santhanam, K. S.; Haas, O., Electrochemically Active Polymers for Rechargeable Batteries. *Chem Rev* **1997,** *97* (1), 207-282, doi: 10.1021/cr941181o.

48.   Giraud, L.; Grelier, S.; Grau, E.; Hadziioannou, G.; Brochon, C.; Cramail, H.; Cloutet, E., Upgrading the chemistry of π-conjugated polymers toward more sustainable materials. *Journal of Materials Chemistry C* **2020,** *8* (29), 9792-9810, doi: 10.1039/d0tc01645d.

49.   Kurosaki, T.; Lee, K. W.; Okawara, M., Polymers having stable radicals. I. Synthesis of nitroxyl polymers from 4-methacryloyl derivatives of 2,2,6,6-tetramethylpiperidine. *Journal of Polymer Science Part A-1: Polymer Chemistry* **1972,** *10* (11), 3295-3310, doi: 10.1002/pol.1972.170101116.

50.   Nishide, H.; Iwasa, S.; Pu, Y.-J.; Suga, T.; Nakahara, K.; Satoh, M., Organic radical battery: nitroxide polymers as a cathode-active material. *Electrochimica Acta* **2004,** *50* (2), 827-831, doi: https://doi.org/10.1016/j.electacta.2004.02.052.

51.   Janoschka, T.; Hager, M. D.; Schubert, U. S., Powering up the future: radical polymers for battery applications. *Adv Mater* **2012,** *24* (48), 6397-409, doi: 10.1002/adma.201203119.

52.   Muench, S.; Wild, A.; Friebe, C.; Haupler, B.; Janoschka, T.; Schubert, U. S., Polymer-Based Organic Batteries. *Chem Rev* **2016,** *116* (16), 9438-84, doi: 10.1021/acs.chemrev.6b00070.

53.   Winsberg, J.; Hagemann, T.; Janoschka, T.; Hager, M. D.; Schubert, U. S., Redox-Flow Batteries: From Metals to Organic Redox-Active Materials. *Angew Chem Int Ed Engl* **2017,** *56* (3), 686-711, doi: 10.1002/anie.201604925.

54.   Tomlinson, E. P.; Hay, M. E.; Boudouris, B. W., Radical Polymers and Their Application to Organic Electronic Devices. *Macromolecules* **2014,** *47* (18), 6145-6158, doi: 10.1021/ma5014572.

55.   Zhang, K.; Monteiro, M. J.; Jia, Z., Stable organic radical polymers: synthesis and applications. *Polymer Chemistry* **2016,** *7* (36), 5589-5614, doi: 10.1039/C6PY00996D.

56.   Hansen, K.-A.; Blinco, J. P., Nitroxide radical polymers – a versatile material class for high-tech applications. *Polymer Chemistry* **2018,** *9* (13), 1479-1516, doi: 10.1039/c7py02001e.

57.   Xie, Y.; Zhang, K.; Yamauchi, Y.; Oyaizu, K.; Jia, Z., Nitroxide radical polymers for emerging plastic energy storage and organic electronics: fundamentals, materials, and applications. *Materials Horizons* **2021,** *8* (3), 803-829, doi: 10.1039/d0mh01391a.

58.   Casado, N.; Mecerreyes, D., Chapter 1. Introduction to Redox Polymers: Classification, Characterization Methods and Main Applications. In *Redox Polymers for Energy and Nanomedicine*, Royal Society of Chemistry: United Kingdom, 2020; pp 1-26.

59.   Kim, J.; Kim, J. H.; Ariga, K., Redox-Active Polymers for Energy Storage Nanoarchitectonics. *Joule* **2017,** *1* (4), 739-768, doi: 10.1016/j.joule.2017.08.018.

60.   Volodarsky, L. B.; Reznikov, V. A.; Ovcharenko, V. I., *Synthetic Chemistry of Stable Nitroxides*. CRC Press: 2017.

61.   Hicks, R. G., *Stable Radicals*. 2010.

62.   Keana, J. F. W., Newer aspects of the synthesis and chemistry of nitroxide spin labels. *Chemical Reviews* **1978,** *78* (1), 37-64, doi: 10.1021/cr60311a004.

63.   Nilsen, A.; Braslau, R., Nitroxide decomposition: Implications toward nitroxide design for applications in living free-radical polymerization. *Journal of Polymer Science Part A: Polymer Chemistry* **2006,** *44* (2), 697-717, doi: 10.1002/pola.21207.

64.   Grubbs, R. B., Nitroxide-Mediated Radical Polymerization: Limitations and Versatility. *Polymer Reviews* **2011,** *51* (2), 104-137, doi: 10.1080/15583724.2011.566405.

65.   Nicolas, J.; Guillaneuf, Y.; Lefay, C.; Bertin, D.; Gigmes, D.; Charleux, B., Nitroxide-mediated polymerization. *Progress in Polymer Science* **2013,** *38* (1), 63-235, doi: 10.1016/j.progpolymsci.2012.06.002.

66.   Yang, D.; Feng, C.; Hu, J., Nitroxide radical coupling reaction: a powerful tool in polymer and material synthesis. *Polymer Chemistry* **2013,** *4* (8), doi: 10.1039/c2py20987j.

67.   Maeda, T.; Otsuka, H.; Takahara, A., Dynamic covalent polymers: Reorganizable polymers with dynamic covalent bonds. *Progress in Polymer Science* **2009,** *34* (7), 581-604, doi: https://doi.org/10.1016/j.progpolymsci.2009.03.001.

68.   Wylie, L.; Blesch, T.; Freeman, R.; Hatakeyama-Sato, K.; Oyaizu, K.; Yoshizawa-Fujita, M.; Izgorodina, E. I., Reversible Reduction of the TEMPO Radical:

One Step Closer to an All-Organic Redox Flow Battery. *ACS Sustainable Chemistry & Engineering* **2020,** *8* (49), 17988-17996, doi: 10.1021/acssuschemeng.0c05687.

69. Gryn'ova, G.; Barakat, J. M.; Blinco, J. P.; Bottle, S. E.; Coote, M. L., Computational design of cyclic nitroxides as efficient redox mediators for dye-sensitized solar cells. *Chemistry* **2012,** *18* (24), 7582-93, doi: 10.1002/chem.201103598.

70. Blinco, J. P.; Hodgson, J. L.; Morrow, B. J.; Walker, J. R.; Will, G. D.; Coote, M. L.; Bottle, S. E., Experimental and theoretical studies of the redox potentials of cyclic nitroxides. *J Org Chem* **2008,** *73* (17), 6763-71, doi: 10.1021/jo801099w.

71. Cao, Q.; Dornan, L. M.; Rogan, L.; Hughes, N. L.; Muldoon, M. J., Aerobic oxidation catalysis with stable radicals. *Chem Commun (Camb)* **2014,** *50* (35), 4524-43, doi: 10.1039/c3cc47081d.

72. Likhtenstein, G. I.; Ishii, K.; Nakatsuji, S., Dual chromophore-nitroxides: novel molecular probes, photochemical and photophysical models and magnetic materials. *Photochem Photobiol* **2007,** *83* (4), 871-81, doi: 10.1111/j.1751-1097.2007.00141.x.

73. Hyodo, F.; Soule, B. P.; Matsumoto, K.; Matusmoto, S.; Cook, J. A.; Hyodo, E.; Sowers, A. L.; Krishna, M. C.; Mitchell, J. B., Assessment of tissue redox status using metabolic responsive contrast agents and magnetic resonance imaging. *J Pharm Pharmacol* **2008,** *60* (8), 1049-60, doi: 10.1211/jpp.60.8.0011.

74. Danhier, P.; Gallez, B., Electron paramagnetic resonance: a powerful tool to support magnetic resonance imaging research. *Contrast Media Mol Imaging* **2015,** *10* (4), 266-81, doi: 10.1002/cmmi.1630.

75. Griffith, O. H.; Keana, J. F. W.; Rottschaefer, S.; Warlick, T. A., Preparation and magnetic resonance of nitroxide polymers. *Journal of the American Chemical Society* **1967,** *89* (19), 5072-5072, doi: 10.1021/ja00995a061.

76. Deng, K.; Zeng, Q.; Wang, D.; Liu, Z.; Qiu, Z.; Zhang, Y.; Xiao, M.; Meng, Y., Single-ion conducting gel polymer electrolytes: design, preparation and application. *Journal of Materials Chemistry A* **2020,** *8* (4), 1557-1577, doi: 10.1039/c9ta11178f.

77. Komaba, S.; Tanaka, T.; Ozeki, T.; Taki, T.; Watanabe, H.; Tachikawa, H., Fast redox of composite electrode of nitroxide radical polymer and carbon with polyacrylate binder. *Journal of Power Sources* **2010,** *195* (18), 6212-6217, doi: 10.1016/j.jpowsour.2009.10.078.

78. Zhang, Y.; Park, A.; Cintora, A.; McMillan, S. R.; Harmon, N. J.; Moehle, A.; Flatté, M. E.; Fuchs, G. D.; Ober, C. K., Impact of the synthesis method on the solid-state charge transport of radical polymers. *Journal of Materials Chemistry C* **2017,** *6* (1), 111-118,

79. Sukegawa, T.; Omata, H.; Masuko, I.; Oyaizu, K.; Nishide, H., Anionic Polymerization of 4-Methacryloyloxy-TEMPO Using an MMA-Capped Initiator. *ACS Macro Letters* **2014,** *3* (3), 240-243, doi: 10.1021/mz400644y.

80. Oyaizu, K.; Suga, T.; Yoshimura, K.; Nishide, H., Synthesis and Characterization of Radical-Bearing Polyethers as an Electrode-Active Material for Organic Secondary Batteries. *Macromolecules* **2008,** *41* (18), 6646-6652, doi: 10.1021/ma702576z.

81. Koshika, K.; Sano, N.; Oyaizu, K.; Nishide, H., An ultrafast chargeable polymer electrode based on the combination of nitroxide radical and aqueous electrolyte. *Chem. Commun.* **2009,** (7), 836-838, doi: 10.1039/b818087c.

82. Suguro, M.; Iwasa, S.; Kusachi, Y.; Morioka, Y.; Nakahara, K., Cationic Polymerization of Poly(vinyl ether) Bearing a TEMPO Radical: A New Cathode-Active Material for Organic Radical Batteries. *Macromolecular Rapid Communications* **2007,** *28* (18–19), 1929-1933, doi: 10.1002/marc.200700300.

83. Katsumata, T.; Satoh, M.; Wada, J.; Shiotsuki, M.; Sanda, F.; Masuda, T., Polyacetylene and Polynorbornene Derivatives Carrying TEMPO. Synthesis and Properties as Organic Radical Battery Materials. *Macromolecular Rapid Communications* **2006,** *27* (15), 1206-1211, doi: 10.1002/marc.200600286.

84.   Katsumata, T.; Qu, J.; Shiotsuki, M.; Satoh, M.; Wada, J.; Igarashi, J.; Mizoguchi, K.; Masuda, T., Synthesis, Characterization, and Charge/Discharge Properties of Polynorbornenes Carrying 2,2,6,6-Tetramethylpiperidine-1-oxy Radicals at High Density. *Macromolecules* **2008,** *41* (4), 1175-1183, doi: 10.1021/ma7020425.

85.   Jahnert, T.; Haupler, B.; Janoschka, T.; Hager, M. D.; Schubert, U. S., Polymers based on stable phenoxyl radicals for the use in organic radical batteries. *Macromol Rapid Commun* **2014,** *35* (9), 882-7, doi: 10.1002/marc.201300791.

86.   Fujii, A.; Ishida, T.; Koga, N.; Iwamura, H., Syntheses and magnetic properties of poly(phenylacetylenes) carrying a (1-oxido-3-oxy-4,4,5,5-tetramethyl-2-imidazolin-2-yl) group at the meta or para position of the phenyl ring. *Macromolecules* **1991,** *24* (5), 1077-1082, doi: 10.1021/ma00005a016.

87.   Dulog, L.; Lutz, S., *Die Makromolekulare Chemie, Rapid Communications* **1993,** *14* (3), 147-153, doi: 10.1002/marc.1993.030140301.

88.   Lopez-Pena, H. A.; Hernandez-Munoz, L. S.; Frontana-Uribe, B. A.; Gonzalez, F. J.; Gonzalez, I.; Frontana, C.; Cardoso, J., Tacticity influence on the electrochemical reactivity of group transfer polymerization-synthesized PTMA. *J Phys Chem B* **2012,** *116* (18), 5542-50, doi: 10.1021/jp301207v.

89.   Bugnon, L.; Morton, C. J. H.; Novak, P.; Vetter, J.; Nesvadba, P., Synthesis of Poly(4-methacryloyloxy-TEMPO) via Group-Transfer Polymerization and Its Evaluation in Organic Radical Battery. *Chemistry of Materials* **2007,** *19* (11), 2910-2914, doi: 10.1021/cm063052h.

90.   Janoschka, T.; Teichler, A.; Krieg, A.; Hager, M. D.; Schubert, U. S., Polymerization of free secondary amine bearing monomers by RAFT polymerization and other controlled radical techniques. *Journal of Polymer Science Part A: Polymer Chemistry* **2012,** *50* (7), 1394-1407, doi: 10.1002/pola.25907.

91.   Bertrand, O.; Ernould, B.; Boujioui, F.; Vlad, A.; Gohy, J.-F., Synthesis of polymer precursors of electroactive materials by SET-LRP. *Polymer Chemistry* **2015,** *6* (33), 6067-6072, doi: 10.1039/c5py00896d.

92.   Aydin, M.; Gorur, M.; Yilmaz, F., Phosphazene-cored star polymer bearing redox-active side groups as a cathode-active material in Li-ion batteries. *Reactive and Functional Polymers* **2016,** *102*, 11-19, doi: 10.1016/j.reactfunctpolym.2016.02.008.

93.   Hung, M.-K.; Wang, Y.-H.; Lin, C.-H.; Lin, H.-C.; Lee, J.-T., Synthesis and electrochemical behaviour of nitroxidepolymer brush thin-film electrodes for organic radical batteries. *J. Mater. Chem.* **2012,** *22* (4), 1570-1577, doi: 10.1039/c1jm13911h.

94.   Yang, J.-J.; Li, C.-C.; Yang, Y.-F.; Wang, C.-Y.; Lin, C.-H.; Lee, J.-T., Superparamagnetic core–shell radical polymer brush as efficient catalyst for oxidation of alcohols to aldehydes and ketones. *RSC Advances* **2016,** *6* (68), 63472-63476, doi: 10.1039/c6ra02739c.

95.   Liu, S.; Wang, H.; Chu, X., Nitroxide polymer brushes as efficient and recoverable catalysts for the selective oxidation of primary alcohols to aldehydes. *Journal of Applied Polymer Science* **2017,** *134* (1), doi: 10.1002/app.44365.

96.   Koshika, K.; Chikushi, N.; Sano, N.; Oyaizu, K.; Nishide, H., A TEMPO-substituted polyacrylamide as a new cathode material: an organic rechargeable device composed of polymer electrodes and aqueous electrolyte. *Green Chemistry* **2010,** *12* (9), 1573, doi: 10.1039/b926296b.

97.   Chikushi, N.; Yamada, H.; Oyaizu, K.; Nishide, H., TEMPO-substituted polyacrylamide for an aqueous electrolyte-typed and organic-based rechargeable device. *Science China Chemistry* **2012,** *55* (5), 822-829, doi: 10.1007/s11426-012-4556-3.

98.   Miyazawa, T.; Endo, T.; Okawara, M., Synthesis and polymerization of 4-o-vinylbenzyl-2,2,6,6-tetramethylpiperidine. *Journal of Polymer Science: Polymer Chemistry Edition* **1985,** *23* (5), 1527-1535, doi: 10.1002/pol.1985.170230524.

99.   Zhang, X.; Li, H.; Li, L.; Lu, G.; Zhang, S.; Gu, L.; Xia, Y.; Huang, X., Polyallene with pendant nitroxyl radicals. *Polymer* **2008,** *49* (16), 3393-3398, doi: 10.1016/j.polymer.2008.06.019.

100.   Zhuang, X.; Zhang, H.; Chikushi, N.; Zhao, C.; Oyaizu, K.; Chen, X.; Nishide, H., Biodegradable and electroactive TEMPO-substituted acrylamide/lactide copolymers. *Macromol Biosci* **2010,** *10* (10), 1203-9, doi: 10.1002/mabi.201000031.

101.   Zhuang, X.; Xiao, C.; Oyaizu, K.; Chikushi, N.; Chen, X.; Nishide, H., Synthesis of amphiphilic block copolymers bearing stable nitroxyl radicals. *Journal of Polymer Science Part A: Polymer Chemistry* **2010,** *48* (23), 5404-5410, doi: 10.1002/pola.24345.

102.   Hauffman, G.; Rolland, J.; Bourgeois, J.-P.; Vlad, A.; Gohy, J.-F., Synthesis of nitroxide-containing block copolymers for the formation of organic cathodes. *Journal of Polymer Science Part A: Polymer Chemistry* **2013,** *51* (1), 101-108, doi: 10.1002/pola.26279.

103.   Takahashi, K.; Korolev, K.; Tsuji, K.; Oyaizu, K.; Nishide, H.; Bryuzgin, E.; Navrotskiy, A.; Novakov, I., Facile grafting-onto-preparation of block copolymers of TEMPO and glycidyl methacrylates on an oxide substrate as an electrode-active layer. *Polymer* **2015,** *68*, 310-314, doi: 10.1016/j.polymer.2015.02.043.

104.   Suga, T.; Pu, Y.-J.; Kasatori, S.; Nishide, H., Cathode- and Anode-Active Poly(nitroxylstyrene)s for Rechargeable Batteries: p- and n-Type Redox Switching via Substituent Effects. *Macromolecules* **2007,** *40* (9), 3167-3173, doi: 10.1021/ma0628578.

105.   Suga, T.; Ohshiro, H.; Sugita, S.; Oyaizu, K.; Nishide, H., Emerging N-Type Redox-Active Radical Polymer for a Totally Organic Polymer-Based Rechargeable Battery. *Advanced Materials* **2009,** *21* (16), 1627-1630, doi: 10.1002/adma.200803073.

106.   Suga, T.; Sugita, S.; Ohshiro, H.; Oyaizu, K.; Nishide, H., p- and n-Type Bipolar Redox-Active Radical Polymer: Toward Totally Organic Polymer-Based Rechargeable Devices with Variable Configuration. *Advanced Materials* **2011,** *23* (6), 751-+, doi: 10.1002/adma.201003525.

107.   Behrends, F.; Wagner, H.; Studer, A.; Niehaus, O.; Pöttgen, R.; Eckert, H., Polynitroxides from Alkoxyamine Monomers: Structural and Kinetic Investigations by Solid State NMR. *Macromolecules* **2013,** *46* (7), 2553-2561, doi: 10.1021/ma400351q.

108.   Aqil, M.; Aqil, A.; Ouhib, F.; El Idrissi, A.; Detrembleur, C.; Jérôme, C., RAFT polymerization of an alkoxyamine bearing acrylate, towards a well-defined redox active polyacrylate. *RSC Advances* **2015,** *5* (103), 85035-85038, doi: 10.1039/C5RA16839B.

109.   Aqil, A.; Vlad, A.; Piedboeuf, M.-L.; Aqil, M.; Job, N.; Melinte, S.; Detrembleur, C.; Jérôme, C., A new design of organic radical batteries (ORBs): carbon nanotube buckypaper electrode functionalized by electrografting. *Chemical Communications* **2015,** *51* (45), 9301-9304,

110.   Chalmers, B. A.; Morris, J. C.; Fairfull-Smith, K. E.; Grainger, R. S.; Bottle, S. E., A novel protecting group methodology for syntheses using nitroxides. *Chem Commun (Camb)* **2013,** *49* (88), 10382-4, doi: 10.1039/c3cc46146g.

111.   Hansen, K.-A.; Chambers, L. C.; Eing, M.; Barner-Kowollik, C.; Fairfull-Smith, K. E.; Blinco, J. P., A Methoxyamine-Protecting Group for Organic Radical Battery Materials-An Alternative Approach. *ChemSusChem* **2020**, doi: 10.1002/cssc.201903529.

112.   Hansen, K.-A.; Nerkar, J.; Thomas, K.; Bottle, S. E.; O'Mullane, A. P.; Talbot, P. C.; Blinco, J. P., New Spin on Organic Radical Batteries–An Isoindoline Nitroxide-Based High-Voltage Cathode Material. *ACS Applied Materials & Interfaces* **2018,** *10* (9), 7982-7988, doi: 10.1021/acsami.7b18252.

113.   Kunz, T. K.; Wolf, M. O., Electrodeposition and properties of TEMPO functionalized polythiophene thin films. *Polymer Chemistry* **2011,** *2* (3), 640-644, doi: 10.1039/C0PY00308E.

114.   Xue, W.; Mutlu, H.; Theato, P., Post-polymerization modification of polymeric active esters towards TEMPO containing polymers: A systematic study. *European Polymer Journal* **2020,** *130*, doi: 10.1016/j.eurpolymj.2020.109660.

115.   Suguro, M.; Mori, A.; Iwasa, S.; Nakahara, K.; Nakano, K., Syntheses and Electrochemical Properties of TEMPO Radical Substituted Silicones: Active Material for Organic Radical Batteries. *Macromolecular Chemistry and Physics* **2009,** *210* (17), 1402-1407, doi: 10.1002/macp.200900251.

116.   Matyjaszewski, K.; Woodworth, B. E.; Zhang, X.; Gaynor, S. G.; Metzner, Z., Simple and Efficient Synthesis of Various Alkoxyamines for Stable Free Radical Polymerization. *Macromolecules* **1998,** *31* (17), 5955-5957, doi: 10.1021/ma9807264.

117.   Lin, W.; Fu, Q.; Zhang, Y.; Huang, J., One-Pot Synthesis of ABC Type Triblock Copolymers via a Combination of "Click Chemistry" and Atom Transfer Nitroxide Radical Coupling Chemistry. *Macromolecules* **2008,** *41* (12), 4127-4135, doi: 10.1021/ma702404t.

118.   Zhang, K.; Hu, Y.; Wang, L.; Monteiro, M. J.; Jia, Z., Pyrene-Functionalized PTMA by NRC for Greater π–π Stacking with rGO and Enhanced Electrochemical Properties. *ACS Applied Materials & Interfaces* **2017,** *9* (40), 34900-34908, doi: 10.1021/acsami.7b09604.

119.   Hu, Y.; Zhang, K.; Hu, H.; Wang, S.; Ye, D.; Monteiro, M. J.; Jia, Z.; Wang, L., Molecular-level anchoring of polymer cathodes on carbon nanotubes towards rapid-rate and long-cycle sodium-ion storage. *Materials Chemistry Frontiers* **2018,** *2* (10), 1805-1810, doi: 10.1039/c8qm00163d.

120.   Fu, Q.; Lin, W.; Huang, J., A New Strategy for Preparation of Graft Copolymers via "Graft onto" by Atom Transfer Nitroxide Radical Coupling Chemistry: Preparation of Poly(4-glycidyloxy-2,2,6,6-tetramethylpiperidine-1-oxyl-co-ethylene oxide)-graft-polystyrene and Poly(tert-butyl acrylate). *Macromolecules* **2008,** *41* (7), 2381-2387, doi: 10.1021/ma7028117.

121.   Jia, Z.; Fu, Q.; Huang, J., Synthesis of poly(ethylene oxide) with pending 2,2,6,6-tetramethylpiperidine-1-oxyl groups and its further initiation of the grafting polymerization of styrene. *Journal of Polymer Science Part A: Polymer Chemistry* **2006,** *44* (12), 3836-3842, doi: 10.1002/pola.21488.

122.   Jia, Z.; Fu, Q.; Huang, J., Synthesis of Amphiphilic Macrocyclic Graft Copolymer Consisting of a Poly(ethylene oxide) Ring and Multi-Polystyrene Lateral Chains. *Macromolecules* **2006,** *39* (16), 5190-5193, doi: 10.1021/ma060934t.

123.   Rostro, L.; Baradwaj, A. G.; Boudouris, B. W., Controlled radical polymerization and quantification of solid state electrical conductivities of macromolecules bearing pendant stable radical groups. *ACS Appl Mater Interfaces* **2013,** *5* (20), 9896-901, doi: 10.1021/am403223s.

124.   Hay, M. E.; Hui Wong, S.; Mukherjee, S.; Boudouris, B. W., Controlling open-shell loading in norbornene-based radical polymers modulates the solid-state charge transport exponentially. *Journal of Polymer Science Part B: Polymer Physics* **2017,** *55* (20), 1516-1525, doi: 10.1002/polb.24406.

125.   Rostro, L.; Wong, S. H.; Boudouris, B. W., Solid State Electrical Conductivity of Radical Polymers as a Function of Pendant Group Oxidation State. *Macromolecules* **2014,** *47* (11), 3713-3719, doi: 10.1021/ma500626t.

126.   Joo, Y.; Agarkar, V.; Sung, S. H.; Savoie, B. M.; Boudouris, B. W., A nonconjugated radical polymer glass with high electrical conductivity. *Science* **2018,** *359* (6382), 1391-1395, doi: 10.1126/science.aao7287.

127.   Groenendaal, L.; Jonas, F.; Freitag, D.; Pielartzik, H.; Reynolds, J. R., Poly (3, 4-ethylenedioxythiophene) and its derivatives: past, present, and future. *Advanced materials* **2000,** *12* (7), 481-494,

128.   Lutkenhaus, J., A radical advance for conducting polymers. *Science* **2018,** *359* (6382), 1334-1335, doi: 10.1126/science.aat1298.

129.   Nakahara, K.; Iwasa, S.; Satoh, M.; Morioka, Y.; Iriyama, J.; Suguro, M.; Hasegawa, E., Rechargeable batteries with organic radical cathodes. *Chemical Physics Letters* **2002,** *359* (5-6), 351-354, doi: 10.1016/s0009-2614(02)00705-4.

130.   Friebe, C.; Schubert, U. S., High-Power-Density Organic Radical Batteries. *Topics in Current Chemistry* **2017,** *375* (1), 19, doi: 10.1007/s41061-017-0103-1.

131.   Zhang, K.; Hu, Y.; Wang, L.; Fan, J.; Monteiro, M. J.; Jia, Z., The impact of the molecular weight on the electrochemical properties of poly(TEMPO methacrylate). *Polymer Chemistry* **2017,** *8* (11), 1815-1823, doi: 10.1039/c7py00151g.

132.   Qu, J.; Fujii, T.; Katsumata, T.; Suzuki, Y.; Shiotsuki, M.; Sanda, F.; Satoh, M.; Wada, J.; Masuda, T., Helical polyacetylenes carrying 2,2,6,6-tetramethyl-1-piperidinyloxy and 2,2,5,5-tetramethyl-1-pyrrolidinyloxy moieties: Their synthesis, properties, and function. *Journal of Polymer Science Part A: Polymer Chemistry* **2007,** *45* (23), 5431-5445, doi: 10.1002/pola.22288.

133.   Qu, J.; Katsumata, T.; Satoh, M.; Wada, J.; Masuda, T., Poly(7-oxanorbornenes) carrying 2,2,6,6-tetramethylpiperidine-1-oxy (TEMPO) radicals: Synthesis and charge/discharge properties. *Polymer* **2009,** *50* (2), 391-396, doi: https://doi.org/10.1016/j.polymer.2008.11.028.

134.   Xu, L.; Yang, F.; Su, C.; Ji, L.; Zhang, C., Synthesis and properties of novel TEMPO-contained polypyrrole derivatives as the cathode material of organic radical battery. *Electrochimica Acta* **2014,** *130*, 148-155,

135.   Yeşilot, S.; Hacıvelioğlu, F.; Küçükköylü, S.; Çelik, K. B.; Sayan, G.; Demir-Cakan, R., Design, Synthesis, and Characterization of Polyphosphazene Bearing Stable Nitroxide Radicals as Cathode-Active Materials in Li-Ion Batteries. *Macromolecular Chemistry and Physics* **2017,** *218* (17), doi: 10.1002/macp.201700051.

136.   Kemper, T. W.; Larsen, R. E.; Gennett, T., Relationship between Molecular Structure and Electron Transfer in a Polymeric Nitroxyl-Radical Energy Storage Material. *The Journal of Physical Chemistry C* **2014,** *118* (31), 17213-17220, doi: 10.1021/jp501628z.

137.   Sukegawa, T.; Masuko, I.; Oyaizu, K.; Nishide, H., Expanding the Dimensionality of Polymers Populated with Organic Robust Radicals toward Flow Cell Application: Synthesis of TEMPO-Crowded Bottlebrush Polymers Using Anionic Polymerization and ROMP. *Macromolecules* **2014,** *47* (24), 8611-8617, doi: 10.1021/ma501632t.

138.   Ernould, B.; Devos, M.; Bourgeois, J.-P.; Rolland, J.; Vlad, A.; Gohy, J.-F., Grafting of a redox polymer onto carbon nanotubes for high capacity battery materials. *Journal of Materials Chemistry A* **2015,** *3* (16), 8832-8839, doi: 10.1039/C5TA00570A.

139.   Zhang, Y.; An, Y.; Yin, B.; Jiang, J.; Dong, S.; Dou, H.; Zhang, X., A novel aqueous ammonium dual-ion battery based on organic polymers. *Journal of Materials Chemistry A* **2019,** *7* (18), 11314-11320,

140.   Koshika, K.; Sano, N.; Oyaizu, K.; Nishide, H., An Aqueous, Electrolyte-Type, Rechargeable Device Utilizing a Hydrophilic Radical Polymer-Cathode. *Macromolecular Chemistry and Physics* **2009,** *210* (22), 1989-1995, doi: 10.1002/macp.200900257.

141.   Sano, N.; Tomita, W.; Hara, S.; Min, C. M.; Lee, J. S.; Oyaizu, K.; Nishide, H., Polyviologen hydrogel with high-rate capability for anodes toward an aqueous electrolyte-type and organic-based rechargeable device. *ACS Appl Mater Interfaces* **2013,** *5* (4), 1355-61, doi: 10.1021/am302647w.

142.   Hatakeyama-Sato, K.; Wakamatsu, H.; Yamagishi, K.; Fujie, T.; Takeoka, S.; Oyaizu, K.; Nishide, H., Ultrathin and Stretchable Rechargeable Devices with Organic Polymer Nanosheets Conformable to Skin Surface. *Small* **2019,** *15* (13), e1805296, doi: 10.1002/smll.201805296.

143.   Janoschka, T.; Martin, N.; Hager, M. D.; Schubert, U. S., An Aqueous Redox-Flow Battery with High Capacity and Power: The TEMPTMA/MV System. *Angewandte Chemie International Edition* **2016,** *55* (46), 14427-14430, doi: 10.1002/anie.201606472.

144.   Janoschka, T.; Martin, N.; Martin, U.; Friebe, C.; Morgenstern, S.; Hiller, H.; Hager, M. D.; Schubert, U. S., An aqueous, polymer-based redox-flow battery using non-corrosive, safe, and low-cost materials. *Nature* **2015,** *527* (7576), 78-81, doi: 10.1038/nature15746.

145.   Winsberg, J.; Janoschka, T.; Morgenstern, S.; Hagemann, T.; Muench, S.; Hauffman, G.; Gohy, J. F.; Hager, M. D.; Schubert, U. S., Poly(TEMPO)/Zinc Hybrid-Flow Battery: A Novel, "Green," High Voltage, and Safe Energy Storage System. *Adv Mater* **2016,** *28* (11), 2238-43, doi: 10.1002/adma.201505000.

146.   Lai, Y. Y.; Li, X.; Zhu, Y., Polymeric Active Materials for Redox Flow Battery Application. *ACS Applied Polymer Materials* **2020,** *2* (2), 113-128, doi: 10.1021/acsapm.9b00864.

147.   Hagemann, T.; Strumpf, M.; Schröter, E.; Stolze, C.; Grube, M.; Nischang, I.; Hager, M. D.; Schubert, U. S., (2,2,6,6-Tetramethylpiperidin-1-yl)oxyl-Containing Zwitterionic Polymer as Catholyte Species for High-Capacity Aqueous Polymer Redox Flow Batteries. *Chemistry of Materials* **2019,** *31* (19), 7987-7999, doi: 10.1021/acs.chemmater.9b02201.

148.   Winsberg, J.; Muench, S.; Hagemann, T.; Morgenstern, S.; Janoschka, T.; Billing, M.; Schacher, F. H.; Hauffman, G.; Gohy, J.-F.; Hoeppener, S.; Hager, M. D.; Schubert, U. S., Polymer/zinc hybrid-flow battery using block copolymer micelles featuring a TEMPO corona as catholyte. *Polymer Chemistry* **2016,** *7* (9), 1711-1718, doi: 10.1039/c5py02036k.

149.   Liu, Y.; Wang, X.; Song, W.; Wang, G., Synthesis and characterization of silica nanoparticles functionalized with multiple TEMPO groups and investigation on their oxidation activity. *Polymer Chemistry* **2015,** *6* (43), 7514-7523, doi: 10.1039/c5py01190f.

150.   Auten, R. L.; Davis, J. M., Oxygen toxicity and reactive oxygen species: the devil is in the details. *Pediatr Res* **2009,** *66* (2), 121-7, doi: 10.1203/PDR.0b013e3181a9eafb.

151.   Vong, L. B.; Nagasaki, Y., Combination Treatment of Murine Colon Cancer with Doxorubicin and Redox Nanoparticles. *Mol Pharm* **2016,** *13* (2), 449-55, doi: 10.1021/acs.molpharmaceut.5b00676.

152.   Yoshitomi, T.; Suzuki, R.; Mamiya, T.; Matsui, H.; Hirayama, A.; Nagasaki, Y., pH-sensitive radical-containing-nanoparticle (RNP) for the L-band-EPR imaging of low pH circumstances. *Bioconjug Chem* **2009,** *20* (9), 1792-8, doi: 10.1021/bc900214f.

153.   Montembault, V.; Fontaine, L., CHAPTER 6. Polyphosphoesters. In *Phosphorus-Based Polymers*, 2014; pp 97-124.

154.   Gleria, M.; De Jaeger, R., Polyphosphazenes: A Review. In *New Aspects in Phosphorus Chemistry V: -/-*, Majoral, J.-P., Ed. Springer Berlin Heidelberg: Berlin, Heidelberg, 2005; pp 165-251.

155.   Steinmann, M.; Markwart, J.; Wurm, F. R., Poly(alkylidene chlorophosphate)s via Acyclic Diene Metathesis Polymerization: A General Platform for the Postpolymerization Modification of Poly(phosphoester)s. *Macromolecules* **2014,** *47* (24), 8506-8513, doi: 10.1021/ma501959h.

156.   David, G.; Negrell-Guirao, C.; Iftene, F.; Boutevin, B.; Chougrani, K., Recent progress on phosphonate vinyl monomers and polymers therefore obtained by radical (co)polymerization. *Polym. Chem.* **2012,** *3* (2), 265-274, doi: 10.1039/c1py00276g.

157.   Royal Society of Chemistry: 2014; Vol. 11.

158.   Allcock, H. R., CHAPTER 7. Phosphazene High Polymers. In *Phosphorus-Based Polymers*, 2014; pp 125-150.

159.   Pelosi, C.;   Tinè, M. R.; Wurm, F. R., Main-chain water-soluble polyphosphoesters: Multi-functional polymers as degradable PEG-alternatives for biomedical applications. *European Polymer Journal* **2020,** *141*, doi: 10.1016/j.eurpolymj.2020.110079.

160.   Wolf, T.; Steinbach, T.; Wurm, F. R., A Library of Well-Defined and Water-Soluble Poly(alkyl phosphonate)s with Adjustable Hydrolysis. *Macromolecules* **2015,** *48* (12), 3853-3863, doi: 10.1021/acs.macromol.5b00897.

161.   Steinbach, T.; Alexandrino, E. M.; Wahlen, C.; Landfester, K.; Wurm, F. R., Poly(phosphonate)s via Olefin Metathesis: Adjusting Hydrophobicity and Morphology. *Macromolecules* **2014,** *47* (15), 4884-4893, doi: 10.1021/ma5013286.

162.   Steinbach, T.; Wurm, F. R., Degradable Polyphosphoester-Protein Conjugates: "PPEylation" of Proteins. *Biomacromolecules* **2016,** *17* (10), 3338-3346, doi: 10.1021/acs.biomac.6b01107.

163.   Bingöl, B.; Hart-Smith, G.; Barner-Kowollik, C.; Wegner, G., Characterization of Oligo(vinyl phosphonate)s by High-Resolution Electrospray Ionization Mass Spectrometry: Implications for the Mechanism of Polymerization. *Macromolecules* **2008,** *41* (5), 1634-1639, doi: 10.1021/ma702225k.

164.   Kosolapoff, G. M., Some Observations Concerning the Acidic Salts of Phosphonic Acids. *Journal of the American Chemical Society* **1952,** *74* (13), 3427-3428,

165.   Yamada, M.; Honma, I., Anhydrous proton conducting polymer electrolytes based on poly(vinylphosphonic acid)-heterocycle composite material. *Polymer* **2005,** *46* (9), 2986-2992, doi: 10.1016/j.polymer.2005.02.056.

166.   Kaltbeitzel, A.; Schauff, S.; Steininger, H.; Bingol, B.; Brunklaus, G.; Meyer, W.; Spiess, H., Water sorption of poly(vinylphosphonic acid) and its influence on proton conductivity. *Solid State Ionics* **2007,** *178* (7-10), 469-474, doi: 10.1016/j.ssi.2007.02.007.

167.   Macarie, L.; Ilia, G., Poly (vinylphosphonic acid) and its derivatives. *Progress in Polymer Science* **2010,** *35* (8), 1078-1092,

168.   Macarie, L.; Ilia, G., CHAPTER 4. Synthesis and Polymerization of Vinylphosphonic Acid. In *Phosphorus-Based Polymers*, 2014; pp 51-67.

169.   Monge, S.; Canniccioni, B.; David, G.; Robin, J.-J., CHAPTER 1. Polymerization of Phosphorus-Containing (Meth)acrylate Monomers. In *Phosphorus-Based Polymers*, 2014; pp 1-18.

170.   Jeanmaire, T.; Hervaud, Y.; David, G.; Boutevin, B., New Phosphonated Methacrylate Monomers with C2/C3 Spacers. *Phosphorus, Sulfur, and Silicon and the Related Elements* **2008,** *183* (9), 2204-2213, doi: 10.1080/10426500701852737.

171.   Senhaji, O.; Robin, J. J.; Achchoubi, M.; Boutevin, B., Synthesis and Characterization of New Methacrylic Phosphonated Surface Active Monomer. *Macromolecular Chemistry and Physics* **2004,** *205* (8), 1039-1050, doi: 10.1002/macp.200400011.

172.   Li, K.; Lei, H.; Zeng, X.; Li, H.; Lai, X.; Chai, S., Preparation of a flame retardant phosphorus-containing polyacrylate/α-zirconium phosphate nanocomposite through in situ emulsion polymerization. *RSC Adv.* **2017,** *7* (78), 49290-49298, doi: 10.1039/c7ra07131k.

173.   Monge, S.; Graillot, A.; Robin, J.-J., CHAPTER 2. Polymerization of Phosphorus-Containing (meth)acrylamide Monomers. In *Phosphorus-Based Polymers*, 2014; pp 19-34.

174.   Klee, J. E.; Lehmann, U., N-alkyl-N-(phosphonoethyl) substituted (meth)acrylamides - new adhesive monomers for self-etching self-priming one part dental adhesive. *Beilstein J Org Chem* **2009,** *5*, 72, doi: 10.3762/bjoc.5.72.

175. Yu, Z.; Zhu, W.-X.; Cabasso, I., Synthesis and polymerization of vinylbenzylphosphonate diethyl ester. *Journal of Polymer Science Part A: Polymer Chemistry* **1990,** *28* (1), 227-230, doi: 10.1002/pola.1990.080280117.

176. Souzy, R.; Ameduri, B.; Boutevin, B.; Virieux, D., Synthesis of new aromatic perfluorovinyl ether monomers containing phosphonic acid functionality. *Journal of Fluorine Chemistry* **2004,** *125* (9), 1317-1324, doi: 10.1016/j.jfluchem.2004.03.010.

177. Ren, Y.; Cheng, B.; Xu, L.; Jiang, A.; Lu, Y., Fire-retardant copolymer of acrylonitrile withO,O-diethyl-O-allyl thiophosphate. *Journal of Applied Polymer Science* **2010,** *115* (3), 1489-1494, doi: 10.1002/app.31154.

178. D'Agosto, F.; Charreyre, M.-T.; Delolme, F.; Dessalces, G.; Cramail, H.; Deffieux, A.; Pichot, C., Kinetic Study of the "Living" Cationic Polymerization of a Galactose Carrying Vinyl Ether. MALDI-TOF MS Analysis of the Resulting Glycopolymers. *Macromolecules* **2002,** *35* (21), 7911-7918, doi: 10.1021/ma0200017.

179. Iftene, F.; David, G.; Boutevin, B.; Auvergne, R.; Alaaeddine, A.; Meghabar, R., Novel dialkyl vinyl ether phosphonate monomers: Their synthesis and alternated radical copolymerizations with electron-accepting monomers. *Journal of Polymer Science Part A: Polymer Chemistry* **2012,** *50* (12), 2432-2443, doi: 10.1002/pola.26020.

180. Komber, H.; Steinert, V.; Voit, B., 1H,13C, and31P NMR Study on Poly(vinylphosphonic acid) and Its Dimethyl Ester. *Macromolecules* **2008,** *41* (6), 2119-2125, doi: 10.1021/ma702662q.

181. Pike, R. M.; Cohen, R. A., Organophosphorus polymers. I. Peroxide-initiated polymerization of diethyl and diisopropyl vinylphosphonate. *Journal of Polymer Science* **1960,** *44* (144), 531-538, doi: 10.1002/pol.1960.1204414424.

182. Sato, T.; Hasegawa, M.; Seno, M.; Hirano, T., Radical polymerization behavior of dimethyl vinylphosphonate: Homopolymerization and copolymerization with trimethoxyvinylsilane. *Journal of applied polymer science* **2008,** *109* (6), 3746-3752,

183. David, G.; Negrell-Guirao, C., CHAPTER 3. Phosphorus-Containing Vinyl or Allyl Monomers. In *Phosphorus-Based Polymers*, 2014; pp 35-50.

184. Canniccioni, B.; Monge, S.; David, G.; Robin, J.-J., RAFT polymerization of dimethyl(methacryloyloxy)methyl phosphonate and its phosphonic acid derivative: a new opportunity for phosphorus-based materials. *Polymer Chemistry* **2013,** *4* (13), doi: 10.1039/c3py00426k.

185. Huang, J.; Matyjaszewski, K., Atom Transfer Radical Polymerization of Dimethyl(1-ethoxycarbonyl)vinyl Phosphate and Corresponding Block Copolymers. *Macromolecules* **2005,** *38* (9), 3577-3583, doi: 10.1021/ma047564y.

186. Suzuki, S.; Whittaker, M. R.; Grondahl, L.; Monteiro, M. J.; Wentrup-Byrne, E., Synthesis of soluble phosphate polymers by RAFT and their in vitro mineralization. *Biomacromolecules* **2006,** *7* (11), 3178-87, doi: 10.1021/bm060583q.

187. Matyjaszewski, K.; Xia, J., Atom transfer radical polymerization. *Chem Rev* **2001,** *101* (9), 2921-90, doi: 10.1021/cr940534g.

188. Hawker, C. J.; Bosman, A. W.; Harth, E., New polymer synthesis by nitroxide mediated living radical polymerizations. *Chem Rev* **2001,** *101* (12), 3661-88, doi: 10.1021/cr990119u.

189. Barner-Kowollik, C., *Handbook of RAFT Polymerization*. 2008.

190. Hirao, A.; Shiraishi, Y.; Martinez, F.; Phung, H. M.; Nakahama, S.; Yamazaki, N., Anionic and radical polymerization of p-triphenyl- and p-tributylgermyl-styrenes. *Die Makromolekulare Chemie* **1983,** *184* (5), 961-967, doi: 10.1002/macp.1983.021840508.

191. Catel, Y.; Degrange, M.; Le Pluart, L.; Madec, P.-J.; Pham, T.-N.; Picton, L., Synthesis, photopolymerization and adhesive properties of new hydrolytically stable phosphonic acids for dental applications. *Journal of Polymer Science Part A: Polymer Chemistry* **2008,** *46* (21), 7074-7090, doi: 10.1002/pola.23013.

192.   Besse, V.; Le Pluart, L.; Cook, W. D.; Pham, T. N.; Madec, P. J., Synthesis and polymerization kinetics of acrylamide phosphonic acids and esters as new dentine adhesives. *Journal of Polymer Science Part A: Polymer Chemistry* **2013,** *51* (1), 149-157, doi: 10.1002/pola.26339.

193.   Sahin, G.; Avci, D.; Karahan, O.; Moszner, N., Synthesis and photopolymerizations of new phosphonated methacrylates from alkyl α-hydroxymethacrylates and glycidyl methacrylate. *Journal of Applied Polymer Science* **2009,** *114* (1), 97-106, doi: 10.1002/app.30449.

194.   Monge, S.; David, G., Phosphorus-Based Polymers: From Synthesis to Applications. **2014,** P001-318, doi: 10.1039/9781782624523.

195.   Kalek, M.; Ziadi, A.; Stawinski, J., Microwave-assisted palladium-catalyzed cross-coupling of aryl and vinyl halides with H-phosphonate diesters. *Org Lett* **2008,** *10* (20), 4637-40, doi: 10.1021/ol801935r.

196.   Lee, H.-S.; Pai, S.-H.; Liao, W.-T.; Yang, X.-J.; Tsai, F.-Y., Mono and double Mizoroki–Heck reaction of aryl halides with dialkyl vinylphosphonates using a reusable palladium catalyst under aqueous medium. *RSC Advances* **2017,** *7* (54), 34293-34299, doi: 10.1039/c7ra06464k.

197.   Altenbuchner, P. T.; Werz, P. D.; Schoppner, P.; Adams, F.; Kronast, A.; Schwarzenbock, C.; Pothig, A.; Jandl, C.; Haslbeck, M.; Rieger, B., Next Generation Multiresponsive Nanocarriers for Targeted Drug Delivery to Cancer Cells. *Chemistry* **2016,** *22* (41), 14576-84, doi: 10.1002/chem.201601822.

198.   Schwarzenbock, C.; Schaffer, A.; Nossner, E.; Nelson, P. J.; Huss, R.; Rieger, B., Fluorescent Polyvinylphosphonate Bioconjugates for Selective Cellular Delivery. *Chemistry* **2018,** *24* (11), 2584-2587, doi: 10.1002/chem.201706034.

199.   Herpel, R. H.; Vedantham, P.; Flynn, D. L.; Hanson, P. R., High-load, oligomeric phosphonyl dichloride: facile generation via ROM polymerization and application to scavenging amines. *Tetrahedron Letters* **2006,** *47* (36), 6429-6432, doi: https://doi.org/10.1016/j.tetlet.2006.06.130.

200.   Maity, P. K.; Faisal, S.; Rolfe, A.; Stoianova, D.; Hanson, P. R., Silica-Supported Oligomeric Benzyl Phosphate (Si-OBP) and Triazole Phosphate (Si-OTP) Alkylating Reagents. *J Org Chem* **2015,** *80* (20), 9942-50, doi: 10.1021/acs.joc.5b01456.

201.   Bordoni, A. V.; Zalduendo, M. M.; Escobar, A.; Amenitsch, H.; Moya, S. E.; Angelomé, P. C., Phosphonate mesoporous hybrid thin films: Synthesis of organophosphosilane by thiol-ene click chemistry and applications in formation and stabilization of silver nanoparticles. *Microporous and Mesoporous Materials* **2020,** *295*, doi: 10.1016/j.micromeso.2019.109958.

202.   Matveeva, E. V.; Shipov, A. E.; Petrovskii, P. V.; Odinets, I. L., Amino acids as suitable N-nucleophiles for the aza-Michael reaction of vinylphosphoryl compounds in water. *Tetrahedron Letters* **2011,** *52* (49), 6562-6565, doi: 10.1016/j.tetlet.2011.09.111.

203.   Fang, Y.; Zhang, L.; Jin, X.; Li, J.; Yuan, M.; Li, R.; Wang, T.; Wang, T.; Hu, H.; Gu, J., α-Phosphonovinyl Arylsulfonates: An Attractive Partner for the Synthesis of α-Substituted Vinylphosphonates through Palladium-Catalyzed Suzuki Reactions. *European Journal of Organic Chemistry* **2016,** *2016* (8), 1577-1587, doi: 10.1002/ejoc.201600056.

204.   Kosolapoff, G. M., Isomerization of alkyl phosphites; some derivatives of 2-bromoethane phosphonic acid. *J Am Chem Soc* **1948,** *70* (5), 1971, doi: 10.1021/ja01185a512.

205.   Salzinger, S.; Rieger, B., Rare Earth metal-mediated group transfer polymerization of vinylphosphonates. *Macromol Rapid Commun* **2012,** *33* (16), 1327-45, doi: 10.1002/marc.201200278.

206.   Soller, B. S.; Salzinger, S.; Rieger, B., Rare Earth Metal-Mediated Precision Polymerization of Vinylphosphonates and Conjugated Nitrogen-Containing Vinyl

Monomers. *Chemical Reviews* **2016,** *116* (4), 1993-2022, doi: 10.1021/acs.chemrev.5b00313.

207. Parvole, J.; Jannasch, P., Polysulfones Grafted with Poly(vinylphosphonic acid) for Highly Proton Conducting Fuel Cell Membranes in the Hydrated and Nominally Dry State. *Macromolecules* **2008,** *41* (11), 3893-3903, doi: 10.1021/ma800042m.

208. Wagner, T.; Manhart, A.; Deniz, N.; Kaltbeitzel, A.; Wagner, M.; Brunklaus, G.; Meyer, W. H., Vinylphosphonic Acid Homo- and Block Copolymers. *Macromolecular Chemistry and Physics* **2009,** *210* (22), 1903-1914, doi: 10.1002/macp.200900284.

209. Chen, E. Y., Coordination polymerization of polar vinyl monomers by single-site metal catalysts. *Chem Rev* **2009,** *109* (11), 5157-214, doi: 10.1021/cr9000258.

210. Yasuda, H.; Ihara, E., Rare earth metal initiated polymerizations of polar and nonpolar monomers to give high molecular weight polymers with extremely narrow molecular weight distribution. *Macromolecular Chemistry and Physics* **1995,** *196* (8), 2417-2441, doi: 10.1002/macp.1995.021960802.

211. Leute, M. Macromolecules with phosphorus functionalities. Universität Ulm, 2007.

212. Seemann, U. B.; Dengler, J. E.; Rieger, B., High-Molecular-Weight Poly(vinylphosphonate)s by Single-Component Living Polymerization Initiated by Rare-Earth-Metal Complexes. *Angewandte Chemie* **2010,** *122* (20), 3567-3569, doi: 10.1002/ange.201000804.

213. Seemann, U. Polyvinylphosphonate und deren Copolymere durch Seltenerdmetall initiierte Gruppen-Transfer-Polymerisation. Technische Universität München, 2010.

214. Salzinger, S.; Soller, B. S.; Plikhta, A.; Seemann, U. B.; Herdtweck, E.; Rieger, B., Mechanistic studies on initiation and propagation of rare earth metal-mediated group transfer polymerization of vinylphosphonates. *J Am Chem Soc* **2013,** *135* (35), 13030-40, doi: 10.1021/ja404457f.

215. Salzinger, S.; Seemann, U. B.; Plikhta, A.; Rieger, B., Poly(vinylphosphonate)s Synthesized by Trivalent Cyclopentadienyl Lanthanide-Induced Group Transfer Polymerization. *Macromolecules* **2011,** *44* (15), 5920-5927, doi: 10.1021/ma200752d.

216. Zhang, N.; Salzinger, S.; Rieger, B., Poly(vinylphosphonate)s with Widely Tunable LCST: A Promising Alternative to Conventional Thermoresponsive Polymers. *Macromolecules* **2012,** *45* (24), 9751-9758, doi: 10.1021/ma3019014.

217. Evans, W. J.; Seibel, C. A.; Ziller, J. W., Unsolvated Lanthanide Metallocene Cations [(C5Me5)2Ln][BPh4]: Multiple Syntheses, Structural Characterization, and Reactivity Including the Formation of (C5Me5)3Nd1. *Journal of the American Chemical Society* **1998,** *120* (27), 6745-6752, doi: 10.1021/ja980534o.

218. Spallek, T.; Hess, O.; Meermann-Zimmermann, M.; Meermann, C.; Klimpel, M. G.; Estler, F.; Schneider, D.; Scherer, W.; Tafipolsky, M.; Tornroos, K. W.; Maichle-Mossmer, C.; Sirsch, P.; Anwander, R., Synthesis and structural diversity of trivalent rare-earth metal diisopropylamide complexes. *Dalton Trans* **2016,** *45* (35), 13750-65, doi: 10.1039/c6dt01568a.

219. Waterman, R., σ-Bond Metathesis: A 30-Year Retrospective. *Organometallics* **2013,** *32* (24), 7249-7263, doi: 10.1021/om400760k.

220. Watson, P. L., Facile C–H activation by lutetium–methyl and lutetium–hydride complexes. *J. Chem. Soc., Chem. Commun.* **1983,** (6), 276-277, doi: 10.1039/c39830000276.

221. Deelman, B.-J.; Stevels, W. M.; Teuben, J. H.; Lakin, M. T.; Spek, A. L., Insertion Chemistry of Yttrium Complex Cp*2Y(2-pyridyl) and Molecular Structure of an Unexpected CO Insertion Product (Cp*2Y)2(.mu.-.eta.2:.eta.2-OC(NC5H4)2). *Organometallics* **1994,** *13* (10), 3881-3891, doi: 10.1021/om00022a025.

222.   Duchateau, R.; van Wee, C. T.; Teuben, J. H., Insertion and C–H Bond Activation of Unsaturated Substrates by Bis(benzamidinato)yttrium Alkyl, [PhC(NSiMe3)2]2YR (R = CH2Ph·THF, CH(SiMe3)2), and Hydrido, {[PhC(NSiMe3)2]2Y(µ-H)}2, Compounds. *Organometallics* **1996,** *15* (9), 2291-2302, doi: 10.1021/om9508142.

223.   Duchateau, R.; Brussee, E. A. C.; Meetsma, A.; Teuben, J. H., Synthesis and Reactivity of Bis(alkoxysilylamido)yttrium η2-Pyridyl and η2-α-Picolyl Compounds. *Organometallics* **1997,** *16* (25), 5506-5516, doi: 10.1021/om970540d.

224.   Kaneko, H.; Nagae, H.; Tsurugi, H.; Mashima, K., End-functionalized polymerization of 2-vinylpyridine through initial C-H bond activation of N-heteroaromatics and internal alkynes by yttrium ene-diamido complexes. *J Am Chem Soc* **2011,** *133* (49), 19626-9, doi: 10.1021/ja208293h.

225.   Nagae, H.; Kundu, A.; Tsurugi, H.; Mashima, K., Propargylic C(sp3)–H Bond Activation for Preparing η3-Propargyl/Allenyl Complexes of Yttrium. *Organometallics* **2017,** *36* (16), 3061-3067, doi: 10.1021/acs.organomet.7b00395.

226.   Soller, B. S.; Salzinger, S.; Jandl, C.; Pöthig, A.; Rieger, B., C–H Bond Activation by σ-Bond Metathesis as a Versatile Route toward Highly Efficient Initiators for the Catalytic Precision Polymerization of Polar Monomers. *Organometallics* **2015,** *34* (11), 2703-2706, doi: 10.1021/om501173r.

227.   Pudasaini, B., Yttrium Catalyzed Dialkyl Vinyl Phosphonate Polymerization: Mechanistic Insights on the Precision Polymerization from DFT. *Organometallics* **2019,** *38* (5), 1091-1098, doi: 10.1021/acs.organomet.8b00884.

228.   Adams, F.; Pahl, P.; Rieger, B., Metal-Catalyzed Group-Transfer Polymerization: A Versatile Tool for Tailor-Made Functional (Co)Polymers. *Chemistry - A European Journal* **2018,** *24* (3), 509-518, doi: 10.1002/chem.201703965.

229.   Schaffer, A.; Weger, M.; Rieger, B., From lanthanide-mediated, high-precision group transfer polymerization of Michael-type monomers, to intelligent, functional materials. *European Polymer Journal* **2020,** *122*, doi: 10.1016/j.eurpolymj.2019.109385.

230.   Schwarzenböck, C.; Schaffer, A.; Pahl, P.; Nelson, P. J.; Huss, R.; Rieger, B., Precise synthesis of thermoresponsive polyvinylphosphonate-biomolecule conjugates via thiol–ene click chemistry. *Polymer Chemistry* **2018,** *9* (3), 284-290, doi: 10.1039/c7py01796k.

231.   Schaffer, A.; Kränzlein, M.; Rieger, B., Synthesis and Application of Functional Group-Bearing Pyridyl-Based Initiators in Rare Earth Metal-Mediated Group Transfer Polymerization.   *Macromolecules*   **2020,**   *53*   (11),   4345-4354,   doi: 10.1021/acs.macromol.0c00642.

232.   Adams, F.; Pschenitza, M.; Rieger, B., Yttrium-Catalyzed Synthesis of Bipyridine-Functionalized AB-Block Copolymers: Micellar Support for Photocatalytic Active Rhenium-Complexes. *ChemCatChem* **2018,** *10* (19), 4309-4316, doi: 10.1002/cctc.201801009.

233.   Pahl, P.; Schwarzenböck, C.; Herz, F. A. D.; Soller, B. S.; Jandl, C.; Rieger, B., Core-First Synthesis of Three-Armed Star-Shaped Polymers by Rare Earth Metal-Mediated Group Transfer Polymerization. *Macromolecules* **2017,** *50* (17), 6569-6576, doi: 10.1021/acs.macromol.7b01007.

234.   Schwarzenbock, C.; Vagin, S. I.; Heinz, W. R.; Nelson, P. J.; Rieger, B., Studies on the Biocompatibility of Poly(diethyl vinyl-phosphonate) with a New Fluorescent Marker. *Macromol Rapid Commun* **2018,** *39* (15), e1800259, doi: 10.1002/marc.201800259.

235.   Schaffer, A.;   Kränzlein, M.; Rieger, B., Precise Synthesis of Poly(dimethylsiloxane) Copolymers through C–H Bond-Activated Macroinitiators via Yttrium-Mediated Group Transfer Polymerization and Ring-Opening Polymerization. *Macromolecules* **2020,** *53* (19), 8382-8392, doi: 10.1021/acs.macromol.0c01639.

236.   Adams, F.; Altenbuchner, P. T.; Werz, P. D. L.; Rieger, B., Multiresponsive micellar block copolymers from 2-vinylpyridine and dialkylvinylphosphonates with a tunable lower critical solution temperature. *RSC Advances* **2016,** *6* (82), 78750-78754, doi: 10.1039/c6ra17160e.

237.   Saurwein, A.; Schaffer, A.; Wieser, C.; Rieger, B., Synthesis, characterisation and functionalisation of BAB-type dual-responsive nanocarriers for targeted drug delivery: evolution of nanoparticles based on 2-vinylpyridine and diethyl vinylphosphonate. *RSC Advances* **2021,** *11* (3), 1586-1594, doi: 10.1039/d0ra08902h.

238.   Soller, B. S.; Sun, Q.; Salzinger, S.; Jandl, C.; Pöthig, A.; Rieger, B., Ligand Induced Steric Crowding in Rare Earth Metal-Mediated Group Transfer Polymerization of Vinylphosphonates: Does Enthalpy Matter? *Macromolecules* **2016,** *49* (5), 1582-1589, doi: 10.1021/acs.macromol.5b01937.

239.   Li, H.; Shakaroun, R. M.; Guillaume, S. M.; Carpentier, J. F., Recent Advances in Metal-Mediated Stereoselective Ring-Opening Polymerization of Functional Cyclic Esters towards Well-Defined Poly(hydroxy acid)s: From Stereoselectivity to Sequence-Control. *Chemistry* **2020,** *26* (1), 128-138, doi: 10.1002/chem.201904108.

240.   Adams, F.; Machat, M. R.; Altenbuchner, P. T.; Ehrmaier, J.; Pothig, A.; Karsili, T. N. V.; Rieger, B., Toolbox of Nonmetallocene Lanthanides: Multifunctional Catalysts in Group-Transfer Polymerization. *Inorg Chem* **2017,** *56* (16), 9754-9764, doi: 10.1021/acs.inorgchem.7b01261.

241.   Weger, M.; Pahl, P.; Schmidt, F.; Soller, B. S.; Altmann, P. J.; Pöthig, A.; Gemmecker, G.; Eisenreich, W.; Rieger, B., Isospecific Group-Transfer Polymerization of Diethyl Vinylphosphonate and Multidimensional NMR Analysis of the Polymer Microstructure. *Macromolecules* **2019,** *52* (18), 7073-7080, doi: 10.1021/acs.macromol.9b01326.

242.   Ciriano, M. V.; Korth, H.-G.; van Scheppingen, W. B.; Mulder, P., Thermal Stability of 2,2,6,6-Tetramethylpiperidine-1-oxyl (TEMPO) and RelatedN-Alkoxyamines. *Journal of the American Chemical Society* **1999,** *121* (27), 6375-6381, doi: 10.1021/ja9837102.

243.   Norcott, P. L.; Hammill, C. L.; Noble, B. B.; Robertson, J. C.; Olding, A.; Bissember, A. C.; Coote, M. L., TEMPO–Me: An Electrochemically Activated Methylating Agent. *Journal of the American Chemical Society* **2019,** *141* (38), 15450-15455, doi: 10.1021/jacs.9b08634.

244.   Hammill, C. L.; Noble, B. B.; Norcott, P. L.; Ciampi, S.; Coote, M. L., Effect of Chemical Structure on the Electrochemical Cleavage of Alkoxyamines. *The Journal of Physical Chemistry C* **2019,** *123* (9), 5273-5281, doi: 10.1021/acs.jpcc.8b12545.

245.   Noble, B. B.; Norcott, P. L.; Hammill, C. L.; Ciampi, S.; Coote, M. L., Mechanism of Oxidative Alkoxyamine Cleavage: The Surprising Role of the Solvent and Supporting Electrolyte. *The Journal of Physical Chemistry C* **2019,** *123* (16), 10300-10305, doi: 10.1021/acs.jpcc.9b01832.

246.   Schwarzenbock, C.; Nelson, P. J.; Huss, R.; Rieger, B., Synthesis of next generation dual-responsive cross-linked nanoparticles and their application to anti-cancer drug delivery. *Nanoscale* **2018,** *10* (34), 16062-16068, doi: 10.1039/c8nr04760j.

247.   Evans, W. J.; Perotti, J. M.; Doedens, R. J.; Ziller, J. W., The tetramethylpiperidinyl-1-oxide anion (TMPO-) as a ligand in lanthanide chemistry: synthesis of the per(TMPO-) complex [(ONC5H6Me4)2Sm(mu-ONC5H6Me4)]2. *Chem Commun (Camb)* **2001,** (22), 2326-7, doi: 10.1039/b106869p.

248.   Murakami, R.; Nakamura, T.; Ishida, T., Doubly TEMPO-coordinated gadolinium(III), lanthanum(III), and yttrium(III) complexes. Strong superexchange coupling across rare earth ions. *Dalton Trans* **2014,** *43* (15), 5893-8, doi: 10.1039/c3dt53586j.

249.   Eggers, S. H.; Schultze, H.; Kopf, J.; Fischer, R. D., Isomorphism of Tris(cyclopentadienyl)lutetium(III) and Tris(cyclopentadienyl)scandium(III): An Unexpected Consequence of the Lanthanoid Contraction. *Angewandte Chemie International Edition in English* **1986,** *25* (7), 656-657, doi: 10.1002/anie.198606561.

250.   Tasdelen, M. A., Diels–Alder "click" reactions: recent applications in polymer and material science. *Polymer Chemistry* **2011,** *2* (10), 2133, doi: 10.1039/c1py00041a.

251.   Chang, C.-M.; Liu, Y.-L., Functionalization of multi-walled carbon nanotubes with furan and maleimide compounds through Diels–Alder cycloaddition. *Carbon* **2009,** *47* (13), 3041-3049, doi: 10.1016/j.carbon.2009.06.058.

252.   Nebhani, L.; Barner-Kowollik, C., Functionalization of Fullerenes with Cyclopentadienyl and Anthracenyl Capped Polymeric Building Blocks via Diels-Alder Chemistry. *Macromolecular Rapid Communications* **2010,** *31* (14), 1298-1305, doi: 10.1002/marc.201000142.

253.   Yuan, J.; Chen, G.; Weng, W.; Xu, Y., One-step functionalization of graphene with cyclopentadienyl-capped macromolecules via Diels–Alder "click" chemistry. *Journal of Materials Chemistry* **2012,** *22* (16), 7929, doi: 10.1039/c2jm16433g.

254.   Vericat, C.; Vela, M. E.; Benitez, G.; Carro, P.; Salvarezza, R. C., Self-assembled monolayers of thiols and dithiols on gold: new challenges for a well-known system. *Chem Soc Rev* **2010,** *39* (5), 1805-34, doi: 10.1039/b907301a.

255.   Elgrishi, N.; Rountree, K. J.; McCarthy, B. D.; Rountree, E. S.; Eisenhart, T. T.; Dempsey, J. L., A Practical Beginner's Guide to Cyclic Voltammetry. *Journal of Chemical Education* **2018,** *95* (2), 197-206, doi: 10.1021/acs.jchemed.7b00361.

9 Supplementary materials

UV-Vis. Calibration curve
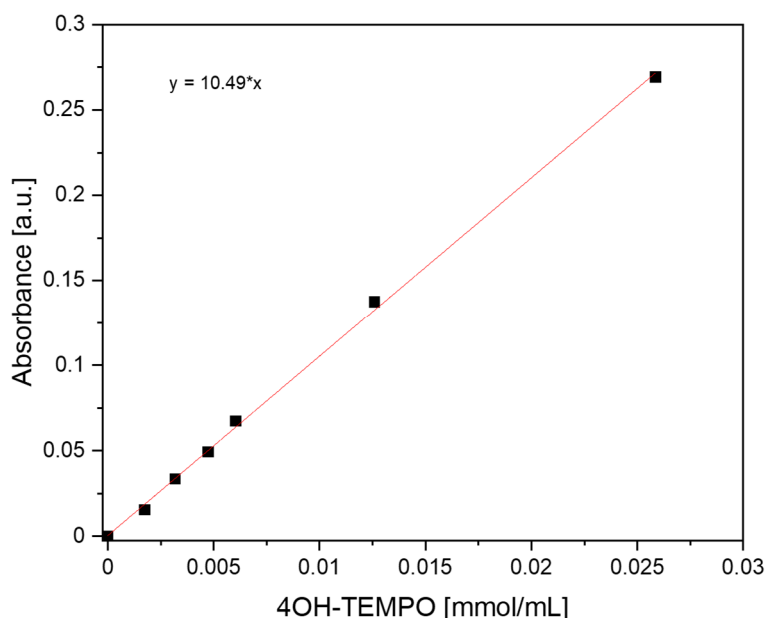
Figure S1: 4OH-TEMPO UV-Vis. Calibration curve in NMP with a 10 mm quartz cuvette

EPR calibration curve in DCM in quartz tubes (I.D. 3 mm)

y = 91809*x
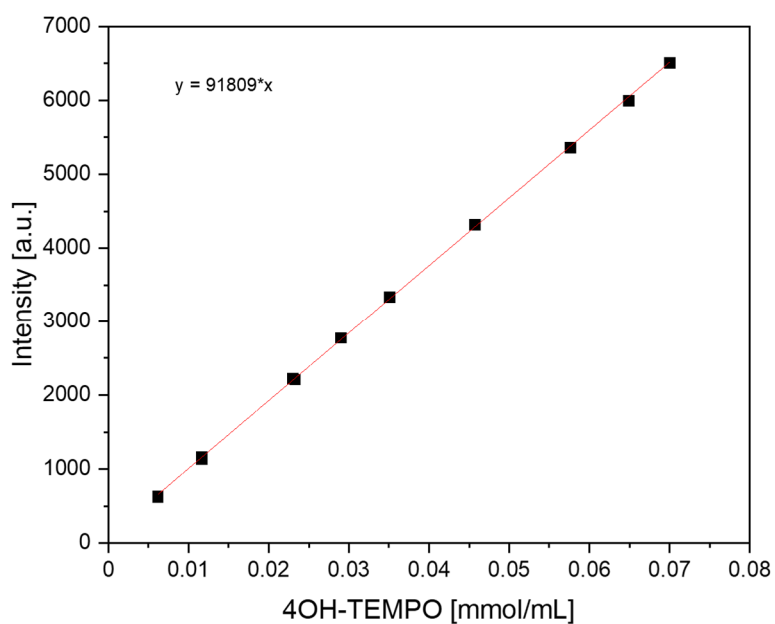
Figure S2: 4OH-TEMPO calibration curve in DCM

EPR calibration curve in NMP in 50 µL microcapillary pipettes

y = 21448*x
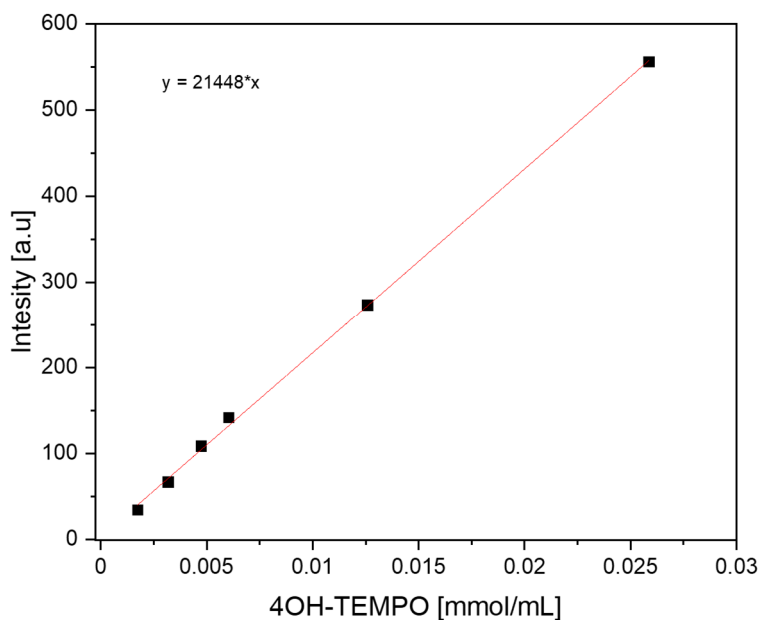
Figure S3: 4OH-TEMPO calibration curve in NMP with 50 µL microcapillary pipettes

154
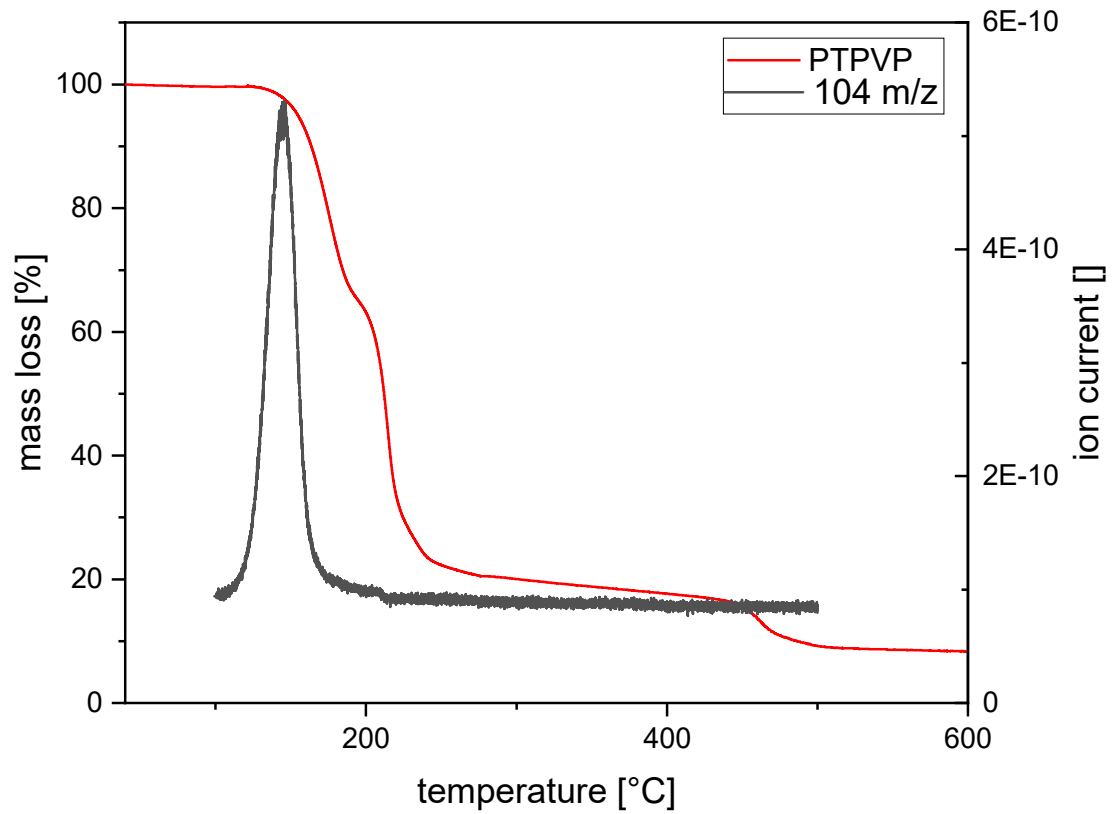
Figure S4: TGA-MS plot for PDTPVP (red) and the ion current at 104 m/z (black). The measurement was performed with a heating rate of 1 Kmin^{-1}

List of Figures

List of Schemes

List of Tables